The physiological functions of different ferredoxins in *Synechocystis* sp. PCC 6803

Dissertation
in fulfilment of the requirements for the degree "Dr. rer. nat."
of the Faculty of Mathematics and Natural Sciences
at Kiel University

submitted by

Yingying Wang

Kiel

August 2018

First referee: Prof. Dr. Rüdiger Schulz

Second referee: Prof. Dr. Wolfgang Bilger

Date of the oral examination: 15. 10. 2018

Life is nothing but an electron looking for a place to rest.

— Albert Szent-Györgyi

List of Abbreviations

a.a.	Amino acid
ADP	Adenosine diphosphate
AG	Arginine plus glucose
AGD	Arginine plus glucose and DCMU
Amp	Ampicillin resistence
AOX	Alternative oxidase
Arg	Arginine
ATP	Adenosine Triphosphate
BG-11	Standard medium for cyanobacteria
BLAST	Basic local alignment search tool
bp	Base pair
CBB cycle	Calvin–Benson–Bassham cycle or Calvin cycle or Calvin-Benson Cycle
cDNA	Complementary DNA
CO_2	Carbon dioxide
Chl	Chlorophyll
CoA	Coenzyme A
COX	Cytochrome c oxidase
Cm	Chloramphenicol
CM	Cytoplasmic membrane
Cyt	Cytochrome
DBMIB	2,5-dibromo-3-methyl-6-isopropyl-p-benzoquinone
DCMU	3-(3,4-dichlorophenyl)-1,1-dimethylurea
ddH2O	Deionized and autoclaved water
DMSO	Dimethyl sulfoxide
DNA	Deoxyribonucleic acid
DNase	Deoxy ribonuclease
dNTPs	Deoxyribonucleotide
DTT	Dithiothreitol
E. coli	*Escherichia coli*
ED	Entner-Doudoroff
EDTA	Ethylene dinitro tetraacetic acid
EMP	Embden-Meyerhof-Parnas
FMN	Flavin mononucleotide
et al.	abbreviation of *et* (“and”) and *alii* (“others”)
Fed/Fd/FDX	Ferredoxin from others work
FNR	Ferredoxin: NADP oxidoreductase
Fx	Ferredoxin in this work
g	Gram / Gravitational acceleration
G	Glucose
GAP	Glyceraldehyde 3-phosphate
GAPDH	Glyceraldehydes-3-phosphate dehydrogenase
Gdh	Glutamate dehydrogenase
Gm	Gentamycin
Gm^r	Gentamycin resistance cassette
GOGAT	Glutamate synthase
GS	Glutamine synthase
H^+	Proton
H_2	Hydrogen
kb	Kilobase pairs
kDa	Kilodalton
Km	Kanamycin
Km^r	Kanamycin resistance cassette

L	Liter
LAHG	Light-activated heterotrophic growth
LB	Standard medium for bacteria *E. coli*
M	Molar
m^2	Square meter
Mb	Mega base pairs
min	Minute
ml	Milliliter
mM	Millimolar
mRNA	Messenger ribonucleic acid
ms	Millisecond
MV	Methyl viologen
N_2	Nitrogen
NAD(H)	Nicotinamide adenine dinucleotide (red/ox)
NADP(H)	Nicotinamide adenine dinucleotide Phosphate (red/ox)
Nar	Nitrate reductase
NCBI	National center of biotechnology information
NaOH	sodium hydroxide
NiFe	Nickel-iron
Nir	Nitrite reductase
O_2	Oxygen
OD	Optical density
OPP	Oxidative pentose phosphate
OPF	Open reading frame
PAM	Pulse amplitude modulated chlorophyll fluorescence
PC	Plastocyanin
PCC	Pasteur culture collection
PCR	Polymerase Chain Reaction
PDH	Pyruvate dehydrogenase
PEP	Phosphoenolpyruvate
PFOR	Pyruvate: ferredoxin / flavodoxin oxidoreductase
pfu	Pyrococcus furiosus
PGP	2,3-bisphosphoglycerate
pH	Latin terms *potentia hydrogenii* (capacity of hydrogen)
PQ	Plastoquinone
PS I	Photosystem I
PS II	Photosystem II
QA	Electron acceptor in Photosystem II
RNA	Ribonucleic acid
RNase	Ribonuclease
rpm	Round per minute
RT	Room temperature
RT-Mix	Reverse transcription mixture
RT-PCR	Reverse transcription-polymerase chain reaction
RTO	Respirational terminal oxidase
SDH	Succinate dehydrogenase
SDS	Sodium Dodecyl Sulfonate
SOB	Super optimal broth medium
SOC	Super optimal broth plus glucose
sp.	Species
Taq	Thermus aquaticus
TBE	Tris/boric acid/EDTA buffer
TCA cycle	Tricarboxylic acid cycle or Krebs cycle
WT	Wild-type of *Synechocystis* sp. PCC6803 in this work

Contents

1. Introduction

1.1 Cyanobacteria

Cyanobacteria (blue-green algae or cyanophytes) are a division of microorganisms that are related to the bacteria but are capable of oxygenic photosynthesis, likewise algae and plants involving two photosystems (PSII and PSI) (Gutekunst 2018, Stanier and Bazine 1977). Their light-harvesting pigments mainly contain chlorophyll a and phycobiliproteins and are therewith distinguishable from that of the other groups of photosynthetic bacteria that rely on one photosystem only: purple bacteria, green sulfur bacteria, green non-sulfur, heliobacteria, and acidobacteria (Hanada 2016, Stanier and Bazine 1977). Cyanobacteria are defined as gram-negative prokaryotes because of the special structure and chemical composition of the cell wall (Lang 1968).

Cyanobacteria are among the oldest and morphologically most diverse prokaryotic phyla on our planet. Early Archean microfossils from Warrawoona Group, Australia suggest that cyanobacteria and therewith oxygen-producing photosynthesis, may reach back 3.3 billion to 3.5 billion years (Schopf and Packer 1987). Among cyanobacteria, there are unicellular, colonial and filamentous species and some diazotrophic strains, that are capable to fix atmospheric nitrogen. Based on their morphology, cyanobacteria are divided into five sections (subgroups): I—unicellular cyanobacteria, that reproduce by binary fission or budding; II—unicellular cyanobacteria, that reproduce by multiple fission alone or by both multiple fission and binary fission; III—multicellular cyanobacteria, that linearly dividing in a single plane; IV—multicellular filamentous cyanobacteria, that contain specialized cells (vegetative, heterocysts, and akinetes); and V—multicellular filamentous branched cyanobacteria (Rippka et al. 1979).

To date (10th June 2018), the genome of 85 cyanobacterial strains (83 species and 2 subspecies) have been completely sequenced (http://dev-genome.annotation.jp/cyanobase). With respect to genome size, cyanobacterial genomes are notably different, extending from 1.44 Mb (*Candidatus Atelocyanobacterium thalassa* ALOHA) to 9.06 Mb (*Nostoc punctiforme* PCC 73102) (Prabha et al. 2016).

Cyanobacteria occupy almost every habitat on earth, such as marine, freshwater, deserts, soil, ranging from polar to topical climate zones (Whitton and Potts 2007). In addition, some cyanobacteria are also involved in symbiotic relationships with a wide range of eukaryotic hosts, mostly plants and fungi, and provide fixed nitrogen or carbon to the host (Adams 2000).

Oxygen accumulated 2.3 billion years ago in the primitive earth's atmosphere (the Great Oxidation Event), which is widely assumed as a result of oxygenic photosynthesis performed by cyanobacteria (Allen and Martin 2007, Bekker et al. 2004, Kopp et al. 2005, Rasmussen et al. 2008). Cyanobacteria are even nowadays very important members of the global ecosystem and contribute up to 30% of the yearly oxygen production (DeRuyter and Fromme 2008) and 40% of the yearly carbon fixation (Falkowski and Raven 1997) on the planet and approximately 50% of the production of biologically available nitrogen in the oceans (Stal 2009).

Therefore, cyanobacteria are crucial and fundamental for the composition of the atmosphere and for the net primary production of organic matter and global food chains.

Recent research has pointed out the potential application of cyanobacteria to produce clean and renewable energy by converting light energy and CO_2 (Deng and Coleman 1999, Lubner et al. 2011, 2013, Quintana et al. 2011, Varman et al. 2013a). Technical improvements in synthetic biology make it easier to unlock the potential of this application (Berla et al. 2013, Knight et al. 2012).

1.2 *Synechocystis* sp. PCC 6803

The unicellular, non-nitrogen fixing cyanobacterium *Synechocystis* sp. strain PCC 6803 (hereafter *Synechocystis*), was the first photosynthetic organism and the first cyanobacterium whose genome was completely sequenced (Kaneko et al. 1996a). Its chromosome genome size is 3.57 Mb with a total of 3168 genes (Kaneko et al. 1996b). Furthermore, the genome of *Synechocystis* also contains three small plasmids: pCC5.2 (5.2 kb), pCA2.4 (2.4 kb), pCB2.4(2.4 kb) and another four large plasmids: pSYSM (120 kb), pSYSX (106 kb), pSYSA (103kb), pSYSG (44 kb) (Kaneko et al. 2003).

As shown in Fig. 1.2, *Synechocystis* cells are essentially spherical immediately after cell division (van de Meene et al. 2006). Furthermore, *Synechocystis* cells have an internal system of thylakoid membranes (see white arrowheads in Fig. 1.2) (van de Meene et al. 2006), which is the main site of respiratory as well as photosynthetic electron transport (Howitt and Vermaas 1998). Respiration does additionally take place in the cytoplasmic membrane.

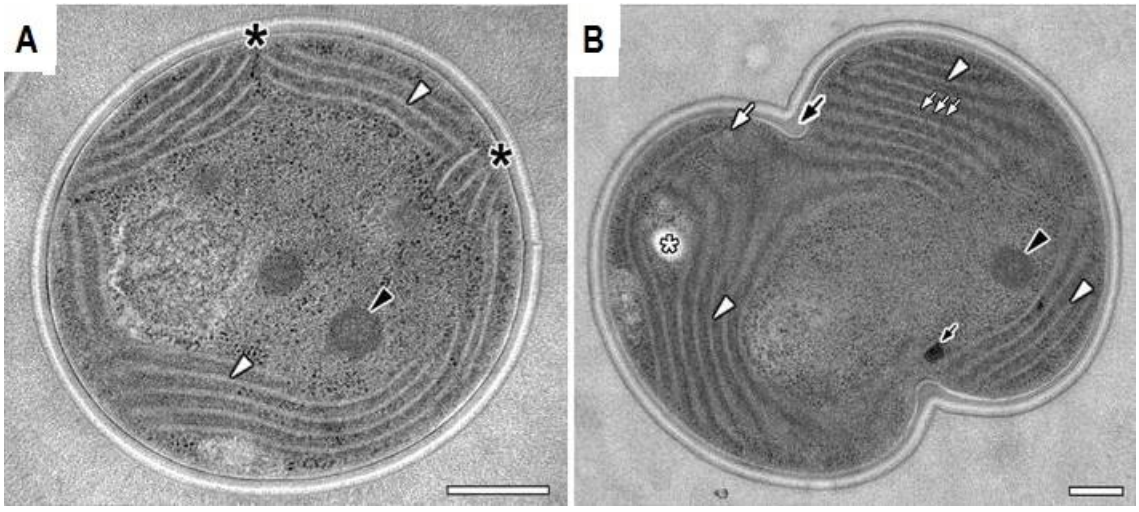

Fig. 1.2. Standard TEM images of cells of *Synechocystis* sp. PCC 6803 at different division phase. A: non-dividing cell; B: a cell in early division. *white arrowheads*: thylakoid membrane; *black asterisks*: cytoplasmic membrane; *black arrowheads*: carboxysomes; *small black arrow*: polyphosphate bodies; *white asterisk*: PHA granule; *large white arrow*: lipid bodies; *small white arrows*: phycobilisome; *large black arrow*: invaginating septum. *Bars*=200 nm. (modified after van de Meene et al. 2006).

Synechocystis is one of the most extensively studied types of cyanobacteria as it can grow under diverse growth conditions, including phototrophic and mixotrophic growth during light periods (Rippka et al. 1979, Williams 1988) as well as light-activated heterotrophic growth in the absence of light (Anderson and Mcintosh 1991). It furthermore survives under fermentative conditions. Moreover, *Synechocystis* readily takes up exogenous DNA and integrates in via homologous recombination into its genome thereby facilitating large-scale genetic modifications and targeted mutagenesis (Vermaas 1996).

1.3 Metabolic characterization of *Synechocystis* under various trophic growth conditions

Cyanobacteria, such as *Synechocystis*, are well known for their ability to grow under various trophic conditions, including photoautotrophic and mixotrophic growth during light periods (Rippka et al. 1979, Williams 1988) as well as light-activated heterotrophic (LAHG) and fermentative growth in the absence of light (Anderson and Mcintosh 1991), and to perform different and flexible modes of metabolism to adapt to various natural environments (Lau et al. 2015, Stal 1995).

1.3.1 Photoautotrophic growth conditions

Photoautotrophic growth is the simplest and most common growth conditions in the nature and in the lab for studying photosynthesis in *Synechocystis*. Under this condition ATP and NADPH are generated by water-splitting photosynthesis and are mainly used for CO_2 fixation via the Calvin-Bension cycle, which subsequently drives glycogen accumulation and the TCA cycle for amino acid and lipid precursors synthesis (Knoop et al. 2010). Therefore, the use of photosynthetic cyanobacteria to convert CO_2 to renewable chemicals or industrially important compounds, has become an emerging area of interest (Lau et al. 2015, Yu et al. 2013).

1.3.2 Mixotrophic growth conditions

Both inorganic carbon sources, such as CO_2 and $NaCO_3$, and exogenous organic carbon sources, such as glucose, can be simultaneously used by *Synechocystis* under mixotrophic conditions (Yang et al. 2002b) (Wan et al. 2015), resulting in a faster growth rate but a slower photosynthesis rates than under autotrophic conditions (Fang et al. 2017, Takahashi et al. 2008, Yoshikawa et al. 2013). The degradation of organic substrates, such as glucose, under mixotrophic conditions provides additional carbon and energy sources including ATP, NAD(P)H, and biosynthetic precursors for amino acids, nucleotides and fatty acids (Nakajima et al. 2014).

It is general knowledge that cyanobacteria as well as plants oxidize carbohydrates via glycolysis [the Embden–Meyerhof–Parnas (EMP) pathway] and the oxidative pentose phosphate (OPP) pathway as the amounts of metabolic intermediates of both pathways accumulated upon the addition of glucose into autotrophic cultures (Takahashi et al. 2008, Yang et al. 2002b, You et al. 2014). Moreover, under mixotrophic conditions, as the pentose phosphate pathway can either run in its oxidative mode (OPP pathway) to oxidize carbohydrates or in its reductive mode (Calvin–Benson cycle) to fix CO_2 and both the EMP and OPP

pathways share several intermediates with the Calvin–Benson cycle, the enhanced EMP and OPP pathways upon the addition of exogenous glucose might slow down the Calvin-Benson cycle to prevent a futile cycle (Chen 2014, Chen et al. 2016, Narainsamy et al. 2013, Wan et al. 2015). However, recent work has proven that both cyanobacteria and plants possess a third overlooked glucose degradation pathway: the Entner–Doudoroff (ED) pathway (Fig. 1.3.1), which is physiologically even more significant than the other two pathways, especially under mixotrophic conditions and under autotrophic conditions in a day/night cycle (Chen et al. 2016). The ED pathway does not share any intermediates with the Calvin–Benson cycle and should therefore not generate futile cycles (Chen et al. 2016).

Acetate, besides glucose, is also one common and important carbon sources for both bacteria and eukaryotic microalgae (Wright and Hobbie 1966). Exogenous acetate can increase the intracellular pool of pyruvate available for biosynthetic reactions in *Syneehoeoccus* and *Aphanocapsa* 6308 (Ihlenfeldt and Gibson 1977). Although it was suggested that some cyanobacteria could also assimilate acetate as the sole carbon and energy source (Pearce and Carr 1967), *Synechocystis* almost cannot grow on supplemented acetate alone (Knoop et al. 2013, Varman et al. 2013b, You et al. 2014). The genes encoding isocitrate lyase and malate synthase, two key glyoxylate shunt enzymes required for acetate assimilation, are absent in the genome of *Synechocystis* (Zhang and Bryant 2015). Moreover, neither those enzymatic activities (Knoop et al. 2013) nor a functional glyoxylate cycle (You et al. 2014) were detected in *Synechocystis* cells.

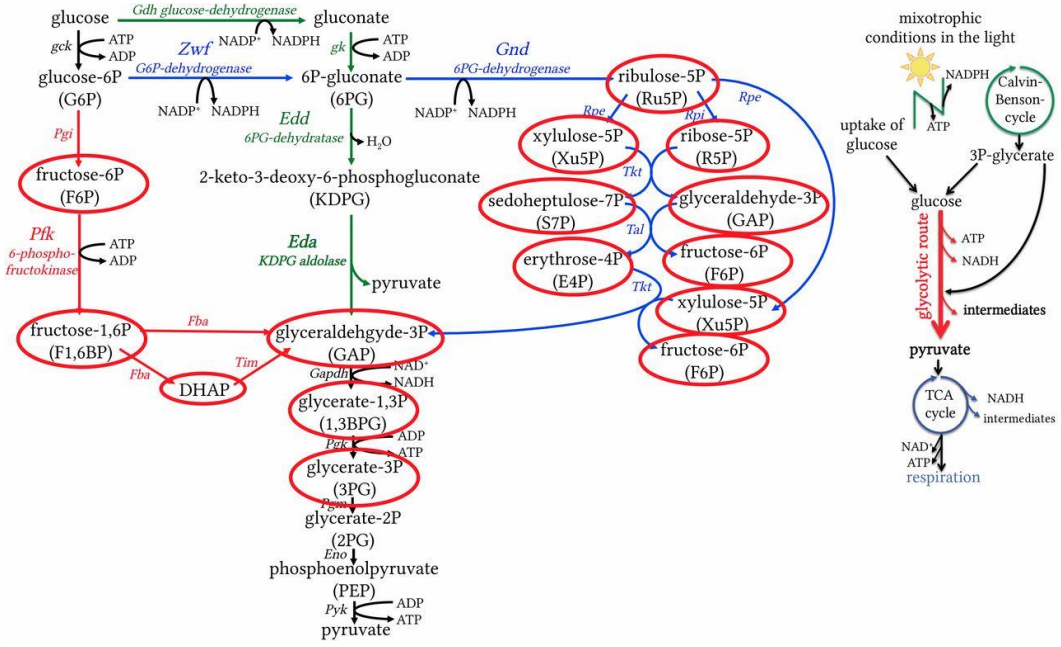

Fig. 1.3.1 The glucose degrading pathway under mixotrophic conditions. Both the EMP (red) and the OPP (blue) pathways share intermediates with the Calvin–Benson cycle (circled in red), but not the ED (green) pathway. (Chen et al. 2016)

Using isobaric labeling-based quantitative proteomics, it was suggested that proteins involved in nitrogen assimilation and light-independent chlorophyll synthesis are upregulated when exogenous glucose is supplied, along with a dramatic reduction of PII phosphorylation that senses carbon and nitrogen (C/N) balance status (Fang et al. 2017, Forchhammer 2004, Selim et al. 2018). These results indicate that the addition of exogenous glucose in the light causes a nitrogen deficiency conditions for *Synechocystis* as the C/N balance has been shifted to the side of carbon (Fang et al. 2017, Muro-Pastor et al. 2001). Furthermore, the combination of light and glucose triggers an oxidative stress for *Synechocystis* under mixotrophic conditions investigated by using the PFPP-LC/MS system (Narainsamy et al. 2013). This stress might result from the glucose-mediated down regulation of the Calvin-Benson cycle, which normally consumes the majority of photosynthetic electrons for CO_2 fixation, leaving the spared electrons to recombine with photosynthetic oxygen, thereby generating toxic reactive oxygen species (ROS) such as superoxide anions, hydrogen peroxide and hydroxyl radicals (Latifi et al. 2009, Narainsamy et al. 2013).

1.3.3 Heterotrophic growth conditions

With glucose as a carbon source, *Synechocystis* can grow, beside under mixotrophic conditions, under photoheterotrophic (continuous photosynthetic illumination in the presence of the photosystem II inhibitor 3-(3,4-dichlorophenyl)-1,1-dimethylurea, DCMU), and light-activated heterotrophic growth (LAHG, or called chemoheterotrophic growth) conditions with a daily pulse of white light (Anderson and Mcintosh 1991, Rippka 1972). They furthermore survive in the absence or presence of glucose in a day/night cycle, which represents the most common condition in nature.

LAHG conditions

When cells grow to a high cell density and light or CO_2 become limited under mixotrophic conditions, cyanobacteria up-regulate their OPP pathway to consume more glucose and reduce its net CO_2 fixation rate via slowing down the Calvin-Benson cycle (You et al. 2014). If heterotrophically incubated in complete darkness, *Synechocystis* fails to grow on glucose unless given a daily pulse of white light or low intensity blue light, which probably activates and regulates some biochemical activities (glucose metabolism) and cell division or other photomorphogenic processes (Anderson and Mcintosh 1991, Tabei et al. 2009). Therefore, this growth condition is called light-activated heterotrophic growth (LAHG).

Cyanobacterial glycolytic routes were deemed to be foremost important under heterotrophic conditions in the dark (Knowles and Plaxton 2003). Under LAHG conditions with glucose as sole organic carbon source, only the OPP pathway, neither EMP or ED pathway, are essential for survival (unpublished). The tricarboxylic acid (TCA) cycle operates to generate ATP, NADPH and carbon skeletons (such as 2-oxoglutarate), which are used as precursors for the biosynthesis of nucleotides, amino acids and fatty acids (Ball and Morell 2003, Zhang and Bryant 2011). Under such conditions, Cox, a thylakoid terminal oxygenase (see chapter 1.3.4), is essential for the growth of *Synechocystis* (Pils et al. 1997).

The heterotrophic metabolism of *Synechocystis*, in comparison to the autotropic mode of growth, has been characterized at protein level via proteomic and lipidomic analyses (Kurian et al. 2006, Plohnke et al. 2015). The significant reduction in the expression levels of Rubisco and CO_2-concentrating mechanism (CCM) proteins indicates the downregulation of photosynthetic activity, which is well in line with the decreased rate of oxygen evolution under saturated light (Kurian et al. 2006). The expression level of proteins involved in glycogen synthesis and glucose degradation including the EMP pathway, the OPP pathway as well as the TCA cycle is increased under LAHG condition (Kurian et al. 2006, Plohnke et al. 2015). In addition, the synthesis of protein and amino acids (such as histidine and serine) is also enhanced under this condition (Kurian et al. 2006, Plohnke et al. 2015, Tabei et al. 2009). It's particularly necessary to point out that superoxide dismutase (SodB or Slr1516)(Bhattacharya et al. 2004) catalyzing the scavenging of superoxide anion radicals, as well as two antioxidant protein (or called peroxiredoxins), Slr1198 and Sll1621 (Hosoya-Matsuda et al. 2005), which are involved in the protection from oxidative stress in cyanobacteria, are strongly upregulated in their protein expression under LAHG conditions (Kurian et al. 2006, Plohnke et al. 2015).

A proteome analysis, which compared mixotrophic to LAHG conditions, revealed that the expression of proteins that are involved in glycogen synthesis increased whereas those involved in glycogen degradation decreased, however an accumulation of glycogen was not observed under these conditions (Plohnke et al. 2015). Furthermore, the expression of proteins that are involved in the OPP pathways increased under LAHG conditions (Plohnke et al. 2015), confirming its importance under LAHG conditions (Lex and Carr 1974, Pelroy et al. 1972, Plohnke et al. 2015, Yang et al. 2002a). Even though nitrate is present in the medium under LAHG conditions, cyanobacteria developed an unexpected nitrogen-starvation response by increasing the abundance of several important proteins that function as nitrogen regulators, such PipX (Taroncher-Oldenberg et al. 2000), NtcA and PII (Osanai and Tanaka 2007), possibly because they sense an C/N imbalance due to the supplementation of glucose (Plohnke et al. 2015). Interestingly, similar to the glucose-elicited oxidative stress which was observed under mixotrophic conditions (Narainsamy et al. 2013), cyanobacteria also increase the abundance of proteins associated with oxidative stress, such as SodB (Slr1516), catalase (Sll1987), thioredoxin (Slr0623), peroxiredoxin (Sll0755), glutathione peroxidase-like NADPH peroxidase (Gpx2, Slr1992), heat shock protein HtpG, as well as several other chaperones involved in a general stress response, under LAHG conditions (Hosoya-Matsuda et al. 2005, Plohnke et al. 2015). Because of the heterotrophic growth conditions, also proteins involved in carbon metabolism and C/N-balance were severely affected.

Photoheterotrophic conditions with DCMU

The herbicide DCMU is used to specifically block the PQ binding site of PSII and to interrupt the linear photosynthetic electron transport (Kyle et al. 1984). Cyanobacteria treated with DCMU cease to grow under autotrophic conditions, whereas they are able to grow when they are supplemented with glucose in addition resulting in photoheterotrophic conditions (Anderson and Mcintosh 1991, Rippka 1972, Tabei et al. 2009).

Under such inhibitory circumstances, cyanobacteria catalyzed the glucose oxidation mainly via the OPP pathway combined with the glucose-6-phosphate isomerase (PGI) reaction to support the requirement of NADPH and operated the cyclic electron flow around PSI and NAD(P)H oxidation for the generation of ATP (You et al. 2015). Even though the Calvin-Benson cycle is not fully functional, RubisCO is still active to fix CO_2 and synthesize 3-phosphoglycerate (3-PG) for glycolysis (You et al. 2015). The minimal flux through the tricarboxylic acid (TCA) cycle and succinate dehydrogenase (SDH) indicates that the TCA cycle might not be the pathway to generate significant NADPH and ATP for cyanobacteria under photoheterotrophic conditions (You et al. 2015).

Furthermore, the ratio of NADP(H) to NAD(H) in cyanobacteria cells is influenced by the availability of carbon and light. For example, the ratio of NADP(H) to NAD(H) in *Synechococcus* PCC7942 cells under dark conditions is 3.8, while it is 6.5 in these cells in the light (Tamoi et al. 2005). It was reported that the NADP(H)/NAD(H) ratio in *Synechocystis* decreased from 2.3 to 1.4 upon the addition of glucose in the light (Takahashi et al. 2008).

1.3.4 Fermentative conditions

During dark anoxic periods (called fermentative conditions), cyanobacteria survive at the expense of endogenous glycogen, which accumulates during photosynthetic conditions in the light or originates from glucose that was consumed from the medium (Heyer and Krumbein 1991, Lee et al. 2014, Smith 1983, Stal and Moezelaar 1997). Glycogen is degraded via the OPP pathway to CO_2, hydrogen and organic products such as formate, acetate, lactate, succinate and alcohols, while NAD(P)H and ATP are generated by substrate-level phosphorylation (Appel et al. 2000a, Carrieri et al. 2009, Carrieri et al. 2010, Gutthann et al. 2007, Hasunuma et al. 2016, Heyer and Krumbein 1991, McNeely et al. 2010).

In comparision to autotrophic conditions, *Synechococcus* sp. PCC 7002 and *Synechocystis* downregulate the expression levels of genes involved in light harvesting, photosystems, photosynthetic electron transport, chlorophyll biosynthesis and Rubiso to adjust to the growth under fermentative conditions (Hasunuma et al. 2016, Ludwig and Bryant 2011). The expression of *pfor* encoding the pyruvate:ferredoxin oxidoreductase (PFOR) is upregulated (Hasunuma et al. 2016, Ludwig and Bryant 2011), whereas transcript levels for pyruvate dehydrogenase (PDH) complex encoding genes, *pdhA* and *pdhB*, decrease approximately two-fold (Ludwig and Bryant 2011). These results suggest a global decrease in transcripts for respiratory proteins and sindicate that cells employ an alternative phosphoenolpyruvate degradation pathway via PFOR, instead of PDH under fermentative conditions (Hasunuma et al. 2016, Ludwig and Bryant 2011).

Cyanobacterial NiFe-Hydrogenase receives electrons from PFOR directly via flavodoxin/ferredoxin for hydrogen production under fermentative conditions (Gutekunst et al. 2014). Nitrate reduction can function as alternative electron sink under low oxygen concentration conditions and fermentative conditions (Appel et al. 2000a, Gutthann et al. 2007, McNeely et al. 2010). Both of them compete each other in the reductans (ferredoxin or flavodoxin) utilization.

1.4 Photosynthesis, respiration and alternative electron transport pathways

Cyanobacteria are significant primary producers and are found in almost every environment on our planet (DeRuyter and Fromme 2008, Falkowski and Raven 1997), especially in the oceans (Stal 2009). They are able to perform oxygenic photosynthesis and respiration simultaneously and have furthermore evolved a variety of alternative electron transport pathways to dissipate excess electrons via photoprotection (Lea-Smith et al. 2016). There are two membrane systems: the cytoplasmic membrane and a series of internal thylakoid membranes, in almost all cyanobacterial species except for *Gloeobacter violaceus*, which lacks thylakoid membranes (Rexroth et al. 2011). The light reactions of photosynthesis occur solely in thylakoid membranes, whereas respiratory electron flow takes place in both the thylakoid and cytoplasmic membranes (Vermaas 2001).

The following part will give a short review on electron transport pathways in each of the membrane systems and the function of alternative electron transport pathways (cyclic electron transport and Mehler-like reaction) that are involved in photoprotection. Unless a different species is indicated, this review will focus on electron transport pathways in *Synechocystis*.

1.4.1 Photosynthesis and photosynthetic linear electron transport

Photosynthesis, a process in which light energy is converted into chemical energy, sustains life on the Earth by providing both carbohydrate and the oxygen we breathe (Falkowski and Raven 1997). Those organisms, that are able to do photosynthesis are called photoautotrophs, including plants, algae (diatoms, green algae), some unicellular eukaryotes (Euglena), and bacteria (cyanobacteria and anoxygenic photosynthetic bacteria) (Falkowski and Raven 1997, Fromme and Grotjohann 2008). In the first stage, light reactions capture the energy of light and use it to generate ATP and NADPH (Fig. 1.4.1) (Fromme and Grotjohann 2008, Ort and Yocum 1996). In the second stage of photosynthesis, ATP and NADPH that were produced in the light reactions are used to fix atmospheric carbon dioxide (CO_2) in carboxysomes and further to reduced it to carbohydrates via the Calvin-Benson-Bassham (CBB) cycle in the cell cytoplasm (Fig. 1.4.1) (Cannon et al. 2001, Hugler and Sievert 2011). The glycogen stored during photosynthesis provides raw material for cellular respiration and anabolic pathways that synthetize proteins, lipids and other products (Falkowski and Raven 1997, Hugler and Sievert 2011).

There are four major types of integral membrane protein complexes, photosystem I (Dutta and Vermaas), photosystem II (PSII), cytochrome *b*6*f* complex (Cyt *b*6*f*) and ATP synthase (ATPase), that catalyze the photosynthetic light reactions and drive a linear electron transport (LET) in the thylakoid membrane (Fig. 1.4.1) (Hervas et al. 2003, Mustila 2017). The plastoquinone (PQ) which reduces the cytochrome b6f complex is one of the main regulators for electron transfer between photosynthesis and respiration in *Synechocystis* (Berry et al. 2002, Fujita et al. 1987).

The photons absorbed by light-harvesting antennae, phycobilisomes (PBS), excite the reaction center chlorophylls of the two photosystems, PSI and PSII, and trigger the electron transfer (Wildman and Bowen

1974). Excitation of reaction center P680, a specialized *Chl a* pair, in PSII leads to primary charge separation, followed by the electron transfer to the primary and secondary quinone acceptors, Q_A and Q_B, and subsequently to plastoquinones (PQ) (Hervas et al. 2003). The lost electron of $P680^+$ is replaced by an electron derived from H_2O splitting (Zehr et al. 2008). The water oxidation of PSII is catalyzed by an oxygen-evolving complex (OEC), by which two water molecules split into four electrons, four protons and an oxygen molecule (Bricker and Frankel 2011, Vinyard et al. 2013). The cyanobacterial OEC consists of several extrinsic subunits, PsbO, PsbV, PsbU, CyanoP and CyanoQ, which corporately protect the inorganic core of OEC and may play a role in proton evolution (Bricker et al. 2012, Vinyard et al. 2013).

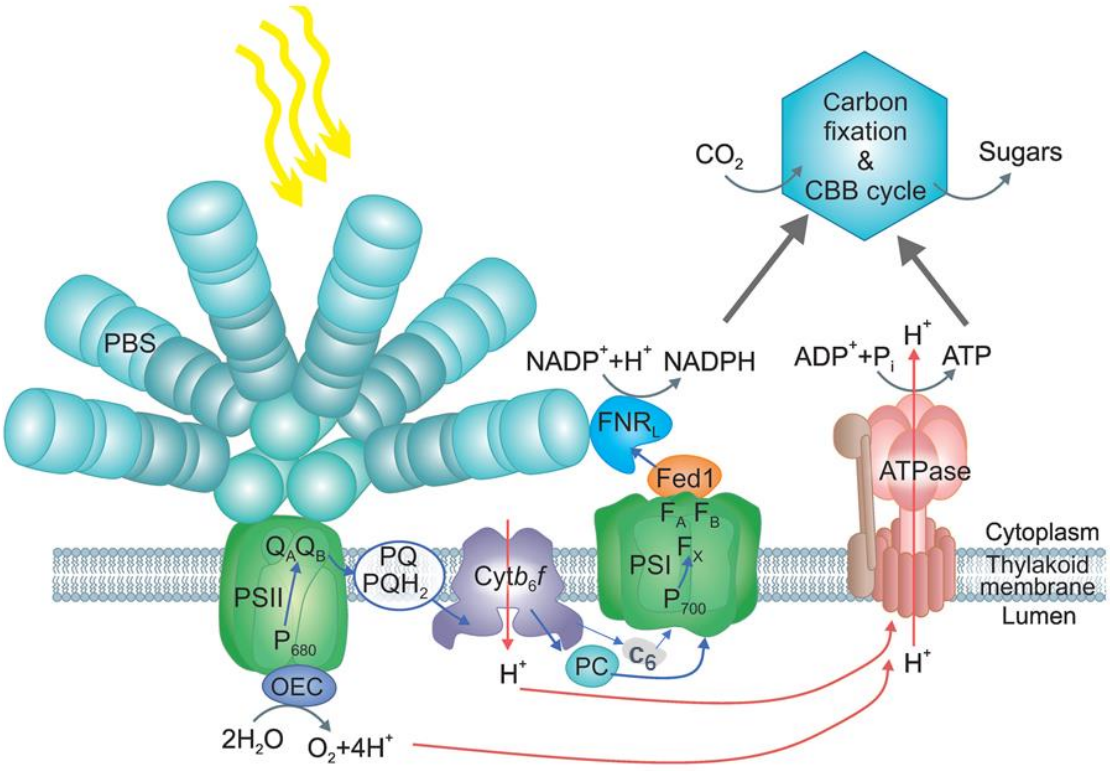

Fig. 1.4.1. A simplified scheme of the photosynthetic linear electron transport chain in the thylakoid membrane of *Synechocystis*. Blue arrows indicate electron transfer, and red arrows indicate proton translocation across the membrane. See the abbreviations from the text. (Modified from Mustila 2017)

The reduced Q_B then delivers electrons to the Cyt *b6f*, which can be interrupted by the widely used photosynthesis inhibitor 3-(3,4-dichlorophenyl)-1,1-dimethylurea, DCMU, via displacing Q_B from its PSII binding site (Kyle et al. 1984). In the Cyt *b6f* complex, 2 electrons are delivered to plastocyanin (Pc) or cytochrome c6 (Cyt c6) and 4 protons into the lumen (Dur n et al. 2004, Hervas et al. 2003). Overall, the Cyt *b6f* complex mediates electron transport between PSII and PSI and converts redox energy into an electrochemical-potential gradient (proton gradient, *ΔpH*; or protonmotive force, *pmf*) for ATP formation

(Stock et al. 1999). Two protons, at the same time, will be translocated across the thylakoid membrane for one electron that is passed from Pc/Cyt c6 to PSI (Hervas et al. 2003, Stock et al. 1999).

PSI catalyzes the oxidation of a soluble electron carrier, Pc or Cyt c_6, on the lumenal side and the reduction of ferredoxin on the cytoplasmic side of the thylakoid membrane by absorbed light energy (Hervas et al. 2003). The reaction center proteins of PSI, PsaA and PsaB, harbor the primary electron donor P700 (a dimer of Chl *a* molecules) and a [4Fe-4S] cluster (Jordan et al. 2001). Two other [4Fe-4S] clusters (F_A and F_B) are bound in the peripheral PsaC subunit (Jordan et al. 2001). The P700 becomes oxidized after being excited by a photon, like in PSII, followed by transferring the electron to the primary electron acceptor of PSI, ferredoxin, and then ferredoxin-$NADP^+$ reductase (FNR), giving rise to conversion of $NADP^+$ to NADPH on the cytoplasmic side (Jordan et al. 2001, Karlusich and Carrillo 2017, Kurisu et al. 2001).

In summary, the splitting of one water molecule directly forms 2 protons and furthermore the photosynthetic LET translocates 4 protons into the lumen, therefore an electrochemical gradient is formed across the thylakoid membrane equivalent to 6 protons. Given that 4.67 (Pogoryelov et al. 2007) or 4 protons (VanWalraven et al. 1996) are required for 1 ATP in *Synechocystis*, 1.28 or 1.5 ATPs can be produced for each NADPH (Lea-Smith et al. 2016). It should be noted that these calculated values only are suitable for standard photoautotrophic conditions without considering alternative electron transfer pathways, such as cyclic electron transfer.

1.4.2 Cyclic electron transport around PSI

In cyclic electron transport (CET) around PSI, electrons are recycled from PSI via ferredoxin and PQ to the Cyt *b6f* complex, which generates a proton gradient, ΔpH. CET around PSI, as well as photosynthetic LET, contribute to form a ΔpH for ATP synthesis. However, in contrast to LET, CET only generate ATP without the production of NADPH because electrons from PSI are recycled from ferredoxin to PQ (Shikanai 2007). Therefore, CET can fine tune the ATP/NADPH ratio as required for the CBB cycle (Kramer and Evans 2011).

Several possible routes of CET have been suggested (Fig. 1.4.2) (Lea-Smith et al. 2016, Shikanai 2014). Firstly, the electron transfer to $P700^+$ through PQ pool from both the respiratory donor and the photoreductant generated in PSI (CET around PSI) via ferredoxin is severely decreased in M55, the NADPH dehydrogenase 1 (NDH-1)-defective mutant of *Synechocystis*, suggesting that NDH-1 participates in both of these bioenergetic pathways in cyanobacteria (Mi et al. 1992). The ferredoxin binding site in the NdhS subunit of NDH-1 complex have been identified in higher plant and cyanobacteria (He et al. 2015, Yamamoto and Shikanai 2013). Furthermore, it was suggested that a putative ferredoxin:plastoquinone reductase (FQR), encoded by *ssr2016* in *Synechocystis*, with substantial sequence similarities to PGR5 of Arabidopsis thaliana, plays a role in CET around PSI (Yeremenko et al. 2005). An indirectly role for succinate dehydrogenase (SDH) in CET around PSI was found and characterized (Cooley et al. 2000). Electrons might be directly transferred to PQ from ferredoxin (Fd in Fig. 1.4.2) via FNR, which may operate as the fourth pathway for CET around PSI in *Synechocystis* (Matthijs et al. 2002, Yeremenko et al. 2005).

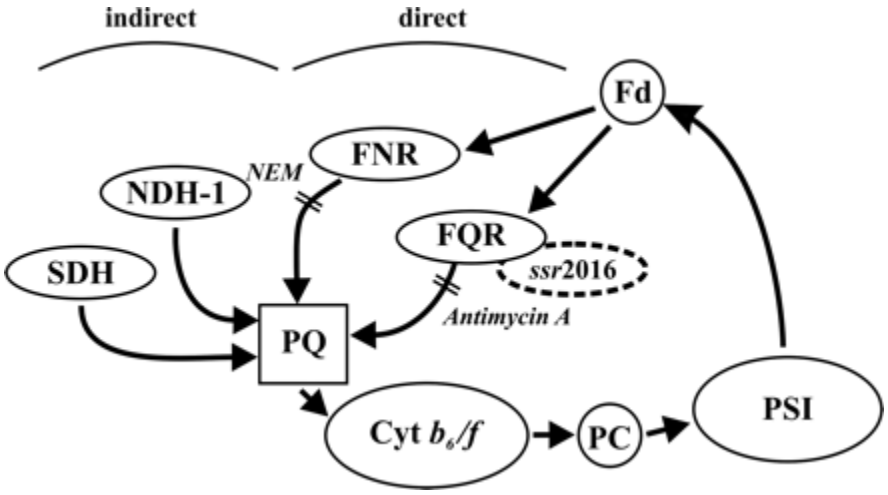

Fig. 1.4.2. A scheme of various routes of CET around PSI in the cyanobacterium *Synechocystis*. At least four parallel operating routes exist. The routes have different electron flux capacities and attributed function. See the abbreviations from the text. (Yeremenko et al. 2005).

In contrast to mitochondrial complex I/NDH enzymes in eukaryotes that play a single role in respiration, the NDH-1 complex in cyanobacteria is involved in a variety of bioenergetic reactions, such as respiration, CET around PSI and CO_2 acquisition (Battchikova and Aro 2007, Battchikova et al. 2011, Shikanai 2014). The NDH-1-dependent pathway of CET is believed to constitute the major pathway in cyanobacteria and to play an important role in coping with various environmental stresses, as high temperature or high light (Battchikova and Aro 2007, Battchikova et al. 2011, Ma and Ogawa 2015, Shikanai 2014, van Thor et al. 2000).

1.4.3 Flavodiiron-proteins and Mehler-like reaction

Flavodiiron proteins (Flvs, also called FDPs) are wildly present in anaerobic prokaryotes and participate in the protection from O_2 and/or NO toxicity (Allahverdiyeva et al. 2015, Gardner et al. 2002, Silaghi-Dumitrescu et al. 2005). All of these Flv proteins contain two conserved redox centers: a flavin mononucleotide (FMN), functioning as an electron acceptor, and a non-heme diiron center as an active site for the reduction of NO or O_2 (Vicente et al. 2008, Vicente et al. 2002). Photoreduction of O_2 to hydrogen peroxide (H_2O_2) by the photosynthetic electrons from PSI complex was discovered and characterized for the first time in spinach chloroplasts by Mehler and is therefore named as the Mehler reaction (Mehler 1951a, b, Mehler and Brown 1952). Later on, it has been proposed that the primary product of the Mehler reaction is a superoxide anion (O_2^-), and H_2O_2 was specified as a disproportionation product resulting from the function of superoxide dismutase (Asada et al. 1974). The Mehler reaction contributes to the generation of a proton gradient across the thylakoid membrane and thus allows the synthesis of ATP, without the accumulation of NADPH, for cellular metabolism (Foyer and Noctor 2000).

Contrary to the Mehler reaction in plants, the cyanobacterial ‘Mehler-like reaction’ driven by Flv proteins (Flv1 and Flv3) does not produce reactive oxygen species (ROS) but instead reduces oxygen to water directly

(Helman et al. 2003). Four genes (*sll1521*, *sll0219*, *sll0550*, and *sll0217*) encoding Flv proteins (Flv1, Flv2, Flv3, and Flv4, respectively) have been found in the genome of *Synechocystis* (Zhang et al. 2009). Cyanobacterial Flv proteins, compared to those in plant and other eukaryotic organisms, possess an additional specific NAD(P)H:flavin oxidoreductase module fused at the C terminus of the protein (Vicente et al. 2008, Vicente et al. 2002). A global transcriptomic analysis of genome-wide DNA microarray data has shown that the transcript levels of *flv3*, *flv2* and *flv4* were remarkable regulated under inorganic carbon (Ci)-limitation, Fe-depletion and different dark/light regimes (Allahverdiyeva et al. 2015). Unlike other *flvs*, the *flv1* transcript level did not respond to high light or Ci-limitation (Allahverdiyeva et al. 2015). Interestingly, a slight up-regulation in *flv1* transcript levels was observed under oxidative stress (methyl viologen and H_2O_2 treatment) (Houot et al. 2007, Kobayashi et al. 2004) and heat stress conditions (Rowland et al. 2010).

Flv2- and Flv4-encoding genes in *Synechocystis*, normally appeared as the *flv2- flv4* pair, are unique for unicellular and filamentous, non-heterocystous β-cyanobacteria (Allahverdiyeva et al. 2015). Flv2 and Flv4 play an essential role in photoprotection of the PSII complex from high light under ambient CO_2 conditions (e.g., air level CO_2) (Allahverdiyeva et al. 2011, Bersanini et al. 2014, Zhang et al. 2009). A Japanese group furthermore reported that the Flv2 and Flv4 proteins are involved in the photoreduction of O_2 to H_2O under CO_2-limiting conditions in *Synechocystis* (Shimakawa et al. 2015).

Both *in vitro* and *in vivo* studies proved that Flv1 and Flv3 proteins functions as a NAD(P)H: oxygen oxidoreductase and play an essential role in the photoreduction of O_2, in the so called Mehler-like reaction, at the PSI stroma side (Helman et al. 2003, Vicente et al. 2002). The extent of Flv1 and Flv3-mediated photosynthetic electron flow to O_2 varies depending on the availability of carbon and light. It was reported that about 20% of electrons originating from PSII are utilized in the photoreduction of O_2 via Flv1 and Flv3 under ambient CO_2 and high light (300–500 μmol photons m^{-2} s^{-1}) conditions (Allahverdiyeva et al. 2011). Furthermore, Flv1 and Flv3 provide a strong electron sink and are crucial for the growth of *Synechocystis* under fluctuating light conditions (50/250 μmol photons m^{-2} s^{-1}), when low background light (50 μmol photons m^{-2} s^{-1}) is regularly interrupted with high light pulse (250 μmol photons m^{-2} s^{-1}) (Allahverdiyeva et al. 2013). In contrast to the Flv2 and Flv4 proteins, which only functions under CO_2-limited conditions, Flv1 and Flv3 continuously operate regardless of the CO_2 availability (Shimakawa et al. 2015, Zhang et al. 2009, Zhang et al. 2012). However, the absence of Flv1 or/and Flv3 has almost no influence under standard autotrophic growth conditions in *Synechocystis*, even under high light condition, as alternative electron transport routes probably compensate for their loss (Allahverdiyeva et al. 2011, Allahverdiyeva et al. 2015, Allahverdiyeva et al. 2013, Zhang et al. 2009).

Moreover, the absence of Flv1 and Flv3 causes a specific lag-phase in oxidation of P700 at the onset of light exposure, after a dark period, when the Calvin-Benson cycle enzymes are still inactivated and therefore the electron sinks for PSI are strong limited and plastoquinone (PQ)-pool is highly reduced (Allahverdiyeva et al. 2013). Subsequently, the reduced PQ-pool recovers to the normal Wild-type level due to the light-activation of the main electron sink, the Calvin-Benson cycle or alternative electron transfer pathways

(Helman et al. 2003, Schuurmans et al. 2014). Therefore, Flv1- and Flv3-free mutants cultivated under diurnal dark/light regime did not show a growth phenotype (Schuurmans et al. 2014). Last but not least, it is important to note that, except for the Mehler-like reaction and dark respiration, photorespiration is also responsible for the consumption of partial O_2 under inorganic carbon-deprivation conditions in *Synechocystis* (Allahverdiyeva et al. 2011).

All the class C Flvs in oxygenic photosynthetic organisms contain an additional flavin reductase-like domain, which should enable reduced NAD(P)H to function as a direct electron donor. However, Flv1 and Flv3 in *Synechocystis* (Hanke et al. 2011) and FlvB (high homology to *Synechocystis* Flv3) in *C. reinhardtii* (Peden et al. 2013) were found to interact with Fed1 (Ferredoxin) and FDX1 (Ferredoxin), respectively. The interaction between Flvs and Fed1 (Fx1 in this work) in *Synechocystis* could either take place directly or through FNR (Hanke et al. 2011). Furthermore, Cassier-Chauvat et al (2014) found by using the bacterial adentlate cyclase two-hybrid (BACTH) system, that Fed9 (Fx9 in this work) specifically interacts with Flv3 (Cassier-Chauvat and Chauvat 2014a). Given that electrons are always transferred from the most to the least electronegative proteins and the predicted redox potentials of both Fed1 and Fed9 are approximately -420mV, it is conceivable that both Fed1 and Fed9 with a lower redox potential are more favorable and feasible than NADPH to function as electron donor to Flv3 (Cassier-Chauvat and Chauvat 2014a).

1.4.4 Respiration

Respiration is essentially regard as a reverse version of the photosynthesis process because of the released energy in the form of ATP and the conversion from glycogen (or other carbon storage molecules) to CO_2 and H_2O. Cyanobacteria accumulate glycogen as a major carbon storage source by photosynthesis-driven CO_2 fixation during the day and then use it as a carbon source through respiration during the night (Saha et al. 2016). The thylakoid membrane is the main site of respiratory electron transport, as well as photosynthetic electron transport, in *Synechocystis* (Fig. 1.4.3A). Several components including PQ, cyt *b6f* and the soluble electron carriers Pc/cyt c6 are shared among both of the two bioenergetic processes (Lea-Smith et al. 2016, Vermaas 2001). Furthermore, the respiratory electron transport chain is situated in the cytoplasmic membranes (Schmetterer 1994, Vermaas 2001).

A series of dehydrogenases (Fig. 1.4.3) catalyzes the oxidation of NADPH, NADH or succinate and directly delivers electrons to the thylakoid membrane electron transport chain via PQ (Lea-Smith et al. 2016). Succinate dehydrogenase (SDH) catalyzes the oxidation of succinate to fumarate, as one step of the TCA cycle (Zhang and Bryant 2011), and was suggested to act as the main respiratory donor to the PQ pool because the absence of SDH lowered the initial respiratory electron flow into the PQ pool by an order of magnitude in *Synechocystis* (Cooley et al. 2000). Type 2 NAD(P)H dehydrogenase (NDH-2) encoded by *ndbB*, as well as SDH, are located both in the thylakoid membrane and in the cytoplasmic membrane and serve as electron donors for the PQ pool without forming a membrane electrochemical gradient (Battchikova et al. 2011, Howitt et al. 1999, Lea-Smith et al. 2016). The type 1 NAD(P)H dehydrogenase (NDH-1) complex, a homolog to mitochondrial Complex I (Ellersiek et al. 1991), can transfer electrons from a reduced electron

donor, NADH or NADPH, to PQ, generating a *pmf* across the thylakoid membrane used for ATP synthesis (Battchikova et al. 2011). Numerous studies have revealed that NDH-1 complexes in cyanobacteria play an important role in CET around PSI, in CO_2 uptake and in respiration (Battchikova and Aro 2007, Battchikova et al. 2011).

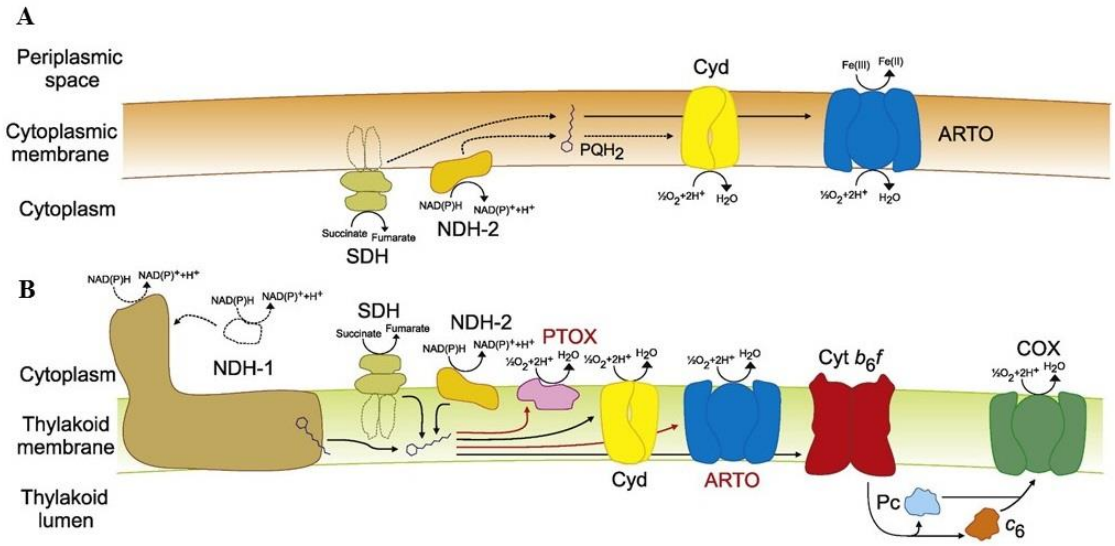

Fig. 1.4.3. Schematic diagram of the cytoplasmic membrane (A) and thylakoid membrane (B) respiratory electron transport chains in cyanobacteria. Broken lines indicate possible electron transport pathways or proteins not yet verified experimentally. Red lines indicate pathways not present in *Synechocystis*. PQ—plastoquinone, PQH2—plastoquinol, cyt b6f—cytochrome b6f, Pc—plastocyanin, Cyt c6—cytochrome c6, NDH-1—NAD(P)H dehydrogenase 1, SDH—succinate dehydrogenase, NDH-2—NAD(P)H dehydrogenase 2, PTOX—plastid terminal oxidase, Cyd—bd-quinol oxidase, ARTO—alternative respiratory terminal oxidase, COX—cytochrome-c oxidase, FQR—ferredoxin-plastoquinone reductase. (Lea-Smith et al. 2016)

Moreover, several terminal oxidases, including cytochrome bd-quinol oxidase (Cyd) (Berry et al. 2002), the alternative respiratory terminal oxidase (Mendel et al. , Nomura et al. 2006) and plastidal terminal oxidase (PTOX) (McDonald et al. 2011), that are present in the thylakoid membranes of cyanobacteria accept electrons directly from the PQ pool (Fig. 1.4.3, reviewed by Lea-Smith, et al, 2016). However, *Synechocystis* does only possess Cyd in the thylakoids membrane and possible ARTO in the cytoplasmic membrane (Berry et al. 2002, Lea-Smith et al. 2016). Under illumination, especially when the electron transfer is inhibited or severely limited at the cytochrome b6f site or PSI, Cyd is the major respiratory terminal oxidases oxidizing PQH2 (Ermakova et al. 2016). Another terminal oxidase, an aa3-type cytochrome-c oxidase complex (COX) in *Synechocystis* thylakoid accepts electrons from soluble electron carriers, Pc/cyt c6, which contributes to the *pmf* formation and increases ATP production at the expense of NADPH (Howitt and Vermaas 1998, Lea-Smith et al. 2016, Schmetterer et al. 1994, Vermaas 2001). The encoding genes of COX are extensively present in all sequenced cyanobacterial genomes so far, which demonstrates that COX might be the major terminal oxidase in cyanobacteria (Lea-Smith et al. 2013). The physiological significance of COX could also

be found under pulsing but not constant light conditions (Lea-Smith et al. 2013), light-activated heterotrophic (or called chemoheterotrophic) conditions (Pils et al. 1997) and for dark respiration (Ermakova et al. 2016, Vermaas et al. 1994).

1.5 Ferredoxin and flavodoxin

1.5.1 Definition, classification and structure

Ferredoxins (Fx) are small (6-13 kDa), soluble iron-sulfur cluster containing proteins with low oxidation reduction potential that transfer electrons to reductive reactions in various metabolic pathways (Bruschi and Guerlesquin 1988, Mortenson et al. 1962). The first ferredoxin was discovered, named and characterized by Mortenson et al. (1962) over 55 years ago in an anaerobic non-photosynthetic bacterium, *Clostridium pasteurianum* (Mortenson et al. 1962). Ferredoxins are among the oldest of iron-sulfur proteins which were one of the earliest biocatalysts on Earth and widely used by anaerobes prior to the appearance of oxygen evolution (Karlusich and Carrillo 2017, Wachtershauser 2007).

According to the location within organisms, ferredoxins are classified as plant-type, adrenodoxin-type ferredoxins, and bacteria-type ferredoxins. Plant-type ferredoxins are further divided into chloroplast-type (or leaf-type) and root-type ferredoxins (Hanke and Mulo 2013). According to the number of iron atom-sulfur cluster in the protein, ferredoxin are classified as two-iron ferredoxins (including plant-like [2Fe-2S], adrenodoxin-type [2Fe-2S], bacterial-type [2Fe-2S]), three-iron ferredoxins (including bacterial-type [3Fe-4S]), four-iron ferredoxins (bacterial-type [4Fe-4S]), seven-iron ferredoxins (bacterial-type [3Fe-4S] [4Fe-4S]), and eight-iron ferredoxins (bacterial-type [4Fe-4S][4Fe-4S]) (Bruschi and Guerlesquin 1988). Furthermore, according to the difference on the basis of amino acid sequences, 2[4Fe–4S] ferredoxins could be classified to two distinct subfamilies: Clostridial ferredoxin (CauFd) and Alvin-like ferredoxin (AlvinFd) (Giastas et al. 2006). In comparison to CauFd, AlvinFd are characterized by a fragment of six amino acids between two cysteine in the second iron-sulfur cluster and an extensive C-terminal α-helix (approximately 20 residues) (Elsen et al. 2010, Giastas et al. 2006).

For electron transport proteins, like ferredoxins, the kinetics of electron transfer between proteins is a sensitive function of their relative redox potentials (Stephens et al. 1996). Therefore, the redox potentials of their iron-sulfur clusters are of central importance to their biological function (Stephens et al. 1996). The redox potentials of [Fe-S] clusters in ferredoxins vary widely (Liu et al. 2014), the most positive being >+400 mV (vs. SHE) while the most negative is <-600 mV (Stephens et al. 1996). In electron transfer processes the redox potentials range of the $[2Fe\text{-}2S]^{1+/2+}$ ferredoxins lie within a very narrow range: -240 to -440 mV; $[4Fe\text{-}4S]^{1+/2}$ in [4Fe-4S]: -300 to -430 mV; $[4Fe\text{-}4S]^{1+/2}$ in [4Fe-4S][4Fe-4S]: -430 mV to -500 mV; $[4Fe\text{-}4S]^{1+/2}$ in [3Fe-4S][4Fe-4S]: -430 mV to -690 mV; $[3Fe\text{-}4S]^{0/1+}$ in [3Fe-4S][4Fe-4S]: -120 mV to -430 mV (Liu et al. 2014). The observed redox potential of several ferredoxins has been determined so far and shown in Table 1.2 (Stephens et al. 1996).

The 3D-structures of total 88 ferredoxins isoforms (42 of [2Fe-2S] containing ferredoxins; 13 of [4Fe-4S] containing ferredoxins, 6 of [3Fe-4S] containing ferredoxins; 4 of [4Fe-4S][3Fe-4S] containing ferredoxins; 5 of [4Fe-4S][4Fe-4S) containing ferredoxins; 9 of adrenoredoxin; 9 other kind of ferredoxins) from various organisms have been determined till now (Updated on 14-May-2017) according to the Proteopedia (http://proteopedia.org/wiki/index.php/Ferredoxin).

Table 1.2. Characterization of ferredoxin containing different iron-sulfur cluster (Stephens et al. 1996).

Iron-sulfur cluster	**Ferredoxins**	**Cysteine cluster**	**Observed redox potential (mV vs. SHE)**
[2Fe-2S]	AnhetFd, AnvegFd, EaFdI, and SpFd	C-X_4-C-X_2-C-X_n-C	-380 to -440 mV
[4Fe-4S]	BtFd, DaFdI	C-X_2-C-X_2-C-X_n-C	-280 mV[a], -385 mV
[3Fe-4S] [4Fe-4S]	AvFdI	C-X_2-C-X_2-C; C-X_2-C-X_2-C-X_n-C	-425 mV[b] or -650 mV[c]
[4Fe-4S] [4Fe-4S]	PaFd, CaFd	C-X_2-C-X_2-C-X_n-C[d]	-430 mV, -420 mV

Notes: a: This redox potential is for *Bacillus stearothermophilus* ferredoxin (BsFd). BsFd is the D64E; E81D mutant of BtFd. b: Oxidized AvFdI at pH 8.0. c: Oxidized AvFdI at pH 6.5. d: Four cysteine motifs comes from clostridial ferredoxin (Elsen et al. 2010), such as PaFd, CaFd. There are two sets of coordinates for D58 and E66; each have 60%:40% occupancy.

1.5.2 Evolution and biological function of ferredoxin

Based on abundance in anaerobic, thermophilic environments and high network centrality (Harel et al. 2014) and a phylogenomic analysis (Dupont et al. 2010), it has been concluded that [4Fe–4S] clusters were the first to be formed and assembled into proteins in the O_2-free primordial oceans and they are more flexible and chemically versatile than their [2Fe–2S] counterparts (Karlusich and Carrillo 2017). The profile-vs.-profile and position-specific iterative-BLAST alignments indicated that ferredoxins with [4Fe–4S] clusters were the ancestral representatives of the family, from which [2Fe–2S] ferredoxins followed by duplication and divergence (Harel et al. 2014, Karlusich and Carrillo 2017).

The two-iron (or [2Fe-2S]) ferredoxins are not only found in eukaryotic photosynthetic organisms (like plant, algae) but also in various bacteria (Bruschi and Guerlesquin 1988). It was suggested that plant- and bacterial-type ferredoxin share a common ancestral form (Matsubar.H et al. 1969, Schwartz and Dayhoff 1978). According to a phylogenetic tree of all the bacterial- and chloroplast-type ferredoxins, [2Fe-2S] ferredoxins from the chloroplast type and the halo-bacterial type have been generated by gene triplication of the ancestor followed by structural change of the cluster (Matsubara et al. 1979). Bacterial-type [2Fe-2S] ferredoxins possess a similar active site as that of chloroplast-type ferredoxins, however, they do not function in the

photoreduction of $NADP^+$ (Bruschi and Guerlesquin 1988). The overall structure of two-iron ferredoxins in cyanobacteria, algae and higher plant retain a conserved amino acid motif ($Cx_4Cx_2Cx_nC$) for forming a proper [2Fe-2S] cluster that facilitates the insertion to the apoprotein and electron transfer to/from the mature enzyme (Bertini et al. 2002, Kameda et al. 2011).

The eight-iron ferredoxins containing two [4Fe-4S] clusters are, so far, found only in bacteria, mainly in anaerobic fermenters (e.g. *Clostridia*, *Peptococci*, sulfate-reducing bacteria), but also in photosynthetic bacteria (e.g. *Synechocystis*, *Chlorobium*, *Chromatium*) (Bruschi and Guerlesquin 1988). These kinds of ferredoxins have amino acid sequences in which two sets of four cysteine residues are in each of two halves of the peptide chain (Tanaka et al. 1966). Because of the close relationship in sequence between the two halves, the ancestral form of ferredoxin must have been internally duplicated to produce an active electron carrier similar to the present eight-iron ferredoxin (Orme-Johnson 1973, Tanaka et al. 1966). The eight-iron ferredoxins have a midpoint potential of about -400 mV and play an important role in the metabolism of anaerobic bacteria and are able to accept two electrons from pyruvate oxidation or H_2 oxidation in bacteria (Bruschi and Guerlesquin 1988).

Both four-iron ferredoxins and eight-iron ferredoxins shared conserved cysteines motif ($Cx_2Cx_2Cx_nC$) (Bruschi and Guerlesquin 1988). Moreover, the four-iron ferredoxins contain only one [4Fe-4S] cluster and are very similar to the eight-iron ferredoxins in redox properties and the disappearance of the second iron-sulfur cluster and are thought to be correlated to the presence of only four or six cysteines in the protein (Bruschi and Guerlesquin 1988). However, the four-iron ferredoxins that contain a single cluster seem to be functioning as single-electron carriers.

Ferredoxins, functioning as electron carrier, are an important central hub for the electrons from photosystem I (Dutta and Vermaas) to various processes depending on reducing power (Goss and Hanke 2014). In plants, algae and cyanobacteria the primary photosynthetic ferredoxin is a plant-type ferredoxin harboring a [2Fe-2S] cluster, and in cyanobacteria it is designated as Fx1 (Cassier-Chauvat and Chauvat 2014a, Hanke and Mulo 2013). Ferredoxins function as electron carriers with a low reduction potential that participate in a variety of essential metabolic reactions including, but not limited to: $NADP^+$ reduction by Fd-$NADP^+$ reductase (FNR), nitrogen assimilation by Fd-dependent nitrate/nitrite reductase and glutamate synthase (Nar/Nir and GlsF), hydrogen evolution by hydrogenase, sulfite reduction by an Fd-dependent sulfite reductase, cyclic electron transport for generation of proton gradient necessary for ATP evolution, thioredoxin reduction by ferredoxin: thioredoxin reductase (FTR), fatty acids desaturation by Acy-ACP desaturase (Fig. 1.5.2) (Batie and Kamin 1986, Buchanan et al. 2002, Garcia-Sanchez et al. 1997, Gutekunst et al. 2014, Hanke and Mulo 2013, Luque et al. 1994a, Staples et al. 1996, Tagawa et al. 1963, Yang et al. 2015).

Ferredoxins function not only as the central hub connecting the photosystem I to cellular metabolism in the light (Mondal and Bruce 2018), but also as electron carriers for a variety of electron transfer reactions in the dark, etc. cytochrome c550 reduction (Arnon and Chain 1979), regulation of glucose-6-phosphate

dehydrogenase (G6PDH) via FTR (Buchanan 1991), fermentative hydrogen production by hydrogenase (Gutekunst et al. 2014) and nitrogen reduction by nitrite reductase (Paneque et al. 1964), when photosynthesis becomes inactive.

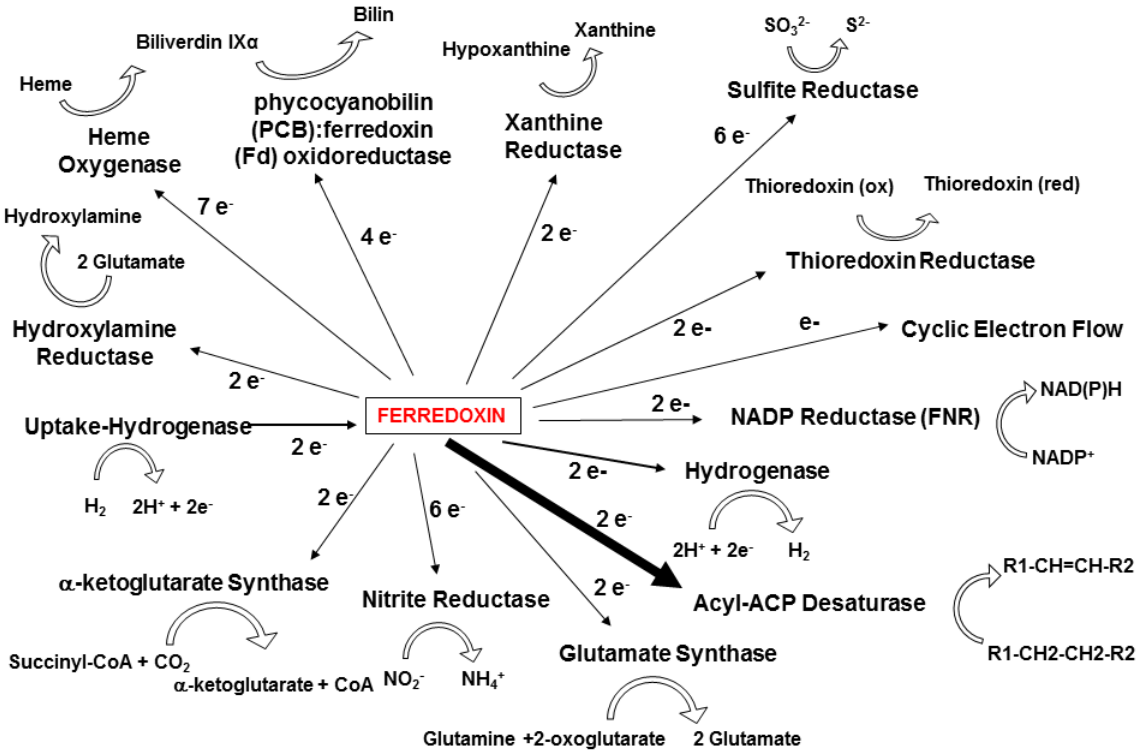

Fig. 1.5.2. Ferredoxin-mediated electron transfer reactions in green algal *Chlamydomonas reinhardtii* (Yang et al. 2015). Ferredoxins participate in a variety of electron transfer reactions, including those depicted; these reactions require donation of between 1 (CEF) and 7 (heme oxygenase) electrons. However, the ferredoxin-dependent α-ketoglutarate synthesis from succinate and carbon dioxide catalyzed by α-ketoglutarate synthase is not present in cyanobacteria *Synechocystis*.

1.5.3 Classification, function and regulation of ferredoxins in *Synechocystis*

To date, 9 Fx isoforms are known in the *Synechocystis* genome and therewith are designated as follows: *fx1* (ssl0020), *fx2* (sll1382), *fx3* (slr1828), *fx4* (slr0150), *fx5* (slr0148), *fx6* (ssl2559), *fx7* (sll0662), *fx8* (ssr3184) and *fx9* (slr2059) (Cassier-Chauvat and Chauvat 2014a). The iron-sulfur centers ([2Fe-2S], [3Fe-4S] [4Fe-4S]) in *Synechocystis* Fx are classified as plant-like [2Fe-2S], bacterial-type [2Fe-2S], bacterial-type [3Fe-4S], and bacterial-type [4Fe-4S] according to their nature and the organisms in which they were isolated for the first time (Bruschi and Guerlesquin 1988, Cassier-Chauvat and Chauvat 2014a). The *Fx1-4* belong to the plant-like [2Fe-2S] ferredoxins (two-iron ferredoxins); *Fx5-6* to bacterial-type [2Fe-2S] ferredoxins (two-iron ferredoxins); *Fx7* is a bacterial-type [4Fe-4S] ferredoxin (four-iron ferredoxin); *Fx8* is a bacterial-type [3Fe-4S][4Fe-4S] ferredoxin (seven-iron ferredoxin); and *Fx9* is a bacterial-type [4Fe-4S][4Fe-4S]

ferredoxin (eight-iron ferredoxins) (Bruschi and Guerlesquin 1988, Cassier-Chauvat and Chauvat 2014a). All nine Fx-encoding genes are highly conserved in cyanobacteria, in agreement with the pivotal role of ferredoxins in electron transfers (Cassier-Chauvat and Chauvat 2014a).

To date, the function and regulation of only a few of the nine *Synechocystis* ferredoxins have been studied in any detail.

The plant-type Fx1 (or PetF) is the most abundant protein in *Synechocystis* (Bottin and Lagoutte 1992a), which is in agreement with the highly expressed transcripts of *fx1* under standard photoautotrophic conditions (Poncelet et al. 1998). These results, combined with the failures to completely delete this ferredoxin from the genome of *Synechocystis*, shows that Fx1 is essential for photoautotrophic growth of *Synechocystis* (Cassier-Chauvat and Chauvat 2014a). The abundant transcription of the *fx1* gene is rapidly induced by active photosynthesis in the light and become scarce after a 15-min shift to darkness (Mazouni et al. 2003). So, the downregulated Fx1 in darkness could probably give other less-abundant ferredoxins (Fx2-9) the opportunity to play a role in *Synechocystis*. Moreover, the transcription of the *fx1* gene is downregulated by treatment with specific inhibitors (DCMU, MV, DBMIB) (Singh et al. 2010), hydrogen peroxide (H_2O_2) and heavy metals such as cadmium (Cd) and selenite (Se), which all are toxic and may lead to oxidative stress (Mazouni et al. 2003). Under iron depletion conditions the Fx1 becomes ineffective but is replaced by a flavodoxin (IsiB or Fld), a non-iron containing electron-transfer protein (Bottin and Lagoutte 1992b). The abundance of *Synechocystis fx1* transcripts is regulated by different light intensities instead of glucose availability (Poncelet et al. 1998). The structure of Fx1 in *Synechocystis*, was determined over 20 years (Lelong et al. 1995).

In contrast to the high abundant Fx1, the other low abundant ferredoxin genes (Fx2-9) of *Synechocystis* have received little attention so far (Cassier-Chauvat and Chauvat 2014a).

There are three additional plant-type ferredoxins with a [2Fe-2S] cluster in *Synechocystis*, Fx2, Fx3 and Fx4. Fx2 and Fx3 were declared as essential for photoautotrophic growth of *Synechocystis* due to the failure to make completely segregated mutants (Cassier-Chauvat and Chauvat 2014a). Furthermore, there are two additional [2Fe-2S] center proteins, Fx5 with adrenodoxin-like and Fx6 with bacterial type, the second of which is proposed to be necessary to the photoautotrophic growth of *Synechocystis* (Cassier-Chauvat and Chauvat 2014a). The genes for Fx4 and Fx5, *fx4* (*slr0150*) and *fx5* (*slr0148*), belong to one well-conserved gene cluster, the *slr0144-slr0152* cluster, and are encoded within the same operon, which has been named and described as the photosystem II assembly proteins (PAP) operon (Cassier-Chauvat and Chauvat 2014a, Wegener et al. 2008). The absence of the PAP operon reduces PSII-mediated oxygen evolution and alters the distribution of the S-states of the catalytic manganese cluster in *Synechocystis* (Wegener et al. 2008). In addition, the phosphorylation of Fx5 is driven by SpkG (Slr0152, also named PknD), which encodes a Ser/Thr kinase, and could be regulated by the Slr0151 protein encoded by the gene preceding *spkG* in the gene cluster (Angeleri et al. 2018). However, the exact function of Fx5 and especially its phosphorylation still only poorly understood.

The last three bacterial-type ferredoxins contain variable iron-sulfur clusters. Fx7 and Fx9 appeared to be essential to photoautotrophic growth of *Synechocystis* whereas Fx8 was declared as being dispensable (Cassier-Chauvat and Chauvat 2014a). It was also proposed that Fx7 and Fx9, as well as Fx1, play important roles in the tolerance to oxidative and metal stresses by running a possible Ferredoxin-Glutaredoxin-Thioredoxin (Fx1/Fx9-FTRc-TrxA/Fx7) crosstalk pathway, where electrons from PSI are transferred via ferredoxin to the ferredoxin-thioredoxin reductase catalytic chain (FTRc) (Cassier-Chauvat and Chauvat 2014a, b, Marteyn et al. 2009). Interestingly, by using the bacterial adentlate cyclase two-hybrid (BACTH) system, they also found that Fx9 specifically interacts with a flavodiiron protein (Flv3) (Cassier-Chauvat and Chauvat 2014a), which functions in the Mehler-like reaction (the NADPH-driven photoreduction of O_2 to H_2O) (Helman et al. 2003). Mustila *et al* (2014) suggested that the absence of Fx7 would increase Chl a and PSI levels but reduce the abundance and activity of PSII. Fx7 is considered to play an important role in tolerance to photooxidative stress (low CO_2 and high light) conditions, which significantly induce the transcription of *fx7* (Mustila et al. 2014).

Table 1.3. Regulation of the *Synechocystis* ferredoxin genes in response to environmental challenges (Updated and modified summary from Cassier-Chauvat C. & Chauvat F. 2014).

Name	**Conditions Triggering Upregulation of the *fx* Genes**	**Conditions Triggering Downregulation of the *fx* Genes**
fx1	Light [a,b]; $NaHCO_3$ [b];	Darkness [a]; Cd, LFe, H_2O_2 [b,c]; Se [b]; HZn [c]; DCMU, DBMIB, LiC, HT°, SS [d]; LiC [i]; BR [j]
fx2	Cd, H_2O_2, HZn [c]; HL, UV [d]	Glu [a]; Na_2SeO_4 [b]; LiC [d]
fx3	BR [d, j]	Cd [c]; H_2O_2 [c,d]; SS, LiC [d,i]; NS [k]
fx4	LL [a]; H_2O_2 [c]	Cd, LFe, HZn [c]; HL, LiC, SS [d]; NS [k]
fx5	LL [a]; H_2O_2 [c]; BR [d, j]	Cd, LFe, HZn [c]; HL, LiC, SS [d]; NS [k]
fx6	BR [d, j]; NS [k]	-
fx7	LFe [c]; HL [d, e, h]; LiC [e,h,i]; H_2O_2 [b, f]; Se [f]	Cd, HFe [c]; BR [j]
fx8	H_2O_2, Cd [b]; HL, LiC [d];	LFe [d]
fx9	HL, HT° [d]; H_2O_2, Se, Cd [f]	EtOH [g]

Note: BR, red light (PSII light) vs. blue light (PSI light) (one out of the six time points); Cd, cadmium; DCMU, (3-(3,4-dichlorophenyl)-1,1-dimethylurea); DBMIB, 2,5-dibromo-3-methyl-6-isopropyl-*p*-benzoquinone; Glu, glucose; H_2O_2, hydrogen peroxide; LiC, inorganic carbon limitation; HFe, high iron; LFe, iron starvation; nitrogen starvation: NS; HL, high light; LL, low light; SS, salt stress; HT°, high temperature; HZn, high zinc. [a]: (Poncelet et al. 1998); [b]: (Mazouni et al. 2003); [c]: (Houot et al. 2007); [d]: (Singh et al. 2010); [e]: (Mustila et al. 2014); [f] (Cassier-Chauvat and Chauvat 2014a) [g]: (Song et al. 2014); [h]: (Mustila et al. 2014); [i]: (Eisenhut et al. 2007); [j] (Singh et al. 2009); [k] (Carrieri et al. 2017).

A bulk of data from DNA microarrays, transcriptome, and/or northern blot analysis together indicate that the expressions of the ferredoxin genes are differently regulated by a variety of environmental stress (Cassier-Chauvat and Chauvat 2014a), etc. light (blue light, red light, HL and darkness), oxidative stresses (HL, H_2O_2), metal stresses (Fe, Cd, Se, Zn), electron-transfer inhibitors (DCMU, DBMIB, MV), and the availability of nutrition source (inorganic carbon/nitrogen/sulfur) (Table 1.3). However, the results from different microarray experiments might be erroneous or unreliable or even contradictory sometimes because of the personal operation and the detecting sensitivity level of microarray. For example, several groups have verified that the transcription of *fx1*, the encoding gene of the well-known main photosynthetic ferredoxin Fx1, is induced by light and enhanced with increasing light (Hihara et al. 2001, Mazouni et al. 2003, Poncelet et al. 1998), however, Singh. et al 's microarray raw data showed that *fx1* is downregulated by high light at six different time point (Singh et al. 2008).

1.6 Carbon metabolism

1.6.1 PFOR and PDH complex

Pyruvate plays a central role both under aerobic and anaerobic conditions (Noth et al. 2013, van Lis et al. 2013). In mitochondria and most aerobic bacteria, oxidative decarboxylation of pyruvate to form acetyl-coenzyme A, a crucial step in energy metabolism, is carried out by the multienzyme pyruvate dehydrogenase complex (PDHc) with the reduction of NADH (Chabriere et al. 1999, Patel et al. 2014, Patel and Roche 1990). In archaea, most anaerobes and amitochondriate eukaryotes, the same reaction is catalyzed reversibly by a single enzyme, the pyruvate:ferredoxin oxidoreductase (PFOR, encoded by *nifJ* or *pfor*) with the simultaneous reduction of ferredoxin or flavodoxin (Chabriere et al. 1999, Ludwig and Bryant 2011). Ferredoxin and flavodoxin have a much lower redox potential than the $NADH/NAD^+$ couple (Tittmann 2009). Reduced ferredoxin can be used directly to reduce nitrate, sulfite, and other substrates or can be used to produce NADPH via ferredoxin:$NADP^+$ oxidoreductase (FNR). The availability of reducing equivalents with low redox potentials provides an energetic benefit for cells when respiration is not possible.

Transcripts for the PDHc encoding genes, *pdhA* and *pdhB*, are 10-fold lower, while PFOR encoding gene *pfor* increase 130-fold in the cyanobacterium *Synechococus* under dark anoxic conditions (Ludwig and Bryant 2011, Xu 2010). Similar results were observed in algal cells (Mus et al. 2007). These results indicate that the oxidative decarboxylation of pyruvate for the conversion of phosphoenolpyruvate to acetyl-CoA via PDHc might be replaced by PFOR under fermentative conditions (Fig. 1.6.1.1) (Ludwig and Bryant 2011).

1.6.1.1 Pyruvate:ferredoxin oxidoreductase PFOR

The pyruvate:ferredoxin oxidoreductase (PFOR) catalyzes the oxidative decarboxylation of pyruvate and reduces either ferredoxin or flavodoxin during fermentative conditions. 40% of all fully sequenced cyanobacteria possess the PFOR-encoding gene *pfor* in their genome (Nakao et al. 2010). Even though this enzyme is known to be sensitive to O_2 (McNeely et al. 2011, Plaga et al. 1992, Schmitz et al. 2001), is has been reported to be expressed under oxic conditions in the cyanobacteria *Synechococcus* sp. PCC7002,

Synechococcus 6301, and *Synechocystis* and an oxygen resistant enzyme is furthermore known in *Desulfovibrio africanus* (Burgstaller 2017, Chabriere et al. 1999, Chen 2014, Schmitz et al. 2001).

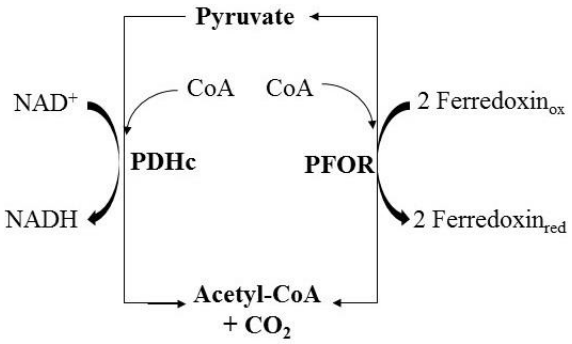

Fig. 1.6.1.1. Scheme of the pyruvate metabolism reactions catalyzed by PFOR or PDHc in *Synechococus* sp. strain PCC 7002, which is also valid for *Synechocystis*. (Modified from McNeely, *et al.*, 2011).

The PFOR from *Desulfovibrio africanus* is a homodimer, of which each subunit contains one TPP, two ferredoxin-type [4Fe-4S] clusters and one [4Fe-4S] cluster (Fig. 1.6.1.2) (Chabriere et al. 1999). These clusters exhibit three different midpoint potentials of -390, -515 and -540 mV, although these potential values have not yet been assigned to the individual clusters (Pieulle et al. 1997). The amino acid sequence of *Desulfovibrio africanus* PFOR is very similar to those of other homodimeric PFORs except for an extension of 63-residue-long C-terminal (Fig. 1.6.1.2C), which contains two cysteine residues (Cys1195 and Cys1212) possibly used for forming a disulfide bridge (Pieulle et al. 1997). Compared to the other homodimeric PFORs, the *Desulfovibrio africanus* PFOR is unusually stable to oxygen (Chabriere et al. 1999). It was supposed that the unique C-terminal end of one of the monomers covers the proximal [4Fe-4S] cluster by forming a disulfide bridge between Cys1195 and Cys1212, and thereby protects the cluster from degradation via oxygen (Fig. 1.6.1.2) (Chabriere et al. 1999, Pieulle et al. 1995, Pieulle et al. 1997).

By operating multiple alignment of the amino acid sequences via ClustalX, it was shown that the unique Domain VII in the C-terminal of *Desulfovibrio africanus* PFOR amino acid sequence contains two cysteine residues that are not present in *Synechococcus* and *Synechocystis* PFOR, which indicates that cyanobacterial PFOR should be oxygen-sensitive. This is well in line with the enhanced transcripts of PFOR encoding gene under dark anoxic conditions described above and the impaired autotrophic growth of a *pdhA*-deletion mutant of *Synechococcus* sp. PCC 7002 (Xu 2010). Previous work in our group showed that the absence of PFOR in *Synechocsytis* causes an impaired growth at the nonexponential phase under mixotrophic conditions (Chen 2014). Moreover, the replacement of nitrate, one important electron sink for ferredoxin or flavodoxin, with arginine as nitrogen source did further inhibit the mixotrophic growth of this mutant (Chen 2014). This came as a surprise as the oxygen-sensitive PFOR of *Synechocystis* seems to be of physiological importance under oxic conditions.

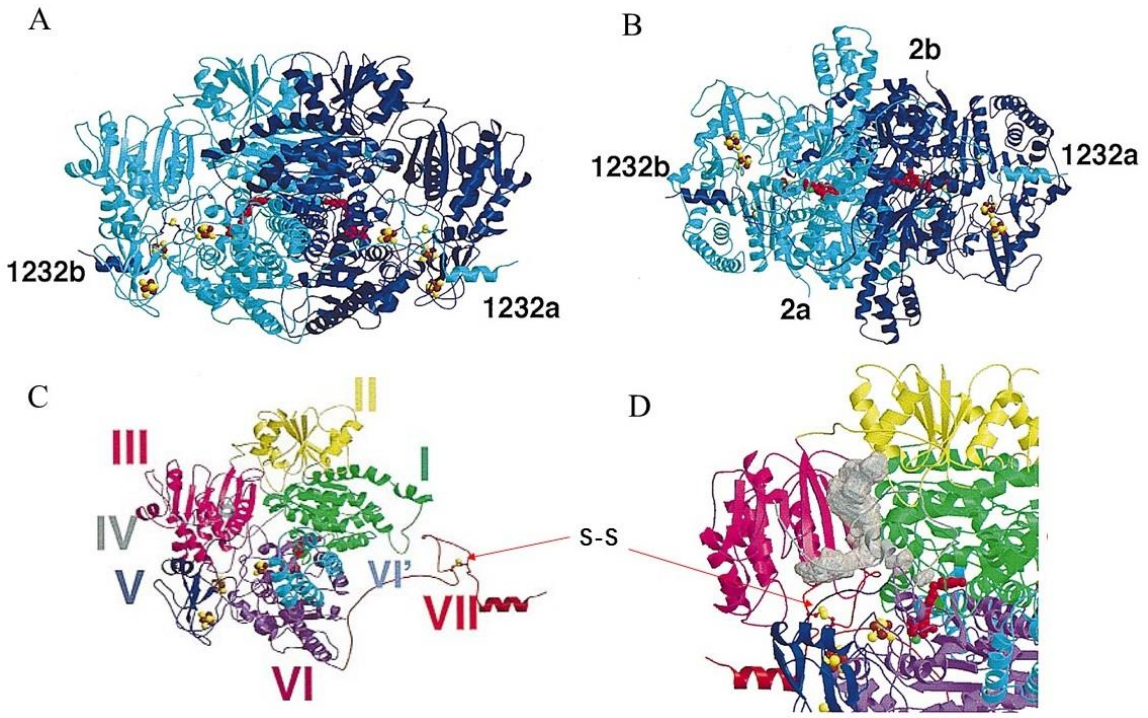

Fig. 1.6.1.2. Ribbon drawings of the homodimeric *Desulfovibrio africanus* PFOR. **A-B**: Two perpendicular views were show. Two subunits are shown in light blue and dark blue, respectively. **C**: Stereoview, shown in the same orientation as A, of one subunit containing 1232 residues, depicting the structural domains I–VII in different colors. **D**: Stereo picture of cavities and channels in PFOR. The view and the domain colors are the same as in C. The cavities, shown in light gray, were calculated from the refined model, without ordered solvent molecules, using an accessible probe radius of 1.4 Å. Red arrows means the disulfide bridge between Cys 1195 and Cys 1212 and also shows that the C-terminal end of one of the monomers covers the proximal [4Fe-4S] cluster of the other. TPP cofactors are highlighted in bright red, Mg ions in green, iron atoms in brown and sulfur atoms in yellow (modified after Chabriere et al. 1999).

1.6.1.2 PDH complex

The pyruvate dehydrogenase complex (PDHc) is present in most prokaryotic and eukaryotic organisms (Patel and Korotchkina 2003). It links the glycolytic pathways with the TCA cycle. PDHc plays a vital role in cellular metabolism of microorganisms and catalyzes the oxidative decarboxylation of pyruvate and the subsequent acetylation of coenzyme A (Bruland et al.) to acetyl-CoA (Balakrishnan et al. 2012, de Kok et al. 1998, Patel and Korotchkina 2003, Robinson et al. 1996). PDHc contains three enzymatic components, including the pyruvate dehydrogenase (E1), dihydrolipoamide acetyltransferase (E2), and dihydrolipoamide dehydrogenase (E3), and a number of cofactors (Alvarez et al. 1991, de Kok et al. 1998, Patel and Korotchkina 2003, Stephens et al. 1983). The first step catalyzed by E1 of the PDHc is the rate-limiting step (Nemeria et al. 2004, Zhou et al. 2017).

In mammals, pyruvate dehydrogenase E1 alpha chain, PdhA, has 3 phosphorylation sites (Ser264, site 1; Ser271, site 2; and Ser203, site 3), which are phosphorylated at high NADH concentration and thereby

inactivated (Patel and Korotchkina 2001, 2003, Patel et al. 2014). Phosphorylation of site 1 completely abolishes the activity of the PDH complex whereas phosphorylation of sites 2 and 3 results in moderate catalytic activities in human PDH complexes (Korotchkina and Patel 2001, Patel and Korotchkina 2001). It was shown that phosphorylation of site 1 blocks the access to the active site and thereby impedes binding of pyruvate (Schriek et al. 2007). As shown in Fig. 1.6.1.3, mammalian, plant, and nematode PDH (named PDC in the figure) are regulated by reversible phosphorylation/dephosphorylation, which is catalyzed by two additional regulatory enzymes, pyruvate dehydrogenase kinase (PDK), and phosphopyruvate dehydrogenase phosphatase (PDP) (Patel and Korotchkina 2003). The products of the PDH reaction, NADH and acetyl-CoA, increase PDK activity whereas it inhibits the activity of PDP (Patel and Korotchkina 2001, 2003). In contrast, the substrates of this reaction, pyruvate, NAD^+, and CoA inhibit the PDK activity (Patel and Korotchkina 2001, 2003). Therefore, the presence of active (dephosphorylated) PDH is determined by the NADH/NAD^+ and acetyl-CoA/CoA ratios (Korotchkina and Patel 2000, Patel and Korotchkina 2001, 2003, Patel and Roche 1990). Furthermore, activities of PDKs are affected by the ATP/ADP ratio as ADP and phosphate anion inhibit of PDK activity (Patel and Korotchkina 2003). The PDP activities are enhanced by plenty of divalent metal ions (Mg^{2+} and Ca^{2+}), insulin, and polyamines (Patel and Korotchkina 2003, Patel and Roche 1990).

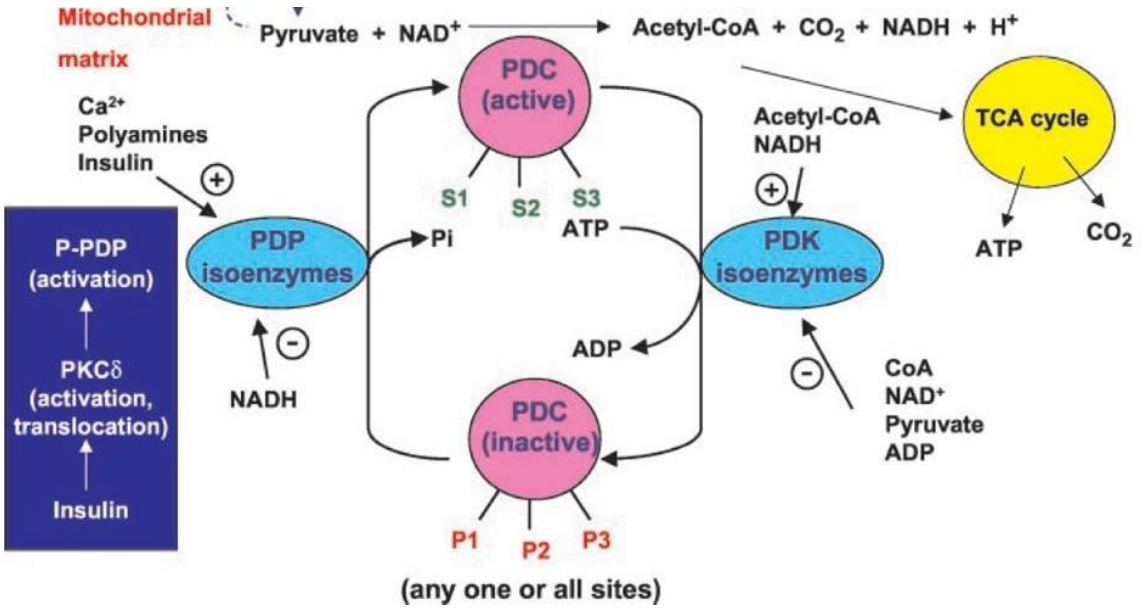

Fig. 1.6.1.3 Regulation of PDC (or PDHc in our work) activity by phosphorylation/dephosphorylation catalyzed by PDKs and PDPs. Three serine residues of E1 phosphorylation sites are shown as S1, S2, and S3 in dephosphorylated condition and as P1, P2, and P3 when phosphorylated. (Patel and Korotchkina 2003)

There are two kinds of PDHc, mitochondrial PDHc (mPDHc) and plastid PDHc (pPDHc), in plants (Patel and Korotchkina 2003, Tovar-Mendez et al. 2003). However, only the mitochondrial one is reported to be regulated by phosphorylation (Patel and Korotchkina 2003, Patel et al. 2012, Tovar-Mendez et al. 2003). Furthermore, light is an important factor for the activity of PDHc in plants (Patel et al. 2012, Tovar-Mendez

et al. 2003). Photosynthesis and photorespiration decrease mPDHc activity due to phosphorylation activated by the elevated concentration of ATP (Patel et al. 2012, Tovar-Mendez et al. 2003). The pPDHc activity, on the contrary, is enhanced due to the increased pH and Mg^{2+}concentration during photosynthesis (Patel et al. 2012, Tovar-Mendez et al. 2003).

The crystal structure of PDHc-E1 from cyanobacteria has not been reported (Zhou et al. 2017), and the information about the regulation of the cyanobacterial PDHc is very limited.

It has been suggested that the PDHc of *Synechococcus* sp. PCC 7002 funciton under anoxic conditions, at least in the abence of PFOR, accourding to the nonzero level of excreted acetate in *pfor*-deletion mutant under fermentative conditions (McNeely et al. 2011). PDHc, beside PFOR, is also reported to contribute to fermentative metabolism in bacteria *Enterococcus* (*Streptococcus*) as well (Deibel and Niven 1964). Furthermore, glycerol decreases the fermentative produciton of acetate from pyruvate at two possible points: acetate-CoA synthase (Acs) and PDHc (McNeely et al. 2011), which have been shown to be inhibited by glycerol in chloroplasts (Lawrence et al. 2004) and yeast (Roughan and Ohlrogge 1994), respectively. Specific inhibition of PDHc by glycerol eliminates acetate production, decreases the produciton of reductant and H_2 of *pfor*-deletion cells compared to *Synechococcus* sp. PCC 7002 Wild-type cells (McNeely et al. 2011). These results indicate that PFOR is not the sole source of reductant for hydrogen production by the bidirectional [Ni-Fe]-hydrogenase under fermentative conditions (McNeely et al. 2011).

PDHc in gram-negative bacteria is inhibited by an elevated NADH:NAD^+ ratio (de Kok et al. 1998). In cyanobacteria, the redox poise might be elevated when growth conditions are shifted from autotrophic to mixotrophic, according to the redox state of cells supplemented with exogenous glucose during fermentation (Kujat and Owttrim 2000, McNeely et al. 2011).

It was reported that there are four PDH kinases (PDK1, PDK2, PDK3, and PDK4) and two PDH phosphatase (PDP1 and PDP2) in humans (*Homo sapiens*). The yeast *Saccharomyces cerevisiae* (strain ATCC 204508 / S288c) also has two PDH kinases (PDK1, PDK2) and two PDH phosphatase (PDP1 and PDP2). Analogously, cyanobacteria may use eukaryotic-like components for signal transduction as well because serine/threonine kinases (STKs) and serine/threonine phosphatases (STPs) have been found in an increasing number of prokaryotes (Zhang et al. 2005, Zhang et al. 2007). Cyanobacterium *Synechocystis* possesses seven STKs and seven STPs (Table 1.6.1) (Zhang et al. 1998, Zhang et al. 2005, Zhang et al. 2007). A variety of reports through genetic, molecular and functional genomic analyses have demonstrated that STKs and STTs play an important role in the regulation of various activities and cell metabolisms, such as cell motility, carbon and nitrogen metabolism, photosynthesis and stress response (Zhang et al. 2005, Zorina et al. 2011). Therefore, the STKs and STPs found in *Synechocystis* are candidates that could overtake the phosphorylation and dephosphorylation of the PDH complex.

Table 1.6.1. Eukaryotic-type signal transducers in *Synechocystis* (Zhang et al. 1998)

ORF	Similarity to
sll0776	protein STK
sll1574–75	protein STK
slr0152	protein STK
slr0599	protein STK
slr1225	protein STK
slr1443	protein STK
slr1697	protein STK
sll1365	protein STP (PPM family)
sll1387	protein STP (PPM family)
slr0114	protein STP (PPM family)
slr0328	protein STP (PTP family)
slr1860	protein STP (PPM family)
slr1983	protein STP (PPM family)
slr2031	protein STP (PPM family)
slr1234	protein kinase C interacting protein
slr0593	protein kinase A regulatory chain

1.6.2 The TCA cycle in *Synechocystis* sp. PCC 6803

Pyruvate is the product of lower glycolysis. Decarboxylation of pyruvate results in acetyl-CoA, which can be further fed into the tricarboxylic acid cycle (TCA cycle, also known as the citric acid cycle or Krebs cycle) which contribute to the generation of ATP, reduction equivalents and precursor metabolites, such as 2-oxoglutarate (2OG), for biosynthesis (Knoop et al. 2013, Krebs 1970, Xiong et al. 2014). Until several years ago, it was assumed that cyanobacteria possess an incomplete TCA cycle due to the lack of 2-oxoglutarate dehydrogenase, which converts 2-oxoglutarate to succinyl–CoA (Schmitz et al. 2001, Schwarz et al. 2011, Zhang and Bryant 2011). However, cyanobacteria possess an alternative pathways to close the incomplete TCA cycle (Knoop et al. 2013). Zhang and Bryant (2011) found that many cyanobacteria, including *Synechocystis*, possess 2-oxoglutarate decarboxylase and succinic semialdehyde dehydrogenase, which convert 2-oxoglutarate to succinate and thus functionally replace the missing 2-oxoglutarate dehydrogenase and succinyl-CoA synthetase (Zhang and Bryant 2011). These Enzymes are present in all cyanobacterial genomes except those of *Prochlorococcus* and marine *Synechococcus* and also exist in many bacteria, including some anaerobes (e.g., *Methanosarcina* and *Clostridium*) (Zhang and Bryant 2011). The presence of a possible glyoxylate shunt (Shastri and Morgan 2005) or a GABA shunt (Knoop et al. 2010, Xiong et al. 2014) is also characterized in details recently. The latter one constitutes a bypass from 2-oxoglutarate, via glutamate, γ-aminobutyrate (Saux et al.) and succinate semialdehyde, to succinate and each is catalyzed by different enzymes (Knoop et al. 2010, Xiong et al. 2014).

The flux of a complete TCA cycle in cyanobacteria is affected by light availability (Knoop et al. 2010, Xiong et al. 2014). Interestingly, it was found that for the TCA cycle of *Synechocystis* in the light, there is a flux to glutamate (tetrapyrrole biosynthesis) and succinate in the right branch, but no significant flux to fumarate in

the left branch (Knoop et al. 2013, Knoop et al. 2010, Xiong et al. 2014), which is somehow similar to the situation in plant mitochondria (Sweetlove et al. 2010). However, flux from succinate to fumarate catalyzed by SDH becomes restored in the dark (Xiong et al. 2014). These results indicate that whereas cyanobacteria carry all enzymes for an intact TCA cycle, the presence of light goes against the flux through succinate dehydrogenase and therefore causes a functional disconnection between the two TCA cycle branches (reductive TCA cycle and oxidative TCA cycle) (Steinhauser et al. 2012, Xiong et al. 2014). The presence of a complete TCA cycle with some pathway plasticity helps cyanobcateria to adjust to rapid changes in respiratory electron depending on the light intensity, the intracellular redox state and energy charge (Xiong et al. 2014).

1.7 Nitrogen metabolism

1.7.1 Nitrogen sources and their uptake

As shown in Fig. 1.7.1, nitrogen sources commonly used by cyanobacteria include nitrate (NO_3^-), nitrite (NO_2^-), urea, and ammonium (NH_4^+) (Flores and Herrero 2005a, Flores and Herrero 2005b). Cyanobacteria that possess heterocysts can also assimilate atmospheric N_2, and some strains are as well able to assimilate some amino acids, such as arginine or glutamine (Flores and Herrero 2005a, Flores and Herrero 2005b). Most of these nitrogen sources normally have to be finally reduced to ammonium (Fig. 1.7.1), which is a preferred nitrogen source for cyanobacteria and therefore inhibits the assimilation of other nitrogen source (Flores and Herrero 2005b, Muro-Pastor et al. 2005).

The uptake of these nitrogen-containing compounds is driven through permeases that are located in the cytoplasmic membrane (Fig. 1.6). Multicomponent ABC (ATP-binding cassette)-type permeases driven by ATP are required for the transport of nitrite (Omata et al. 1993), urea (Valladares et al. 2002), arginine and glutamine (Quintero et al. 2001), while a secondary permease from the major facilitator superfamily (MFS) is responsible for the uptake of ammonium (Montesinos et al. 1998), as well as nitrate and nitrite in some marine cyanobacteria (Sakamoto et al. 1999).

1.7.2 Assimilation of nitrate and nitrite and its regulation

As nitrate is the most widely used nitrogen source, the assimilatory reduction of nitrate is a key step of the nitrogen cycle in nature (Flores et al. 2005). Nitrate reduction to ammonium in cyanobacteria is catalyzed by nitrate reductase (Nar) and nitrite reductase (Nir) (Fig. 1.7.1), which is reduced by 2-electron and 6-electron reductions, respectively (Flores et al. 2005). Reduced ferredoxin/flavodoxin serves as an electron donor and is not only provided at PSI via the photosynthetic electron transfer in the light (Flores et al. 2005) but also from some enzymes, such as PFOR via carbohydrate oxidation in the dark (McNeely et al. 2011). However, the high presence of reduced ferredoxin under photosynthetic conditions results in elevated consumption of nitrate in the light compared to darkness in photosynthetic organisms, such as algae (Lillo 2004).

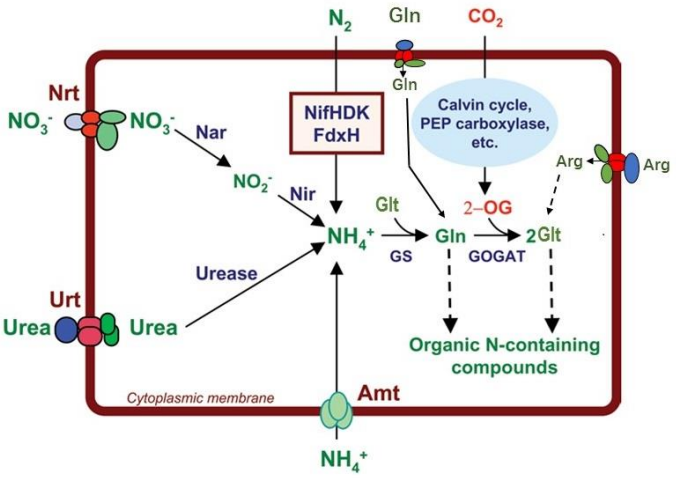

Fig. 1.7.1 Main nitrogen assimilation pathways in cyanobacteria. Combined nitrogen sources are taken up through permeases and metabolized to ammonium, which is incorporated into carbon skeletons through the GS-GOGAT pathway. Nitrogen is then distributed from glutamine or glutamate to the other nitrogen-containing organic compounds. Exogenous glutamine can be incorporated into glutamate synthesis directly. Nrt, ABC-type nitrate/nitrite transporter; Urt, ABC-type urea transporter; Amt, ammonium permease; Nar, nitrate reductase; Nir, nitrite reductase; NifHDK, nitrogenase complex; FdxH, heterocyst-specific ferredoxin; PEP carboxylase, phosphoenolpyruvate carboxylase; 2-OG, 2-oxoglutarate; GS, glutamine synthetase; GOGAT, glutamate synthase. Gln: glutamine; Arg: arginine; The urease reaction releases two molecules of ammonium and one molecule of CO_2 per molecule of urea degraded (not indicated). Nitrogenase and FdxH are boxed to note that in some filamentous cyanobacteria N2 fixation takes place in heterocysts. (Modified after Flores and Herrero 2005b)

Nitrate assimilation genes are quite conserved and commonly found in the following operon structure: *nir* (nitrite reductase)-permease gene(s)-*narB* (nitrate reductase) in cyanobacterial genomes (Flores et al. 2005). Nar and Nir activities are repressed in ammonium-grown cyanobacterial cells (Herrero et al. 1981, Herrero and Guerrero 1986), however, this repression by ammonium can be abolished with the supplement of MSX, an inhibitor of glutamine synthetase (Flores et al. 2005, Herrero et al. 1981). This is well in line with the expression of the *nir* operon at the mRNA level under similar conditions (Aichi et al. 2001, Suzuki et al. 1993). Furthermore, when cyanobacterial cells perceive a high C to N ratio or suffer under nitrogen starvation (Flores et al. 2005, Flores and Herrero 2005b), the transcription of the Nir operon is promoted and regulated by NtcA, a global nitrogen-control regulator that belongs to the CRP (or CAP) family of bacterial transcription factors (Luque et al. 1994b), and in addition NtcB, a pathway-specific regulator that belongs to the LysR family of bacterial transcription factors (Aichi et al. 2001, Suzuki et al. 1995), and PII, the signal transduction protein for regulation of the activity of the ABC-type nitrate/nitrite transporter (Heinrich et al. 2004, Hisbergues et al. 1999).

1.7.3 Assimilation of ammonium and glutamine and its regulation

Under either autotrophic or heterotrophic conditions, the ammonium resulting from nitrate reduction or after transport by specific permeases is incorporated into carbon skeletons via glutamate dehydrogenase (GDH)

or the glutamine synthetase/glutamate synthase (GS-GOGAT) cycle, the latter being the primary ammonium assimilation pathway in cyanobacteria (Flores et al. 2005). Glutamine, as one important nitrogen source in the form of amino acid, can be taken up by cyanobacteria and directly incorporated into glutamate synthesis catalyzed by glutamate synthases (GOGAT, see Fig. 1.7.1) (Flores and Herrero 2005a, Muro-Pastor et al. 2005).

Two GS, encoded by *glnA* and *glnN*, respectively, and three GOGAT, encoded by *glsF*, *gltB* and *gltD*, respectively, are characterized in detail in *Synechocystis* (Flores et al. 2005, Flores and Herrero 2005b). The glutamine biosynthesis catalyzed by GS is an ATP-dependent amidation of glutamate to glutamine (Purich 1998). The three GOGATs are classified into two types according to their specificities for electron donors: GlsF uses ferredoxin and belongs to Fd-GOGAT, both GltB and GltD use NADH as electron donor and belong to NADH-GOGAT (Flores and Herrero 2005a, Muro-Pastor and Florencio 2003, Muro-Pastor et al. 2005, Suzuki and Knaff 2005).

Fd-GOGAT has been found only in higher plants, algae and cyanobacteria, whereas some bacteria have another type of GOGAT, which uses NADPH as electron donor (Kameya et al. 2007, Temple et al. 1998, van den Heuvel et al. 2004). In higher plants Fd-GOGAT plays an important role in photorespiratory metabolism (Kendall et al. 1986, Somerville and Ogren 1980). In cyanobacteria *Synechocystis* and *Plectonema boryanum*, neither Fd-GOGAT nor NADH-GOGAT is indispensable for their photoautotrophic growth with different nitrogen source (Muro-Pastor et al. 2005). The Fd-GOGAT of the cyanobacterium *Plectonema boryanum* is supposed to be the most important for nitrogen assimilation at increasing availabilities of carbohydrates from photosynthate or exogenously added glucose (Okuhara et al. 1999).

The main photosynthetic ferredoxin, petF (Fx1 or Ssl0020 in *Synechocystis*) functions as electron donor to Fd-GOGAT in most investigated photosynthetic organisms (Hirasawa et al. 1996, Knaff 1996, Navarro et al. 2000, Staples et al. 1996), and was hence used to construct a complex between GOGAT and ferredoxin (Hirasawa et al. 2017, Schmitz et al. 1996, Tripathy et al. 2015). However, besides the main ferredoxin, Fx1, *Synechocystis* contains eight more ferredoxins, including three bacterial-type ferredoxins carrying [4Fe-4S] clusters (Cassier-Chauvat and Chauvat 2014a). Such a diversity of analogous proteins probably could replace the function of Fx1 as electron donor for Fd-GOGAT or other ferredoxin-dependent metabolic processes, especially when the expression of Fx1 are downregulated or repressed.

Surprisingly, *Hydrogenobacter thermophilus*, a hydrogen-oxidizing chemoautotrophic bacterium, was supposed to possess a novel Fd-GOGAT, GltS, which is a homologous to Fd-GOGAT from photoautotrophs and also the first reported Fd-GOGAT existing in a nonphotosynthetic organism (Kameya et al. 2007). Moreover, this *H. thermophilus* Fd-GOGAT did only react with two bacterial ferredoxins (HtFd1 and HtFd2), each of which contain single [4Fe-4S] clusters instead of a plant-type ferredoxin containing [2Fe-2S] cluster (Ikeda et al. 2005, Kameya et al. 2007). Interestingly, these two tandemly arranged ferredoxin genes are overlapped by four bp and also co-transcribed as an operon (Ikeda et al. 2005). HtFd1 was furthermore shown to act as an electron donor for PFOR and 2-oxoglutarate: ferredoxin oxidoreductase (Pogoryelov et al.),

catalyze carboxylation of acetyl-CoA and succinyl-CoA respectively, from *H. thermophilus* (Yoon et al. 1997). A unique loop, which was thought to be present in all Fd-GOGATs but absent from all NAD(P)H-GOGATs (van den Heuvel et al. 2003, Vanoni and Curti 2008), is unexpectedly missing in Fd-GOGAT from *H. thermophilus* (Kameya et al. 2007).This result could prove that this loop is not essential for the interaction between ferredoxin and Fd-GOGAT (Tripathy et al. 2015).

Due to the absence of 2-OG dehydrogenase in cyanobacteria (Zhang and Bryant 2011), 2-OG that is synthesized by the isocitrate dehydrogenase (encoded by *icd*) during the TCA cycle serves only as the sole carbon skeleton substrate of the GS-GOGAT pathway, in which the amide group is transferred from glutamine to 2-OG with the generation of two molecules of glutamate (Lee et al. 1992, Temple et al. 1998, van den Heuvel et al. 2004).

The presence of ammonium in the growth medium inhibits the uptake of nitrate and transcription of the nitrate assimilatory genes by quickly depleting the 2-OG pool through its metabolism via the GS-GOGAT cycle in cyanobacteria (Muro-Pastor and Florencio 2003, Muro-Pastor et al. 2001). The low level of 2-OG further induces the PII protein, which inhibits the nitrate transporter and nitrate reductase (Muro-Pastor and Florencio 2003, Muro-Pastor et al. 2001, 2005). Therefore, the key intracellular signal for this inhibition is 2-oxoglutarate (2-OG) instead of ammonium (Muro-Pastor et al. 2001). In contrast, when nitrogen is limiting or ammonium is absent, the intracellular amount of 2-OG rapidly increases and thus binds to PII to prevent it from inhibiting nitrate assimilation (Muro-Pastor and Florencio 2003, Muro-Pastor et al. 2001). Furthermore, the transcription factor NtcA is also activated by accumulation of 2-OG, to induce transcription of the nitrate assimilation genes (Flores and Herrero 2005a, Herrero et al. 2001, Luque et al. 1994a, Tanigawa et al. 2002).

1.7.4 Arginine metabolism (Biosynthesis and degradation pathways)

1.7.4.1 Arginine and arginine catabolism

The amino acid L-arginine, besides glutamine, can serve as efficient nitrogen source for many cyanobacteria (Flores and Muropastor 1990, Savary and Flores 1994). Furthermore, it can be taken up by a common transport system called Bgt permease system (Quintero et al. 2001). However, in contrast to L-arginine, the growth of *Synechocystis* with glutamine was inhibited in the presence of other nitrogen source such as nitrate or ammonium (Flores and Muropastor 1990).

Synechocystis grown on L-arginine as sole nitrogen source leads to high accumulations of cyanophycin, which is similar to the phenotype of cells grown under nutrient deficient conditions (Stephan et al. 2000). Furthermore, it also causes big morphological and physiological changes including degraded thylakoid membranes, the partial loss of pigments as well as reduced photosynthetic activity (Stephan et al. 2000).

All these described phenotypes grown on arginine are well in line with results of the correspondent transcript profiling analysis by DNA microarray (Schriek et al. 2008). Comparison of the transcriptomes of *Synechocystis* cells grown on nitrate to that on L-arginine reveal that the transcript levels of glutamine

synthase (GS), including GlnA and GlnN, are upregulated while GS-inactivating factors, IF7 and IF17, are downregulated (Schriek et al. 2008). Transcript levels of the nitrate/nitrite transport system called NrtA-D system are decreased, while the urea transporter-related transcripts are upregulated (like periplasmic urea transporter substrate-binding protein encoding by *urtA*, increased 6.5 folds) (Schriek et al. 2008). Probably the majority of urea produced from arginine catabolism (Quintero et al. 2000) cannot be effectively reduced to ammonium by *Synechocystis*, and is then released into the medium, even though there are still no specific reports about urea excreted from *Synechocystis* cells. In additions, most detectable genes encoding proteins involved in the assembly and biosynthesis of phycobilisome and PSII are to downregulated (Schriek et al. 2008).

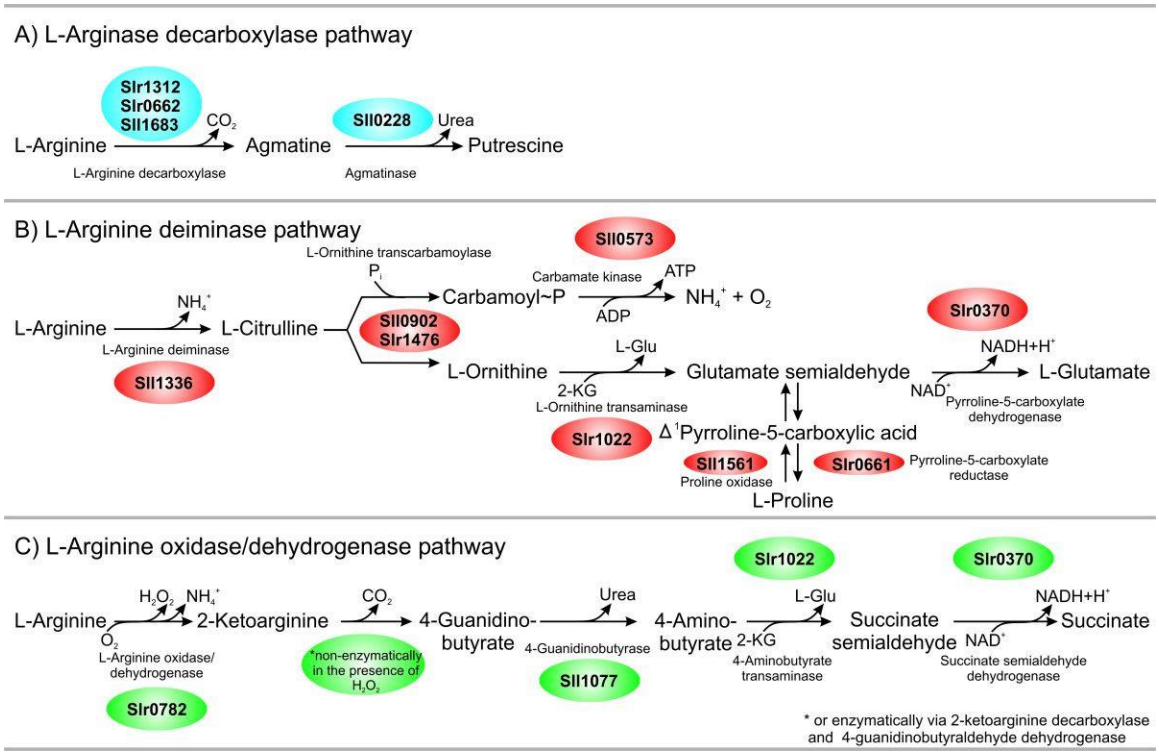

Fig. 1.7.4 Schematic presentation of the three L-arginine-degrading pathways in *Synechocystis* sp. PCC 6803 with the corresponding enzymes, intermediates, cofactors, and final products (Schriek et al. 2007).

The growth efficiency on arginine was reported to be similar to that on nitrate (Flores and Muropastor 1990). When grown on L-arginine, *Synechocystis* takes up L-arginine effectively (Montesinos et al. 1997), however, it surprisingly exhibits a decreased carbamate kinase transcript, a candidate for the last enzyme of the L-arginine oxidase/dehydrogenase pathway, and an increased level of transcripts encoding some enzymes (like ArgG and ArgJ) involved in the L-arginine biosynthetic pathway (Schriek et al. 2008). These results indicate that the arginine biosynthetic pathway might still be active and play an unknown role in the arginine catabolism (Schriek et al. 2008). Furthermore, the enhanced transcription of isocitrate dehydrogenase (Schriek et al. 2008), functioning for the biosynthesis of 2-OG, and the downregulated transcription of

glutamate dehydrogenase (Gdh) (Schriek et al. 2008), functioning for the consumption of 2-OG, indicate that GOGAT is an important pathway for 2-OG as substrate. Therefore, it was suggested that *Synechocystis* is not capable of consuming L-arginine effectively, thus resulting in nitrogen starvation condition (Schriek et al. 2008).

1.7.4.2 Arginine catabolic pathways

Arginine was proposed to function as an amino acid for protein synthesis and as a nitrogen buffer, storing excess nitrogen in the form of cyanophycin (Maheswaran et al. 2006). According to bioinformatic analysis, cyanobacteria possess five putative pathways for L-arginine catabolism, which include the L-arginine decarboxylase pathway, an arginase pathway, an L-arginine amidinotransferase pathway, an L-arginine deiminase pathway, and an L-arginine dehydrogenase pathway (Schriek et al. 2009, Schriek et al. 2007). In *Synechocystis*, the L-arginine deiminase pathway and the L-arginine dehydrogenase pathway seem to be of physiological importance while the L-arginine decarboxylase pathway most likely only functions in polyamine biosynthesis (see Fig. 1.7.4) (Schriek et al. 2007). It has been shown that the L-arginine dehydrogenase pathway is the most important arginine degradation pathway when cells are grown on arginine at 200 µmol photons m^{-2} s^{-1} (Schriek et al. 2009, Schriek et al. 2007). Slr0782, which is involved in this pathway, functions as an L-arginine dehydrogenase and transfers electrons from L-arginine oxidation via the PQ pool into the respiratory electron transport chain using oxygen as electron acceptor via cytochrome oxidase (Schriek et al. 2009). Furthermore, if the photosynthetic electron pressure is reduced, as e.g. true for the PsbO-free mutant, which is inhibited in water splitting at PSII, L-arginine oxidation catalyzed by Slr0782 is enhanced and results in much faster growth (Schriek et al. 2008, Schriek et al. 2009, Stephan et al. 2000).

1.7.4.3 Arginine biosynthesis

Cyanobacteria perform a cyclic pathway of arginine biosynthesis, during which NAG kinase (NAGK) represents the committed step, which can be feedback regulated by arginine (Caldovic and Tuchman 2003, Hoare and Hoare 1966). PII controls this committed step as non-phosphorylated PII activates NAGK activity by complex formation (Heinrich et al. 2004, Maheswaran et al. 2004). Under conditions of nitrogen excess, non-phosphorylated PII strongly activates the catalytic activity of NAGK, which promotes arginine synthesis and then induce cyanophycin synthesis (Heinrich et al. 2004). In contrast, when under nitrogen starvation conditions, the phosphorylated PII decomposes the PII-NAGK complex and then downregulates the NAGK catalytic activity and subsequent arginine biosynthesis (Maheswaran et al. 2006). Besides increasing NAGK catalytic activity, formation of PII-NAGK complex also severely limits or prevent arginine feedback inhibition (Maheswaran et al. 2006, Selim et al. 2018).

2. Aims of the present study

Three different questions were to be addressed in this thesis as described below.

1) Ferredoxins are soluble iron-sulfur cluster containing proteins with low reduction potential that transfer electrons to reactions in various metabolic pathways (Bruschi and Guerlesquin 1988, Mortenson et al. 1962). In total, nine ferredoxin-encoding genes (Fx1-Fx9) are predicated in the unicellular cyanobacterium *Synechocystis* (Cassier-Chauvat and Chauvat 2014a). Different ferredoxins may be involved in different metabolic pathways. In contrast to the highly abundant protein Fx1, which is well studied, the functions of the low-abundant ferredoxins (Fx2-Fx9), are only poorly understood. The main aim of this PhD work is to characterize the physiological function of those low abundant ferredoxins under various growth conditions, including photoautotrophic, mixotrophic, LAHG, fermentative conditions.

2) A central step in the energy and carbon metabolism is the decarboxylation of pyruvate to acetyl-CoA, which connects lower glycolysis to the TCA cycle. In *Synechocystis* this reaction is catalyzed by the pyruvate-dehydrogenase complex (PDHc) or alternatively by the pyruvate:ferredxin oxidoreductase (PFOR). The latter enzyme is oxygen sensitive and there is general agreement that PDHc is most important under aerobic conditions and replaced by PFOR under fermentative conditions. It therefore came as a surprise that deletion of PFOR in a previous work resulted in a mutant with impaired growth under mixotrophic conditions at high $NADH/NAD^+$ ratios in the presence of oxygen (Chen 2014). The question arose why PDHc does not suffice under these conditions. It is known from eukaryotes but not from prokaryotes that PDHc contains conserved phosphorylation sites that are phosphorylated at high $NADH/NAD^+$ ratios and thereby inactivate this enzyme complex. One of the aims of this thesis was thus to investigate if PDHc might get phosphorylated and thereby probably inactivated at high $NADH/NAD^+$ ratios under mixotrophic conditions in *Synechocystis*, which would partly explain the growth impairment of *Δpfor* under mixotrophic conditions.

3) It was furthermore shown that ferredoxin instead of NAD(P)H is the direct electron donor to the bidirectional NiFe-hydrogenase in *Synechocystis* (Gutekunst et al. 2014). As this finding was called into question by another group (Dutta et al. 2016), the issue should be further examined and clarified.

3. Materials and Methods

3.1. Cyanobacteria strains and growth conditions

The unicellular, freshwater cyanobacterium *Synechocystis* Wild-type (WT) and its mutants were cultivated and studied in this work (Table 3.1). It can survive under photoautotrophic (BG-11 medium in the light), mixotrophic (BG-11+glucose, in the light), LAGH (BG-11+glucose, bubbled with air in the dark), and fermentative (BG-11+glucose in anaerobic and dark) conditions. BG-11_0 medium was regarded as nitrogen starvation. Different nitrogen source, including nitrate (17.6 mM), nitrite (17.6 mM), ammonium (10 mM), arginine (5 mM), glutamine (5mM), glutamate (5 mM), was added in BG-11_0 medium for growth experiments with *Synechocystis* (Table 3.2). For mixotrophic, LAGH and fermentative conditions 10 mM glucose was added. For the LAGH or fermentative growth in darkness, cells were exposed for 10 min to light (40 µmol photons m^{-2} s^{-1}) every day. Cultures were bubbled with nitrogen for 10 min after illumination in order to discard oxygen and create an anaerobic condition in fermentative growth experiments.

Mutants used in this work, were either created during this work or by colleagues in this group (Appel et al. 2000a, Chen 2014, Gutekunst et al. 2014, Schreiber 2016) . All the mutants are listed in the following as a summary (Table 3.1).

Table 3.1. Mutant strains listed with their genes deletion and antibiotic resistance cassette.

Mutants	Deleted genes or ORF	Deleted or added protein	Resistance cassettes	Reference
Δpfor	*nifJ or pfor* (*sll0741*)	pyruvate:ferredoxin oxidoreductase	Em	Gutekunst et al. 2014
ΔpdhA	*pdhA* (*slr1934*)	subunit of pyruvate dehydrogenase	Sp	this work
Δzwf	*zwf*	glucose-6-phosphate dehydrogenase	Cm	Chen 2014
Δgdh	*gdh* (*sll1709*)	glucose dehydrogenase	Gm	Chen 2014
Δeda	*eda* (*sll0107*)	KDPG aldolase	Gm	Chen 2014
Δgnd	*gnd* (*sll0329*)	6-phosphogluconate dehydrogenase	Em	Chen 2014
Δflv3	*sll0550*	Flavodiiron protein Flv3	Cm	Schreiber 2016
Δflv24	*sll0217-sll0219*	Flavodiiron protein Flv2 and Flv4	Gm	Schreiber 2016
ΔhoxH	*hoxH*	large subunit of [NiFe]- Hydrogenase	Km	Appel et al. 2000
ΔhoxEH	*sll1220-sll1226, ssl2420*	[NiFe]-Hydrogenase	Km	Schreiber 2016
$fx1_{petE}$	*ssl0020*	[2Fe-2S] plant-like Ferredoxin-1	Gm	this work

Mutants	Deleted genes or ORF	Deleted or added protein	Resistance cassettes	Reference
fx2/Δfx2	*sll1382*	[2Fe-2S] plant-like Ferredoxin-2	Km	Schreiber 2016
Δfx3	*slr1828*	[2Fe-2S] plant-like Ferredoxin-3	Em	Schreiber 2016
Δfx4	*slr0150*	[2Fe-2S] plant-like Ferredoxin-4	Cm	Schreiber 2016
fx5/Δfx5	*slr0148*	[2Fe-2S] plant-like Ferredoxin-5	Km	this work
Δfx6	*ssl2559*	[2Fe-2S] plant-like Ferredoxin-6	Gm	this work
Δfx7	*sll0662*	[4Fe-4S] bacterial type Ferredoxin-7	Sp	Schreiber 2016
fx8/Δfx8	*ssr3184*	[3Fe-4S][4Fe-4S] bacterial type Ferredoxin-8	Cm	this work
Δfx9	*slr2059*	[4Fe-4S][4Fe-4S] bacterial type Ferredoxin-9	Km	Schreiber 2016
ΔisiB	*sll0284*	Flavodoxin	Gm	Schreiber 2016
Δfx7Δfx9	*sll0662, slr2059*	Ferredoxin-7 and -9	Sp, Km	Schreiber 2016
Δfx7Δfx8Δfx9	*sll0662, ssr3184, slr2059*	Ferredoxin-7, -8 and -9	Sp, Cm, Km	this work
Δfx9ΔisiB	*slr2059, sll0284*	Ferredoxin-9, Flavodoxin	Gm, Km	Schreiber 2016
F1h	-	Ferredoxin-1 with His-tag	Km	this work
F1s	-	Ferredoxin-1 with Strep-tag	Em	this work
F9h	-	Ferredoxin-9 with His-tag	Km	this work
F9s	-	Ferredoxin-9 with Strep-tag	Em	this work
F1hF9s	-	Ferredoxin-1 with His-tag	Km, Em	this work
F1sΔfx9	*slr2059*	Ferredoxin-1 with Strep-tag	Km, Em	this work
F1sF9h	-	Ferredoxin-1 with Strep-tag Ferredoxin-9 with His-tag	Km, Em	this work

Table 3.2. The medium compositions under various growth conditions with different nitrogen and carbon source. Star (*) means the short name marked in the part of results.

Growth conditions	Medium*	N-source	C-source
Autotrophic	BG11	17.6 mM $NaNO_3$	CO_2
	$BG11_0+NH_4^+$	10 mM NH_4Cl	CO_2
	$BG11_0$+Arg	5 mM arginine	CO_2
	$BG11_0$+Gln	5 mM glutamine	CO_2
	$BG11_0$+Urea	5 mM urea	CO_2
Mixotrophic	BG11+G	17.6 mM $NaNO_3$	10 mM glucose; CO_2
	$BG11_0$+G+N	10 mM NH_4Cl	10 mM glucose; CO_2
	$BG11_0$+AG	5 mM arginine	10 mM glucose; CO_2
	$BG11_0$+Urea+G	5 mM urea	10 mM glucose; CO_2
Photo-heterotrophic	BG11+G+DCMU	17.6 mM $NaNO_3$	10 mM glucose
	$BG11_0$+Urea+G+DCMU	5 mM urea	10 mM glucose
	$BG11_0$+AG+DCMU	5 mM arginine	10 mM glucose
LAHG	BG11+Glu	17.6 mM $NaNO_3$	10 mM glucose
	$BG11_0+NO_2^-$+G	10 mM $NaNO_2$	10 mM glucose
	$BG11_0+NH_4^+$+G	10 mM NH_4Cl	10 mM glucose
	$BG11_0$+Urea+G	5 mM urea	10 mM glucose
	$BG11_0$+Arg+G	5 mM arginine	10 mM glucose
Fermentative	BG11+G	17.6 mM $NaNO_3$	10 mM glucose

3.2. Chemicals, buffers and mediums

Unless otherwise stated, all chemicals used in this work were mainly obtained from Bio-Rad, BioVision, Biozym, Fermentas, Invitrogen, Merck, Millipore, Qiagen, Promega, Roche, Roth, Sigma-Aldrich, Thermo. For the preparation of all medium and solutions, the water used was taken from a distillation machine (PURELAB® Chorus 1 Type I Ultrapure Water System, ELGA LabWater, or Seralpur pro 90 CN, O. Kohl Chemie-Pharma-Laborbedarf, Germany) and was additionally autoclaved at 120 ℃ for at least 20 min. For primer dilution or other specific molecular experiments, the nuclease free, sterile filtered, autoclaved water was used.

The buffers and mediums used in normal experiment are listed below (Table 3.3 and 3.2.2). Some special ones will be mentioned in relevant experiments. *Synechocystis* mutants or *E. coli* was incubated or grown in BG-11 medium or LB-medium, respectively, with appropriate antibiotic solution (in the case of mutants), which are shown in the list of Table 3.5.

Table 3.3. Buffers used in this work and their compositions.

Name	**Reagents**
TBE	890 mM Tris (pH 8.3), 890 mM H_3BO_3, 25 mM Na_2EDTA
TE	10 mM Tris (pH7.4), 1 mM Na_2EDTA (pH 8.0)
80% Glycerin	80g Glycerin in 100 ml H_2O, autoclaved
PBS	81% (v/v) of 20 mM K_2HPO_4, 19% (v/v) of 20 mM KH_2PO_4, 0.15 M NaCl
5 x DNA loading buffer	50 % (v/v) glycerol, 50 % (v/v) 10x buffer TBE, 0.2 mg/ml bromophenol blue
TES	0.5M TES, pH 8.0

For preparation of liquid BG-11 medium (1 L for example), firstly, the reagents stock solution 100 x BG-11, K_2HPO_4, Na_2CO_3, TES (Note: open TES stock in sterile bench) were added, with the final concentration marked in Table 3.4, in graduated cylinder (beaker) containing 500 ml double-distilled H_2O, followed by filling up to 1 L with distilled H_2O before autoclaving at 120 °C for 20 min. $FeNH_4$-Citrat (Table 3.4) and the corresponding antibiotic (Table 3.5) were added when the temperature of the autoclaved medium cooled down to 55 °C.

For preparation of solid BG-11 medium (for agar plate), $FeNH_4$-Citrat and additional sodium thiosulfate ($Na_2S_2O_3$) and agar were added to the liquid BG-11 medium before autoclaving.

Table 3.4. Medium used in this work and their compositions.

Medium name	**Reagents**
BG-11	17.6 mM $NaNO_3$, 0.304 mM $MgSO_4 \cdot 6H_2O$, 31.2 µM citric acid, 2.79 µM Na_2EDTA, 46.3 µM H_3BO_3, 4.15 µM $MnCl_2 \cdot 4H_2O$, 1.61 µM $NaMoO_4 \cdot 2H_2O$, 188.7 µM $NaCO_3$, 175.1 µM K_2HPO_4, 0.77 µM $ZnSO_4 \cdot 7H_2O$, 10 mM TES (pH 8.0), 22.8 µM $FeNH_4$-citrate, 0.32 µM $CuSO_4 \cdot 5H_2O$, 5 µM $NiCl_2$
$BG\text{-}11_0$	BG-11 medium without $NaNO_3$
LB	1 % (w/v) NaCl, 1 % (w/v) peptone, 0.5 % (w/v) yeast extract
SOB	0.5 % (w/v) yeast extract, 2 % (w/v) tryptone, 10 mM NaCl, 2.5 Mm KCl, 10 mM $MgCl_2$, 10 mM $MgSO_4$
SOC	SOB medium with 20 mM glucose

Table 3.5. Antibiotic used in medium and agar plate are listed with relevant concentrations for *Synechocystis* and *E. coli* mutants.

Full Name	Abbreviation	Concentration (stock solution)	Concentration (working solution)	Solvent
Kanamycin	**Km**	50 mg/ml	50 µg/ml	H_2O
Chloramphenicol	**Cm**	25 mg/ml	25 µg/ml	ethanol
Spectinomycin	**Sp**	20 mg/ml	20 µg/ml	H_2O
Ampicillin	**Amp**	100 mg/ml	100 µg/ml	H_2O
Erythromycin	**Em**	25 mg/ml	25 µg/ml	ethanol
Gentamycin	**Gm**	10 mg/ml	10 µg/ml	H_2O

3.3. Oligonucleotides or primers

All the oligonucleotides or primers used in this work were synthesized by Sigma-Aldrich (Steinheim, Germany) and provided as a dry or lyophilized powder, which was further dissolved in distilled water as stock solution (100 µM). Primers for the Polymerase Chain Reaction (PCR) were diluted to a final concentration of 5 µM. Both the stock and working solution for primers was placed at -20 °C.

Table 3.6. Primers used in this work. The sequences of all primers are listed in 5'→ 3 'direction.

Name	Sequence	Notes (product or function)
M13-F	AGGGTTTTCCCAGTCACGACGTT	pCR2.1 TOPO
M13-R	GAGCGGATAACAATTTCACACAGG	
Em-F	GTCGACGAAAAAAGAAATTAGATAAA	Erythromycin (Em) gene
Em-R	GTCGACTTACTTATTAAATAATTTATAGC	
Cm-F	TCAATAATATCGAATTCCTGCAG	Chloramphenicol (Cm) gene
Cm-R	AGCGAGGTGCCGCCATCAAGCTT	
Gm.1	GTCGACGGATGAAGGCACGAACC	Gentamycin (Gm) gene
Gm.2	GTCGACGAATTGTTAGGTGGCG	
Km-F	CCACGTTGTGTCTCAAAATCTCTGAT	Kanamycin (Km) gene
Km-R	ATCGCCCCATCATCCAGCCAGAAAG	

Name	Sequence	Notes (product or function)
Sp-F	TCGCGCAGGCTGGGTGCCAA	Spectinomycin (Sp) gene
Sp-R	GCCCTCGCTAGATTTTAATGCGGAT	
Fed1.1	CGGAGGGGGAAACGGAAGAA	Fusion PCR for *fx9* (*slr2059*)
Fed1.in1	ATCAGAGATTTTGAGACACAACGTGG GGCATTTGCACCGCACTACG	
Fed1.in2	CTTTCTGGCTGGATGATGGGGCGAT CATCTTTGCCGACTCCGCCA	
Fed1.2	AATTCCAAAATAAATACCCC	
Fed2.1	GCGGGGCTACCAGGGTTTGA	Fusion PCR for *fx7* (*sll0662*)
Fed2.in1	TTGGCACCCAGCCTGCGCGA CAGGCACTCCAGCGTTGCAC	
Fed2.in2	ATCCGCATTAAAATCTAGCGAGGGC TTAATTGGGTGATGGAATCT	
Fed2.2	CTCCTAAATATTCCTCGGTGC	
Fdx1.1	CCGGTCCTTAAAACTCCCTT	Fusion PCR for *fx1* (*ssl0020*)
Fdx1.in1	TTGGCACCCAGCCTGCGCGA ACAGTAGAGAGATTGCCTCAT	
Fdx1.in2	ATCCGCATTAAAATCTAGCGAGGGC GGTAATAATGCTGGCCATGG	
Fdx1.2	TTAATCTACCCTTCGTTTCCC	
Fdx2.1	CTCTCATATTCCGACCTACC	Fusion PCR for *fx2* (*sll1382*)
Fdx2.in1	ATCAGAGATTTTGAGACACAACGTGG TTATGGGCTGGTTTGAATCCA	
Fdx2.in2	CTTTCTGGCTGGATGATGGGGCGAT GTAGGCTACAACTACAACCTG	
Fdx2.2	TCTGGGCAACGGCGTTTAAT	
Fdx3.1	CAATTACAGCCATCCTGTTTG	Fusion PCR for *fx4* (*slr0150*)
Fdx3.in1	TCAATAATATCGAATTCCTGCAG GAATGACCCAAACAATGGACT	
Fdx3.in2	AGCGAGGTGCCGCCATCAAGCTT AATGTTAGTCCAGCGGAGTT	
Fdx3.2	TTAGCAGGCAAGACCACACT	
Fdx4.1	CGTCTGCCGTACTGTTAGAT	Fusion PCR for *fx3* (*slr1828*)
Fdx4.in1	AGAGATTTATCTAATTTCTTTTTTCGTCGAC CCATGGCAAAGCGGTAATAA	
Fdx4.in2	GCTATAAATTATTTAATAAGTAAGTCGAC TTCGGCTGGAATTCTCCCTT	
Fdx4.2	GCAAAGACTCAAAGGACTGG	

Name	Sequence	Notes (product or function)
Fx5.1	CGATTCAGAACTCGGCATTG	Fusion PCR for *fx5* (*slr0148*)
Fx5.in1	ATCAGAGATTTTGAGACACAACGTGG CATAATGGTGGCATGGTCATG	
Fx5.in2	CTTTCTGGCTGGATGATGGGGCGAT CGTTGACTCGTCTCACCATTG	
Fx5.2	TCAGTGCTGGTAACACCATGG	
Fx6.1	TTCTCCACGCAGTTGGTGAC	Fusion PCR for *fx6* (*ssl2559*)
Fx6.in1	GGTTCGTGCCTTCATCCGTCGAC ACCAGCATGGTATGGCGATC	
Fx6.in2	CGCCACCTAACAATTCGGTCGAC TTGTCCGATGGAACCTAAGC	
Fx6.2	AAGCTCTGGACGCCATTACC	
Fx8.1	CGTTGGCTAGCATGTCACTG	Fusion PCR for *fx8* (*ssr3184*)
Fx8.in1	TCAATAATATCGAATTCCTGCAG TAAGGGTAGCGGACGTTCAA	
Fx8.in2	AGCGAGGTGCCGCCATCAAGCTT GGTTGGGAGGGGTCTAACTG	
Fx8.2	CTCTGCCACTGTTAGGCTGC	
IsiB.1	ATGGATCATCCTCACACTTG	Fusion PCR for *isiB* (*sll0284*)
IsiB.in1	GGTTCGTGCCTTCATCCGTCGAC GATTACTGGAAAGTTACTAAGC	
IsiB.in2	CGCCACCTAACAATTCGGTCGAC GCAATCCTAGGTAACCTAAG	
IsiB.2	CTGGTTTGTCATGGTAGGAG	
1/9GmFd_1.1	ATCCAACAGGTAGCCATAGCCT	Fusion PCR for *fx1* (*ssl0020*) with Gm and petE promoter
10GmFd_1.2	CGCTATGAATCCTTGACAGTAGAGAGATTGCCTCATG	
11GmFd_2.1	CAATCTCTCTACTGTCAAGGATTCATAGCGGTTG	
6/12GmFd_2.2	GGTATAGGATGCCATACTTCTTGGCGATTGTATC	
7/13GmFd_3.1	CAATCGCCAAGAAGTATGGCATCCTATACCGTTAAATTG	
14GmFd_3.2	CTTCATCCGTCGACGCATTATTACCCTTAGTAGAG	
15GmFd_4.1	AGGGTAATAATGCGTCGACGGATGAAGGCACGAAC	
16GmFd_4.2	CCATGGCCAGCATTAGTCGACCGAATTGTTAGGTG	
17GmFd_5.1	TAACAATTCGGTCGACTAATGCTGGCCATGGGCTAGT	
8/18GmFd_5.2	CTCACGGTGCAACTGTTGGAAG	

Name	Sequence	Notes (product or function)
1/9SpFd_1.1	ATCCAACAGGTAGCCATAGCCT	Fusion PCR for *fx1* (*ssl0020*) with Sp and petE promoter
2SpFd_1.2	CTCAATCAATCACGCACAGTAGAGAGATTGCCTCATG	
3SpFd_2.1	CAATCTCTCTACTGTCGGTGATTGATTGAGCAAGC	
4SpFd_2.2	CGCTATGAATCCTTGGGATCCGGTGATTGATTGAG	
5SpFd_3.1	TCAATCACCGGATCCCAAGGATTCATAGCGGTTG	
6/12SpFd_3.2	GGTATAGGATGCCATACTTCTTGGCGATTGTATC	
7/13SpFd_4.1	CAATCGCCAAGAAGTATGGCATCCTATACCGTTAAATTG	
8/18SpFd_4.2	CTCACGGTGCAACTGTTGGAAG	
PdhA.1	CAGGCGATCGCGTAACCGTTG	*pdhA* (*slr1934*) fragment with Sp
PdhA.in1	TTGGCACCCAGCCTGCGCGATCTATGCGAAGTCGGTCAGC	
PdhA.in2	ATCCGCATTAAAATCTAGCGAGGGCACGTTCACCGTTTGGGAGAA	
PdhA.2	GACACCCAACCGCTAATGGA	

3.4. Plasmids and Bacteria

Once the desired PCR product was made, it was introduced into the TOPO®-clone pCR™2.1-TOPO® vector and transformed into competent *E. coli* cells. Plasmids and bacteria used in this work are listed in Table 3.7 and Fig.3.4.

Table 3.7. Plasmid and bacteria used in this work

Plasmid/*E. coli*	Description	Reference
Top10 (*E. coli*)	Genotype: F- *mcr*A *Δ*(*mrr-hsd*RMS-*mcr*BC) φ80*lacZΔ*M15 *ΔlacX*74 *rec*A1 *ara*D139 *Δ*(*ara-leu*) 7697 *gal*U *gal*K *rpsL* (Str^R) *end*A1 *nup*G Notes: Do not require IPTG to induce expression from the *lac* promoter	Invitrogen
pCR2.1 TOPO	Lac*Z*α fragment; M13 reverse priming site; Multiple cloning site; T7 promoter/priming site; M13 Forward (-20) priming site; f1 origin; Kanamycin resistance ORF; Ampicillin resistance ORF; pUC origin;	Invitrogen

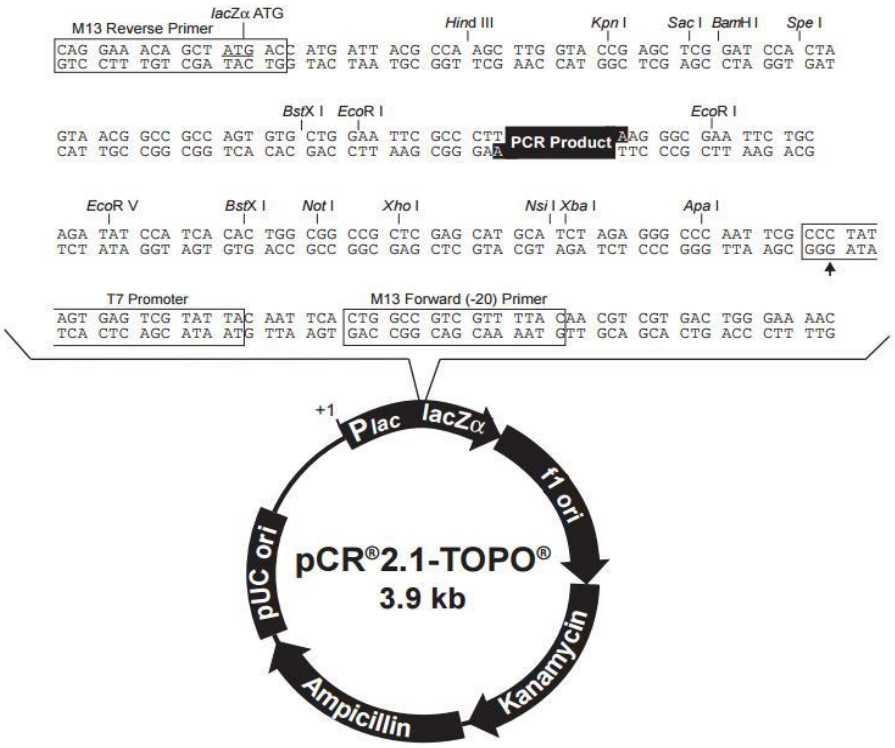

Fig.3.4. Map of vector pCR™2.1-TOPO. The above map shows the features of the pCR™2.1-TOPO vector and the sequence surrounding the TOPO Cloning site. Restriction sites are labeled to indicate the actual cleavage site. The arrow indicates the start of transcription for T7 polymerase. The sequence of the pCR™2.1-TOPO vector is available from *www.lifetechnologies.com/support*.

3.5. Restriction Enzymes

A restriction enzyme is an enzyme that cleaves DNA into fragments at a specific recognition site. All of the Thermo Scientific FastDigest Restriction Enzymes used in this work were bought from Fermentas (Thermo Scientific™, Life Technologies GmbH, Germany) and are listed in Table 3.8. The digested products were checked by loading them on a 0.8% (w/v) agarose gel (Section 3.8.2.1).

Table 3.8. FastDigest restriction enzymes used in this work. Specific recognition sites were marked with a caret in sequence. The reaction time marked here is only suitable for FastDigest restriction enzymes.

Enzyme name	Cut site and Sequence (5' → 3')	Reaction time	Optimal reaction temperature (°C)
EcoRI	G^AATTC	5-15 min	37
HindIII	A^AG CTT	5-15 min	37
BclI	T^GATCA	5-15 min	37
BglII	A^GATCT	5-15 min	37

3.6. Cultivation of bacteria (*Escherichia coli*)

Transformation of *Escherichia coli* (*E. coli*) Top10 cells was performed as described by the manufacturer (Invitrogen, Karlsruhe, Germany) except that only 1/4 of the reaction was used. Transformed *E. coli* Top10 cells (Invitrogen, Karlsruhe, Germany) were grown for 1 hour in SOC medium on a shaker at 37 °C and 180 rpm (4400 Innova Incubator Shaker, New Brunswick Scientific, Nürtingen, Germany). Transformed cells of *E. coli* were plated on LB agar plates supplemented with 50 µg/ml kanamycin. They were incubated at 37 °C overnight in an incubator (T5050E, Heraeus, Hanau, Germany).

For short-term storage, the plates were sealed with sealing film (PARAFILM® M, Carl Roth GmbH, Karlsruhe, Germany) and kept in a refrigerator at 4 °C. For long-term storage, freezing cultures were prepared as described for *Synechocystis* and stored at -80 °C.

3.7. Physiological Methods

3.7.1 Optical density determination

The optical density (OD) of culture was determined by photometrical analysis (UV 2501 PC Photometer, Shimadzu, Kyoto, Japan) and its data was recorded and analyzed by the affiliated software UVProbe 2.33 (Shimadzu, Kyoto, Japan). Normally, the cell density of *Synechocystis* was indicated as the absorbance at 750 nm (OD_{750}) with fresh BG-11 medium, which was used to inoculate the cultures, as blank reference. Samples were diluted with BG11 medium by 1:10 when samples showed an OD_{750} value above 0.5. OD_{750}.

3.7.2 Absorption spectrum of photosynthetic pigments

There are several kinds of photosynthetic pigments, including carotenoids (an orange pigment), phycocyanin (PC), and chlorophyll a (Chl a, a blue-green pigment) present in *Synechocystis.* Absorption spectra for wavelengths from 400 to 800 nm were recorded using an integrating sphere method with a UV spectrophotometer (UV 2501 PC Photometer, Shimadzu, Kyoto, Japan), with slit size adjusted to 0.5 nm or 1.0 nm.

3.7.3Chlorophyll a determination

Chl a absorbs at a wavelength of 400–450 nm and 650–700 nm (Fig. 3.7.2). The Chl a content of cultures was determined as follows (Chen 2014). For Chl a content measurement, 1 ml cell suspension, whose OD_{750} was no more than 0.5, was centrifuged at 16000 g for 10 min (Centrifuge 5415D, Eppendorf, Germany) at room temperature (RT). 1 ml methanol was used to resuspend the pellet and the suspension was vortexed for 10 min to extract Chl a. Dissolved cells were centrifuged down for 10 min at 16000 g and then the supernatants were transferred to a new Eppendorf cup. Measurements of the supernatants' extinctions were carried out at 666.5 nm, 666 nm, 665.5 nm, 665 nm and 750 nm (UV-2501 PC, Shimadzu, Kyoto, Japan)

with fresh methanol as a blank reference. Chl a content was calculated according to the following formula (Lichtenthaler 1987):

$$\text{Chl a content } (\mu g/ml) = \frac{(\text{maximum of OD666.5 to OD665}) - \text{OD750}}{0.0809} \times \text{dilution}$$

0.0809 in this formula means molar extinction coefficient Chl a. This analysis was performed at least in triplicates.

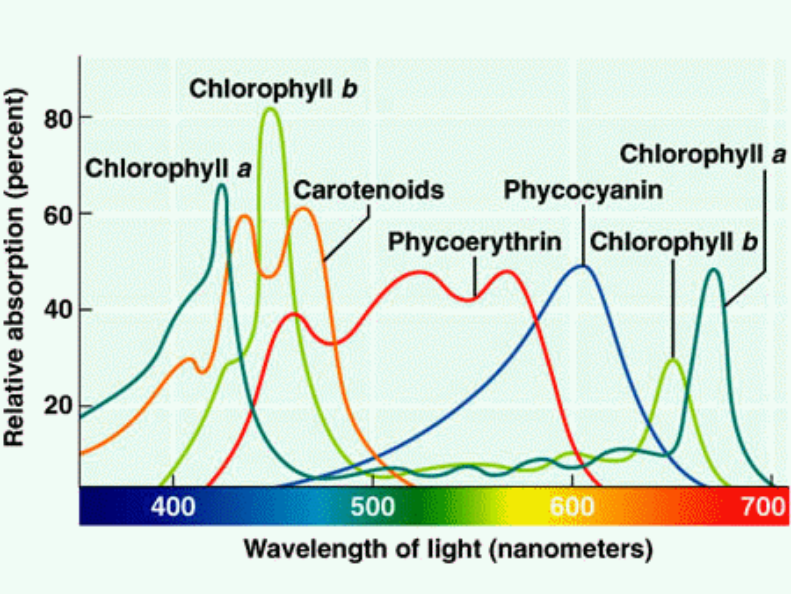

Fig. 3.7.2. Photosynthetic pigments absorb energy from sunlight, which is used during photosynthesis. (http://hyperphysics.phy-astr.gsu.edu/hbasees/Biology/ligabs.html). *Synechocystis* cells contain only carotenoids, phycocyanin and chlorophyll a.

3.7.4Carotenoids determination

Carotenoids absorb at a wavelength of 420–480 nm (Fig. 3.7.2). The carotenoids (mainly β-carotene) content was determined according to the protocol described by Zavřel et al. 2015. 1 ml of cyanobacterial culture suspension was harvested by centrifuge at 15000 g, RT for 7 min and subsequently the supernatant was thoroughly discarded. 1 ml of methanol was added to the pellet and vortexed at 2000 rpm for 4 sec to homogenize the mixture, which was subsequently covered with aluminum foil and incubated at 4 °C for 20 min (up to 2 hours) in order to extract the pigments from the cells. The suspension was pelleted at 15000 g, 4 °C for 7 min. The color of the pellet ranged between bluish and purple without any green color. The supernatant was measured at 470 nm, 665 nm and 720 nm with methanol as a blank. The obtained OD values were used to calculate the concentration of Chl a and carotenoids according to the following equations:

Chl a [μg/ml] = 12.9447 * ($OD_{665} - OD_{720}$)

Carotenoids [μg/ml] = [1000 * ($OD_{470} - OD_{720}$) − 2.86 (Chl a content)]/221

The measurement of every sample was performed at least in triplicates.

3.7.5 Respiration and photosynthesis rate measurement

Respiration and photosynthesis rate of *Synechocystis* cultures were determined as the oxygen uptaken rate in darkness and oxygen evolution rate in the light, which were determined with Unisense oxygen microsensor (Unisense, Denmark), a miniaturized Clark-type oxygen sensor, according to the manufacturer's instruction (Oxygen Sensor User Manual, Version 2014, Unisense, Denmark).

The protocol of the OXYGEN SENSOR USER MANUAL (Unisense, Denmark) was modified as follows:

(a) Connect the oxygen sensors to the Unisense Microsensor Multimeter;

(b) Polarize the oxygen sensors with -0.80 V (Note: On the Microsensor Multimeter, oxygen sensors are automatically recognized and polarization should be pre-set. Incorrect polarization may destroy the oxygen sensor).

(c) Connect the oxygen microsensor to the input terminal (one laptop containing the free Unisense Logger software, Programming Tool and the full SensorTrace Suite), and open the program of SensorTrace Suite and pre-run for at least 1 hour before calibration.

(d) Calibration by making standard curves in the SensorTrace program:

100% oxygen (atmospheric) reading: Place/keep the sensor tip in a complete aeration of the water (by bubbling with air in the Unisense calibration chamber for 5 minutes) and then turn off bubbling. After the water movement has stopped, note the signal reading on the display and add the point to the calibration in the software. Your referenced calibration value at the temperature of bubbled water can be found in the Table in the handbook (See Appendix IV, for example: at 20 °C and 0.21 atm, 0 salinity, 283.9 μmol O_2/l). This signal is your calibration value for atmospheric partial pressure (Sat) conditions.

0% oxygen *reading*: Place the sensor tip in solution of 0.1 M sodium ascorbate (made by dissolving ~2 g sodium ascorbate in 100 ml of 0.1M NaOH) and wait for the signal to stabilize. This zero-calibration solution can be stored in a closed container for 1-2 weeks. The signal reading is the calibration value for zero oxygen partial pressure (S0).

Read the value on the display or add it to the software calibration. Oxygen sensors respond linearly in the range of 0 to 100% oxygen and signals can be linearly converted to partial pressure. So far, the oxygen sensor is ready to be used for oxygen measurement.

(e) Put the calibrated oxygen sensor in a 25 ml culture, which was exposed by 15 min illumination at 100 μmol photons m^{-2} s^{-1} followed by another 15 min in the darkness. The corresponding oxygen evolution rate in the light and oxygen uptake rate in darkness were used to monitor the photosynthetic and respiratory activity, respectively.

(f) Close the program and multimeter after saving data.

(g) Wash the oxygen sensors with 70% ethanol and water in turn before packaging them in the paper box with the protection interlayer;

3.7.6 Hydrogen production

Fermentative hydrogen production could be determined by the hydrogen microsensor (Unisense, Denmark) according to the manufacturer's instruction (Hydrogen Sensor User Manual, Version 2014, Unisense, Denmark). The protocol was modified as follows:

(a) Connect hydrogen sensors to the Unisense Microsensor Multimeter;

(b) Polarize the hydrogen sensors with +1.0 V and make sure the signal for "0" H_2 concentration should stabilize at 0-50 pA (normally < 30 pA for H_2-500; < 20 pA for H_2-50); (Note: On Microsensor Multimeter, hydrogen sensors are not automatically recognized so that the polarization should be manually set. Incorrect polarization may destroy the hydrogen sensor).

(c) Connect the hydrogen microsensor to the input terminal (one laptop containing the free Unisense Logger software, Programming Tool and the full SensorTrace Suite), and open the program of SensorTrace Suite and pre-run for at least 1 hour before calibration.

(d) Calibration by making standard curves in the SensorTrace program:

0% hydrogen reading: Place/keep the sensor tip in water (bubbled with air) and read the signal;

10% hydrogen reading: 30 mL water bubbled with 99% H_2 for at least 15 min in a Conical tube (50 mL) was slowly poured in a beaker containing 270 mL water and mixed gently. Measure the mixed water temperature and calculate the responding 10% hydrogen concentration (μmol/L) according to the reference in Appendix V (for example: 0 salinity at 20 °C, 10%*805.36 = 80.5 μmol/L);

Read the value on the display or add it to the software calibration. Hydrogen sensors respond linearly in the range of 0 to 100% hydrogen and signals can be linearly converted to partial pressure. So far, the hydrogen sensor is ready to be used for hydrogen measurement.

(e) Put the calibrated hydrogen sensor in a Kniese tube containing 70 ml *Synechocystis* culture, whose OD_{750} is about 2.0 (or just make sure all samples have the same OD_{750} values), and make sure that all the heads of tips are placed in same depth (about 6-10 cm).

(f) Set sampling interval as "30 sec" and start the program;

(g) Keep all the cultures in the dark and bubble cultures with 99% N_2 for 10 min until the oxygen is discarded completely to make anaerobic conditions.

(h) Leave the program running overnight (normally for 12 hours) and the fermentative hydrogen production was recorded by the SensorTrace program (normally the visible H_2 production appears in 30 min).

(i) The cultures were exposed by illumination at 300 μmol photons m^{-2} s^{-1} to activate photosynthesis followed by hydrogen uptake.

(j) Close the program and multimeter after saving data.

(k) Wash the hydrogen sensors with 70% ethanol and water in turn before packaging them in the paper box with the protection interlayer.

3.7.7 The measurement of the cyclic electron transport (CET) by DUAL-PAM-100

In order to determine the cyclic electron transport (CET) around PSI, $P700^+$ reduction kinetics were recorded by a pulse amplitude-modulated measurement (DUAL-PAM-100) (Bernat et al. 2009). Complete P700 oxidation was achieved by a 200-ms saturation pulse (I = 10000 µE m^{-2} s^{-1}). P700 reduction kinetics were recorded without any addition as well as in the presence of 10 µM DCMU and fitted with single exponential functions; the resulting rate constants (*b*) were used for quantifying both the linear and the (direct) cyclic electron transport rates. The inhibitor DCMU (10 µM) which blocks electron transfer from PSII to the PQ-pool was added to inhibit the linear electron (LET) pathway, resulting in the sole presence of CET around PSI (Fig. 4.2.2.1).

The protocol for the measurement of $P700^+$ reduction kinetics is shown below:

(a) Preparation and test of the equipment before formal measuring:

- Plug in computer and PAM and start both.

- Start Dual-PAM program in the computer.

- Check the setting under MODE:

Measure Mode: Fluo+ P700

Analysis: SP Analysis (Saturation Pulse)

Fluo: 5 (high)

P700 5 (high)

Damping for both: 1ms (high)

- Check Sat. Pulse (Saturation Pulse)

Intensity 10 (10 000 µE)

Width: 200 ms

P700: interval delay:0

Width: 200 ms

- Choose Trig. Run (Trigger Run)

- Open the program of "Ying 4"

1. *1000 ms XmL on*
2. *51 000 SP.Int 10*
3. *56 000 Trig. Out 0/0/1/0*
4. *300 000 P+F.SP*
5. *330 000 P+F.SP*
6. *360 000 P+F.SP*
7. *390 000 P+F.SP*
8. *420 000 Stop*

- Check slow kinetics by changing default setting from "Manual" to "Trig. Run".

- Press "Bal" until P700 signal is close to 0 (should be stable).

(b) Leave the equipment running for certain time (normally more than 1 hour) until the decreasing signal of P700 became stable. Samples can be prepared during the waiting time.

(c) 2 ml cell suspension (adjust to 10 µg/ml chlorophyll according to Section 3.7.3) was prepared per measurement. Cell cultures were pelleted and resuspend with fresh BG11 medium.

(d) Pipette culture into the cuvette (quartz, with a small magnet inside) and add inhibitor (10 µM DCMU) when necessary.

(e) Stir for 1 min in darkness, then turn stirring off to get a good signal by balancing.

(f) Start the program "*Ying 4*" (Press the "*Start*"). Make sure that "*Acquisition Rate*" should be "1 ms" for conditions without inhibitor, "2 ms" for conditions with inhibitor (10 µM DCMU).

(g) Export data as "*.csv"*-file and save data after every single measurement

(h) Rinse cuvette with 2 times of distilled H_2O, 3 times of 70% ethanol, 3 times of distilled H_2O, in turn, if DCMU was added in the cuvette as inhibitor.

(i) Start new measurement after pressing *"Bal"* again until P700 signal is close to 0 (Signal values of P700 might decrease during the last measurement).

The obtained data in "*csv*" file was changed to excel file and analyzed by Sigma blot to pick up the only exponential decays of the curves to make a nonlinear regression with a single exponential function: $\boldsymbol{y = y_0 + a*e^{-bx}}$ (b is reaction constant k or $T_{1/2}$= *ln2/b*). One example of exponential decays of $P700^+$ reduction curves in WT is shown below (Fig. 3.7.7). The bigger the relative rate constants (*b*) of $P700^+$ rereduction kinetics, the faster the CET.

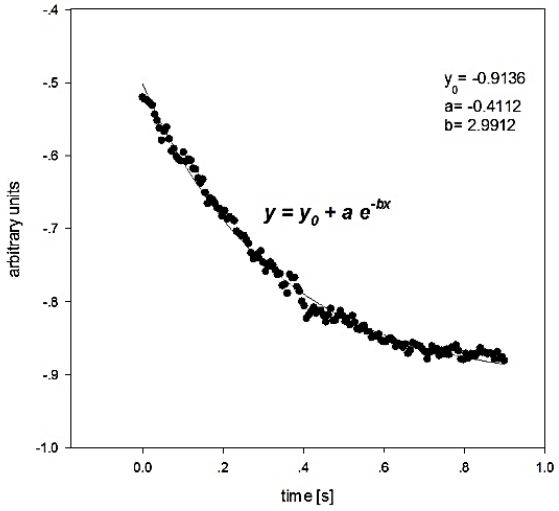

Fig. 3.7.7 The exponential decays of $P700^+$ reduction curves with the addition of 10 µM DCMU. Single exponential function ($\boldsymbol{y = y_0 + a*e^{-bx}}$) was used to stimulate this curve. Acquisition rate was set to 2 ms. Complete P700 oxidation was repeatedly achieved by a 200-ms saturation pulse (10000 µE m^{-2} s^{-1}) and a 30-sec pause.

3.7.8 The quenching analysis of chlorophyll fluorescence by Multi-Color PAM

Although PS II fluorescence is a minor pathway for excitation dissipation, it competes with the quantitatively more important energy dissipation routes of PS II photochemistry, excitation transfer to other pigment systems (such as PS I), and heat dissipation. Therefore, changes in photochemistry or in the nonphotochemical routes causes changes in the fluorescence yield from PS II. A novel multi-color pulse amplitude modulation (Multi-Color PAM, Heinz Walz GmbH, Germany) was used to monitor the chlorophyll fluorescence (Schreiber et al. 2012). The curves were drawn with the software Pam Win-3 v.3.12g.

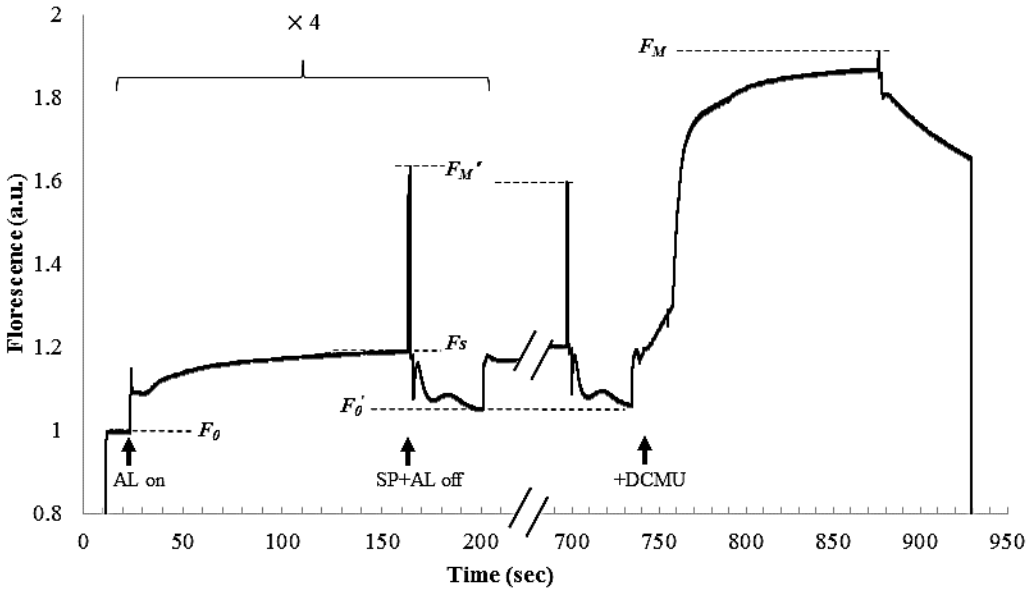

Fig. 3.7.8. Chlorophyll florescence analysis by Multi-Color PAM. Florescence was induced for 120sec by actinic light (AL, 20 µmol photons m^{-2} s^{-1}) followed by a saturation pulse (SP, 10000 µmol photons m^{-2} s^{-1}, 200 ms) and 30sec of actinic light off. 10 µM DCMU was added to interrupt the electron to PQ pool during the 5th actinic light and therefor achieve the maximal fluorescence yield by the saturation pulse. A typical curve of chlorophyll florescence of *Synechocystis* Wild-type cells grown in BG11 was shown. Data are representative of three independent experiments. a.u., Arbitrary units.

Photochemical quenching reflects a lowering of fluorescence below maximal levels through photochemical competition with fluorescence emission. Thus, when all PS II reaction centers are open and the potential for photochemistry is maximal, photochemical quenching of fluorescence is also maximal and fluorescence yield is low (F_0 or F_0' in Fig. 3.7.8). Conversely, when all PS II centers are closed and no photochemistry can occur (with the presence of 10 µM DCMU), photochemical quenching is zero and the fluorescence yield is maximal (F_M or F_M' in Fig. 3.7.8). In practice, photochemical quenching is quantified by the photochemical quenching coefficient (Campbell et al. 1998): $q_P = (F_M'-F_S)/(F_M'-F_O')$. q_P reflects the balance between

excitation of PS II centers, which closes them, and removal of electrons from PS II by the electron transport chain, which reopens the centers.

A specific protocol for the analysis of chlorophyll fluorescence by Multi-Color PAM is shown below:

(a) Connect the Multi-Color PAM with computer and open the software Pam Win-3, followed by loading the program "*Johanna-1*". Make sure all the connection was available. Blue light (wavelength of 440 nm) was used as measuring light for the fluorescence.
(b) Per measurement use 2 ml cell suspension (adjust to 2.5 µg/ml chlorophyll). Pellet the cells and adjust to the cell concentration by discarding the supernatant or adding the old supernatant (note: not the fresh BG11 medium!) if the chlorophyll content is too low.
(c) Pipette culture into the cuvette (quartz, with a small magnet inside).
(d) Stir for 30 sec in darkness, and then turn stirring it off.
(e) Start the program (Press the "*Start*").
(f) After 4 peaks (about 10mins later), add 2ul DCMU (finally 10 µM) into the cuvette and then stir for about 5 sec and stop quickly.
(g) When the program window is closed, press "*MC*" to stop the program.
(h) Press "*Mode*", and change "*measure*" model to "view" model, and choose the correct measurement number in "*View*"- "*Rpt*" (Note: Important step! Check your saved file and if the data is correct).
(i) Export data as *.csv*-file and save data.
(j) Rinse cuvette with 2 times of distilled H_2O, 3 times of 70% ethanol, 3 times of distilled H_2O, in turn, if DCMU was added in the cuvette as inhibitor.
(k) Pick up new cultures and start new measurement.
(l) Data analysis was operated in Excel program with a specific template.

3.7.9NAD(P)$^+$/NAD(P)H determination

Small volume assay of for the determination of NADH/NAD ratios were done with BioVision's NADH/NAD Quantification Colorimetric Kit (BioVision, California, USA) (Chen 2014). The NAD Cycling Enzyme Mix in the kit specifically recognizes NADH/NAD. The reaction specifically detects NADH and NAD, but not NADP nor NADPH. The enzyme cycling reaction significantly increases the detection sensitivity and specificity. NADt (NAD and NADH) or NADH can be easily quantified by comparing with standard NADH.

All the cultures used for NAD$^+$/NADH determination experiments were grown fermentatively in 70 ml BG-11 medium or BG-11_0 medium containing 5 mM arginine. 5 ml to 10 ml cells, equivalent to approximately 1.0 x10^9 cells/ml (10 ml cultures of OD750 of 1) were harvested for the measurements.

The cells were centrifuged at 3500 g at -9 °C for 10 min and the pellets were resuspended with 1 ml of 20 mM cold PBS (Phosphate buffered solution, Table 3.3). The suspension was transferred to a 2 ml reaction cup and was centrifuged at 12000 g, -9 °C, for 1 min. The pellet was resuspended in 50 µl extraction buffer

(BioVision, California, USA), and precooled glass beads (a diameter of 0.18 mm) were added nearly (0.5-1 mm) to the surface of the liquid. The mixture was vortexed 4 times for 1 min at 4 °C and chilled on the ice for 1 min intermediately. 150 µl extraction buffer was added again and the mixture was centrifuged at 3500 g, -9 °C, for 10 min. The liquid phase was transferred as much as possible into a new reaction cup and centrifuged at maximum speed for 30 min at -9 °C.

The supernatant was transferred into precooled 10 kD spin columns (BioVision, California, USA). The sample was centrifuged at 10000 g, -9 °C, for 10 min. The flow through liquid was divided into two 30 µl portions. One was incubated with 30 µl NADH extraction buffer (BioVision, California, USA) at 60 °C for 30 min and chilled on ice immediately and then was quickly spun to remove any precipitate to determine the amount of NADH present in the cells. To the other one 30 µl NADH extraction buffer (BioVision, California, USA) was added on ice.

2 times 25 µl heated and 2 times 25 µl non-heated samples were placed in four wells of a 96-well microtiterplate, and 2.5 µl of all these samples were also placed with 22.5 µl NADH extraction buffer as concentration control. 50 µl NAD Cycling Mix (BioVision, California, USA) was well mixed and pipetted into each well and incubated for 5 min at room temperature. Then 10 µl NADH developer (BioVision, California, USA) was added into each well and incubated for 1 to 4 hours before measuring absorbance at 450 nm by TECAN GENios machine (TECAN Group Ltd., Austria). The reactions were stopped by adding 5 µl of stop solution (BioVision, California, USA) into each well. The color should be stable for 48 h with the stop solution and was sealed at 4 °C with foil. The plates were read at OD 450 nm. The values were collected by the software Magellam.

10 µl of 1 nmol/µl NADH standard was diluted (Biovision, California, USA) with 990 µl NADH/NAD Extraction Buffer to generate 10 pmol/µl standard NADH. Addition of 0, 1, 2, 3, 4, 5 µl of the diluted NADH standard into labeled 96-well plates in duplicate, generated 0, 20, 40, 60, 80, 100 pmol/well standards. A final volume to 25 µl was achieved by addition of NADH/NAD extraction buffer. (Note: diluted NADH solution is unstable, and must be used within 4 hours.) All the diluted NADH standards were treated as other samples mentioned above.

With the aid of the standard curve the different concentrations of total NAD^+/NADH and NADH alone can be calculated.

Similar procedure for small volume assays was performed with BioVision's NADPH/NADP Quantification Colorimetric Kit (BioVision, California, USA).

3.7.10 Glucose quantification with the HK/G6PDH assay

The basic idea of this quantification system is the coupling of glucose consumption to the generation of NADPH which has, in contrary to glucose, a distinguishable absorption maximum and is thus photometrically

quantifiable. This is achieved by combining the activity of two enzymes: Hexokinase (HK) and glucose-6-phosphate dehydrogenase (G6PDH or ZWF) (see below).

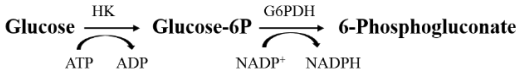

When excessive amounts of ATP and $NADP^+$ are present, the reaction can be drawn towards the product site resulting in a state where all glucose is consumed. The amount of NADPH that is formed in the meantime is proportional to the initial amount of glucose and can be measured photometrically as a change in absorption at 340 nm. A glucose standard curve is used to calibrate the change in absorption to a glucose concentration.

The 96-well plate reader (Plate Reader Infinite M200Pro, Tecan, Austria) was used to do the photometric measurement with the help of Dr. Christoph Plieth. An overview of the procedure is shown below.

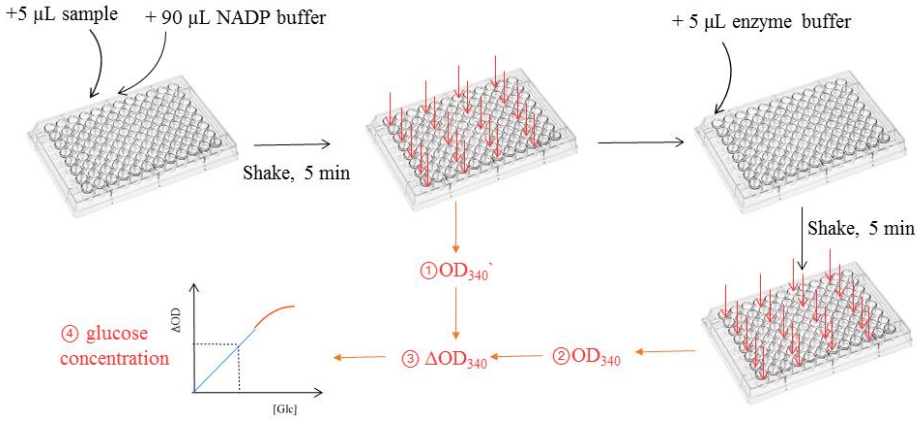

Fig. 3.7.10. The procedure of glucose quantification assay with a 96-well plate reader (Alexander Makowka, unpublished).

As shown in Fig. 3.7.10, the whole process contains five steps: 1) determination of baseline absorbance (OD_{340}'); 2) determination of endpoint absorbance (OD_{340}); 3) calculation of net absorbance (ΔOD_{340}); 4) preparation of standard curve and read-out of sample concentration.

(a) Step 1 & 2: Measuring baseline and endpoint absorbance (OD_{340}' and OD_{340})

Step one and two are the only steps that are done inside the laboratory, all other steps involve evaluation and are done at the computer. However, it is necessary to talk about the three kinds of solutions that are involved here: 1) the sample/standard, 2) the NADP buffer and 3) the enzyme buffer.

For assays with the 96-well plate reader, a sample volume of 5 µl (containing less than 5 mM glucose) was added in 100 µl of the whole reaction volume (Table 3.9). The final whole reaction volume is recommended to be a larger volume (200 µl or 250 µl) as well, however, if you do that you might have to make further adaptations in the concentrations of other reagents as well as the standard range. Dilution of the sample is normally necessary due to too high concentration of glucose in samples. The diluting factor depends on the

growth conditions of *Synechocystis* cells. According to our experience, normally samples grown under autotrophic, mixotrophic, and heterotrophic conditions are recommended to be diluted 2, 10, and 5 times, respectively.

Table 3.9. Composition of reaction of HK/G6PDH assay.

Reagent	**Stock conc.**	**Final conc.**	**Dilute factor**	**Final vol.**	**NADP buffer vol.**	**Enzyme buffer vol.**
sample/standard	< 5 mM	< 0.25 mM	20	50 µl	-	-
NADP	150 mM	2 mM	75	13.33 µl	13.33 µl	-
ATP	150 mM	2 mM	75	13.33 µl	13.33 µl	-
MgCl2	300 mM	3 mM	100	10 µl	10 µl	-
Hk/G6PDH	-	0.5 U	-	0.5 µl	-	0.5 µl
Tris-HCL	100 mM	91.3 mM	1.1	912.83 µl	863.33 µl	49.5 µl
Total (x 10)	-	-	-	1000 µl	900 µl	50 µl

The NADP buffer comprises the main part of the reaction mixture and contains everything that is needed for the reaction except the enzymes. The enzymes are part of the enzyme buffer which is added lastly and has the purpose to start the reaction. Table 3.9 shows exemplarily concentrations and volumes of the used solutions, including the concentrations of the stock solutions (second column), final concentration of each reagent in the reaction (third column), the dilution factor (fourth column), the final volume of each reagent in the reaction (fifth column), as well as the volumes of each reagent required for the preparation of 900 µl NADP buffer (sixth column) and 50 µl enzyme buffer (seventh column). For the purpose of understanding it might be noteworthy that an addition of all volumes in the sixth and seventh column yield the fifth column. When preparing the buffers, the volumes in the table can easily be scaled up to fit the number of your samples. The buffers should always be prepared freshly.

(b) Step 3: Calculation of net absorbance (ΔOD_{340})

The next step is the calculation of net absorbance (ΔOD_{340}) which can be defined as the change of absorption caused by enzymatic consumption of glucose. Basically, this is just the subtraction of the baseline absorbance from the endpoint absorbance, however, for an exact calculation the following formula should be used:

$$\textit{Net absorbance } (\Delta OD_{340}) = \textit{endpoint absorbance } (OD_{340}) - 19/20 * \textit{baseline absorbance } (\Delta OD_{340}')$$

The factor (19/20) derives from the fact that addition of enzyme buffer causes a dilution of the sample. This correction can be neglected if the baseline absorbance value is small.

(c) Step 4: Standard curve

The standard curve (or calibration curve) is used to calibrate ΔOD_{340} values to a glucose concentration. This is achieved by measuring sample solutions with a known glucose concentration, so-called standards. An exemplary standard curve is shown below.

The most important parameter of a standard curve is its linearity range. A linear standard curve is a good measure for a complete glucose oxidation, indicating a sufficient incubation time and sufficient substrate (ATP, $NADP^+$) concentrations. Only samples that fall into the linear range of the standard curve should be used. In the exemplary standard curve (Fig. 3.7.10a), the permitted calibration range reaches from 0 to a ΔOD_{340} value of 1.6 which resembles a glucose concentration of 10 mM (note that this is not the actual glucose concentration in the reaction mix but the concentration of the standard prior to putting it into the reaction). Standards with a (Ninfa et al.) concentration of 5 mM, 2.5 mM, 1.25 mM, 0.625 mM and 0 mM in duplicates were recommended in this work. These concentrations can easily be prepared by doing a series dilution.

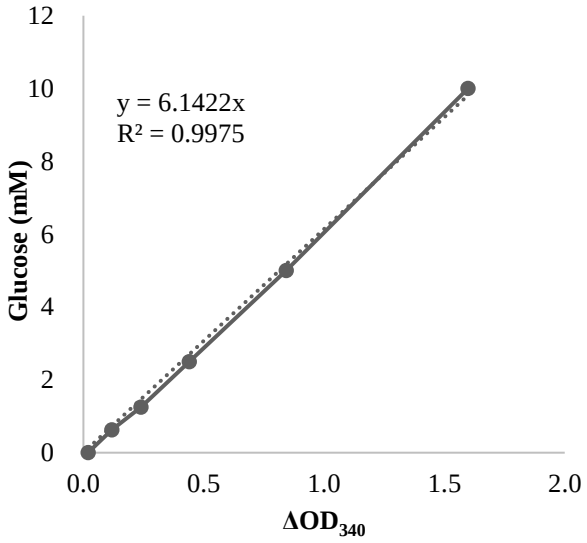

Fig. 3.7.10a: The linear relationship of stand glucose and net absorbance at 340 nm (ΔOD_{340}). Glucose standard buffers with a concentration of 10 mM, 5 mM, 2.5 mM, 1.25 mM, 0.625 mM and 0 mM were measured at 340 nm by the 96-well platereader in duplicates.

Step 5: Calculation of glucose concentration

After applying a linear regression on your standard curve, you can read out the equation which should have a form like this:

$$f(x)=y = m * x + b$$

The variables $f(x)$ and x represent the glucose concentration and ΔOD_{340} respectively. b is set to 0 in this work.

3.7.11 Glycogen quantification

Glycogen cannot be quantified directly and therefore needs to be convert to glucose by amyloglucosidase for subsequent determination. The detailed protocol for glycogen quantification assay used in this work is below (modified from Gründel et al. 2012)

Step 1: Conversion of glycogen to glucose

(a) Harvest 2-15 OD*ml cells by centrifugation (10 min, 10000g, RT).
(b) Resuspend pellet in 300 µl 30 % (w/v) KOH and transfer to 2 ml Eppendorf cup.
(c) Incubate in heat block (at 95 °C) for 2 h.
(d) Add 1000 µl 100 % cold ethanol and incubate at -20 °C (2 h or overnight).
(e) Centrifuge (10 min, 10000 g, 4 °C) and discard supernatant.
(f) Add 1 ml 70 % ethanol and centrifuge (5 min, 10000 g, 4 °C).
(g) Discard supernatant, add 1 ml 100 % ethanol and centrifuge (5 min, 10000 g, 4 °C).
(h) Remove supernatant completely (with pipet) and dry pellet in heat block (50 °C, ~ 10 min).
(i) Add 200 µl AG solution containing 180 µl 100 mM sodium acetate (pH 4.5) and 20 µl (15 mg/ml) amyloglucosidase.
(j) Incubate for 90 min at 60 °C in heat block.
(k) Centrifuge (10 min, 10000 g, RT) and transfer 50 µl supernatant to a new 1.5 ml cup (it might be necessary to dilute mixotrophic samples).

Step 2: Glucose quantification assay

(a) Prepare 50 µl glucose standards with following concentrations: 5 mM, 2.5 mM, 1.25 mM, 0.625 mM and 0 mM.
(b) Add 950 µl glucose test reagent to all samples and standards.
(c) Incubate in cell incubator (37 °C) for 30 min.
(d) Measure absorption at 340 nm (OD_{340}) (UV cuvettes, use water as blank)

Step 3: Calculation of specific glycogen content (µg OD_{750}^{-1} ml^{-1})

a) Plot standard curve and calculate slope (m) and y-intercept (b) as Fig. 3.7.10a.
b) Calculate sample glucose concentration in mM as follows: $[Glc] = (OD_{340} - b)/m$.
c) Convert to glycogen mass in µg by multiplying with 32.4288 if necessary.
d) Divide by OD_{750}*ml (which is the OD_{750} value and volume of original sample/cell culture).

3.7.12 Arginine or cyanophycin extraction and quantification

One molecule of cyanophycin contains one molecule of arginine. Therefore the concentration of cyanophycin equals the amount of arginine. The detailed protocol of cyanophycin quantification is shown below (modified from Elbahloul et al, 2005; Messineo L, 1996).

Step 1: Cyanophycin extraction:

(a) Collect 25 ml culture (OD_{750}=1.0) by centrifugation (10min, 4000 g, RT).

(b) Add 1 ml acetone to the pellet and incubate in a shaker,1400 g for 30 min.

(c) Centrifuge the sample at 13000 g for 10 min and discard the supernatant.

(d) Resuspend the pellet in 1.2 ml 0.1 M HCl and incubate for 1 h at 60 °C and 1400 g shaking;

(e) Centrifuge the sample at 13000 g for 10 min at 4 °C.

(f) Take the supernatant and add 300 µl 0.1 M Tris/HCl, pH 9.0(If applicable, check the pH and adjust it to 7.5-7.8 by adding 100 µl of 1 M NaOH normally).

(g) Incubate for 40 min at 4 °C.

(h) Centrifuge the sample at 18000 g for 15 min and discard the supernatant.

(i) Solve the pellet in 1 ml 0.1M HCl and use for the quantification.

(j) Prepare 1 ml arginine standards with the following concentrations: 0 µg, 10 µg, 20 µg, 30 µg, 40 µg, 50 µg, 60 µg, 70 µg.

Table 3.10. Reagent used for arginine determination in this work

Reagent	**Composition**
A	300 mg KI (Potassium iodide) in 100ml distilled H_2O
B	100 ml 5 M KOH + 2 g Potassium sodium tartrate + 0.1 g 2,4-dichloro-1-naphthol +180 ml absolute Ethanol + x ml NaClO
C	5%(v/v) NaClO with distilled H_2O

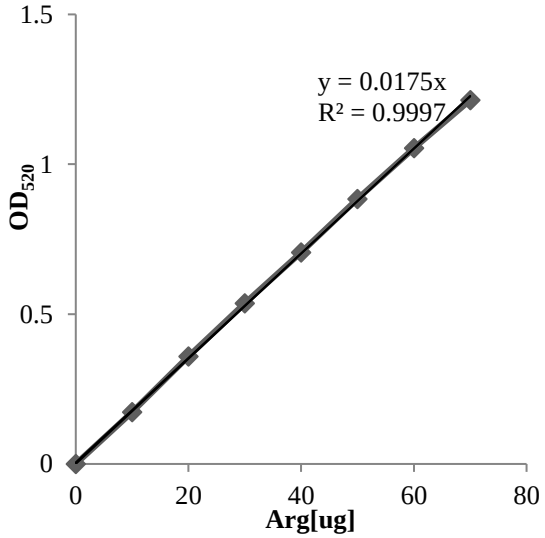

Fig. 3.7.12. Standard curve generated using the absorbance at 520 nm (OD_{520}) for known concentrations of arginine (Arg). Arginine standards with a concentration of 0 µg, 10 µg, 20 µg, 30 µg, 40 µg, 50 µg, 60 µg and 70 µg were measured in duplicates, respectively.

Step 2: Cyanophycin quantification using the Sakaguchi Reaction:

(a) Add 166 µl Reagent A (Table 3.10) to 166 µl sample/standard containing from 10 to 100 µg arginine (0.057 µM - 0.5 µM, 0.1 M HCl).
(b) Add 500 µl of Reagent B (Table 3.10) and incubate for 1 hour at RT.
(c) Add 166 µl of Reagent C (Table 3.10) and incubate for exactly 10 min.
(d) Immediately read the absorption at 520 nm against a blank without arginine/cyanophycin.

3.7.13 Nitrite determination

The present protocol is based on versatile spectrometry with cheap reagents, making it practicable for many researchers. Under acidic conditions, nitrite reacts with sulfanilamide hydrochloride to produce a diazonium compound that undergoes diazocoupling with *N*-(1-naphthyl)-ethylene-diamine dihydrochloride to form a pink azo compound. The amount of the azo dye formed is proportional to the initial concentration of nitrite over a wide range of concentrations (0 -10 µM) (Grasshoff et al. 2009). This method is very sensitive and is unaffected by the presence of other constituents normally occurring in seawater (Grasshoff et al. 2009). The detailed procedure is shown below (modified from Grasshoff et al, 2009).

(a) Dilute samples whose concentrations exceeds 3 µM nitrite (the dilution factor is 1:3000) with distilled water.
(b) Prepare a nitrite standard series using sodium nitrite (0, 0.1, 0.5, 1.0, 2.0, 3.0, and 5.0 µM) with ddH_2O.
(c) Transfer 1ml of samples/standards (containing 0-5.0 µM of nitrite) or ddH_2O to 2 ml Eppendorf cups.
(d) Add 20-30 µl sulphanilamide (Reagent 1) and mix and leave reaction for 1 min (at RT or 4 °C).
(e) Add 20-30 µl aromatic amide (Reagent 3, *N*-(1-naphthyl)-ethylene-diamine dihydrochloride) and shake and the azo dye is allowed to develop for at least 15 min.
(f) Measure the absorbance at 540 nm against a reference of the respective ZW within 1 h after the addition of the reagents.
(g) Calculate the concentration of samples according to the standard curve as reference.

For the nitrite excretion determination, similar operations were done as described above except that the optical denstiy cultures grown under heterotrophic conditions should be enough low (OD_{750} < 0.5). Ortherwise, the turbid color of supernant or the chemicals excreted into medium will affect the absorbance at 540 nm and subsequnectly affect final values, no matter it is after or before reacting with aromatic amine to form a diazonium.

3.7.14 Nitrate determination

One method for the determination of nitrate is based on the reduction of nitrate to nitrite in the presence of Zn/NaCl (Narayana and Sunil 2009). The produced nitrite is subsequently diazotized with sulphanilamide and then coupled with aromatic amide to form an azo dye and was measured at 540 nm, which have been introduced in the method of nitrite determination (Grasshoff et al. 2009). The detailed procedure is shown below.

(a) Dilute samples whose concentrations exceeds 3 μM nitrate (the dilution factor is 1:5000) with distilled water.
(b) Prepare a nitrate standard series using potassium nitrate (0, 0.5, 1.0, 2.0 and 4.0 μM KNO_3).
(c) Transfer 1000 μl aliquots of sample/standard containing 0-5 μM of nitrate to 2 ml Eppendorf cup.
(d) Add 500 μl of Conc. HCl and 200 μl of Zn/NaCl granular mixture and stand for 30 mins, occasionally stirring to form nitrite or put on mixture inverter.
(e) Centrifuge at 10000 g for 5 min and transfer the supernatant to new 2 ml Eppendorf cup.
(f) Pick up 1 ml samples (containing 0-5.0 μM of nitrite converted from nitrate) or ddH_2O and transfer in 2 ml Eppendorf cups.
(g) Continue the measurement as the procedure of nitrite determination in Section 3.7.13.
(h) Calculate the nitrate concentration of samples according to the standard curve as reference.

Another method we used in this work is the detection of nitrate directly by absorbance at 210 nm (Kloft and Forchhammer 2005). The cells were removed from the medium by centrifugation, and the absorbance of nitrate was measured at 210 nm. Since the absorbance at 210 nm detects both nitrate and nitrite, the apparent nitrate values were corrected for the presence of nitrite. However, the excreted nitrite to the medium (BG11 containg 10 mM Glucose) was negliable after 5000 times of dilution.

Fig. 3.7.14b indicats that there is a significant trend of linear correlationship between the absorance at 210 nm (OD_{210}) and nitrate concentration in the standard medium. However, the absorbance at 210 nm of mixotrophic media (BG11 containing 10 mM glucose) was reduced, which means that certain chemical components in the medium affect the absorbance of nitrate at 210 nm (Fig. 3.7.14c.A). Furthermore, supernatants from cultures grown under heterotrophic conditions were also determined by this method. The unexpected higher concentration of nitrate on the 4^{th} and 6^{th} day than that on 1^{st} day indicates that some dissolved organic carbon (such as acetate, succinate) or other chemicals possessing high absorbance at 210 nm were excreted into the medium during the growth under heterotrophic conditions. In summary, this described method by UV spectrophotometry is only suitable for BG11 medium without glucose but not the supernatant from culture grown with glucose.

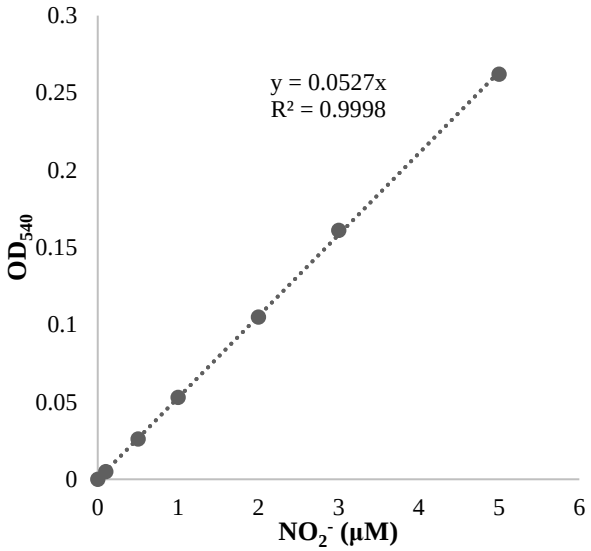

Fig. 3.7.13. Standard curve generated using the absorbance at 540 nm for known concentrations of nitrite (NO_2^-). Nitrite standards (KNO_2) with a concentration of 0 µM, 0.1 µM, 0.5 µM, 1.0 µM, 2.0 µM, 3.0 µM and 5.0 µM were measured in duplicates via the spectrophotometer, respectively

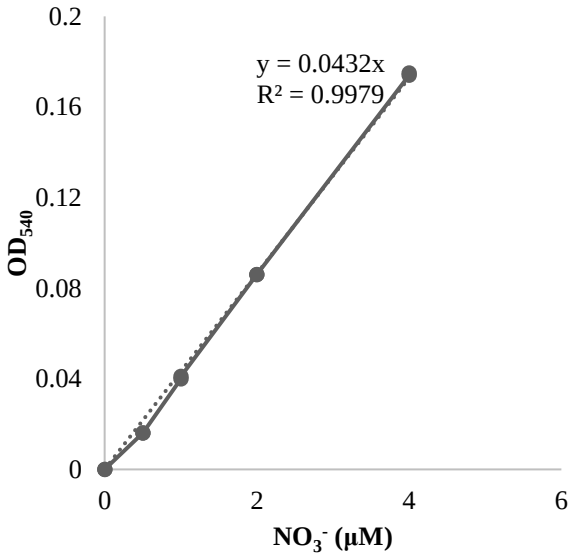

Fig. 3.7.14a. Standard curve generated using the absorbance at 540 nm for known concentrations of nitrite (NO_2^-) convered from nitrate (NO_3^-). Nitrite standards (KNO_3) with a concentration of 0, 0.5, 1.0, 2.0 and 4.0 µM were measured in duplicates via the spectrophotometer, respectively

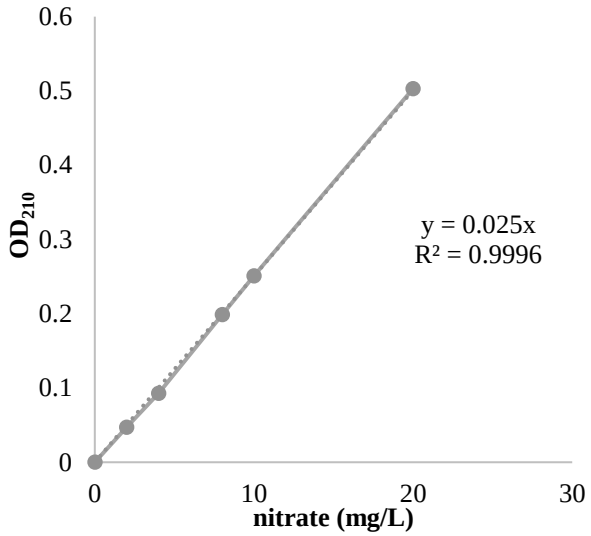

Fig. 3.7.14b. The standard calibration line for nitrate determination at 210 nm. Nitrite standards (KNO_3) with a concentration of 0, 2, 4, 8, 10 and 20 mg/l were measured in duplicates via the spectrophotometer, respectively.

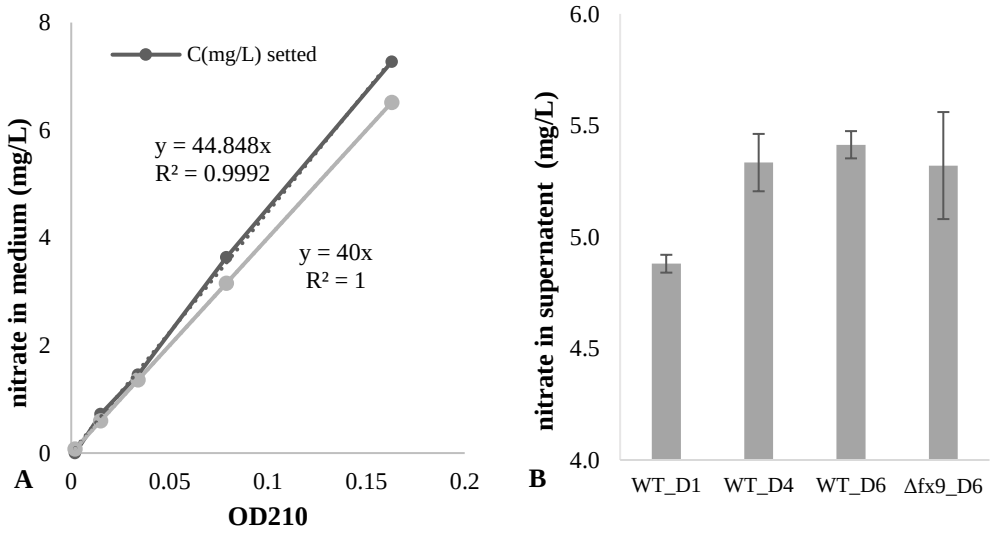

Fig. 3.7.14c. Nitrate determination in BG11 medium containing glucose. A: The absorbance of standard BG11 medium with 10 mM glucose at 210 nm. Nitrite standards (KNO_3) with a concentration of 0, 0.73, 1.46, 3.64 and 7.28 mg/l were measured in duplicates via the spectrophotometer, respectively. B: Nitrate determination in supernatant from heterotrophic cultures of Wild-type and *Δfx9*. D1 means picking up sample on 1st day. Three biological repeats per sample.

3.7.15 Transmission Electron microscopy (TEM)

Synechocystis cells in 30 ml cultures were harvested at 8000 g for 3 min and resuspended with 2 ml old growth medium. The concentrated cells were fixed with 2 ml of a solution containing 5% glutaraldehyde

(GA) and 2% paraformaldehyde (FA) in 0.2 M cacodylate buffer (pH 7.3). Samples were put in 4 °C refrigerator (up to a week) or directly sent to the technician (Ms. Marita Beese) and subsequently treated according to the methods and techniques used at the TEM Center Kiel.

3.8. Molecular Biological Methods

3.8.1 Extraction and purification of DNA

3.8.1.1 High-copy plasmid DNA preparation from *E. coli*

A single colony was used to inoculate 3 ml of liquid LB medium containing the appropriate antibiotic(s) and the cells were incubated overnight at 37 °C under vigorous shaking. Cells of the 2 ml culture were harvested and used to isolate plasmids. High-copy plasmid DNA preparations from *E. coli* were performed using the NucleoSpin Plasmid Kit (MACHEREY-NAGEL, Düren, Germany) according to the manufacturer's instructions (see Plasmid DNA purification User manual 2017, Rev. 10, p.15).

3.8.1.2 Small scale isolation of chromosomal DNA from *Synechocystis*

Small scale isolation of chromosomal DNA from *Synechocystis* was performed according to the phenol-chloroform extraction method devised by Dr. Josef Komenda (Institute of Microbiology, Trebon, Czech Republic). A pea-sized glob of *Synechocystis* cells from a BG-11 agar plate was resuspended in 200 µl of TE buffer and 200 µl of phenol were added. The suspension was extracted twice for 20 sec by hand and centrifuged in a microfuge (Eppendorf Centrifuge 5415D, Eppendorf, Germany) at maximum speed for 2-5 min. The upper phase was transferred to a new tube and 150 µl of chloroform was added. The mix was extracted for 30 sec by hand and centrifuged in a microfuge at maximum speed for 2-5 min. The aqueous phase was transferred to a new tube and a tenth sample volume of 3 M sodium acetate (pH = 4.8) together with two volumes of 99 % (v/v) ethanol were added and then mixed gently. The sample was kept at –20 °C overnight followed by centrifuge at maximum speed for 30 min (at 4 °C). The obtained pellet was washed with 500 µl 70 % (v/v) ethanol, resuspended in 100 µl nuclease-free water and stored at 4 °C or –20 °C. 1 µl of obtained DNA could be used for 50 µl PCR as template directly.

3.8.1.3 Total cellular DNA extraction from *Synechocystis*

Total cellular DNA extraction from *Synechocystis* was performed according to the phenol-chloroform extraction method devised by Dr. Kirstin Gutekunst.

Synechocystis cells were pelleted or directly scratched from one half of an agar plate and transferred into a 2 ml sterile Eppendorf cup. The cells were resuspended in 100 µl TE buffer (pH 7.4). 100 µl Phenol-chloroform-isoamylalcohol (25:24:1) and an equal volume of sterile glass beads (0.25-0.5 mm), followed by the addition of 2 µl 10 % (w/v) SDS. The cell walls were disrupted by vortexing this mixture for 10 min (1

min x 10) at 4 °C, cooled on ice in-between, and then centrifuged at 10000 g for 10 min (Centrifuge 5804R, Eppendorf, Germany). The aqueous supernatant containing the nucleic acids was transferred into a new 1.5 ml cup and diluted with equal volume of phenol chloroform isoamylalcohol (25:24:1). After another centrifugation step for 10 min at 10000 g, the upper phases were transferred into a new reaction cap. This step was repeated until the interphase disappeared or was barely visible. Then the cup was filled with chloroform isoamylalcohol (24:1) whose volume was the same as the upper liquid phase and centrifuged for 10 min at 10000 g. This step extracted the phenol out of the upper phase and was repeated several times until the pink color in the upper phase mostly disappeared. The supernatant was then transferred to a new cup. DNA precipitation was done by addition of a tenth of the supernatant-volume of 3 M sodium acetate (pH 4.8) and a 2.5-fold volume of 100 % ethanol (-20 °C). After incubation at -20 °C overnight, DNA was centrifuged down for 15 min at 13000 g and -9 °C. The pellets were washed with 70 % (v/v) ethanol and centrifuged again for 5 min at 10000 g. The supernatant was discarded and the pellet was dried at 37 °C in an incubator (Memert, Schwabach, Germany). The dry pellet was dissolved in 20 - 50 µl TE buffer (pH 7.4) and stored at 4 °C or –20 °C.

3.8.1.4 Estimation of DNA concentration and quality

DNA concentration was determined by two methods in parallel. A Nanodrop (NanoDrop ND-1000 Spectrophotometer, Thermo Scientific, USA) was used to measure the concentration of nucleic acids in 1µl sample from the genomic DNA extraction. The other measuring way was to separate the DNA sample on 0.8% (w/v) agarose gels. By this way, DNA concentration was estimated by comparing the bright of the band to a Lambda DNA/HindIII marker (Thermo Scientific™, Life Technologies GmbH, Germany) with defined DNA concentration.

3.8.2 DNA manipulations

3.8.2.1 Agarose gel electrophoresis

Agarose gel electrophoresis allows the separation of DNA fragments according to their sizes. Gels were prepared with molecular grade agarose dissolved in TBE buffer (Fig. 3.2.1) and 1 µg/ml ethidium bromide. Samples were loaded in the wells after the addition of 0.2 volumes (v/v) of 5 x loading buffer (Fig. 3.2.1). GeneRuler™ 1 kb DNA Ladder (Thermo Scientific™, Life Technologies GmbH, Germany) was used to calibrate the size and 1 ng/µl Lambda DNA/HindIII marker (Thermo Scientific™, Life Technologies GmbH, Germany) was utilized to determine the DNA concentration of the sample. Electrophoresis was performed with power supply at 5 V/cm (High Voltage Power Pack P30, Biometra, Goettingen, Germany) for 50 min. DNA could be visualized by using a UV light (TF 20 M Vilber Lourmat, Torcy, France) and photographs were taken by a PC connected live camera (EOS 2000D, Canon, Japan)

3.8.2.2 DNA purification from agarose gels

DNA fragments from agarose gels were purified using the high pure PCR product purification kit (Roche, Mannheim, Germany) according to the manufacturer's instructions. DNA was eluted from the spin column with two times 15 µl of nuclease-free water and stored at –20 °C.

3.8.2.3 Amplification of DNA fragments by polymerase chain reaction (PCR)

The polymerase chain reaction (PCR) is a biochemical technology to amplify nucleic acid fragments *in vitro* across several steps that are initiated by changes in temperature, generating thousands to millions of copies of these particular DNA sequences. PCR depends on a number of different parameters, for example the template, the primers, salt concentration, DNA polymerase etc.

Thermo Scientific™ Phusion™ High-Fidelity DNA Polymerase (Thermo Scientific™, Life Technologies GmbH, Germany) were used to amplify DNA fragments for high fidelity cloning and overlap extension. Due to the nature of Phusion DNA Polymerase, the optimal reaction conditions may differ from PCR protocols for standard DNA polymerases. Due to the high salt concentration in the reaction buffer, Phusion DNA Polymerase tends to work better at elevated denaturation and annealing temperatures. A detailed description of these steps used in this assay is listed in Table 3.11.

Table 3.11. Steps of PCR protocol.

Cycle step	Temperature/°C	Time	Cycles
Initial denaturation	98	30 s	1
Denaturation	98	5-10 s	
Annealing	X	10-30 s	30-40
Extension	72	15-30 s/kb	
Final extension	72	10 min	1
Incubation	4	+∞	1

Specific primers in Table 3.6 were designed by Primer-BLAST (https://www.ncbi.nlm.nih.gov/tools/primer-blast/) and produced by Sigma-Aldrich (Steinheim, Germany). The annealing temperature was calculated depending on the specificity and affinity between DNA template and primers. The elongation time was dependent on the length of the expected PCR product and the DNA polymerase. The lid of the PCR machine was heated during the program to prevent sample evaporation and condensation in the lid of the tube. Each PCR reaction contained in a total volume of 50 µl the following components (Table 3.12) in 200 µl caps and was programmed by the thermocycler (DNA- Engine PTC-200, Bio-Rad Laboratories, USA).

The reaction mixture and the PCR program were varied when the standard procedure did not yield an optimum amplification.

Table 3.12. Pipetting instructions: add items in this order

Component	Volume per 50 µl	Final concentration
H_2O	add to 50 µl	-
5x Phusion HF Buffer	10 µl	1 x
2.5 mM dNTPs	4 µl	200 µM each
Forward primer (5 µM)	5 µl	0.5 µM
Reverse primer (5 µM)	5 µl	0.5 µM
Template DNA (2 ng/µl)	5 µl	0.2 ng/µl
Phusion DNA Polymerase	0.5 µl	0.02 U/µl

3.8.2.4 DNA ligation

For transforming DNA fragments into chemically competent Top10 *E. coli* cells (Invitrogen, Karlsruhe, Germany), the fragments were ligated into the pCR2.1 TOPO vector (Invitrogen, Karlsruhe, Germany). The ligation was performed by using the TOPO TA cloning kit (Invitrogen, Karlsruhe, Germany) following the manufacturer's instructions, except that ¼ reactions were used. All the cups and tips here were prechilled before use. More details about Top10 *E. coli* cells and pCR2.1 TOPO vector could be found in Section 3.4.

3.8.2.5 DNA sequencing

All of the plasmid and DNA sequencing (Sanger et al. 1977) was carried out by the institute for clinical molecular biology (IKMB) in Kiel.

3.8.3 Construction of mutants

All mutants listed in Table 3.1 were constructed by inserting an antibiotic resistance cassette into the genome of *Synechocystis* via homologous recombination thereby replacing the target gene. The whole procedure containing the fusion-PCR, Topo TA-cloning, transformation of *Synechocystis* is shown in Fig. 3.8.3.

3.8.3.1 Fusion-PCR

DNA sequence of target genes listed in Table 3.1 were obtained from Cyanobase (http://genome.microbedb.jp/cyanobase/). The primers were designed for the upstream 200 bp to 500 bp sequence of the target gene, named gene-1, gene-in1. Additional primers were designed for the downstream

200 bp to 500 bp sequence of the target gene, named gene-in2, gene-2. All the primers used in this work are listed in Table 3.6.

Before conducting fusion PCR (Fig. 3.8.3), three normal PCRs were set up to amplify the upstream (with primer pairs: gene-1and gene-in1) and downstream (with primer pairs: gene-in2 and gene-2) fragments of the target gene, and the fragment of the antibiotic resistance cassette. The total amount of PCR products for the fusion PCR was 100 ng, which consists of three PCR products with an equal ratio according to their fragment sizes (upstream length: antibiotic resistance cassette: downstream length; 1:1:1). In contrast to the standard PCR, in the Fusion-PCR a of mixture of three PCR products as templates and Pfu-DNA-Polymerase (Promega, USA), instead of Phusion HF Buffer, as DNA polymerase, were used. The diluted Fusion-PCR product functions as template and primer for the 2nd Fusion-PCR, which is catalyzed by Taq-DNA-Polymerase (Thermo Scientific, USA), instead of Pfu-DNA-Polymerase, with primer pairs of gene-1 and gene-2. The temperature program steps are listed in table 3.11 (DNA-Engine PTC-200, Bio-Rad Laboratories, USA).

PCR products were run on 0.8% (m/v) agarose gels and compared to the Lambda DNA/HindIII Marker (Thermo Scientific™, Life Technologies GmbH, Germany) in order to estimate the concentrations of the products.

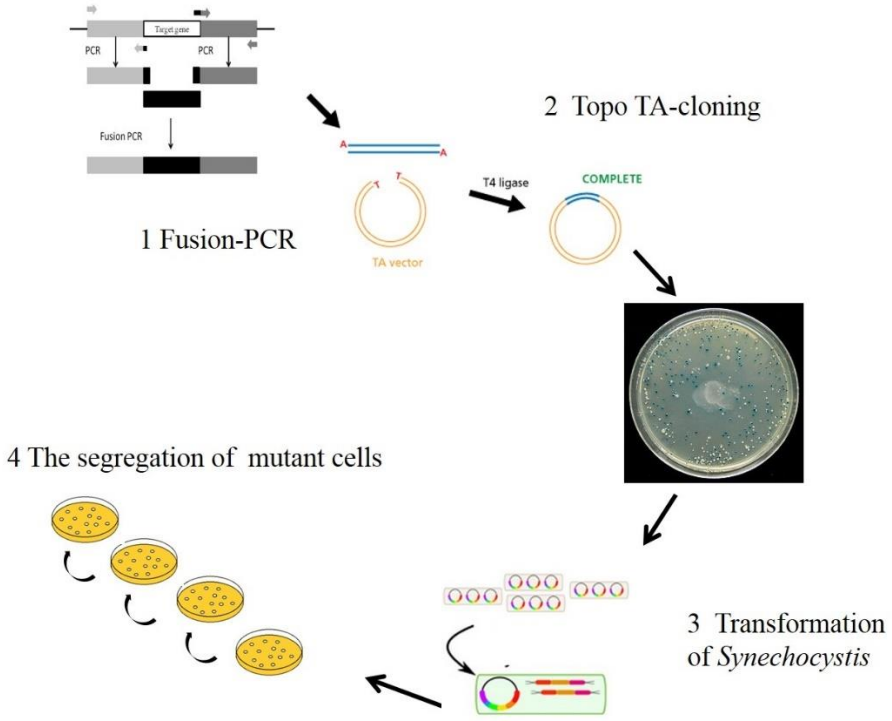

Fig. 3.8.3. Procedure of mutant construction in this work. All the mutants were constructed by inserting an antibiotic resistance cassette into the genome of *Synechocystis* via homologous recombination thereby interrupting the target gene. The mutant after the screen for at least ten generations were detected by normal PCR or the Southern-blot.

3.8.3.2 Topo-TA Cloning

The 2nd Fusion-PCR products were purified from agarose gels (see Section 3.8.2.2) and then transformed into chemically competent Top10 *E. coli* cells by ligation into the pCR2.1 TOPO vector (see Section 3.8.2.4).

X-galactose was supplemented on the solid LB medium (agar plate) containing antibiotic Kanamycin to select the positive clones, which were grown overnight in liquid medium containing the corresponding antibiotic (Fig. 3.8.3). When X-galactose is digested by the beta-galactosidase, which is expressed by the gene lacZ, a blue by-product will be produced. The pCR2.1 TOPO vector carries lacZ in its multiple cloning sites. Therefore, if the plasmids of the cell colonies carry an inserted sequence in their multiple cloning sites, the gene lacZ cannot be expressed and the colonies are white. Otherwise, the cells without any insert will get a blue staining due to the cleavage of galactose. Obviously, the positive clones with the required gene appear white, while the others are blue.

After overnight incubation, white colonies were picked with sterilized tooth-sticks and grown in 3 ml LB liquid medium with kanamycin in a shaker (4400 Innova Incubator Shaker, New Brunswick Scientific, Germany) at 180 rpm and 37°C overnight. High copy plasmid DNA of positive clones was extracted from cultures according to Section 3.8.1.

3.8.3.3 Transformation of *Synechocystis*

Cultures of *Synechocystis* were pre-grown at an optical density (OD_{750}) of 0.15 in 250 ml Kniese tubes (EYDAM, Kiel, Germany) with fresh BG-11 medium at 28 °C and 50 µE/m^2/s light intensity and were continuously bubbled with air for 24 hours. 250 ml cultures were used for 2 transformations. On the second day, 250 ml culture was harvested by centrifugation at 5000 g, RT, for 10 min and re-suspended in 1.5 ml of fresh BG-11 medium. 300 µl of the cell suspension was mixed with 6-18 µg plasmid DNA with the fusion PCR product cloned inside. The mixture was incubated in the shaker at 30 °C for 6 hours, during which these samples were inverted gently every 30 min.

After incubation, 100 µl of cells were spread on autoclaved nitrocellulose membrane filters (Poresize 0.45 µm, MACHEREY- NAGEL, Düren, Germany), which were laid on BG-11 agarose plates without any antibiotics. Triplicates were made and incubated in continuous light of 28 µE/m^2/s at 30 °C for 2 days. Then the filters were transferred to new plates supplemented with the corresponding antibiotic as described in Table 3.1. Two weeks later, single colonies could be picked and streaked onto new agar plates containing suitable antibiotic(s). Transformants were restreaked at least three times, until PCR analyses were performed to test for segregation. Copies of new segregated mutant grown in BG11 medium were stored at -80 ° C with half volume of 80% glycerol.

For the double mutant or triple mutant construction, the same procedure was used as described above. The only difference was that mutant cells instead of Wild-type *Synechocystis* cells were used for the transformation.

3.8.4 Protein biochemistry techniques

3.8.4.1 Small-scale protein isolation from *Synechocystis*

Synechocystis cells were pelleted from 10 or 50 ml culture at 3000 g, 4°C for 10 min and resuspended in 500 µl ACA buffer (25 mM Tris/HCl pH = 7.5, 1 mM ε-amino caproic acid). The suspension was transferred to a new 2 ml Eppendorf tube containing ~200 µl of glass beads (0.17-0.18 mm, Sigma Aldrich, Germany) were added. The mixture was vortexed at 4°C for 2 min (12 cycles: 10 seconds on followed by 10 seconds off at maximum speed). The glass beads were pelleted (centrifuge at 5000 g, 4°C for about 1 min) at the bottom of the tube and the supernatant was transferred to a new 1.5 ml Eppendorf tube. The pooled supernatants were centrifuged (centrifuge at 7000 g for 1 min) to pellet unbroken cells. The supernatant was transferred to a new Eppendorf tube and centrifuged again (centrifuge at 12000 g, 4°C for 20 min, 4 °C). The supernatant should be blue now.

3.8.4.2 Standard protein isolation from *Synechocystis*

Synechocystis cells were pelleted from a 250-ml culture grown in Kinese tube and resuspended in a 50 ml Falcon tube with 2 ml Puffer W (100 mM Tris, 150 mM NaCl, pH 8 (adjust pH with HCL). Glass beads (0.17-0.18 mm) were added to the suspension in which 2 mm (or more) liquid is still visible above the beads. The suspension mixture was cooled for 5 min on ice and subsequently vortexed for 10 x 1 min at full speed in the +4°C room, followed by centrifuge for 1 min at 2750 g, 4°C. The left supernatant was transferred to a new Eppendorf tube and pelleted again for 10 min at 3500 g, 4°C, followed by transferring the supernatant without glass beads to a new tube. The green supernatant could be checked under the microscope if there are still whole cells in the supernatant. In order to get soluble protein, the supernatant was centrifugated for 15 min at 14000 g, 4°C, to get rid of the membranes. Till now, the obtained supernatant should be blue color and was transferred to a new Eppendorf cup.

3.8.4.3 Determination of protein concentration

The protein concentration of a sample was determined via Bradford dye-binding method (Bradford 1976) with the Bio-Rad Protein Assay Kit (Bio-Rad Laboratories GmbH, München, Germany) according to the manufacturer's instructions (assay volume was reduced fourfold). ACA buffer is not compatible with this protein concentration determination method.

3.8.4.4 Protein precipitate

If the protein concentration was too low, samples were precipitated with acetone. In order to precipitate proteins from a sample, four times the sample volume of 100 % acetone (-20 °C) were added, the mixture

vortexed and incubated for at least 15 min (or overnight) at -20 °C. Precipitated proteins were pelleted in a precooled centrifuge at 14000 g for 10 min and resuspended in an appropriate volume of a desired buffer.

3.8.4.5 Polyacrylamide gel electrophoresis (PAGE)

Polyacrylamide gel electrophoresis (PAGE) was performed to separate complex protein mixtures according to their size differences into distinctive bands in a polyacrylamide gel matrix (Laemmli 1970).

Samples for SDS-PAGE analyses were prepared by mixing with protein loading buffer (2 x PLP: 125 mM Tris pH 6.8, 4% w/v SDS, 40% v/v glycerol, 0.2% w/v bromophenol blue, 10 mM dithiothreitol (DTT, added freshly before each use)). The mixture was incubated for 10 min at 95 °C, followed by transfer to ice and incubation for 1 min. Insolubilized material was pelleted by centrifuge very short time. Samples were either flash frozen in liquid nitrogen for storage at –20 °C or loaded into the stacking gel wells at maximum volumes of 15 µl for 15-well gels. 5 µl of the PageRuler™ Plus Prestained Protein Ladder (Thermo Scientific™, Life Technologies GmbH, Germany) was loaded as protein molecular weight markers for PAGE in this work. The gels were self-cast, 0.75 mm thick and routinely run in the Bio-Rad Mini-PROTEAN III vertical gel system (Bio-Rad Laboratories GmbH, München, Germany). was poured on the bottom of 4 % (w/v) stacking gel. The stacking gel, 4 % (w/v) polyacrylamide SDS-PAGE gel, was poured on top of the separation gel, a typical 10 % (w/v) continuous polyacrylamide SDS-PAGE gel (Table 3.13). When gels are polymerized, they could be used directly or covered with moist paper and kept at 4 °C.

Table 3.13. Separation gel and spacer gel made for SDS-PAGE

10 % separation gel		**4% spacer gel**	
Volume	**Reagent**	**Volume**	**Reagent**
3.75 ml	Buffer A (40 % acrylamide; 1.06 % Bisacrylamide)	0.9 ml	Buffer A (40 % acrylamide; 1.06 % Bisacrylamide)
5 ml	Buffer B (3M Tris/HCl pH 8.5; 0.3% SDS)	3 ml	Buffer B (3M Tris/HCl pH 8.5; 0.3% SDS)
6.25 ml	H_2O	5.1 ml	H_2O
5 µl	TEMED	20 µl	TEMED
50µl	10 % APS	100 µl	10 % APS

The gels were pre-run at 30 Volts until samples form a distinct band and continue with a constant voltage of 90 Volts for a period of 4 to 6 h using a Bio-Rad PowerPac Basic (Bio-Rad Laboratories GmbH, München, Germany) in a variant of the Laemmli running buffer (25 mM Tris, 190 mM glycine, 0.1 % (w/v) SDS, pH = 8.3) (Laemmli 1970). The obtained gels were either stained with Coomassie (see Section 3.8.4.6) or used for immunoblotting analyses (see Section 3.8.4.7)

3.8.4.6 Coomassie-brilliant-blue-R-250-staining of polyacrylamide gel

Gels were incubated for at least two hours, but preferably overnight, under gentle shaking in staining solution (40 % (v/v) ethanol, 10 % (v/v) acetic acid and 0.2 % (w/v) Coomassie-brilliant-blue-R-250). Background as well as stained proteins could be destained by incubation in the first destaining solution (40 % (v/v) ethanol and 10 % (v/v) acetic acid). Incubating the gel in the second destaining solution (10 % (v/v) acetic acid) would not destain proteins but would eventually completely remove any background staining.

3.8.4.7 Immunoblotting analysis (Western Blot)

SDS-PAGE gel was used for immunoblotting analyses using a protocol from Dr. Kirstin Gutenkunst. As shown in Fig. 3.8.4.7, protein transfer was performed for about 30 min in transfer buffer (3 mM Na_2CO_3, 10 mM $NaHCO_3$ and 20 % (v/v) methanol) onto nitrocellulose membrane (Roti-NC, 0.2 µm Transfer membrane for protein analyses, Carl Roth, Germany). The current to be used was calculated using the following formula: size of gel in cm^2 x 0.8 = current to be used in mA.

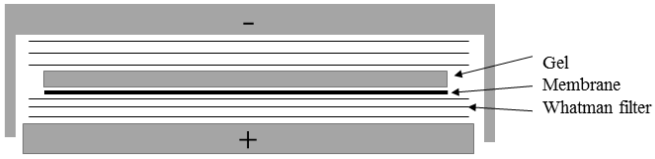

Fig. 3.8.4.7. Schema graph of Sandwich-Structure transblot. 6 moisten Whatman filter was used to cover gel and membrane. Gel: SDS-PAGE gel; Membrane: nitrocellulose membrane.

After the proteins were blotted, the nitrocellulose membrane was washed with TBS buffer (50 mM Tris-Cl, pH 7.5; 150 mM NaCl) for 2 x 10 min and subsequently blocked for 1h in Blocking Buffer (50 ml TBS, 2.5 g BSA, 0.05 g Tween, always prepare freshly). The membrane was then briefly washed at 4 °C with 1x PBS-Tween/Triton buffer (50 ml TBS, 0.025 g Tween, 0.1 g Triton) for 2 x 10 min, subsequently followed by being washed for10 min in TBS buffer and incubated overnight at 4 °C on rocking shaker with a primary antibody (40 ml TBS, 0.04 g Tween, 400 µl Anti-Phospho-Serin (0.1 mg/ml, Qiagen, Germany). On the following day the primary antibody solution was recycled and stored at -20 °C and the membrane was washed in 1x PBS-Tween/Triton buffer for 2 x 10 min and subsequently in 1x PBS buffer for 10 min. incubated at RT for 1 h with the appropriate secondary antibody (anti-mouse IgG+IgM) (1:10000 = 3 µl antimouse IgG+IgM (0.8 mg/ml) in 30 ml TBS with 3 g milk powder and 0.03 g Triton, always prepare freshly). Unbound secondary antibody was removed by washing the membrane for 4 x 10 min with 1x PBS-Tween/Triton. To obtain the optimum chemiluminescent signal, it was important to omit Tween 20 from the last two washing steps, as the detergent seemed to inhibit the peroxidase activity. The secondary antibody was detected by the enhanced chemiluminescence procedure. The membrane was incubated for 1-30 sec in a 1:1 mixture of Luminol Solution A (100 mM Tris/HCl pH = 8.5, 0.4 mM p-coumaric acid (90 mM stock

solution in DMSO), 2.5 µM luminol (250 mM stock solution in DMSO)) and Luminol Solution B (100 mM Tris/HCl pH = 8.5, 100 mM H_2O_2), put into a new freezing bag and exposed to a Röntgenfilm (Thermo Scientific™ CL-XPosure™ Film, Life Technologies GmbH, Germany) for 2 sec to 5 min. The film was developed according to the manufacturer's instructions (5 min in developer followed by being briefly washed in H_2O and then 15 min in Fixer followed by extensively washed for 30 min) and hanged up to let it dry.

3.9. Database and Bioinformatic programs

The databases, internet-based servers, software and programs that were used for the bioinformatic analyses in this work are listed below. The specific settings for these tools can be found in the respective result chapter.

Database:

Cyanobase: http://genome.microbedb.jp/cyanobase/

NCBI: https://www.ncbi.nlm.nih.gov/

NCBI proteins: https://www.ncbi.nlm.nih.gov/protein

UniProt or Swiss-Prot: https://www.uniprot.org/

Proteopedia: http://proteopedia.org/wiki/index.php/Ferredoxin

Programs and softwares:

BLAST (Johnson et al. 2008): http://www.ncbi.nlm.nih.gov/Blast.cgi

Primer-Blast (Ye et al. 2012): http://www.ncbi.nlm.nih.gov/tools/primer-blast/

GeneView (Thomas et al. 2012): https://omictools.com/geneview-tool

Reverse Complement: http://www.bioinformatics.org/sms/rev_comp.html

Nebcutter V2.0: http://tools.neb.com/NEBcutter2/

ProtParam tool (Gasteiger et al. 2003): https://web.expasy.org/protparam/

Clustal X (Version 1.81) (Larkin et al. 2007): http://www.clustal.org/clustal2/

BioEdit (version 7.2.6) (Hall et al. 2011): http://www.mbio.ncsu.edu/BioEdit/bioedit.html

3D Structure Viewer (NGL Viewer) (Rose and Hildebrand 2015): https://www.rcsb.org/pages/help/3dview

Phylogeny.fr (Dereeper et al. 2008): http://www.phylogeny.fr/index.cgi

4. Results

4.1. Construction of the ferredoxin mutants in *Synechocystis*

4.1.1Construction of the ferredoxin deletion mutants in *Synechocystis*

To date, nine highly-conserved ferredoxin-coding genes (*fx1-fx9*) and one flavodoxin (*isiB*) are known in the genome of the cyanobacterium *Synechocystis* sp PCC 6803 (Cassier-Chauvat and Chauvat 2014a). In order to study the function of ferredoxins and flavodoxin *in vivo*, deletion mutants of *Synechocystis* were created by deleting the ferredoxin-coding genes from the genome of *Synechocystis* and replacing them with antibiotic resistance cassettes.

Several ferredoxin deletion mutants, including *Δfx2*, *Δfx3*, *Δfx4*, *Δfx7*, *Δfx9*, and the flavodoxin deletion mutant *ΔisiB* (Appendix I.1-6) had been previously constructed in our group. However, their segregation had not been checked yet. In addition, two double mutants, *Δfx7Δfx9 and Δfx9ΔisiB*, were created by deleting *fx7* or *isiB* in the genome of *Δfx9*, respectively.

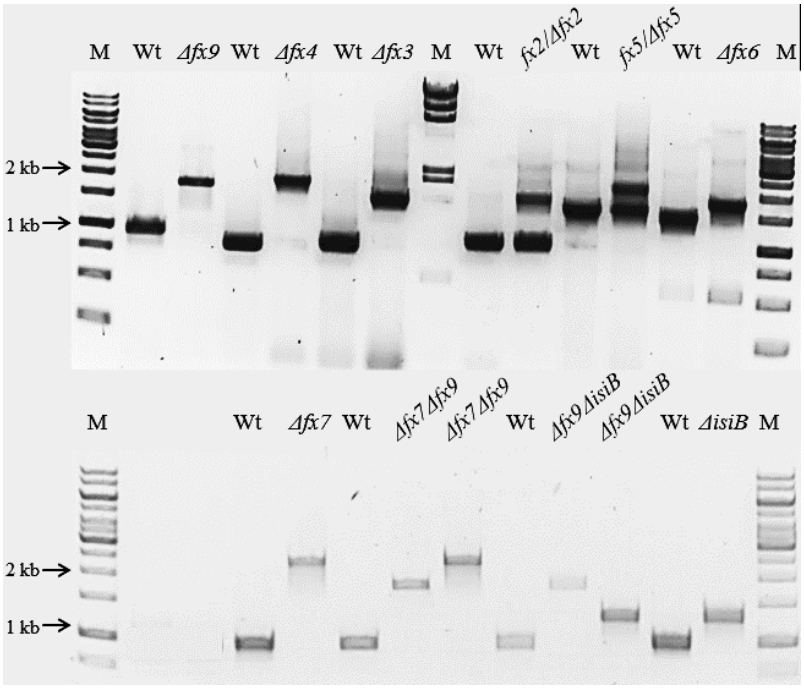

Fig. 4.1.1.1. Segregation of the ferredoxin and flavodoxin mutants checked by PCR. Absence of the WT target gene and presence of the corresponding antibiotic resistance cassette were verified regularly by polymerase chain reaction (PCR) on genomic DNA of the strains. Double mutants were amplified by specific primers for two target genes respectively. GeneRuler™ 1 kb DNA Ladder and Lambda DNA/HindIII marker was added as DNA marker (M).

All these mutants mentioned above were checked by PCR with primers listed in Table 3.3.3. PCR results from the WT and the mutants (Fig. 4.1.1.1, Table 4.1) showed that deletion of *fx3*, *fx4*, *fx7*, *fx9*, and *isiB* resulted in completely segregated mutants (*Δfx3*, *Δfx4*, *Δfx7*, *Δfx9*). The absence of *fx7* or *isiB* in *Δfx9*

indicated that the double mutants, *Δfx7Δfx9 and Δfx9ΔisiB*, were segregated as well. However, the presence of both *fx2* and the Kanamycin (*Km*) antibiotic resistance cassette in the *fx2* deletion strain showed incomplete segregation of the mutant, even after segregation for over three years.

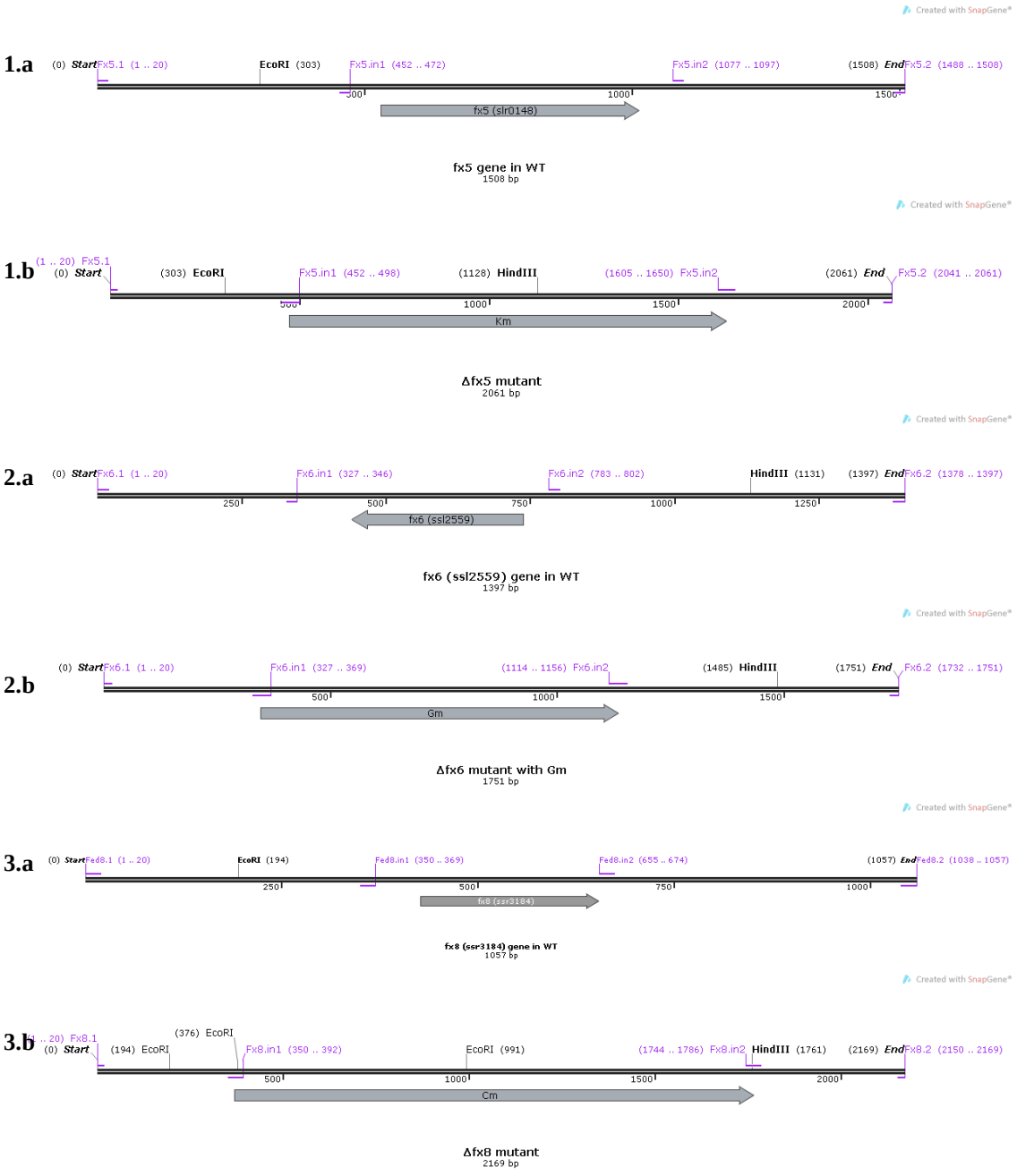

Fig. 4.1.1.2. Schematic representations of the ferredoxin (Fx5, Fx6, Fx8) deletion construct and the positions of the primers used. The ORF of the gene targeted for mutagenesis (a) was replaced by various antibiotic resistance gene (b). The restriction sites of *HindIII* and *EcoR I* were marked on the fragment containing the region upstream and downstream of target gene. Km: Kanamycin, Cm: Chloramphenicol, Gm: Gentamycin.

Table 4.1. The expected lengths of the different PCR products of Figure 4.1.1.1. "W" means *Synechocystis* Wild-type DNA as template for PCR; "M" means mutant DNA as template for PCR.

Mutant		***fx2/Δfx2***	***Δfx3***	***Δfx4***	***fx5/Δfx5***	***Δfx6***	***Δfx7***	***fx8/Δfx8***	***Δfx9***	***ΔisiB***
Primer pairs		*Fdx2.1/Fdx2.2*	*Fdx3.1/Fdx3.2*	*Fdx4.1/Fdx4.2*	*Fx5.1/Fx5.2*	*Fx6.1/Fx6.2*	*Fed2.1/ Fed2.2*	*Fx8.1/Fx8.2*	*Fed1.1/ Fed1.2*	*IsiB.1/ IsiB.2*
Product size	**W**	929 bp	827 bp	866 bp	1508 bp	1397 bp	969 bp	1057 bp	953 bp	997 bp
	M	1716 bp	1903 bp	1557 bp	2061 bp	1751 bp	2317 bp	2169 bp	1755 bp	1284 bp

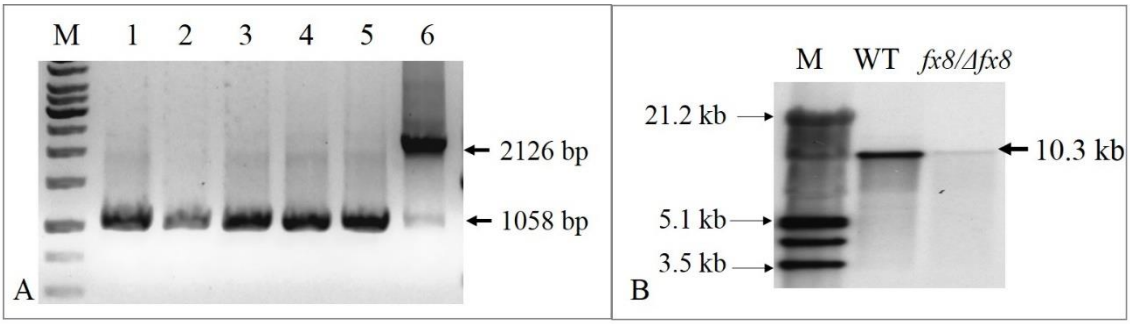

Fig. 4.1.1.3. Segregation of the Fx8 deletion mutant and its triple knockout mutant (*Δfx7Δfx8Δfx9*) checked by PCR and Southern blot. A: Absence of the WT target gene and presence of the corresponding antibiotic resistance cassette were checked by PCR with specific primers *Fx8.1* and *Fx8.2*. No. 1, 3 and 5: Wilde-type; No. 2 and 4: putative *fx8/Δfx8*; No. 6: *Δfx7Δfx8Δfx9*; GeneRuler^{TM} 1 kb DNA Ladder was added as marker (M). B: Southern blot of the putative Fx8 deletion mutant (*fx8/Δfx8*). Fragment length in WT and mutant should be 10.3 kb and 5.1 kb, respectively.

Furthermore, it was attempted to delete and replace *fx5*, *fx6* and *fx8* with kanamycin (Km), gentamycin (Gm), and chloramphenicol (Cm) resistance cassettes, respectively. The knockout mutants were checked via PCR and southern blot with the primers listed in Table 3.3.3 and Fig. 4.1.1.2. As shown in Fig. 4.1.1.1 and 4.1.1.3, *fx6* could be deleted from all genome copies, whereas the *fx5* deletion strain could not be segregated and the deletion of *fx8* failed. However, as the same amount of DNA was loaded onto the southern-blot (Fig. 4.1.1.3B) from WT and putative *fx8/Δfx8* DNA, and as the signal in the putative *fx8/Δfx8* lane is much weaker, it cannot be ruled out completely that less *fx8* is present in the respective mutant. The mutant is therefore referred to as putative *fx8/Δfx8* mutant throughout this thesis. As outlined in the "future perspectives" part, all results that were obtained with this mutant should be interpreted cautiously. Additionally, a new *Δfx8* mutant should be constructed and experiments should be repeated.

Furthermore, it was further attempted to delete the open reading frame (ORF) of *fx8* from the genome of *Δfx7Δfx9*, resulting in a triple mutant, *Δfx7Δfx8Δfx9*. The absence of *fx8* in *Δfx7Δfx8Δfx9* and presence of the Cm^R cassette were verified by PCR of the genomic DNA of the strain (Fig. 4.1.1.3A) and the growth on agar plates containing three antibiotics (Km + Sp + Cm).

4.1.2Construction of the Fx1 mutant by adding a copper-regulated *petE* promoter in *Synechocystis*

According to earlier works, it was not possible to delete *fx1* (*ssl0020*) from the genome of *Synechocystis* as *fx1* is essential for growth (Gutekunst et al. 2014, Poncelet et al. 1998). The few strategies described up to date in the literature that allow to study the function of Fx1 in cyanobacteria include the expression of *fx1* via the metal-inducible promoter, P_{petE} (plastocyanin gene) which can be controlled via copper (Briggs et al. 1990).

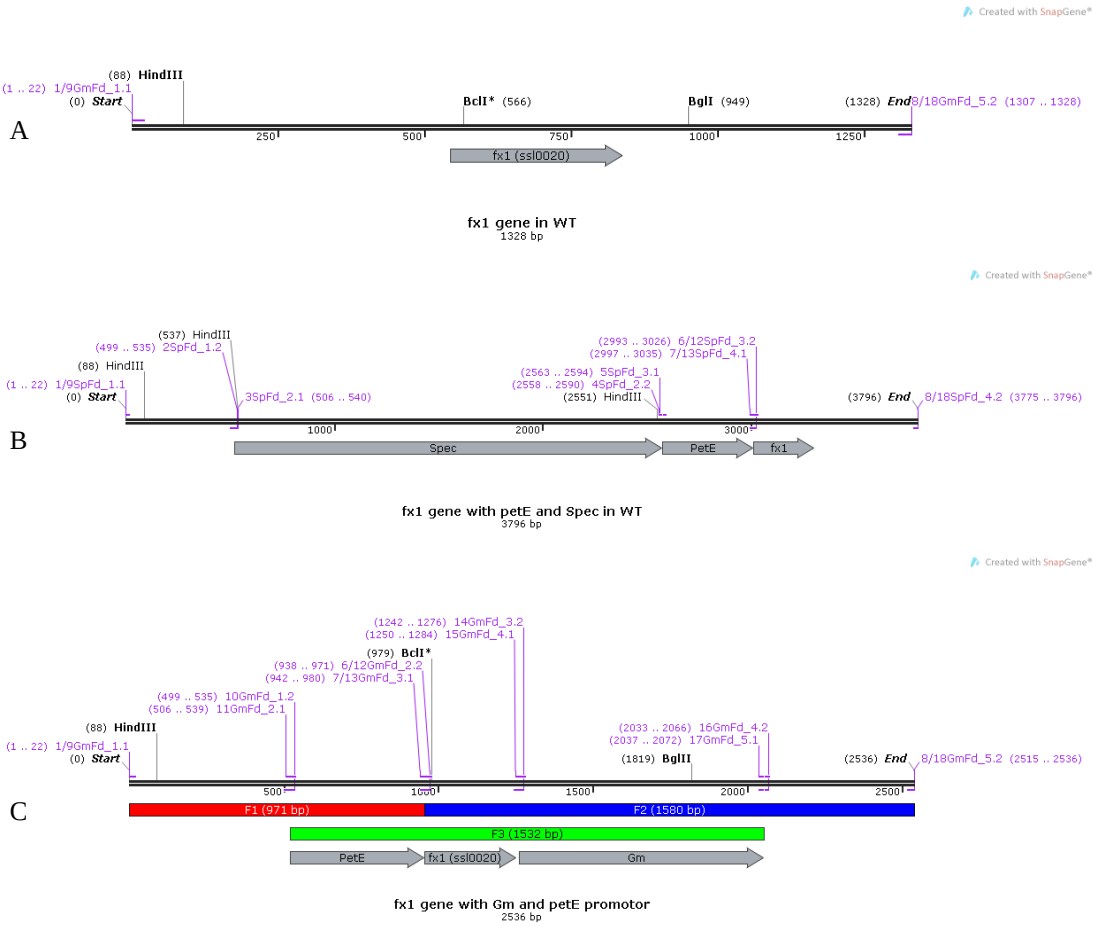

Fig. 4.1.2.1. The genomic structure of the *fx1* construct containing the native metal-inducible promoter element and the antibiotic resistance cassette. A: Schematic representations of the ORF of *fx1* (*ssl0020*) and the positions of the primers used in WT genome. B: The genomic structure of the native metal-inducible promoter element following the spectinomycin (Spec) cassette; One terminal coding 'TAA' was add in the end of Spec. C: The genomic structure of the native metal-inducible promoter element followed by the target gene *fx1* and the gentamycin (Gm) cassette; F1-3: three sub-fragments were separately amplified to verify the correct fusion product of P_{petE}-fragments and Gm^R cassette fragment. The positions of the primers used and the restriction sites of specific enzymes (*HindIII*, *BclI* and *BglII*) were marked in purple and black lines, respectively. Gm: Gentamycin; Spec: Spectinomycin.

Fig. 4.1.2.1 showed two strategies to construct a genomic structure by inserting the native metal-inducible promoter (P_{petE}) and a responding antibiotic resistance cassette (Gm^R or Sp^R) into the genome of *Synechocystis* via homologous recombination without interrupting the target gene *fx1*. After transformation, we only obtained one potential *Δfx1*$_{petE}$ strain with the ability to grow on agar plates containing Gm^R.

In Wild-type *Synechocystis*, P_{petE} normally regulates transcription of the gene encoding plastocyanin under copper-replete conditions. When copper is present in the medium, P_{petE} is transcribed, whereas its expression is heavily down regulated in the absence of copper (Briggs et al. 1990). Therefore, the potential *Δfx1*$_{petE}$ was grown in BG11 medium with different concentration of copper. For copper-replete conditions, standard BG-11 medium, which contains about 0.3 µM $CuSO_4$, was used. Preliminary results showed that there was no difference in the growth between WT and *Δfx1*$_{petE}$ in the presence (0.3µM) and absence (0 µM) of copper (Fig. 4.1.2.2).

The poor regulation observed in the potential *Δfx1*$_{petE}$ strain could either be due to the loss of the *petE* promoter fragment in *Δfx1*$_{petE}$ and/or difficulties to remove all residual copper in medium and laboratory glassware. To explore the first scenario, the strain was checked by PCR (primers *1/9GmFd_1.1* and *8/18GmFd_5.2* listed in Table 3.3.3). Fig. 4.1.2.1C. shows that the amplified fragment size (2.1 kb) in *Δfx1*$_{petE}$ is shorter than expected (2.5 kb), which might be caused by the lost 436 bp of *petE* promoter fragment (Fig. 4.1.2.3A). Further digestion of PCR product in *Δfx1*$_{petE}$ using the high-fidelity restriction enzyme *BglII* produced a 1.6 kb length of fragment, which is as well shorter than expected (Fig. 4.1.2.3B).

In order to check for the presence of the *petE* promoter fragment in *Δfx1*$_{petE}$, three sub-fragments, F1-3, were separately amplified by PCR with three pairs of primers marked in Fig. 4.1.2.1C. As expected, we got the correct length of F2, but neither F1 nor F3 (4.1.2.3B). The loss of the *petE* promoter fragment might contribute to the failures to amplify the F1 and F3 in *Δfx1*$_{petE}$.

In summary, the potential *Δfx1*$_{petE}$, could not be used to regulate the expression of *fx1* because of the absence of a functional *petE* promoter fragment. Thus, all the ferredoxin and flavodoxin deletion mutants (*fx2/Δfx2, Δfx3, Δfx4, fx5/Δfx5, Δfx6, Δfx7, fx8/Δfx8, Δfx9, Δfx7Δfx9, Δfx7Δfx8Δfx9, Δfx9ΔisiB, ΔisiB*), except for the Fx1-deletion mutant, are available.

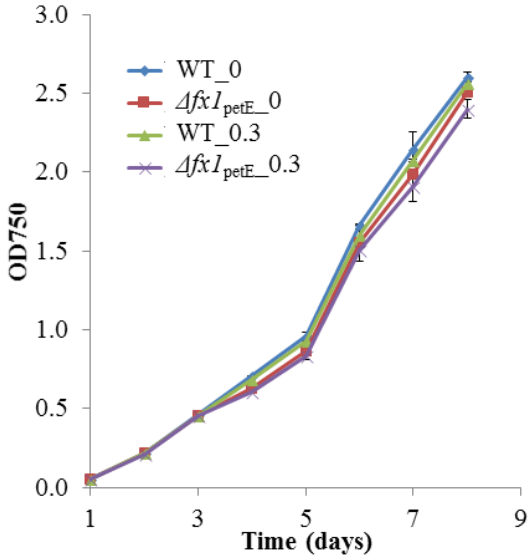

Fig. 4.1.2.2. Phototrophic growth of *Synechocystis* Wild-type and *Δfx1*$_{petE}$ in the presence and absence of copper. For copper-replete conditions, standard BG-11 medium, which contains about 0.3 μM $CuSO_4$, was used. For copper-deficient conditions, $CuSO_4$ was omitted from BG11 medium, as indicated by '0'. The data points and error bars represent mean ± S.D. of two independent cultures.

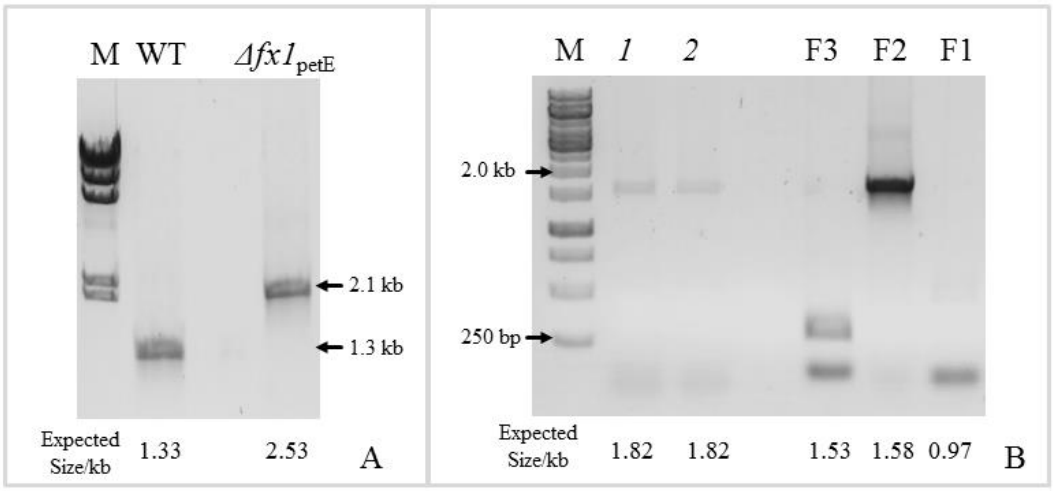

Fig. 4.1.2.3. Segregation of the suspected *fx1* mutant (*Δfx1*$_{petE}$) checked by PCR and digestion of restriction enzyme. A: Segregation of *Δfx1*$_{petE}$ checked by PCR with primer showed in Fig. 4.1.2.1. B: *Lane 1* and *2*, The PCR product of *Δfx1*$_{petE}$ shown in A was digested by the restriction enzyme *BglII*, whose specific cutting site was shown in Fig. 4.1.2.1C. *Lane F1-F3*, see Fig. 4.1.2.1C.

4.1.3 Construction and analysis of the *Synechocystis* strains containing a C-terminal StrepII-tagged or 6xHistidine-tagged ferredoxin

In order to purify distinct ferredoxins and to study the expression of Fx1 and Fx9 in *Synechocystis*, a StrepII-tag (Strep-tag or s) or a 6xHistidine-tag (His-tag or h) was added at the C-terminus of these ferredoxins to get the recombinant proteins (Appendix II). Erythromycin (Em) or Kanamycin (Km) resistance cassette were inserted following the ORFs of ferredoxin-encoding genes. Segregation of all the strains (F1s, F9s, *Δfx9*F1s, F1h, F1hF9s, F9h, F9hF1s) was checked by PCR with primers GmFd_1.1/GmFd_5.2 and Fed1.1/Fed1.2.

Fig. 4.1.3.1 shows that all strains (F1s, F9s, *Δfx9*F1s, F1h, F1hF9s, F9h, F9hF1s) are completely segregated.

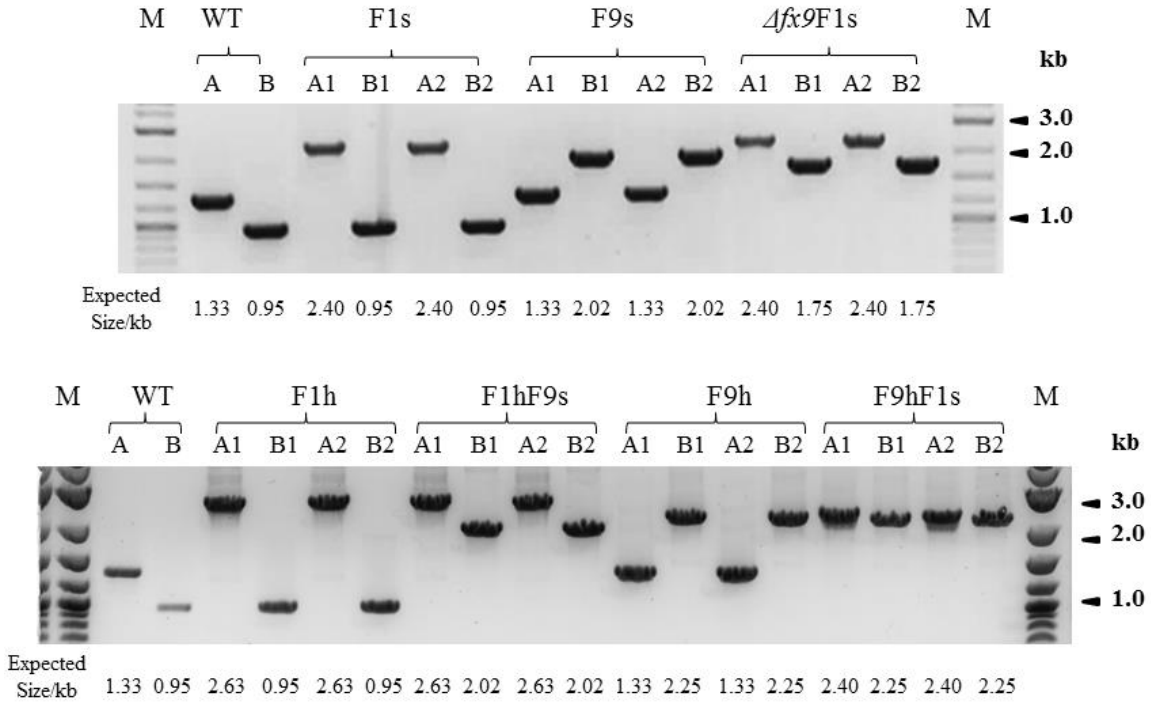

Fig. 4.1.3.1 Segregation of the *Synechocystis* strains containing a Strep-tag or a His-tag at the C-terminus of recombinant ferredoxins (Fx1 and Fx9) was checked by regular PCR. Primers GmFd_1.1/GmFd_5.2 (A) and Fed1.1/Fed1.2 (B) shown in Appendix II were used to amplify the fragments containing *fx1* and *fx9*, respectively. The expected size of every PCR product was shown at the bottom of gel picture.

In order to investigate the expression of Fx1 and Fx9, all the strains (F1s, F9s, *Δfx9*F1s, F1h, F1hF9s, F9h, F9hF1s) were grown under photoautotrophic and mixotrophic conditions for 5 days and subsequently harvested for protein isolation. The expression of Fx1 and Fx9 under these conditions was investigated by Western blot using antibodies against the Strep-tag and His-tag.

As shown in Fig. 4.1.3.2, only the His-tagged Fx1 was found in strains F1h and F1hF9s, both containing a His-tag at the C-terminus of recombinant Fx1, under autotrophic and mixotrophic conditions. The absence of signals of His-tagged Fx9 might be due to too low abundance of Fx9. When an antibody against the Strep-tag was used, no apparent bands were found in all the strains except for F9hF1s, which contains one weak 17 kDa protein band under mixotrophic conditions (Fig. 4.1.3.2).

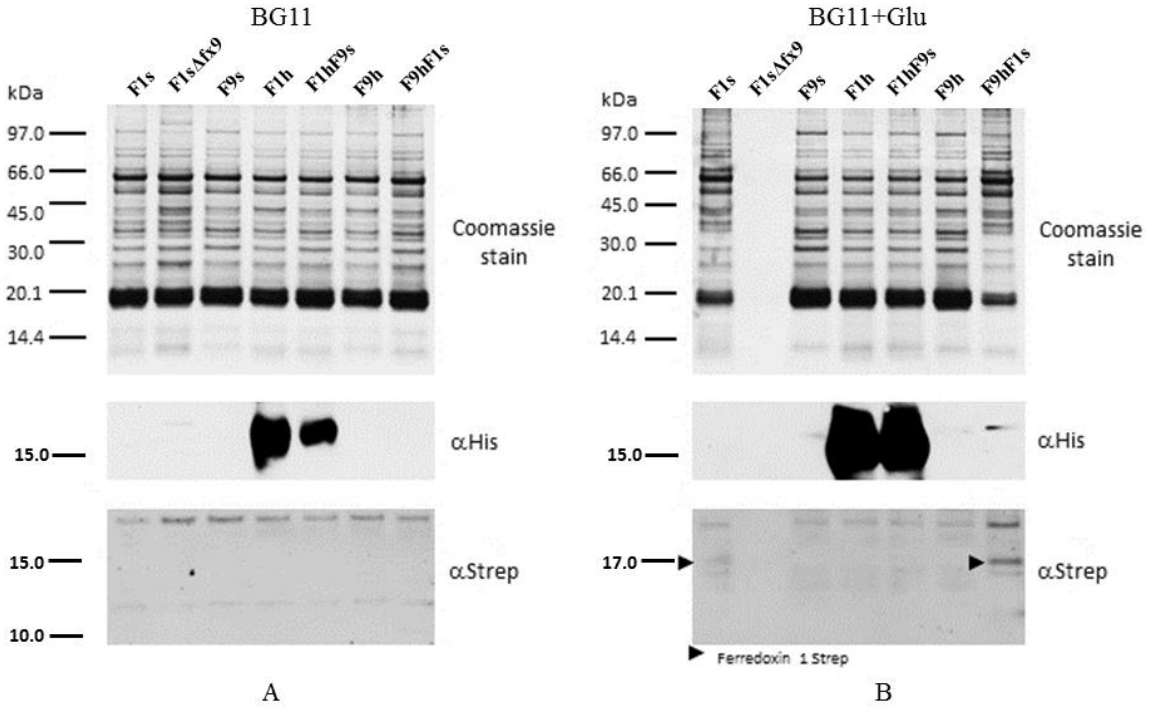

Fig. 4.1.3.2 Expression of recombinant ferredoxins containing a Strep-tag or a His-tag at the C-terminus (F1s, F9s, *Δfx9*F1s, F1h, F1hF9s, F9h, F9hF1s) detected by Western blot analysis using antibodies against the Strep tag or His tag under autotrophic and mixotrophic conditions. 7.5 µg protein per sample was load on the SDS-PAGE gel. Fx1-His has 12 to 25 kDa while Fx1-Strep should be present at about 17 kDa.

4.2 Characterization of ferredoxin deletion mutants in *Synechocystis* under autotrophic conditions

4.2.1 Screening and characterization of *Synechocystis* ferredoxin deletion mutants with different nitrogen sources under autotrophic conditions

Nine ferredoxin-coding genes (*fx1-fx9*) are known in the genome of *Synechocystis* (Cassier-Chauvat and Chauvat 2014a). The light-inducible Fx1 is a highly abundant protein and is essential under photoautotrophic conditions (Mazouni et al. 2003). Under photoautotrophic conditions, ferredoxins Fx2 to Fx9 are expressed at low levels only (Houot et al. 2007, Mazouni et al. 2003, Poncelet et al. 1998). Their functions still remain unclear. To investigate the function of these ferredoxin genes under photoautotrophic conditions, we constructed and grew all obtained ferredoxin/flavodoxin deletion mutants (*fx2/Δfx2, Δfx3, Δfx4, fx5/Δfx5, Δfx6, Δfx7, fx8/Δfx8, Δfx9, Δfx7Δfx9, Δfx9ΔisiB, ΔisiB*). Additionally, a pyruvate: ferredoxin/flavodoxin oxidoreductase (PFOR) deletion mutant (*Δpfor*) was cultivated. Based on current knowledge PSI and PFOR are the only sites in the cells at which ferredoxins can be reduced. Therefore, PFOR was cultivated in parallel in order to possibly find ferredoxins that might be reduced via PFOR and might thus show a similar growth phenotype as *Δpfor.*

When grown under photoautotrophic conditions, as shown in Fig. 4.2.1.1A-D, all these ferredoxin/flavodoxin deletion mutants (*fx2/Δfx2, Δfx3, Δfx4, fx5/Δfx5, Δfx6, Δfx7, Δfx9, Δfx7Δfx9, Δfx9ΔisiB* or *ΔisiB*) and *Δpfor*, with the exception of putative *fx8/Δfx8,* grew like the WT. This indicates that the complete deletion of *fx3, fx4, fx6, fx7, fx9, isiB* or *pfor* alone or the incomplete deletion of *fx2* or *fx5* alone doesn't affect the photoautotrophic growth of *Synechocystis.* Furthermore, the additional deletion of *fx7* or *isiB* in *Δfx9* mutant didn´t cause any changes in growth either. These results showed neither *fx3, fx4, fx6, fx7, fx9, isiB* or *pfor* are essential under photoautotrophic conditions in *Synechocystis*.

Subsequently, the growth behavior of distinct ferredoxin deletion strains was tested under different nitrogen sources. *Synechocystis* can take up L-arginine effectively as an alternative nitrogen source (Schriek et al. 2008, Stephan et al. 2000). The nitrogen in nitrate has an oxidation sate of +5 and therefore needs to be reduced by 8 electrons in order to reach the oxidation state of -3, which is characteristic for the nitrogen in proteins. Nitrate is thus an important electron sink of the photosynthetic electron chain under photoautotrophic conditions. The nitrogen in arginine by contrast has an oxidation state of -3 already and does thus not have to be reduced for protein biosynthesis. However, the carbon skeleton in arginine is oxidized delivering electrons either to the PQ-pool in the thylakoid membrane or to $NAD(P)^+$ (Schriek et al. 2009, Schriek et al. 2007). The replacement of nitrate by arginine thus probably results in a surplus of electrons in the thylakoid membrane. Ferredoxins might thus get important under these conditions to relieve the cells of these surplus electrons. All the mutant strains mentioned above were autotrophically grown with 5 mM arginine, instead of 17.6 mM nitrate.

Figure 4.2.1.1E-H shows that *Δfx9, Δfx7Δfx9, Δfx9ΔisiB, ΔisiB* and *Δpfor* displayed impaired growth compared to WT on arginine. Mutant (*fx5/Δfx5*) with the incomplete deletion of *fx5* started to slow down its photoautotrophic growth from the 4th day on. These results indicate that Fx9, IsiB and PFOR are of physiological importance on arginine whereas neither Fx3, Fx4, Fx6 nor Fx7 play a role under these conditions. The growth phenotype of *Δpfor* is remarkable under these conditions as the enzyme is regarded as oxygen sensitive (Hughes et al. 1995, Meinecke et al. 1989, Williams et al. 1987).

The color of the cultures turned from green to yellow on arginine. In order to quantify the pigment contents of the cells, absorption spectra between 400 nm to 800 nm were recorded on the 1st and the 7th day. The relation of chlorophyll a (Chl a) to phycocyanin can be determined by comparison of the peaks at 430 nm (Chl a) and 660 nm (phycocyanin). The broad absorbance peak between 480 nm and 500 nm originates from a mix of Chl a and carotenoids.

As indicated in Figure 4.2.1.2, the content of chlorophyll and phycocyanin decreased while the carotenoid content increased on arginine, in line with the yellow color of the cultures. Furthermore, the relative carotenoid content in *Δfx9, ΔisiB* and *Δpfor* increased during cultivation on arginine and finally became higher than that of the WT (Fig. 4.2.1.3).

Break down of arginine results in the production of urea which is further metabolized to ammonium (Quintero et al. 2000). In order to test the influence of ammonium on the growth, the WT, *Δfx9* and *Δfx7Δfx9* were grown on 10 mM NH_4Cl. Both *Δfx9* and *Δfx7Δfx9* stayed green and grew like the WT on ammonium (Fig. 4.2.1.3 and 4.2.1.4). Furthermore, the oxygen evolution rate of *Δfx9* (458.73 ± 73.0 μM/OD_{750} h^{-1}) was almost twice as high as that of the WT (234.9 ± 20.5 μM/OD_{750} h^{-1}) in light on the 5th day while the oxygen uptake rate of *Δfx9* (91.82 ± 15.5 μM/OD_{750} h^{-1}) was more than twice as high as in the WT (37.1 ± 5.5 μM/OD_{750} h^{-1}) in darkness.

In order to get an impression of the phenotype of the cells, WT and *Δfx7Δfx9* grown either on arginine or ammonium were analyzed via transmission electron microscopy (TEM) on day 6 of the cultivation (Fig. 4.2.1.5A).

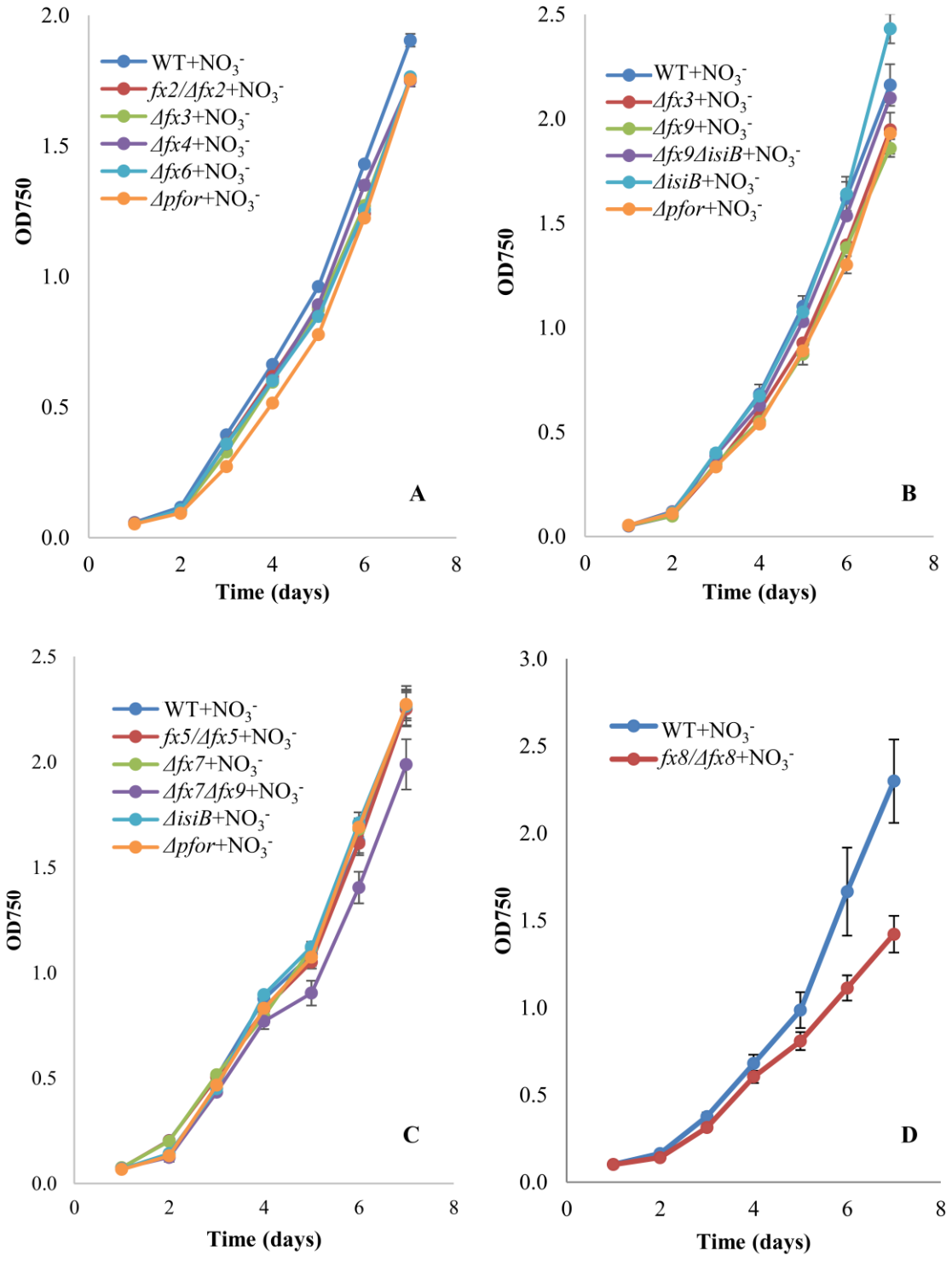

Fig. 4.2.1.1. Standard photoautotrophic growth of WT, selected ferredoxin deletion mutants and *Δpfor*. 17.6 mM nitrate ($+NO_3^-$) was supplemented in cultures as nitrogen source. Reported data result from the mean of three independent experiments ± Standard Deviation.

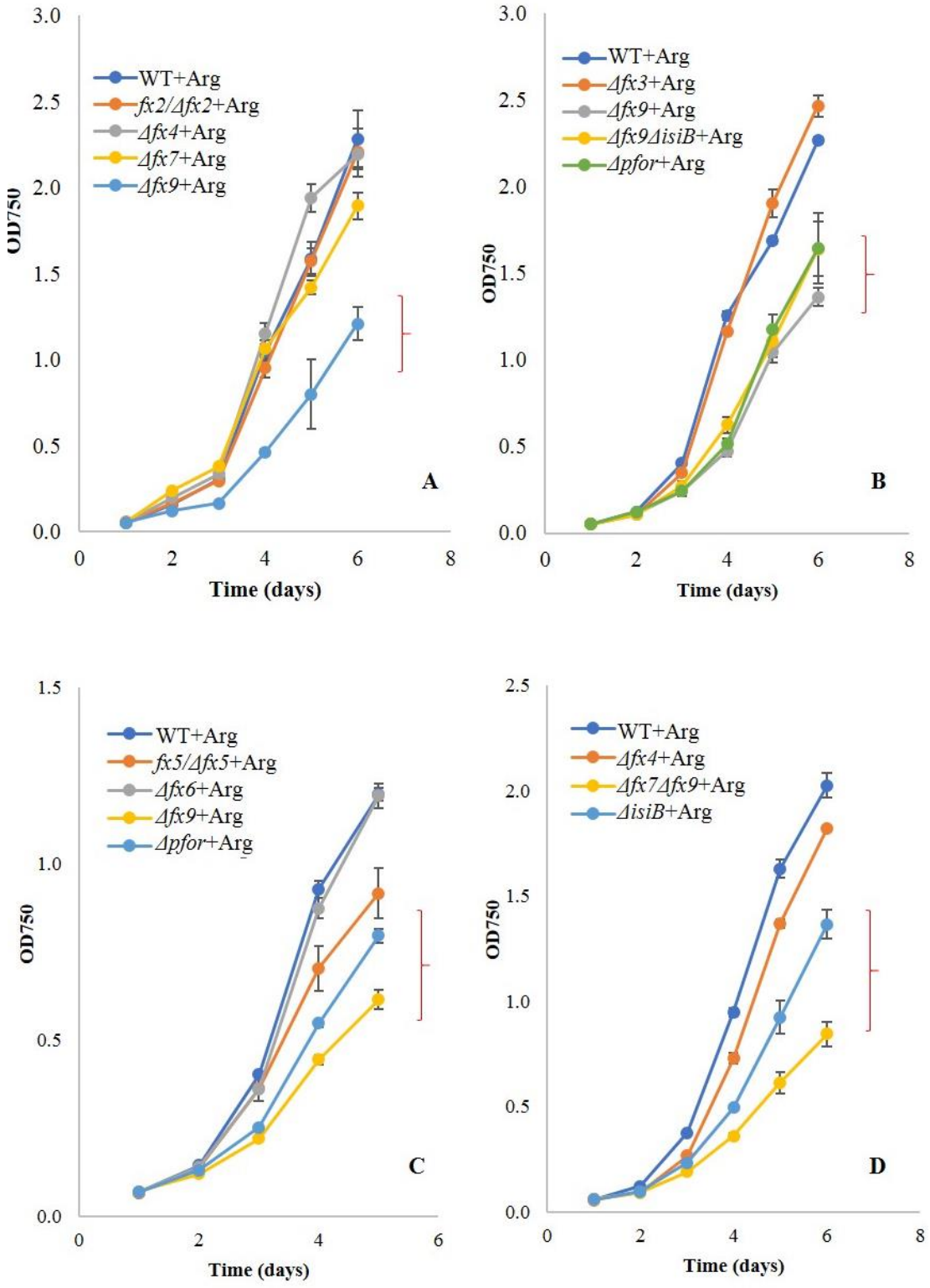

Fig. 4.2.1.2. Photoautotrophic growth of WT, selected ferredoxin deletion mutants and *Δpfor* as indicated with arginine (+Arg). 5 mM arginine was supplemented as nitrogen source in $BG11_0$. Reported data result from the mean of three independent experiments ± Standard Deviation.

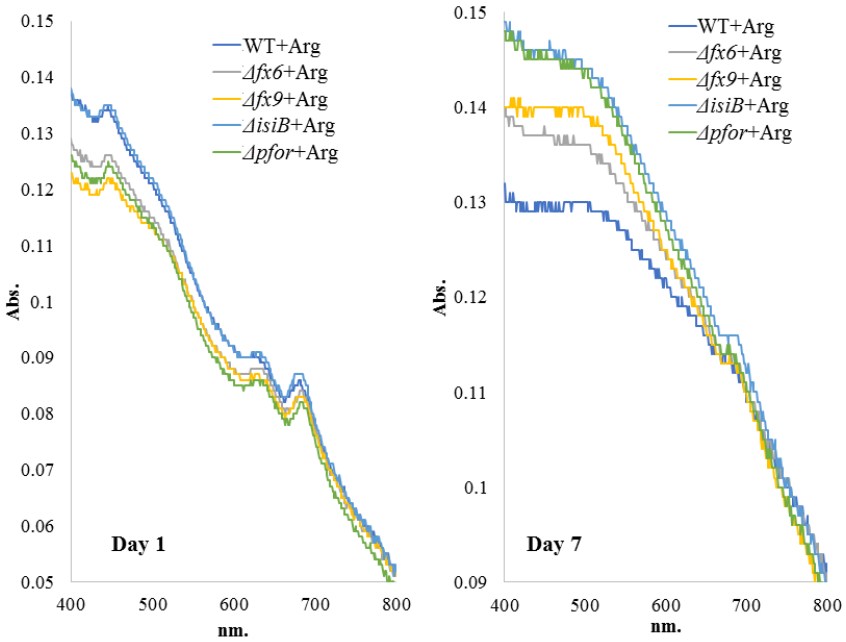

Fig. 4.2.1.3. Absorption spectra of WT, ferredoxin deletion mutants and *Δpfor* grown on arginine recorded at day 1 and 7. Data are representative for three independent experiments.

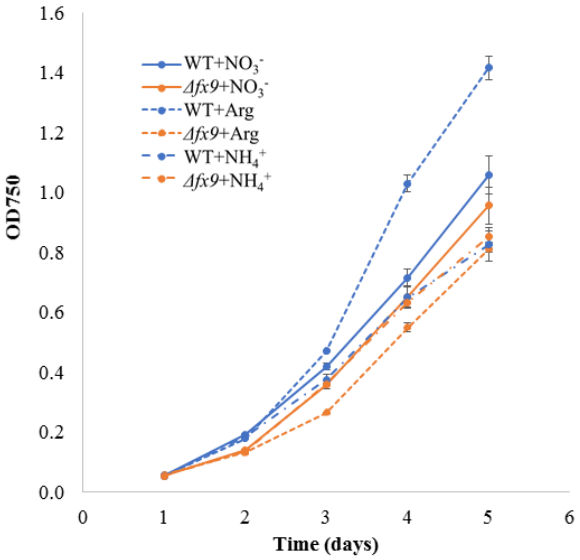

Fig. 4.2.1.4. Growth of WT and Δ*fx*9 on nitrate (+NO_3^-), arginine (+Arg) or ammonium (+NH_4^+). Reported data result from the mean of three independent experiments ± Standard Deviation.

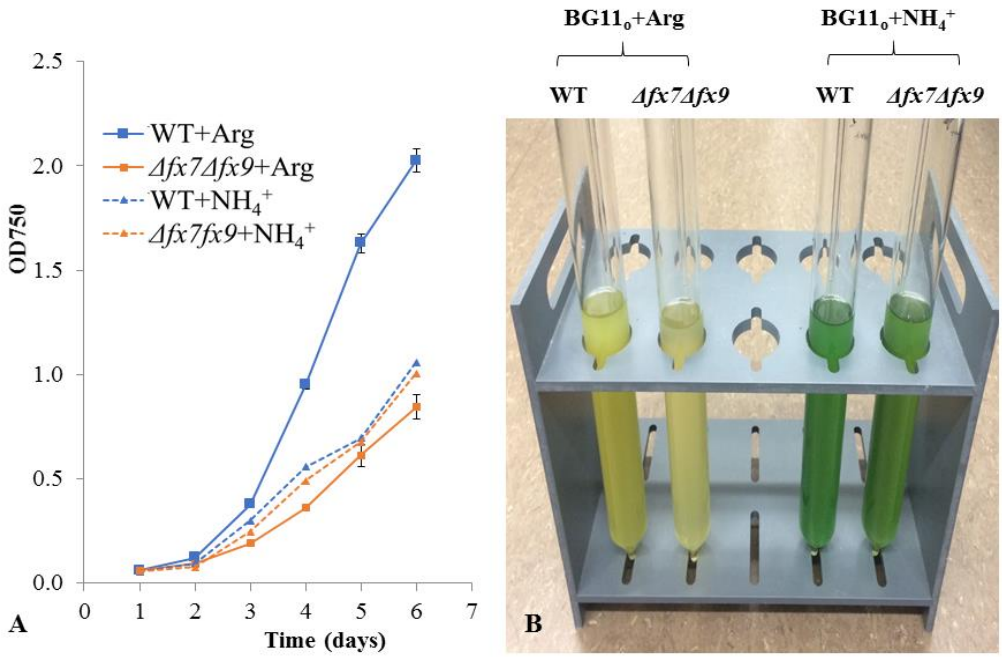

Fig. 4.2.1.5. Growth of WT and *Δfx7Δfx9* on either arginine (+Arg) or ammonium (+NH_4^+). A: Growth; B: Colors of cultures from A (on 4th day); Reported data result from the mean of three independent experiments ± Standard Deviation.

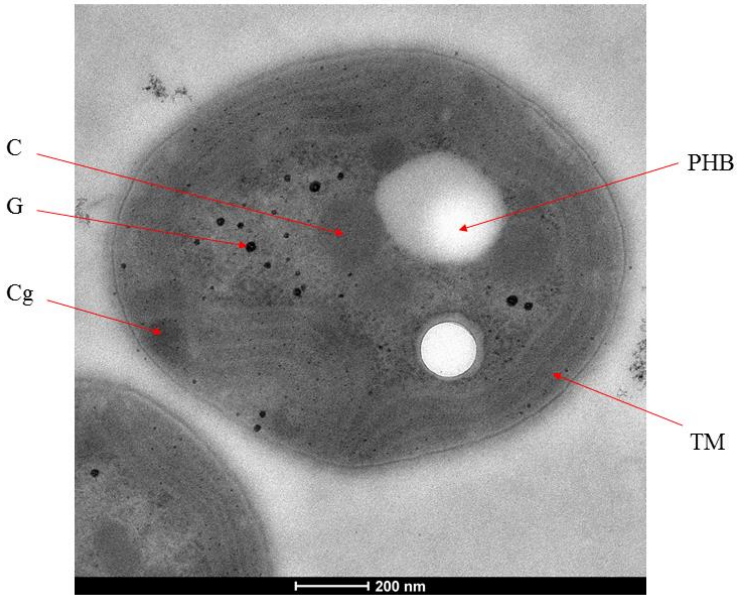

Fig. 4.2.1.6. Morphological Analysis via Transmission Electron Micrographs of *Synechocystis* Wild-type Cells grown in BG11 medium (BG11$_0$+NO_3^-). G, Glycogen granules; PHB, polyhydroxybutyrate granules; Cg, cyanophycin granules; C, carboxysomes; TM, thylakoid membranes.

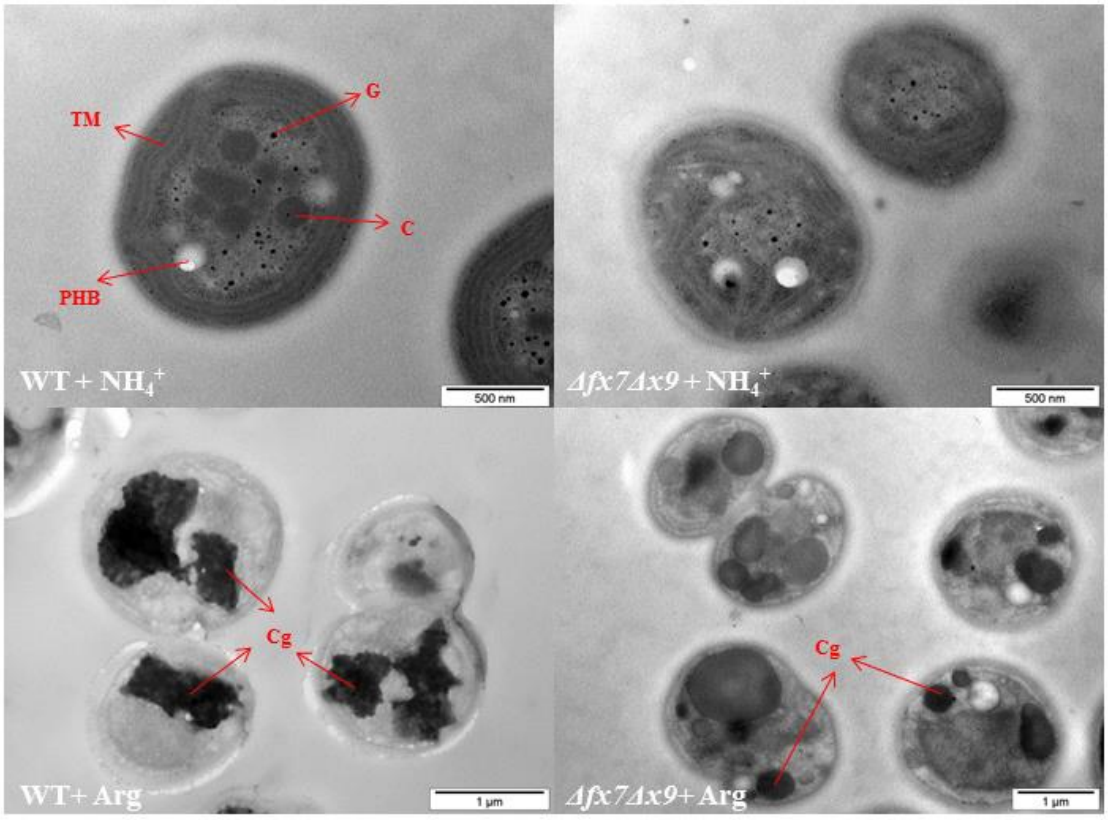

Fig. 4.2.1.7. Representative TEM images of *Synechocystis* WT and *Δfx7Δfx9* cells grown for 6 days on ammonium ($+NH_4^+$) or arginine (+Arg) (from Fig. 4.2.1.5). G: Glycogen granules; PHB: polyhydroxybutyrate granules; Cg: cyanophycin granules; C: carboxysomes; TM: thylakoid membranes. Additional replicates of TEM images can be found in the Appendix III.

The TEM images show that *Δfx7Δfx9* and WT cells look similar to cells grown on standard medium with nitrate (Fig. 4.2.1.6). However, it seems that *Δfx7Δfx9* possesses a smaller number of carboxysomes per cell (*Δfx7Δfx9*: 0.8 ± 1.1 per cell; WT: 5.8 ± 1.7 per cell) in comparison to the WT when grown on ammonium (Fig. 4.2.1.7, see also additional images in the Appendix III). When grown on arginine the phenotypes of the cells changed dramatically. The WT accumulated a lot of cyanophycin granules and the thylakoid membranes were severely degraded. This phenotype was less pronounced in *Δfx7Δfx9* cells (Fig. 4.2.1.7). The changes in the cell phenotype probably come along with metabolic changes that allow the WT to grow better on arginine compared to *Δfx7Δfx9*.

From the results above, it can be concluded that IsiB, PFOR and Fx9 might help the cells to dissipate surplus electrons when cells are grown on arginine and to switch their cell morphology and metabolism in a way that allows growth under these conditions. It is known that PFOR is able to reduce IsiB (Flavodoxin) as indicated by the name pyruvate: ferredoxin/flavodoxin oxidoreductase (Neuer and Bothe 1982). The results indicate that also Fx9 might be reduced by PFOR as the phenotypes of *Δfx9* and *Δpfor* are similar as well. However, this has to be proven in more detail.

Bioinformatic evaluations and transcript analyses indicate that arginine is metabolized in *Synechocystis* either via the arginine deiminase pathway or the arginine dehydrogenase pathway (Schriek et al. 2009, Schriek et al. 2007). Electrons from the oxidation of arginine are either fed into the PQ-pool in the thylakoid membrane or to $NAD(P)^+$. One of the final products in the arginine dehydrogenase pathway is succinate (Schriek et al. 2009). We therefore tried to rescue the impaired growth of *Δfx9* by adding 5 mM succinate. However, addition of succinate had no effect on growth (data not shown).

4.2.2 Screening of *Synechocystis* ferredoxins which are involved in the cyclic electron transport under autotrophic conditions

Theoretically, the linear electron transfer (LET) from water to $NADP^+$ cannot satisfy the ATP/NADPH production ratio required by the Calvin-Benson and photorespiration (black pathway in Fig. 4.2.2.1). Cyclic electron transfer (CET) contributes substantially to the supply of ATP for CO_2 fixation (red pathway in Fig. 4.2.2.1), as does LET (Shikanai 2016). Ferredoxins are proposed to be involved in at least four parallel operating routes of CET around PSI in the cyanobacterium *Synechocystis*, however, if any of the ferredoxins beside Ferredoxin-1 (Fx1) are involved is unknown (Yeremenko, et al. 2005).

In order to check which ferredoxins in *Synechocystis* are involved in the CET pathway, we grew all the strains (*fx2/Δfx2, Δfx3, Δfx4, fx5/Δfx5, Δfx6, Δfx7, Δfx9, Δfx7Δfx9, Δfx9ΔisiB* or *ΔisiB*) under autotrophic conditions and recorded the $P700^+$ reduction kinetics by a pulse amplitude-modulated measurement (DUAL-PAM-100). The pelleted cells were resuspended in fresh BG11 medium at 10 μg/ml Chl concentration. Complete P700 oxidation was achieved by a 100 ms saturation pulse. We monitored the kinetics of reduction of oxidized P700 ($P700^+$) after switching off the actinic light. The resulting rate constants (*b*) were used to quantify both LET and CET rates (Bernat. et al, 2009). If one ferredoxin should be involved in the CET, it can be expected that the $P700^+$ rereduction rate of the respective mutant should be slower and that the *b* value is smaller than that in the WT. The inhibitor DCMU (10 μM) which blocks electron transfer from PSII to the PQ-pool was added to inhibit the LET pathway (Fig. 4.2.2.2).

Fig. 4.2.2.3 shows that the *b* values of M55 is almost zero. The M55 mutant is totally devoid of the NDH-1 complex (Ogawa 1991). Obviously, CET around PSI are completely abolished in the absence of the NDH-1. The *b* values of *Δfx4* and *Δfx6* were reduced about 10 % of the *b* values of the WT, indicating that Fx4 and Fx6 might be directly or indirectly involved in the CET around PSI (Fig. 4.2.2.3). Interestingly, *Δfx9* and its double mutant, *Δfx7Δfx9,* have bigger *b* values compared to the WT (Fig. 4.2.2.3), which might indicate that these ferredoxins are involved in some competitive pathways that dissipate electrons that can be alternatively cycled around PSI in CET. We did not find a ferredoxin deletion mutant that showed a similar phenotype to M55. This indicates that Fx1 is the principle electron carrier for the CET around PSI. Fx4 and Fx6 might play minor roles as well.

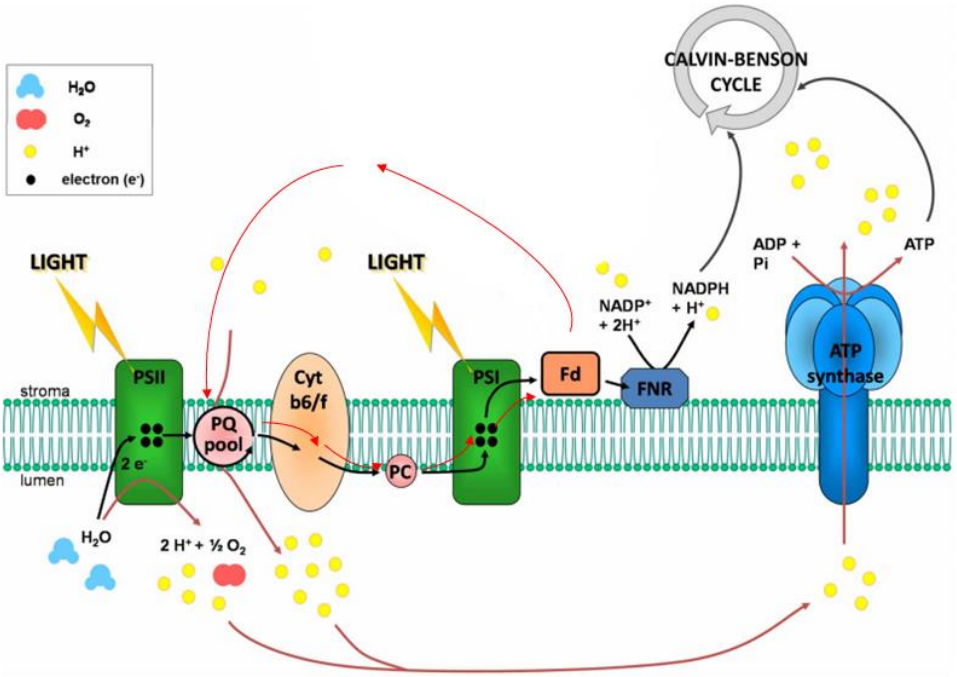

Fig. 4.2.2.1. The photosynthetic electron transfer chain: linear electron transport (LET, black pathway), and cyclic electron transport (CET, red pathway). (Modified from Michelet L. et al, 2013)

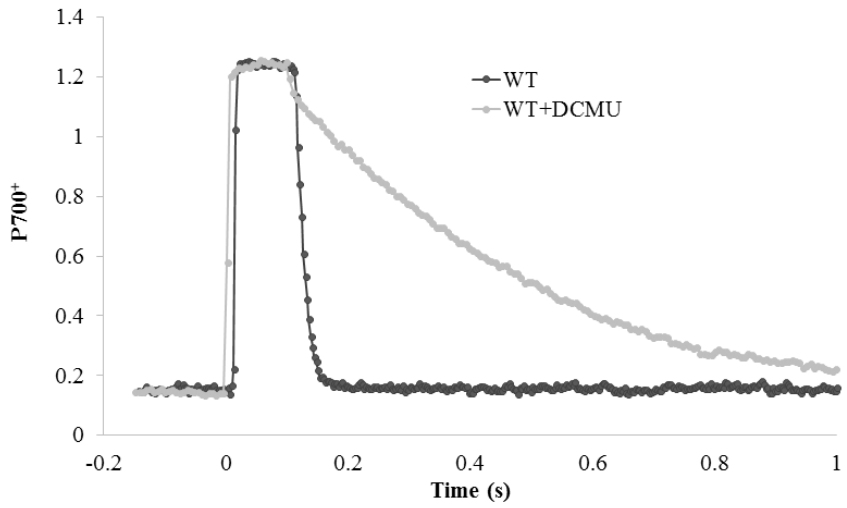

Fig. 4.2.2.2. P700 rereduction kinetics measured with *Synechocystis* WT cells under photoautotrophic conditions in the absence (black) or presence (grey) of 10 µm DCMU. A saturating pulse (100 ms, 10000 µmol photons m^{-2} s^{-1}) was applied to fully oxidize P700, followed by the (dark) rereduction of $P700^+$. Twelve subsequent traces (of the same samples) were recorded and corresponding rate constants (*b*) were determined by fitting the decay curves with single exponential functions.

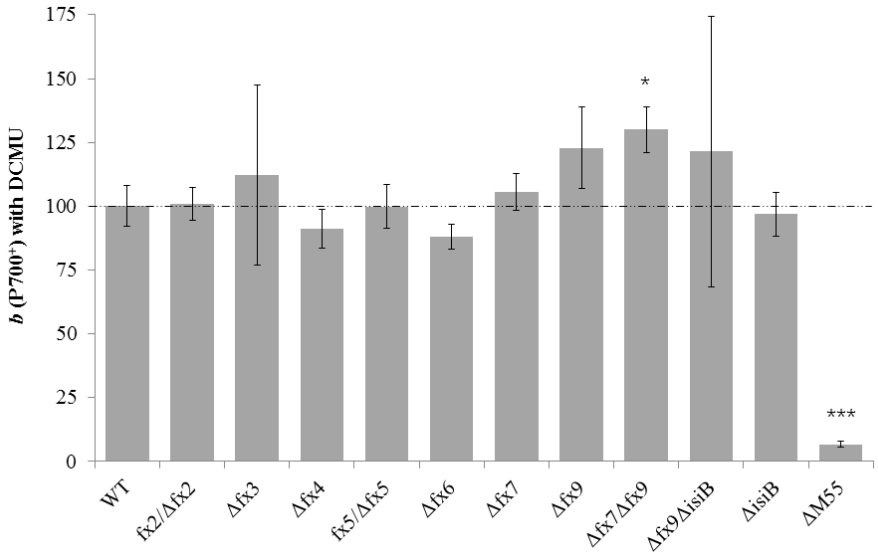

Fig. 4.2.2.3. The relative rate constants (*b*) of $P700^+$ rereduction kinetics of all the ferredoxin/flavodoxin mutants. NDH-1 mutant M55 was set as control. Stars on the column diagram indicates differences between mutant and WT by Tukey's HSD test (*P < 0.05 and ***P < 0.001). Reported data result from the mean of three independent experiments ± Standard Deviation.

4.2.3Is FX9 an electron carrier to the flavodiiron protein Flv3 in *Synechocystis*?

It has been proposed that the bacteria-type Fx9 physically interacts with the flavodiiron protein Flv3, which functions in the NAD(P)H-driven photoreduction of O_2 to H_2O, without concomitant formation of reactive oxygen species, known as Mehler-like reaction (Allahverdiyeva et al. 2011, Cassier-Chauvat and Chauvat 2014a, Helman et al. 2003). Furthermore, the number of carboxysomes per cell was also nearly 2-fold lower in the *Δflv3* mutant compared with the WT, being 3.2 ± 1.10 and 5.8 ± 0.45, respectively (Mustila et al. 2016). In line with this, *Δfx7Δfx9* cell also possess less carboxysomes (0.8 ± 1.1) per cell than the WT (5.8 ± 1.7) when grown on ammonium (Fig. 4.2.1.7).

If Fx9 should be involved in the Mehler-like reaction on arginine, the phenotype of *Δfx9* should be similar to that of the *Δflv3* under these conditions. Arginine is a reduced nitrogen source that needs to be oxidized to ammonia. It has been proposed that electrons from arginine oxidation are fed into the quinone pool of the photosynthetic electron chain and thereby result in a more reduced PQ pool (Schriek et al. 2009). We hypothesized that the Mehler-like reaction might be especially important on arginine as it provides an electron sink for surplus electrons from the photosynthetic electron chain.

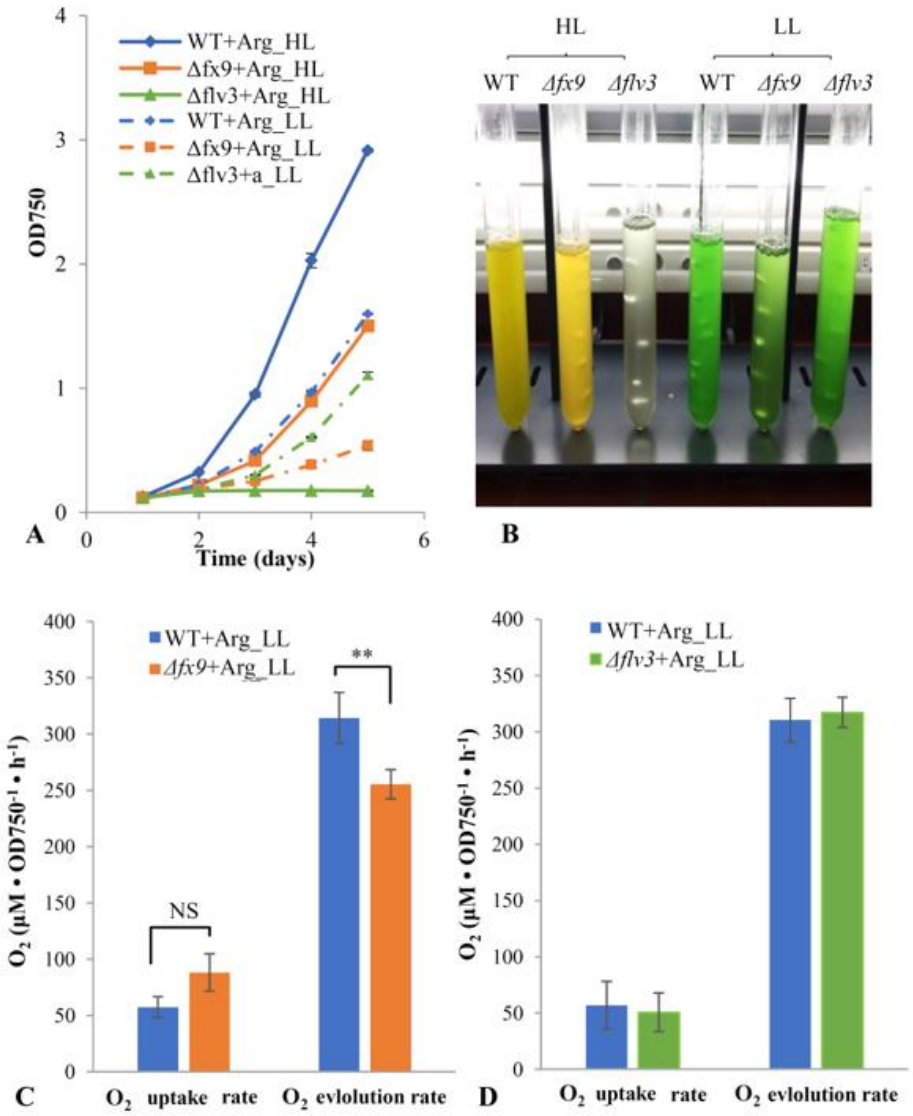

Fig. 4.2.3.1 Autotrophic growth of mutants *Δfx9* and *Δflv3* on arginine under different light intensity. A and B: cultures grown at 300 μmol photons m^{-2} s^{-1} as high light (HL) or at 15 μmol photons m^{-2} s^{-1} as low light (LL); The initial OD750 is set about 0.08. C and D: The oxygen evolution rate in light and the oxygen uptake rate in darkness of the cultures on 7th day in A; Stars on the column diagram indicates differences between mutant and WT by Tukey's HSD test (**P < 0.01). 'NS' indicates not significant. All error bars indicate standard deviation (s.d.) of three independent experiments.

Firstly, *Δflv3* and *Δfx9* were grown on arginine under different light intensity. Interestingly, the flavodiiron protein Flv3 mutant (*Δflv3*) cannot grow at a light intensity of 300 μmol photons m^{-2} s^{-1} on arginine (Fig. 4.2.3.1. A and B). This indicates that the protection of an overreduced photosynthetic electron chain via the photoreduction of O_2 catalyzed by Flv3 is indispensable for *Synechocystis* under the described conditions. As expected, low light (15 μmol photons m^{-2} s^{-1}) could effectively rescue the growth of *Δflv3* and led to a O_2 evolution rate similar to the WT (Fig. 4.2.3.1A and D). In addition, this growth experiment with a higher

OD_{750} (such as 0.5 compared to 0.05) could also partly rescue the impaired growth (Fig. 4.2.3.2), which further indicates that *Δflv3* is distinctly affected by light.

The growth of *Δfx9* was impaired on arginine compared to the WT as displayed by *Δflv3* (Fig. 4.2.3.1A and B). However, its growth on 300 µmol photons m^{-2} s^{-1} was much better that the growth of *Δflv3* and lowering the light intensity to 15 µmol photons m^{-2} s^{-1} did not improve its growth performance as in *Δflv3* but rather deteriorated it (Fig. 4.2.3.1A and B). Furthermore, *Δfx9* produced less oxygen than the WT and *Δflv3* at low light intensity (Fig. 4.2.3.1C and D).

Furthermore, the PSI oxidation status was determined by monitoring P700 using a Dual-PAM-100 measuring system. Fig. 4.2.3.2 shows that the knockout of Flv3 caused a significantly slower oxidation of P700 in PSI, which is especially apparent when the red light is turned on (arrows up) which efficiently excites PSII. When electrons form PSII arrive in PSI, P700 is barely oxidized in *Δflv3*, because of the absence of the Flv3 mediated Mehler-like reaction in its function as an electron sink.

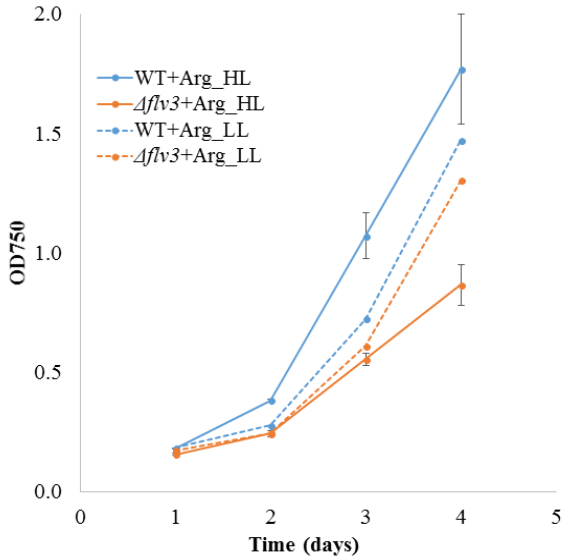

Fig. 4.2.3.2. Autotrophic growth of *Δflv3* on arginine under HL or LL conditions. Cultures were grown from OD750 = 0.2. 300 µmol photons m^{-2} s^{-1} was regarded as HL or 15 µmol photons m^{-2} s^{-1} was regarded as LL.

We did furthermore grow *Δflv3* with ammonium as sole nitrogen source under HL (300 µmol photons m^{-2} s^{-1}) and LL (15 µmol photons m^{-2} s^{-1}) conditions. No apparent difference in the growth of *Δflv3* and WT was observed under these conditions (data not shown). Hence, the mere loss of nitrate, which is an important electron sink, does not affect the growth of *Δflv3* when grown on ammonium. Ammonium chloride can work as uncoupling reagents and prevent the formation of a proton gradient across the thylakoid membrane and consequently remove a constraint on the rate of electron transport and release the stress of surplus electrons (Dean and Miskiewicz 2003).

In summary, these results show that Flv3, which is involved in the Mehler-like reaction, is indispensable under autotrophic conditions on arginine with high light. As *Δfx9* has a distinct phenotype compared to *Δflv3*, its role as an electron carrier to Flv3 can either be compensated for by e.g. Fx1 or another ferredoxin or alternatively it does not interact at all with Flv3.

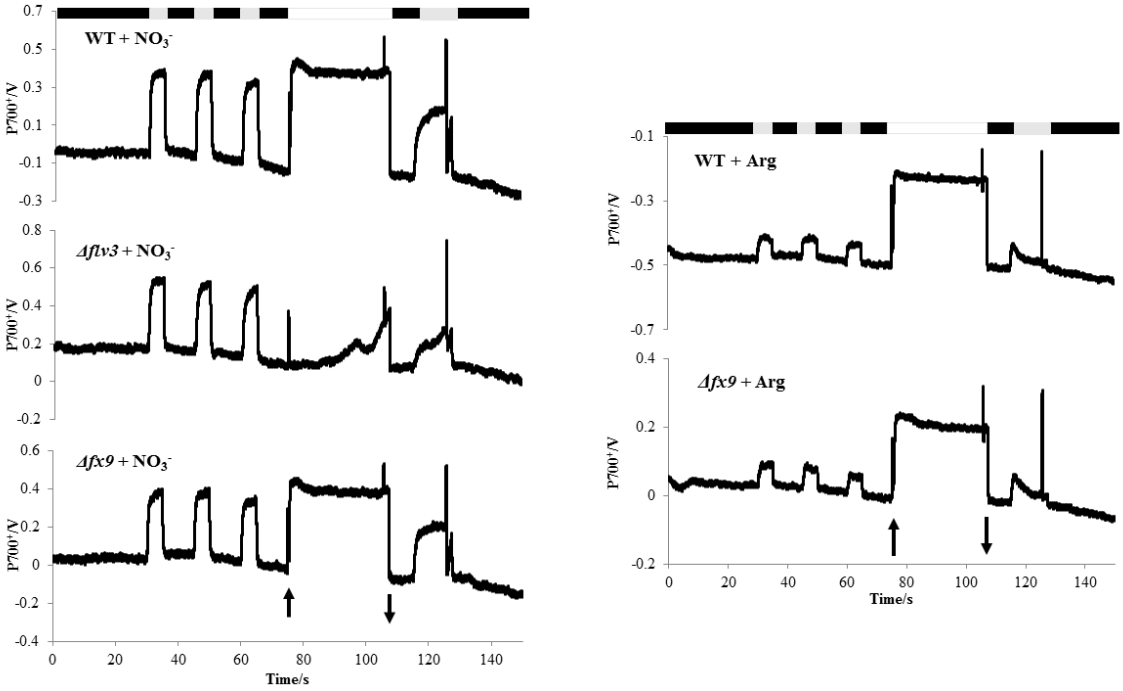

Fig. 4.2.3.2 P700 oxidation in PSI of *Δfx9* and *Δflv3* cells were grown on nitrate (+NO_3^-) or arginine (+Arg). Redox kinetics of P700 was monitored by a Dual-PAM-100. The P700 oxidation formation upon illumination of PSI using 20 µmol photons m^{-2} s^{-1} far red (FR) light (5 s or 10 s, gray bar) or actinic light (AL) under a background of red light (30 s, white bar). Up or down arrow means turning on or off red light, respectively. A saturating pulse (20 ms, 10000 µmol photons m^{-2} s^{-1}) was applied to fully oxidize P700, followed by the (dark) rereduction of $P700^+$. The rest of the time the light was off (black bar) to allow for full re-opening of the reacting centers. Data are representative of three independent experiments.

4.2.4 Characterization of *Δfx9* under autotrophic conditions on different nitrogen sources

Δfx9 was characterized in more detail on different nitrogen sources. The WT and *Δfx9* were again grown on either nitrate or arginine for 5 days. The growth experiment was started with a higher OD_{750} (0.5 compared to 0.05) this time in order to have more cells to measure additional parameters. The growth of *Δfx9* showed the same characteristics as in the experiment that had been started at a lower optical density (Fig. 4.2.4.1A and B). The Chl a content of the cultures was determined every day revealing that *Δfx9* cells possess less Chl a both on nitrate and arginine in comparison to the WT (Fig. 4.2.4.1C). However, the photochemical quenching (q_P) of PSII was not affected in *Δfx9* neither on nitrate nor on arginine but was instead similar to the photochemical quenching in the WT (Fig. 4.2.4.1D).

The respiratory and photosynthesis activities of the cultures were measured as O_2 uptake rate in darkness and O_2 evolution rate in the light, respectively. When grown on nitrate or arginine *Δfx9* had higher respiratory activity but similar photosynthetic activity in comparison to the WT (Fig. 4.2.4.2C-D). However, when nitrate was replaced by arginine, the photosynthetic activity of both WT and *Δfx9* decreased, whereas the growth of the WT was elevated (Fig. 4.2.4.2B and D). In addition, the knockout of *fx9* resulted in lower Chl a content.

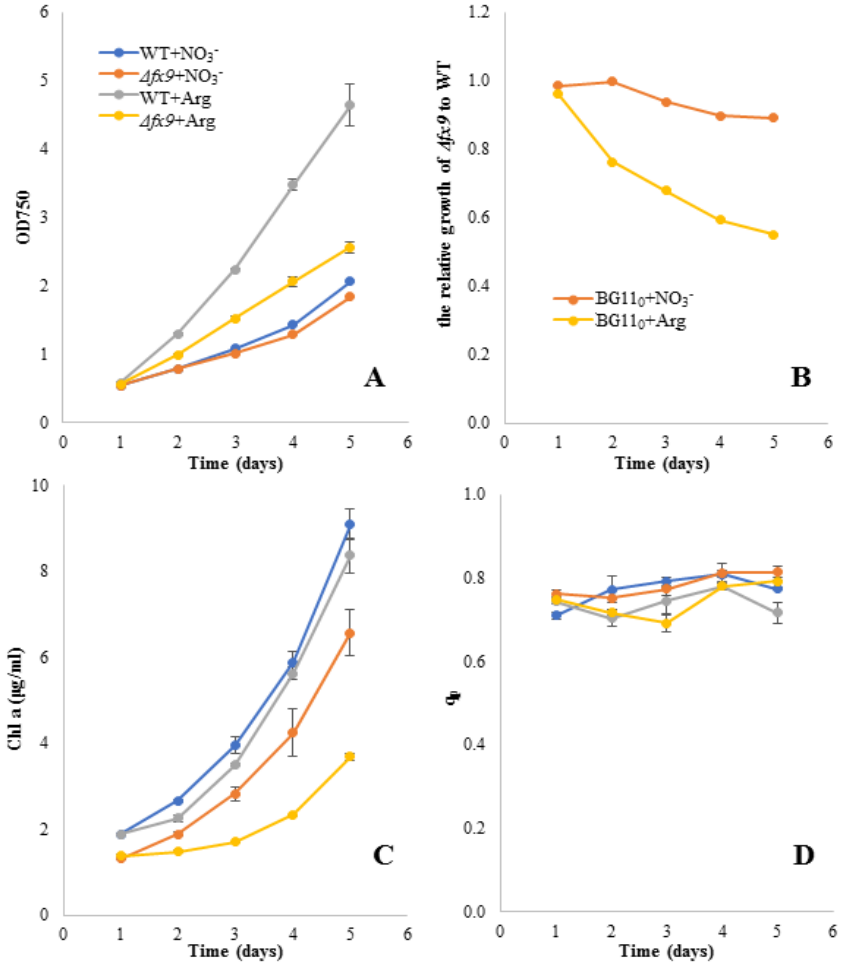

Fig. 4.2.4.1. Growth, Chl a content and photochemical quenching of *Synechocystis* WT and *Δfx9* cells. Strains were grown either with nitrate or L-arginine (+Arg) as sole nitrogen source in continuous light for 5 days. A: Growth is given as a function of OD 750 nm. B: The impaired growth of *Δfx9* on arginine was shown as the ratio of OD_{750} of *Δfx9* to WT; C: Chl a content of WT and Δ*fx9* during the growth in A; D: The photochemical quenching (q_P) induced by actinic light (AL, 20 µmol photons m^{-2} s^{-1}) was determined by Multi-Color PAM (see Materials and methods). $q_P = (F_M' - F_S)/(F_M' - F_0')$. For q_P =1.0, all PS II centers are open. Reported data result from the mean of three independent experiments ± Standard Deviation.

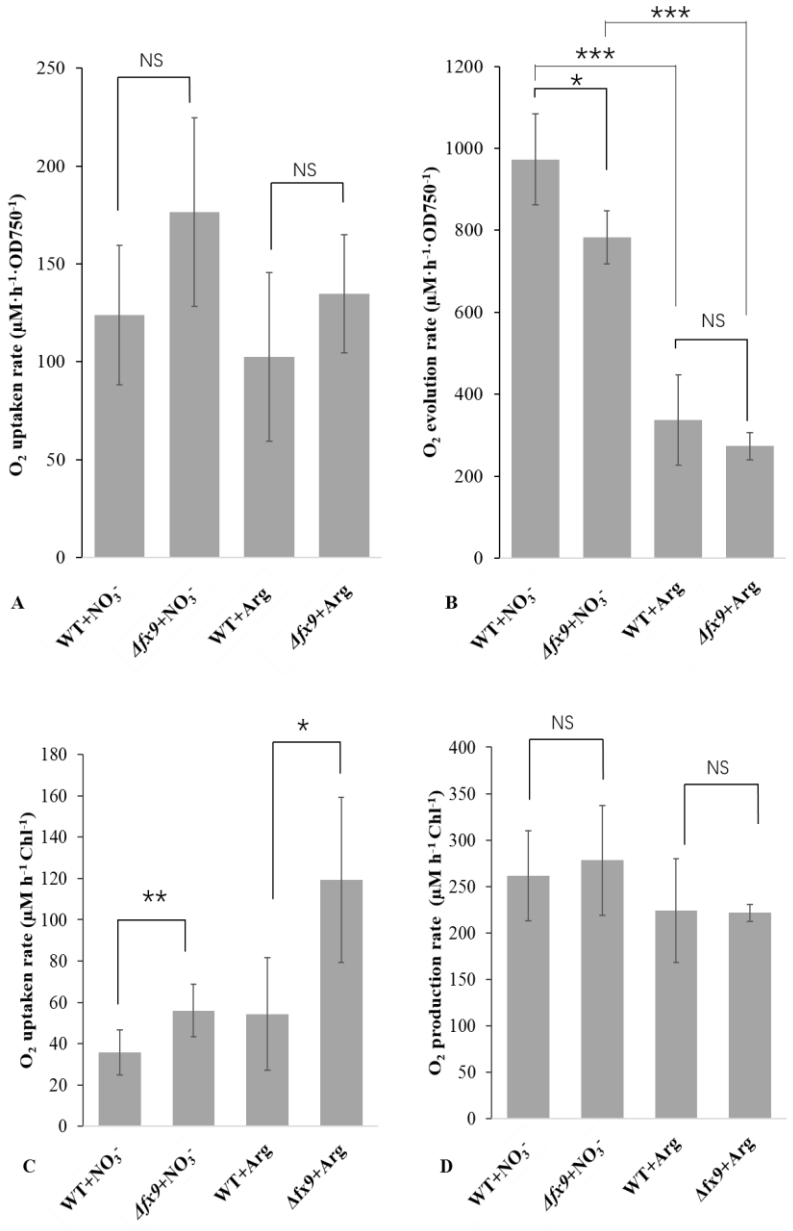

Fig. 4.2.4.2. Respiratory and photosynthetic activity of *Δfx9* grown on nitrate (+NO_3^-) or arginine (+Arg) were monitored as O_2 uptake rate (A and C) and O_2 evolution rate (B and D). Stars on the column diagram indicate differences between mutant and WT by Tukey's HSD test (*P < 0.05, **P < 0.01). Throughout the figure 'NS' indicates 'not significant'. All error bars indicate standard deviation (s.d.) of four daily independent experiments.

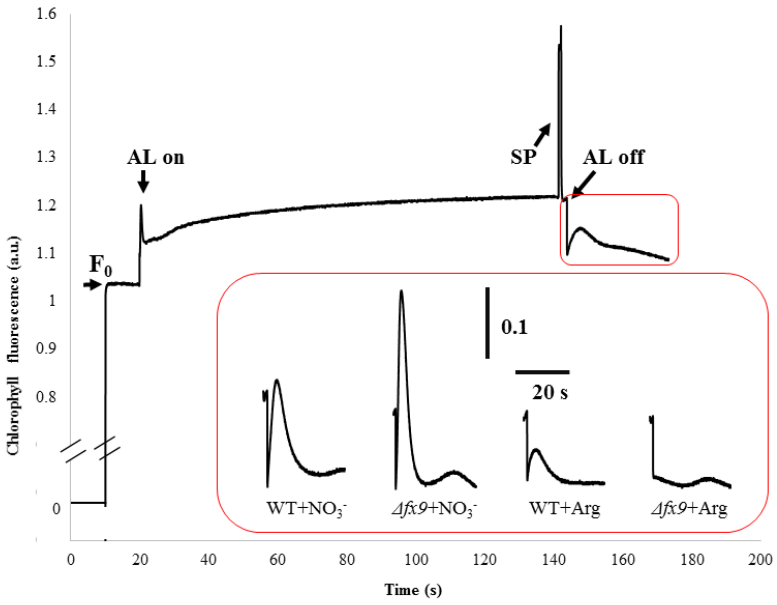

Fig. 4.2.4.3. Monitoring of NDH-CET activity around PSI using chlorophyll florescence analysis by Multi-Color PAM (see Materials and methods). Florescence was induced by actinic light (AL, 20 µmol photons m^{-2} s^{-1}) (see Materials and methods). A typical curve of chlorophyll florescence of WT cells grown in BG11 is shown on the top. The same measurements were also performed with Δ*fx9* cells on nitrate (+NO_3^-) or arginine (+Arg). Data are representative of three independent experiments. a.u., Arbitrary units.

In order to investigate whether the impaired growth of *Δfx9* is a result from an over reduced PQ pool on arginine the post-illumination rise in chlorophyll fluorescence was measured in WT and *Δfx9* both on nitrate and arginine. After giving a saturation pulse, the actinic light was turned off, so that the cells encountered dark conditions (Fig. 4.2.4.3). As PSI is no longer excited it does no longer draw electrons from the photosynthetic electron chain. The post-illumination rise in chlorophyll fluorescence originates from PSII and correlates to the amount of electrons that are present in the PQ pool. The more reduced the PQ pool the higher the fluorescence signal. Electrons that accumulate in this post-illuminated phase in the PQ pool can either originate from the CET in light (Chen et al. 2016a) that flow back into the PQ pool, alternatively, electrons from carbohydrate oxidation can be fed into the PQ pool under these conditions.

Figure 4.2.4.3 shows that the PQ pool of *Δfx9* is more reduced in the post-illumination phase compared to the WT on nitrate. This is in line with the observation of an enhanced CET in *Δfx9* compared to the WT on nitrate (Fig. 4.2.2.3). Interestingly, the reduction of the PQ pool on arginine during the post-illumination phase is lower both in WT and *Δfx9* when compared to conditions on nitrate. Furthermore, the post-illumination rise in *Δfx9* is lower compared to the WT, while the rest of the chlorophyll fluorescence curves of WT and *Δfx9* on arginine are similar to each other. These results suggest that contrary to the condition on nitrate, the absence of Fx9 slows down NDH-CET activity when grown on arginine.

4.2.5 Different efforts to rescue growth of *Δfx9* grown on arginine under autotrophic conditions

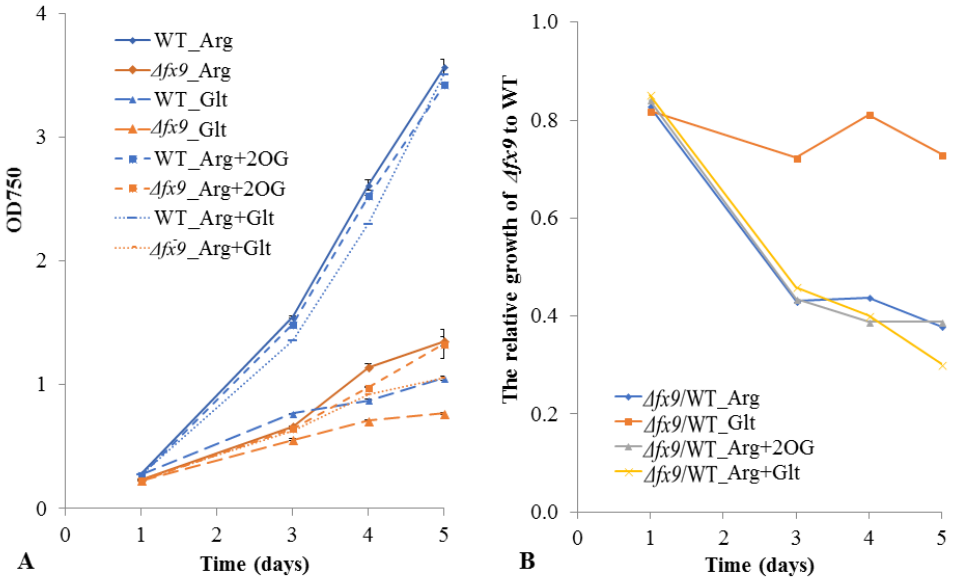

Fig. 4.2.5.1. A: Growth of WT and *Δfx9* on either arginine (Arg), glutamate (Glt), arginine and 2-oxogluatarate (Arg+2OG), or arginine and glutamate (Arg+Glt). B: Relative growth of *Δfx9* to WT. Reported data result from the mean of three independent experiments ± Standard Deviation.

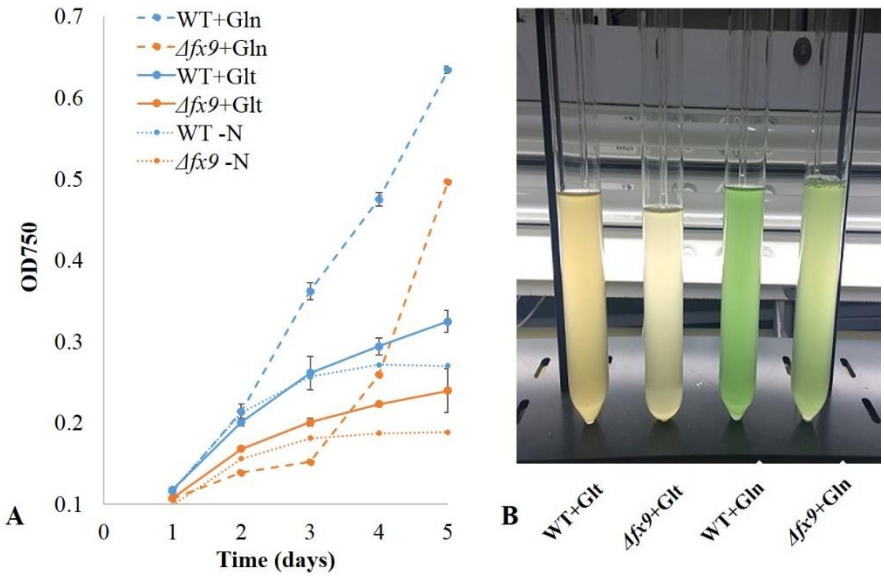

Fig. 4.2.5.2. Autotrophic growth (A) and phenotypical appearance (B) of WT and *Δfx9* with different nitrogen sources. Glt: glutamate; Gln: glutamine; -N: no nitrogen source. Reported data result from the mean of three independent experiments ± Standard Deviation.

Arginine is degraded either via the L-arginine deiminase or the L-arginine dehydrogenase pathway in *Synechocystis* (Schriek et al. 2007). One of the final products of these two pathways is glutamate (see the introduction part). 2-oxoglutarate is required as carbon skeleton for glutamate synthesis in cyanobacteria (Flores and Herrero 2005a) and can be synthesized via a ferredoxin-dependent α-ketoglutarate synthase in green algae (Yang et al. 2015). In order to further confine possible functions of Fx9 on arginine, different efforts were undertaken to rescue its growth and to thereby identify possible metabolic pathways in which Fx9 is involved. Neither the addition of glutamate nor 2-oxoglutarate could rescue the growth of *Δfx9* on arginine (Fig. 4.2.5.1). Both WT and *Δfx9* turned yellow and grew slowly on glutamate as well as with the absence of nitrogen source (Fig. 4.2.5.2).

Transcript profiling indicates that the glutamate synthase (GOGAT) pathway plays a more important role in nitrogen assimilation in response to nitrogen starvation (Krasikov et al. 2012, Schriek et al. 2008). In photosynthetic oxygenic organisms two types of GOGATs have been found; one uses ferredoxin and a second type uses NADH as electron donor (Flores and Herrero 2005a). The ferredoxin-dependent glutamate synthase (Fd-GOGAT or GlsF) uses the amide group of glutamine to reductively aminate 2-oxoglutarate, generating two molecules of glutamate (Flores and Herrero 2005a). To test if the Fx9 works as an electron donor for *Synechocystis* Fd-GOGAT, we grew WT and *Δfx9* cells with 5 mM glutamine as sole nitrogen source. The growth curves show that *Δfx9* displays a sigmoidal growth curve when grown on glutamine (Fig. 4.2.5.2.A), which is in line with the growth of *ΔglsF* in the cyanobacterium *Plectonema boryanum in* which the ferredoxin-dependent glutamate synthase (GlsF) is deleted (Okuhara et al. 1999). This result indicates that Fx9 could potentially be an electron donor for Fd-GOGAT (GlsF). However, this idea would have to be tested in detail.

4.3 Characterization of the ferredoxin deletion mutants in *Synechocystis* under mixotrophic conditions

Previous work in our group showed that the absence of PFOR (Pyruvate: Ferredoxin/Flavodoxin Oxidoreductase) results in impaired growth under mixotrophic conditions as the optical density of the cultures drop at the end of the cultivation time (unpublished). This is astonishing as PFOR is known as an oxygen sensitive enzyme whose absence should thus not result in a growth phenotype under oxic conditions. In order to identify the ferredoxins that might be reduced by PFOR under mixotrophic conditions all available ferredoxin deletion mutants (*fx2/Δfx2*, *Δfx3*, *Δfx4*, *fx5/Δfx5*, *Δfx6*, *Δfx7*, *Δfx9*, *Δfx7Δfx9*, *Δfx7Δfx8Δfx9*, *Δfx9ΔisiB*, *ΔisiB*) and the PFOR mutant *Δpfor* were cultivated under mixotrophic conditions.

4.3.1 Screening and characterization of *Synechocystis* ferredoxin deletion mutants under mixotrophic conditions

All the strains were grown under mixotrophic conditions in the presence of 10 mM glucose on nitrate. As shown in the growth curves in Fig. 4.3.1.1 and Fig. 4.3.1.2A all mutants grew like the WT in the exponential growth phase, however, *Δfx3, Δfx9, Δfx7Δfx9, Δfx7Δfx8Δfx9, Δfx9ΔisiB* and *ΔisiB* started to slow down their growth and decreased their optical density from the 6th day on, which is similar to the growth phenotype in *Δpfor*. Obviously, deletion of either Fx3, Fx9 (alone and in combination with other deleted ferredoxins) or IsiB (flavodoxin) had a strong effect on the growth behavior under mixotrophic conditions. Under mixotrophic conditions a surplus of electrons might accumulate when electrons from water splitting at PSII in photosynthesis are available in parallel to electrons originating from glucose degradation. In previous work (Chen 2014) it was hypothesized that these surplus electrons might be responsible for the impaired growth of *Δpfor* cultures as PFOR might be an important electron sink for *Synechocystis* under mixotrophic conditions, especially at the nonexponential phase. If this hypothesis is correct, Fx3, bacterial-type ferredoxin Fx9 and the flavodoxin IsiB could be involved in accepting electrons from PFOR under mixotrophic conditions.

The mixotrophic cultures of *Δfx3, Δfx9, Δfx7Δfx9, Δfx7Δfx8Δfx9, Δfx9ΔisiB* and *ΔisiB* showed a much lighter green or more yellow color than that of the WT (Fig. 4.3.1.2B), which means that the content of pigments was probably affected. In order to further investigate the variation of pigments in the cultures, an absorption spectrum from 400 nm to 800 nm of the mutants *Δfx9* and *Δfx7Δfx8Δfx9* was recorded. As shown in Fig. 4.3.1.2E, the relative amount of chlorophyll a (Chl a) to phycocyanin are represented by the peaks at 660 nm and 620 nm, respectively. The broad absorbance peak at 480 nm to 500 nm originates both from Chl a and carotenoids. Fig. 4.3.1.2E shows the spectrum absorbance of the cultures on the 9th day of cultivation, at which the WT reached its stationary phase. Much lower Chl a and phycocyanin contents were found in *Δfx9* and its triple mutant *Δfx7Δfx8Δfx9* compared to the WT (Fig. 4.3.1.2E).

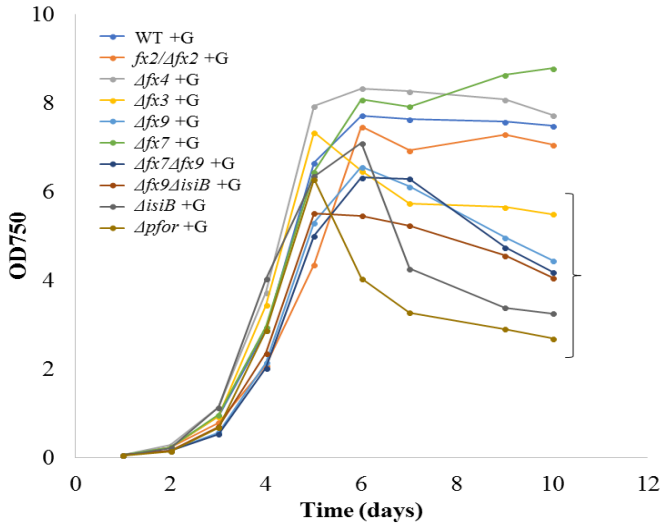

Fig. 4.3.1.1. The growth of ferredoxin deletion mutants under mixotrophic conditions with 10mM glucose (+G) as external carbon source. The PFOR mutant *Δpfor* was monitored in parallel in order to search for ferredoxins that might be reduced by PFOR. The curly brace (}) indicates all the mutants with a similar impaired growth as *Δpfor*. At least three biological repeats were recorded.

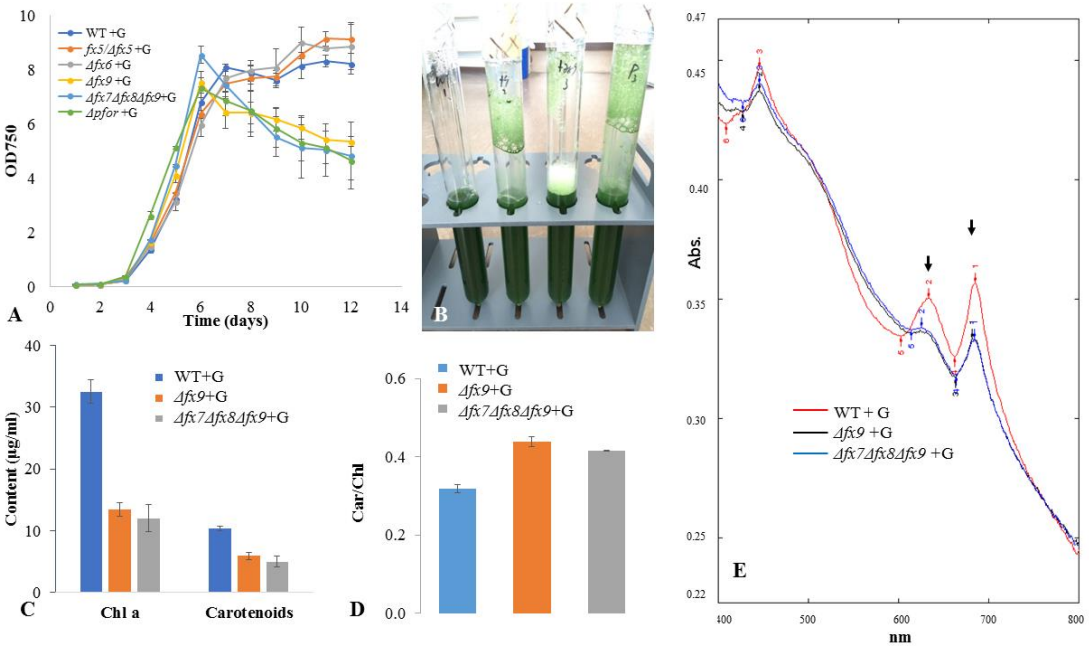

Fig. 4.3.1.2. The growth of ferredoxin deletion mutants under mixotrophic conditions in the presence of 10 mM glucose. The PFOR mutant *Δpfor* was monitored in parallel in order to search for ferredoxins that might be reduced by PFOR. A: Impaired growth of *Δfx9*; B: the foam formed on glass tubes (from right to left: WT, *Δfx9*, *Δfx7Δfx8Δfx9* and *Δpfor*) during mixotrophic growth on the 9th day; C: Chl a and carotenoids content of WT, *Δfx9* and *Δfx7Δfx8Δfx9* on the 9th day; D: the carotenoid-to-chlorophyll (Car/Chl) ratio of WT, *Δfx9* and *Δfx7Δfx8Δfx9* on the 9th day; E: Absorbance spectrum on the 9th day (red line: WT; black line: *Δfx9*; blue line: *Δfx7Δfx8Δfx9*). Arrows at 660 nm and 620 nm indicate the absorbance peak of Chl a and the phycocyanin, respectively.

In addition, the carotenoid contents of WT, *Δfx9 and Δfx7Δfx8Δfx9* were also determined. As shown in Fig. 4.3.1.2C and D the carotenoid contents of *Δfx9 and Δfx7Δfx8Δfx9* were about halved and their carotenoid-to-chlorophyll (Car/Chl) ratio was slightly increased.

The Car/Chl ratio increases when microalgae are starved for nitrogen and exposed to high light (Solovchenko et al. 2008). These are conditions under which the cells have to deal with surplus electrons. Even though both the amount of Chl a and carotenoids was much lower in *Δfx9 and Δfx7Δfx8Δfx9* compared to the WT, the Car/Chl ratio was higher in the mutants, which probably contributed to the yellow color of the mutants grown under mixotrophic conditions. The higher Car/Chl ratio in the mutants indicates that Fx9 might help the cells to dissipate surplus electrons under these conditions. This is well in line with the elevated CET around PSI in *Δfx9* and its problems to grow on arginine.

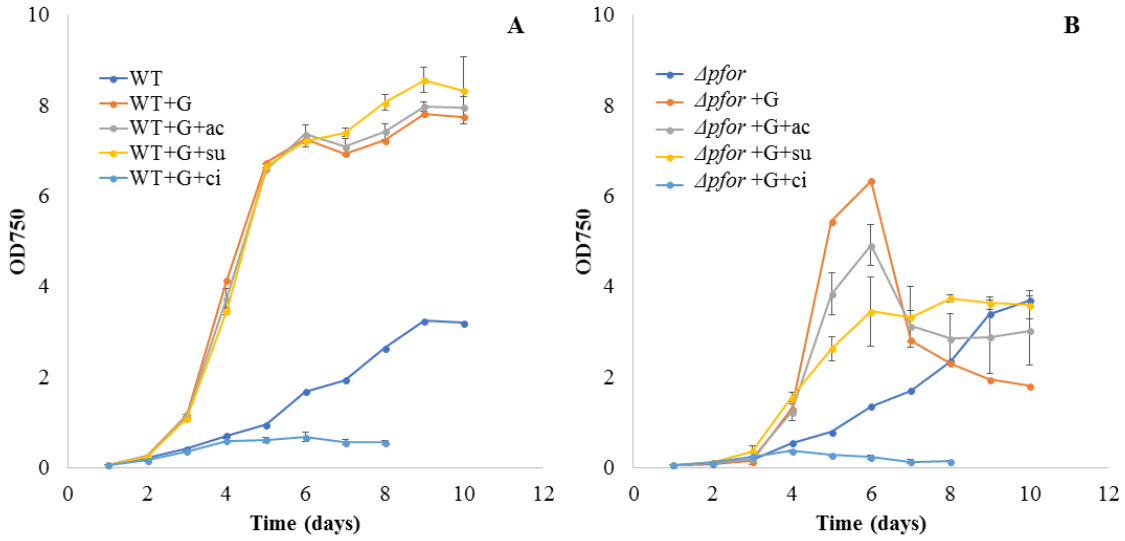

Fig. 4.3.1.3. Growth of *Synechocystis* WT (A) and *Δpfor* (B) under autotrophic, mixotrophic (+G) or mixotrophic conditions with acetate (+G+ac), succinate (+G+su) or citrate (+G+ci). For the last three conditions, at least two biological repeats were measured.

Furthermore, previous work in our group has shown that the PDH complex might be inactivated due to the high $NADH/NAD^+$ ratio in WT and *Δpfor* cultures at a certain time point under mixotrophic conditions, especially at the nonexponential late growth phase (Chen 2014), *Δpfor* thus might have problems to supply the TCA cycle with acetyl-CoA. In order to check whether this could be the reason for the decreased growth of *Δpfor* under mixotrophic conditions, the cultures were supplemented with 10 mM acetate, succinate or citrate, respectively. Acetate can be directly converted to acetyl-CoA to supply the TCA cycle, while succinate or citrate could be used as substrate for the TCA cycle. As shown in Fig. 4.3.1.3, unexpectedly, both *Synechocystis* WT and *Δpfor* could not grow with citrate under mixotrophic conditions. Contrary to Xi Chen's result, supplemented acetate didn't rescue the impaired growth of the mutant. Addition of succinate

abolished the sudden lowering in the OD_{750} which is typical for *Δpfor* under mixotrophic conditions. However, its growth could not be restored to WT levels.

4.3.2 Screening and characterization of *Synechocystis* ferredoxin deletion mutants grown on different nitrogen sources under mixotrophic conditions

Under mixotrophic conditions, ferredoxin could be reduced by PFOR, or alternatively by PSI. The hydrogenase was proposed to be an essential electron sink under mixotrophic, nitrate-limiting conditions (Gutekunst et al. 2014). A hydrogenase deletion mutant was thus not able to grow under mixotrophic conditions on arginine (Burgstaller 2017). In order to further screen which of the ferredoxins might interact with the NiFe-hydrogenase under these conditions, all the ferredoxin deletion mutants (*fx2/Δfx2, Δfx3, Δfx4, fx5/Δfx5, Δfx6, Δfx7, Δfx9, Δfx7Δfx9, Δfx9ΔisiB, ΔisiB*) and the PFOR mutant *Δpfor* were grown on 5 mM arginine instead of nitrate under mixotrophic conditions.

Fig. 4.3.2.1 shows that *Δfx3, Δfx9, Δfx7Δfx9, Δfx7Δfx8Δfx9, Δfx9ΔisiB, ΔisiB,* and *Δpfor* had a very poor growth under mixotrophic conditions on arginine. The merodiploid mutant *fx5/Δfx5* was impaired in its growth as well, even though to a much lesser extent than mutants in which either Fx3, Fx9 or IsiB were deleted (Fig. 4.3.2.1C). The growth phenotype of the PFOR mutant *Δpfor* under mixotrophic conditions on arginine is not consistent (Fig. 4.3.2.1A and C). The mutant did not grow in ten growth experiments (mainly in old climate chamber) but partly grew in seven experiments (mainly in new climate chamber). Occasionally *Δpfor* formed cell aggregates that sank to the bottom of the culture tube. This might have resulted in varying optical densities of the cultures in growth experiments. Previous work in which the *Δpfor* mutant never grew well under mixotrophic conditions on arginine utilized higher concentrations of arginine (10 mM arginine instead of 5 mM arginine) (Chen 2014) which might have resulted in even more oxidized conditions.

The triple mutant *Δfx7Δfx8Δfx9* had a high absorbance in the range of less than 550 nm which indicates together with its yellow color that *Δfx7Δfx8Δfx9* probably has a very high Car/Chl ratio, as the amount of Chl a and phycocyanin was extremely low (Fig. 4.3.2.1D). Arginine can be either utilized as nitrogen source. Alternatively, arginine can be stored as cyanophycin in the cell. The cyanophycin content of the WT and *Δfx7Δfx8Δfx9* was determined on the 6th day. As shown in Fig. 4.3.2.1E *Δfx7Δfx8Δfx9* had a tremendously reduced cyanophycin content in comparison to the WT. This indicates that the mutant which did not grow on arginine and glucose probably did not consume the external arginine.

Ferredoxins/Flavodoxin that are reduced by PFOR can be utilized to reduce nitrate to ammonium. It was hypothesized that the lack of a certain ferredoxin or flavodoxin might affect the reduction of nitrate to ammonium under mixotrophic conditions, especially during the non-exponential growth phase. In order to check whether this might be the reason for the impaired growth of *Δpfor, Δfx9, Δfx7Δfx9, ΔisiB,* and *Δfx9ΔisiB,* the cultures were cultivated with ammonium under mixotrophic conditions. When the cells were cultivated

with 10 mM ammonium (Fig. 4.3.2.2), the growth stopped and decreased from the 4th day on probably because ammonium was lost along with the continuous bubbling of the cultures. *Δpfor*, *Δfx3, fx5/Δfx5, Δfx6, Δfx7, Δfx9, Δfx7Δfx9, Δfx9ΔisiB* and *ΔisiB* grew like the WT before the 4th day, and their growth stopped as observed in the WT from there on (Fig. 4.3.2.2A). The OD_{750} of *Δpfor, Δfx9*, and *ΔisiB* dropped far below the OD_{750} of the WT as had previously also been observed under mixotrophic conditions on nitrate.

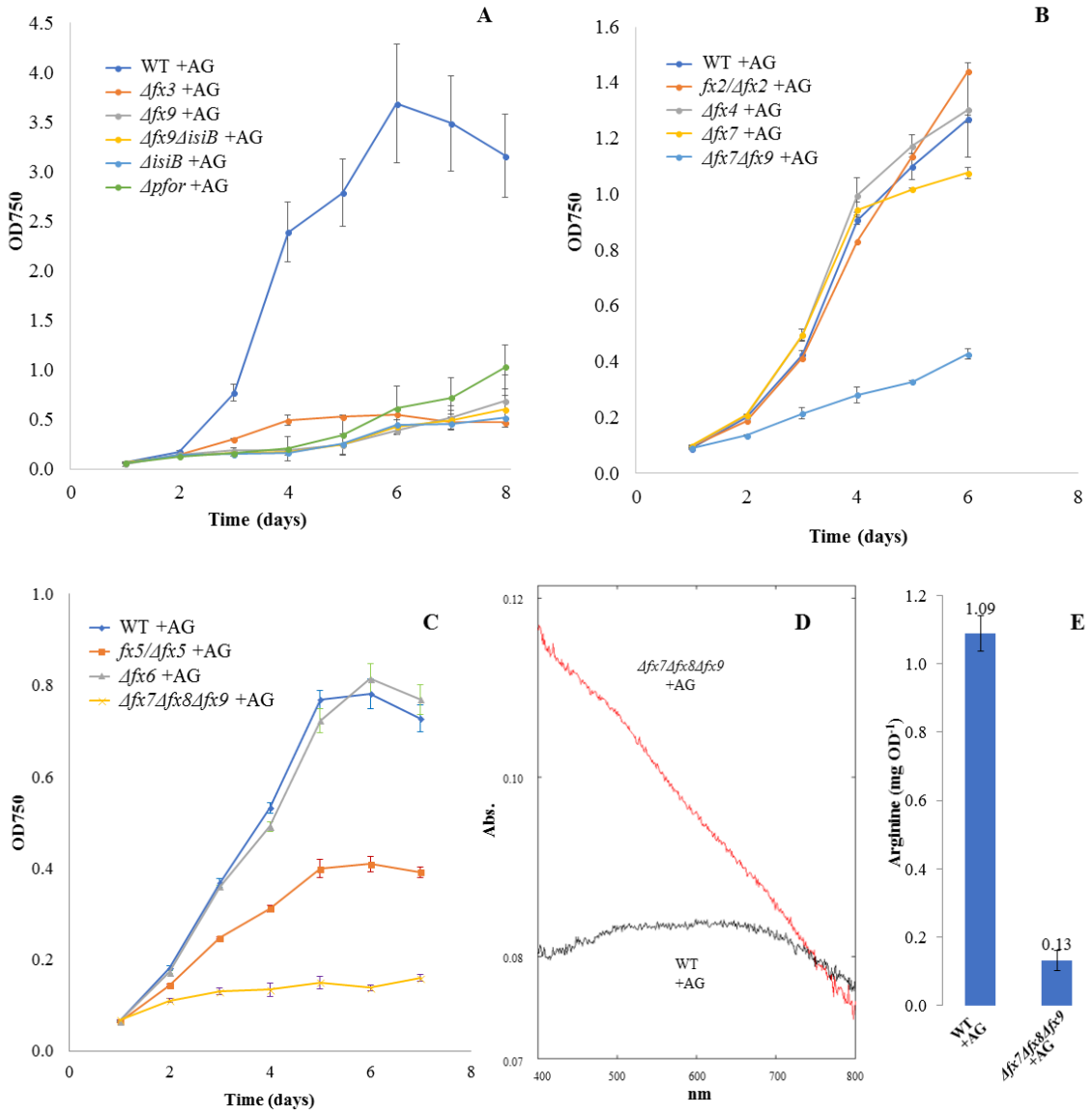

Fig. 4.3.2.1. Growth of ferredoxin deletion mutants and *Δpfor* under mixotrophic conditions on arginine. A-C: Growth of mutants and WT as indicated; D: the absorbance spectrum of cultures on the 6th day (black line: WT; red line: *Δfx7Δfx8Δfx9*); E: Cyanophycin content shown as arginine content in WT and *Δfx7Δfx8Δfx9* on the 6th day.

Interestingly, the putative bacterial-type Fx8 deletion mutant, *fx8/Δfx8*, grew much slower than the WT (Fig. 4.3.2.2B). The triple mutant *Δfx7Δfx8Δfx9* displayed a growth phenotype that can be interpreted as a

combination of the growth phenotypes of *Δfx8* and *Δfx9*. The cells grew slower as *Δfx8* and their OD_{750} dropped to low levels as in *Δfx9* (Fig. 4.3.2.2B).

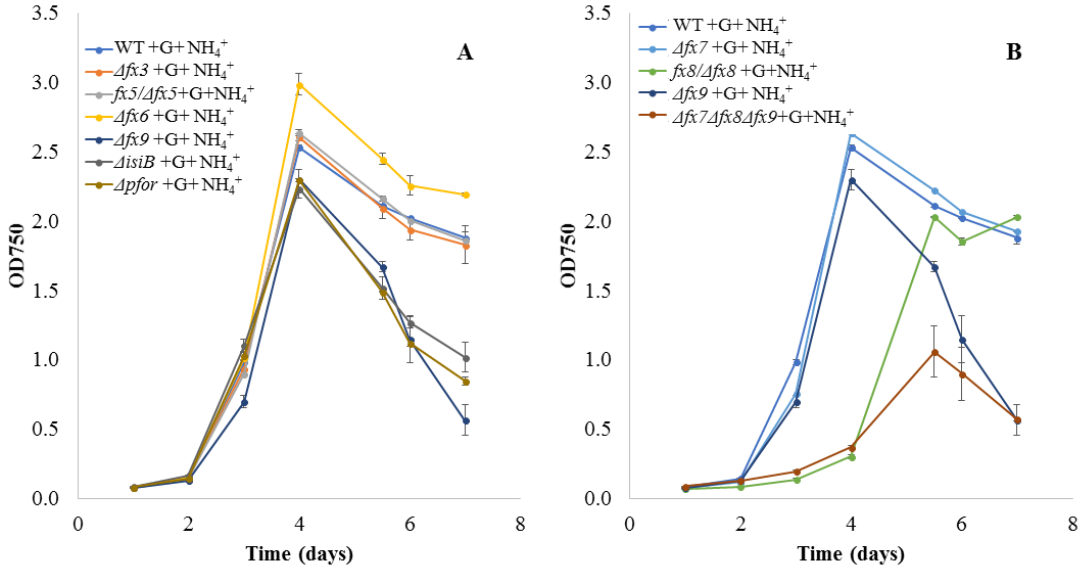

Fig. 4.3.2.2. Growth of *Synechocystis* WT and ferredoxin deletion mutants grown mixotrophically with ammonium as sole nitrogen source (+G+NH_4^+). Two biological repeats were measured.

4.3.3 Characterization of *Δfx9* and hydrogenase-free mutant *ΔhoxH* under mixotrophic conditions on arginine

Deletion of either PFOR, Fx9 or the large subunit of the hydrogenase HoxH in *Synechocystis* inhibits cellular growth under mixotrophic conditions on arginine. PFOR reduces ferredoxin/flavodoxin to provide electrons e.g. for the reduction of nitrate or for fermentative hydrogen production (Gutekunst et al. 2014). In order to understand in more detail why the growth of *Δfx9* and *ΔhoxH* is impaired under the described conditions and how the hydrogenase and Fx9 might be interconnected, both mutants were grown and further characterized under mixotrophic conditions on arginine.

4.3.3.1 Cell phenotype and photosynthesis activity of hydrogenase-free mutant *ΔhoxH* grown under mixotrophic conditions on arginine

The bidirectional NiFe-hydrogenase of *Synechocystis* was suggested to be essential under special oxic conditions regardless of the enzyme´s sensitivity to oxygen (Burgstaller 2017). Furthermore, the impaired growth of *ΔhoxH* could be partly rescued by either lowering the light intensity or by adding the photosynthesis inhibitor DCMU (Burgstaller 2017), which indicates that the hydrogenase functions as one

important electron sink and could be regulated by light and affected by the photosynthetic electron pressure under mixotrophic conditions on arginine.

For cyanobacteria, arginine has several roles. It can be used as a substrate to synthesize cyanophycin, which is a storage form of arginine, or it can alternatively be used as an amino acid directly or oxidized to ammonia for protein synthesis via glutamate and ornithine (Maheswaran et al. 2006). In order to understand in more detail why *ΔhoxH* is not able to grow under mixotrophic conditions on arginine, WT and *ΔhoxH* were further characterized.

In order to check the phenotypes of the cells they were monitored via transmission electron microscopy (TEM). Both strains were grown under photoautotrophic conditions (BG11) and mixotrophic conditions on arginine (BG11o+AG). Cells were collected and immediately treated with fresh sodium cacodylate buffer on the 3rd day to preserve the cells. Under autotrophic conditions, *ΔhoxH* possesses thylakoid membranes like the WT and the overall phenotype of the cells does not differ from the WT (Fig. 4.3.3.1.1), which is in line with their growth under autotrophic conditions (Fig. 4.3.3.1.2). However, when grown mixotrophically on arginine, the phenotypes of the cells of *ΔhoxH* and WT differed tremendously. WT cells accumulated more cyanophycin granules and their thylakoid membranes were heavily degraded (Fig. 4.3.3.1.1), which is in line with the phenotype of *Synechocystis* cell grown autotrophically with arginine (Stephan et al. 2000). However, even though *ΔhoxH* could not grow under mixotrophic conditions on arginine, the cells looked similar to autotrophically grown cells with the only exception that they accumulated more glycogen granules (Fig. 4.3.3.1.1). Cyanophycin granules are only scarcely found in *ΔhoxH* cells. The fact that the cell morphology of *ΔhoxH* changed less than the cell morphology of the WT in combination with a reduced growth, resembles the situation in *Δfx7Δfx9* (or *Δfx9*) on arginine which also changed less than the WT and grew worse (Fig. 4.2.1.7)

Surprisingly, *ΔhoxH* looks as healthy and normal under mixotrophic conditions on arginine as under photoautotrophic conditions even though it is not able to grow. In order to check if the mutant still performs photosynthesis like that under autotrophic conditions, oxygen evolution and oxygen uptake were determined by the Unisense oxygen microsensor in the light and in the dark, respectively.

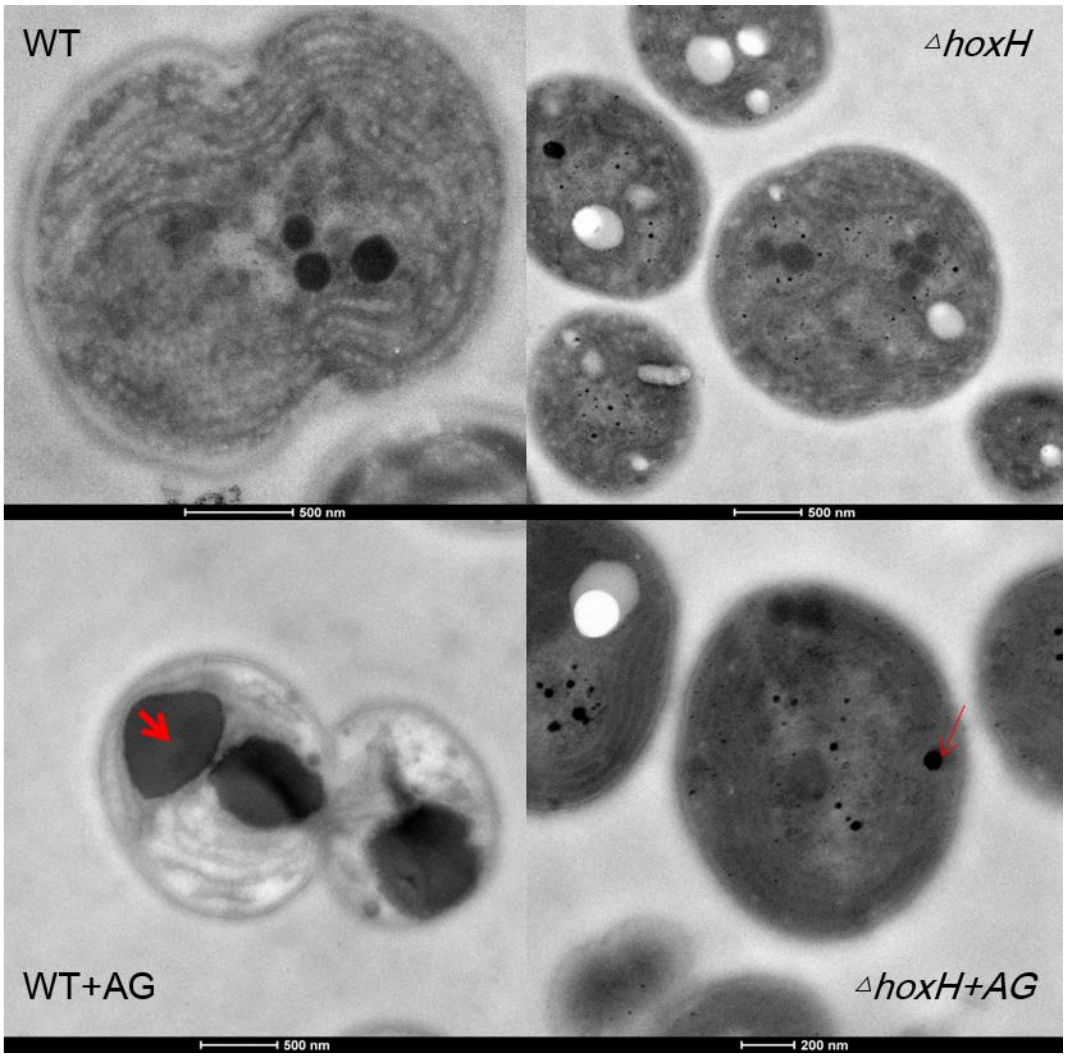

Fig. 4.3.3.1.1. Identification of cyanophycin (red arrows) and the phenotype of whole cells of WT and *ΔhoxH* under autotrophic and mixotrophic conditions on arginine (+AG) via transmission electron microscopy (TEM)

Under autotrophic conditions, *ΔhoxH* and WT display similar oxygen evolution rates (Fig. 4.3.3.1.2C), which means that there is no detectable difference concerning photosynthesis activity. When grown mixotrophically with arginine, both WT and *ΔhoxH* reduce their oxygen evolution rate and thus display much lower photosynthesis activities (Fig. 4.3.3.1.2C). Furthermore, *ΔhoxH* is characterized by a slower oxygen uptake rate in darkness (Fig. 4.3.3.1.2B), which indicates that its respiratory activity is reduced compared to the WT. Remarkably, *ΔhoxH* thus reduces its photosynthesis and respiratory activity even though the cells look normal and healthy with thylakoid membranes and only small amounts of cyanophycin granules. It might thus be that *ΔhoxH* enters a dormant state and does not switch its metabolism as does the WT under mixotrophic conditions on arginine.

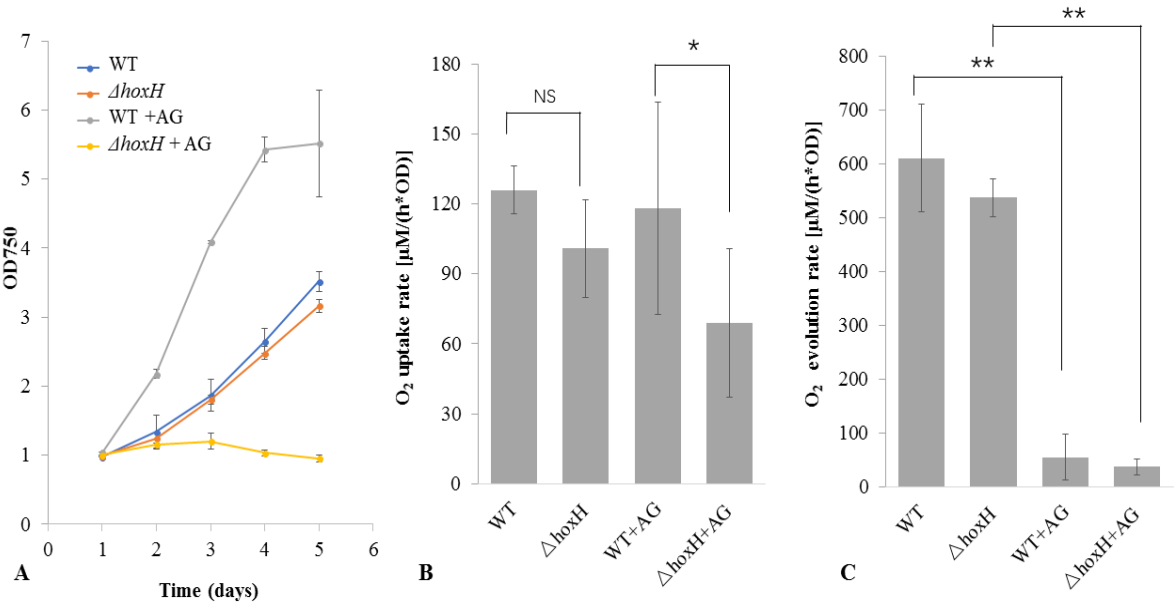

Fig. 4.3.3.1.2. Photosynthetic and respiratory activity of WT and *ΔhoxH* under autotrophic conditions and mixotrophic conditions on arginine (+AG). A: Growth curves of WT and *ΔhoxH*; B and C: Oxygen evolution rates in darkness to monitory respiratory activity and oxygen uptake rate in the light to monitor photosynthetic activity of cultures from the experiment in A (from the 2nd to 4th day). All error bars indicate standard deviation (s.d.) of three daily independent experiments. (NS indicates not significant, *$P < 0.05$, **$P < 0.01$, Student's *t* test).

4.3.3.2 Carbon and nitrogen metabolism of the ferredoxin deletion mutant *Δfx9* and the hydrogenase deletion mutant *ΔhoxH* under mixotrophic conditions on arginine

In order to understand in more detail why *ΔhoxH* and *Δfx9* do not grow under mixotrophic conditions on arginine and in order to analyze their carbon and nitrogen metabolism in comparison to the WT, the consumption of glucose and arginine and the intracellular cyanophycin content were determined.

As shown in Fig. 4.3.3.2.1, WT cells consumed glucose as carbon source and arginine as nitrogen source and grew continuously. They furthermore accumulated large amounts of cyanophycin. In contrast, *ΔhoxH* and *Δfx9* cells that had a poor growth did only consume minor amounts of glucose and arginine and accumulated much smaller amounts of cyanophycin. The results concerning the cyanophycin content in WT and *ΔhoxH* are well in line with the results from the TEM photographs (Fig. 4.3.3.2.1D). Almost 1/3 of the arginine (0.79 mM/2.2 mM on 5th day) that was taken up by WT cells was used for cyanophycin biosynthesis, the residual arginine was probably utilized for protein synthesis (Fig. 4.3.3.2.1B, C and E). Calculating the ratio of intracellular cyanophycin content to the total amount of arginine consumed by cells revealed that WT and *Δfx9* display similar ratios, whereas *ΔhoxH* has a much lower ratio (Fig. 4.3.3.2.1E). This suggests that the reasons for the impaired growth of *Δfx9* and *ΔhoxH* are possibly different.

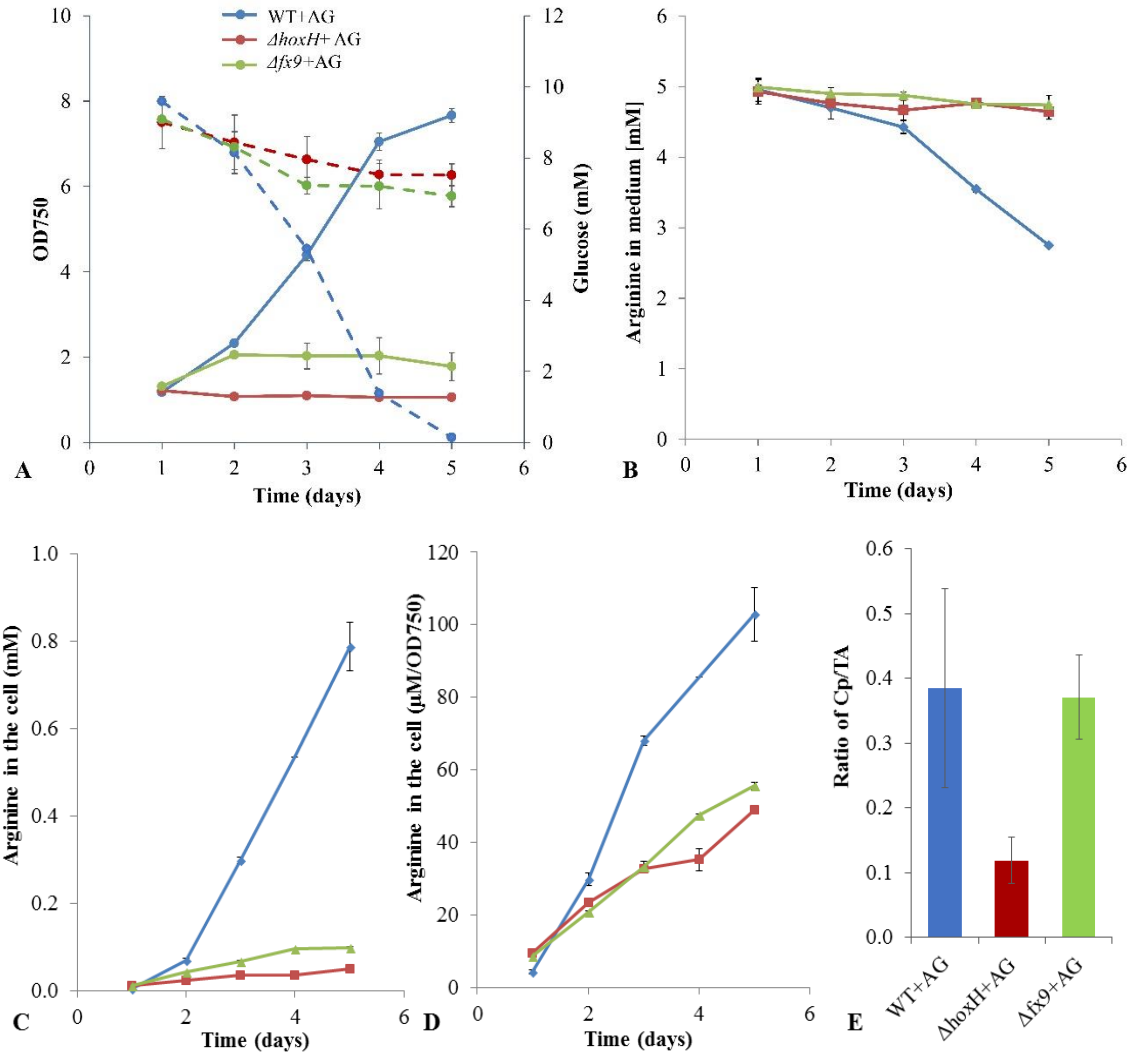

Fig. 4.3.3.2.1. Growth and glucose and arginine consumption of WT, *ΔhoxH* and *Δfx9* under mixotrophic conditions on arginine (+AG). A: Growth (solid line) and glucose consumption (dotted line) measured as glucose concentration in the medium; B: Arginine consumption from medium during the growth experiment in A; C and D: Intracellular cyanophycin content of WT, *ΔhoxH* and *Δfx9* measured as arginine; E: The average ratio of cyanophycin content to total arginine consumption (Cp/TA) from 2nd to 5th day; All error bars indicate standard deviation (s.d.) of at least three daily independent experiments.

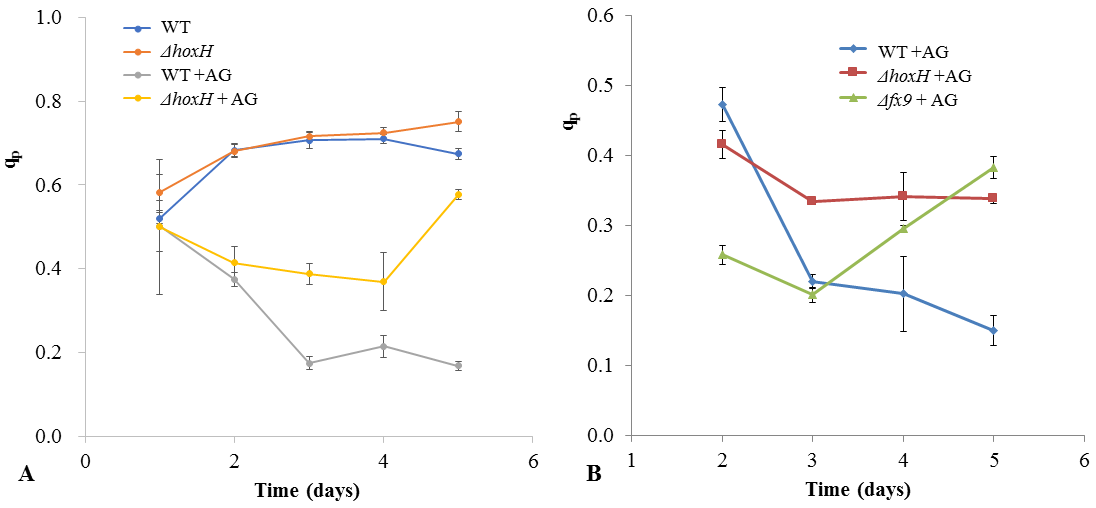

Fig. 4.3.3.2.2. The photochemical quenching (q_p) at PSII determined by measuring the variable fluorescence with a Multi-Color PAM (see Materials and Methods for details). q_p is directly defined by the relative variable fluorescence as: $1 - q_p = V = (F - F_0)/ (F_M - F_0)$; A: The q_p value of WT and *ΔhoxH* (Chl a concentration of 2.5 mg/ml) from Fig. 4.3.3.1.2 A; B: The q_p value of WT and *Δfx9* (Chl a concentration of 2.5 mg/ml) from Fig. 4.3.3.2.1. The given values of *ΔhoxH* are representative of more than five independently repeated experiments, while one experiment with 3 biological repeats are displayed for *Δfx9.*

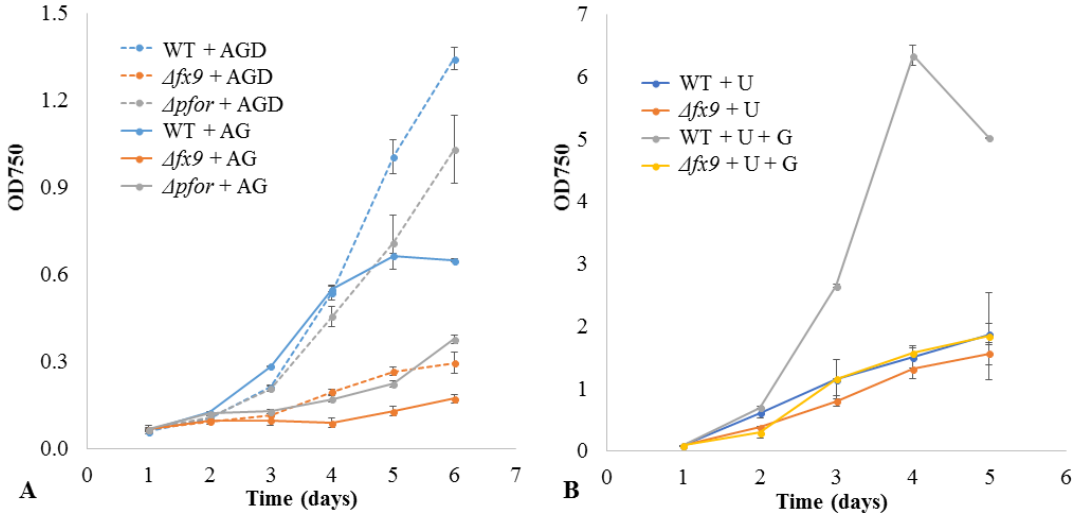

Fig. 4.3.3.3. Attempts to rescue the impaired growth of *Δpfor* and *Δfx9* under mixotrophic conditions on arginine. A: The addition of DCMU, which inhibits the electron transfer between PSII and the PQ pool, could rescue the inhibited growth of *Δpfor,* but had only a minor effect on the growth of *Δfx9.* B: Autotrophic (+U) and mixotrophic (+G+U) growth of WT and *Δfx9* on urea instead of arginine. At least three biological repeats were recorded.

It has been proposed that electrons that are liberated during the oxidation of arginine are fed into the plastoquinone (PQ) pool of the thylakoid membrane utilizing O_2 as an electron acceptor via the cytochrome oxidase (Schriek et al. 2009). The oxidation of arginine might thus result in a reduced PQ pool. Furthermore, electrons from the oxidation of glucose are likewise fed into the PQ pool. The hydrogenase has been suggested to be an electron sink for the photosynthetic electron chain under mixotrophic conditions on arginine (Burgstaller 2017). It was thus hypothesized that *ΔhoxH* might suffer from an over reduced photosynthetic electron chain.

If electrons from arginine and glucose oxidation are fed into the PQ pool in the WT, this should be visible in the photosynthetic electron transport chain and the variable fluorescence. Therefore, the variable fluorescence was recorded with a Multi-Color PAM to check the influence of the absence of HoxH or Fx9 on the photochemical quenching of PSII under autotrophic or mixotrophic conditions on arginine. Fig. 4.3.3.2.2A shows that the deletion of *hoxH* did not have an influence on the photochemical quenching (q_p) of PII under autotrophic conditions. However, under mixotrophic conditions on arginine the photochemical quenching of the WT was reduced indicating that the plastoquinone pool was more reduced (Fig. 4.3.3.2.2A). In contrast to the WT, the values of q_p stayed high in *ΔhoxH* and *Δfx9* which indicates that less electrons were fed into the PQ pool in the mutants (Fig. 4.3.3.2.2A and B). This is well in line with the observation that *ΔhoxH* and *Δfx9* did only consume minor amounts of glucose and arginine. It thus seems that the WT accomplishes a metabolic shift under mixotrophic conditions on arginine. Photosynthetic activity declines, thylakoid membranes are degraded and large amounts of cyanophycin are accumulated, however, growth continues based on the utilization of glucose and arginine. The oxidation of glucose and arginine enhances the reduction of the PQ pool. In contrast, *ΔhoxH* and *Δfx9* stop their growth under these conditions and thus enter a dormant-like state. They barely consume glucose and arginine which thus leaves the PQ pool less reduced compared to the WT. *ΔhoxH* keeps its thylakoid membranes, however, reduces its photosynthetic activity as well and both *ΔhoxH* and *Δfx9* accumulate less cyanophycin in their cells.

4.3.3.3 Attempts to rescue the inhibited growth of *Δfx9* under mixotrophic conditions on arginine

Both the deletions of Fx9 and HoxH result in poor growth under mixotrophic conditions on arginine. The same is true for the deletion of PFOR (*Δpfor*), even though this mutant grows slightly better than either *ΔhoxH* or *Δfx9.* It is therefore nearby to hypothesize that PFOR might reduce Fx9, which further transfers its electrons to the hydrogenase. It has been previously shown that the impaired growth of *ΔhoxH* could be rescued by the addition of DCMU, which inhibits the transfer of electrons from PSII to the PQ pool (Burgstaller 2017). Based on this hypothesis all three mutants *Δpfor*, *ΔhoxH*, and *Δfx9* would suffer from an excess of electrons due to the missing of an electron sink (hydrogenase) and might thus be rescued by the addition of DCMU. Therefore, WT, *Δpfor* and *Δfx9* were grown on glucose and arginine in the presence and in the absence of DCMU. Addition of DCMU rescued the growth of *Δpfor* as had previously been shown for *ΔhoxH*, however, it had only a minor effect on the growth of *Δfx9* (Fig. 4.3.3.3A). This disproves the

hypothesis that Fx9 is the electron shuttle between PFOR and the hydrogenase. It furthermore indicates that the reasons for the growth impairment of *Δfx9* might differ from those of *Δpfor* and *ΔhoxH.*

In order to check if the growth phenotype of *Δfx9* under mixotrophic conditions on arginine is rather due to the absence of nitrate as an electron sink or due to the presence of arginine itself, the mutant was grown on glucose and urea instead of arginine. Urea is an effective nitrogen source that can be taken up and directly and is converted to ammonium by the urease in cyanobacteria (Erratt 2017). Under autotrophic conditions *Δfx9* and WT grew similar (Fig. 4.3.3.3B). However, when grown under mixotrophic conditions on urea, the WT enhanced its growth compared to autotrophic conditions on urea, whereas *Δfx9* did not enhance its growth in the presence of glucose (Fig. 4.3.3.3B). These results show that the deletion of Fx9 also affects the mixotrophic growth of *Synechocystis* on urea, even though to a lesser extent. The impaired growth under mixotrophic conditions might thus be partly due to a special effect of arginine and partly to the absence of nitrate as an electron sink. Another possibility is, that Fx9 is of importance as soon as carbohydrates are provided externally. *Δfx9* displays a reduced growth in the presence of glucose (under mixotrophic conditions) on nitrate, ammonium, arginine and urea (Fig. 4.3.1.2, Fig. 4.3.2.1, Fig. 4.3.2.2, and Fig. 4.3.3.3). Its growth is worst on glucose and arginine and best on glucose and nitrate. Furthermore, growth on arginine alone in the absence of glucose also results in poorer growth of *Δfx9* (Fig. 4.2.1.2). In contrast to urea and ammonium and nitrate, arginine contains carbon. Due to the carbon content of arginine, cultivation on arginine in the absence of glucose could be regarded as partly mixotrophic conditions. In summary, Fx9 in *Synechocystis* might be important for carbohydrates metabolism under mixotrophic conditions.

4.3.4 Characterization of pyruvate dehydrogenase (PDH) under mixotrophic conditions

Both the PDH (pyruvate dehydrogenase complex) complex and PFOR (pyruvate: ferredoxin oxidoreductase) occupy a central position in the energy metabolism as they link glucose metabolism with the tricarboxylic acid (TCA) cycle and subsequent oxidative phosphorylation via the catalysis of pyruvate to acetyl-CoA (Pietrocola et al. 2015). However, the deletion of PFOR causes an impaired growth of *Synechocystis* under mixotrophic conditions as well as on arginine (Fig. 4.3.1.2 and 4.2.1.1), especially at the nonexponential phase. This indicates that the oxygen-sensitive PFOR has a function under aerobic conditions that cannot be compensated for by the PDH complex. However, it is known from eukaryotes that the PDH complex gets phosphorylated and thereby inactivated at high NADH/NAD^+ ratios (Korotchkina and Patel 2001). Indeed, elevated NADH/NAD^+ ratios were measured in the WT under mixotrophic conditions (Chen 2014). Therefore, it was hypothesized that the PDH complex might get phosphorylated and thereby inactivated in the nonexponential phase under mixotrophic conditions, thereby necessitating PFOR to overtake its function.

In order to test the hypothesis that NADH provokes a phosphorylation of E1 of the PDH complex in *Synechocystis* the three following question need to be answered: (1) Does the genome of *Synechocystis* contain homologs to PDH kinases and PDH phosphatases? (2) Does E1 of the PDH complex in *Synechocystis*

contain the phosphorylation sites found in eukaryotes? (3) Is the PDH complex phosphorylated at high $NADH/NAD^+$ ratios?

4.3.4.1 *Synechocystis* holds several annotated serine/threonine kinases and several serine/threonine phosphatases

In eukaryotes, NADH activates a PDH kinase which phosphorylates one of three serine residues in the pyruvate dehydrogenase E1 subunit (Korotchkina and Patel 2001, Patel et al. 2014). Dephosphorylation of E1 is catalyzed by a PDH phosphatase which results in the reactivation of the PDH complex (Reed 1981).

However, BLASTP (http://genome.microbedb.jp/blast/blast_search/cyanobase/Synechocystis/genes) analysis with PDH kinases and PDH phosphatases in human and yeast at the amino acid level showed no sequence identity to any protein of *Synechocystis* in CyanoBase (data not shown). This result indicates that *Synechocystis* does not have a homolog to the PDH kinases and the PDH phosphatase of eukaryotes.

Alternatively, it was reported that the cyanobacterium *Synechocystis* possesses seven STKs and seven STPs (Table 1.6.1) (Zhang et al. 1998, Zhang et al. 2005, Zhang et al. 2007), which are candidates that could overtake the phosphorylation and dephosphorylation of the PDH complex. For further information please check the Chapter 1.6.1.2.

4.3.4.2 E1 of the PDH complex in *Synechocystis* contains one phosphorylation site found in eukaryotes

In mammals, phosphorylation of E1 occurs at three serine residues (Ser264, site 1; Ser271, site 2; and Ser203, site 3) (Fig. 4.3.4.2.1). Phosphorylation of site 1 completely abolishes the activity of the PDH complex whereas phosphorylation of sites 2 and 3 results in moderate catalytic activities in human PDH complexes (Korotchkina and Patel 2001). It was shown that phosphorylation of site 1 blocks the access to the active site and thereby impedes binding of pyruvate (Schriek et al. 2007). In order to study if these three phosphorylation sites are conserved in cyanobacteria as in eukaryotes, several homologs of E1 component subunit alpha of PDH complex from cyanobacteria, higher plant, yeast and mammal were aligned by ClustalW multiple sequence alignment. Fig. 4.3.4.2.1 shows that the first phosphorylation site of E1 is found in cyanobacteria, however, sites 2 and 3 are neither conserved in yeast, in higher plant nor in cyanobacteria. However, as phosphorylation of the first phosphorylation site suffices to inactivate the PDH complex also in mammals, it can be assumed, that the conserved serine residue that is found in cyanobacteria, should be adequate to allow a regulation of the PDH complex via phosphorylation.

We furthermore checked if the first phosphorylation site (S1) that we found in *Synechocystis* is conserved among cyanobacteria and found that it is present in 86 from 91 cyanobacteria in the motif GH**S**LA with serine at the conserved position (Fig. 4.3.4.2.2). Only one *Synechococcus* (GH**S**VA), one *Nostoc* (PH**S**KG), and one *Stanieria* (AH**S**KG) strain carry a deviating sequence with the serine at the conserved position (Fig.

4.3.4.2.2). Furthermore, two *Prochlorococcus* strains do not have a serine at the conserved position (Fig. 4.3.4.2.2).

The PDHA protein (Slr1934) is composed of 342 aa and has a molecular weight of 38.16 kDa (Fig. 4.3.4.2.3A). Its theoretical pI (isoelectric point) is 5.08, suggesting that PDHA is rather electronegative, while its instability index is computed to be 38.40 (smaller than 40), indicating that PDHA is rather stable. The PDHA grand average of hydropathicity (GRAVY) is −0.216, indicating that PDHA is rather hydrophilic. By comparing the homolog of PDHA of *Synechocystis* and other species, one peptide (TKYRREVLKDDGYDQ) which constitutes a long loop connecting an alpha helix and a beta sheet in the secondary structure of PDHA and is located in proximity to conserved potential phosphorylation site was selected and used for the synthesis of a *Pdh-E1* antibody (α-PdhA-E1) (Fig. 4.3.4.2.1 and 4.3.4.2.3).

In summary, phosphorylation site 1 (Fig. 4.3.4.2.3A), which is responsible for the complete inactivation of the PDH complex in eukaryotes, is highly conserved in cyanobacteria.

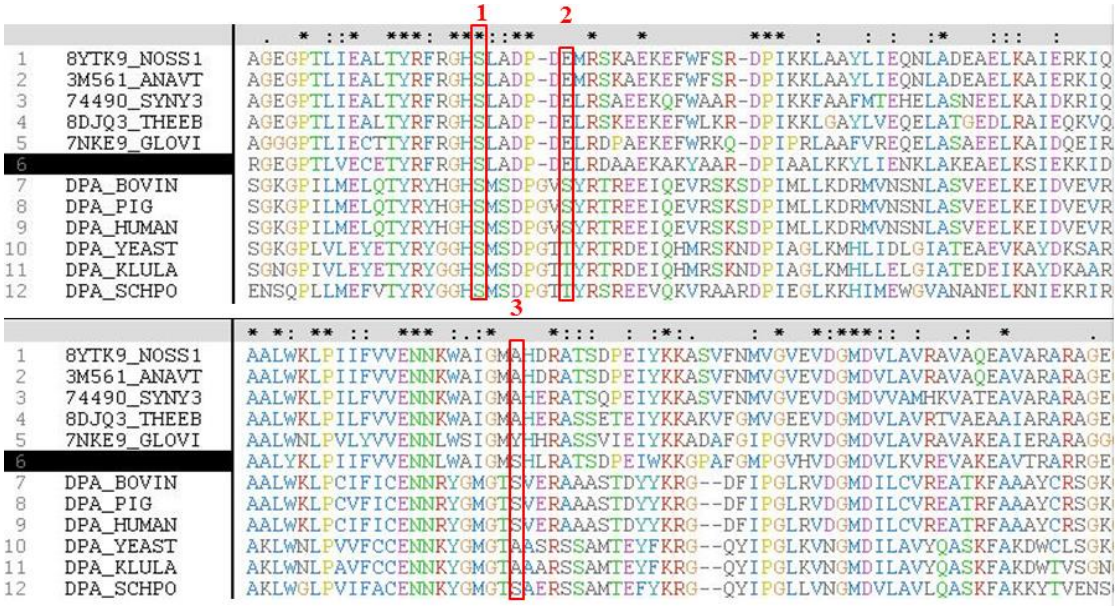

Fig. 4.3.4.2.1. Cutout of a multiple sequence alignment of the complete amino acid sequence of pruvate dehydrogenase E1 component subunit alpha from eukaryotes (higher plant, yeast and mammal) and cyanobacteria. The alignment was generated by using the ClustalW multiple sequence alignment program, using sequences from cyanobacteria *Nostoc* sp. strain PCC 7120 (Line 1, UniProt accession no. Q8YTK9), *Anabaena variabilis* strain ATCC 29413/PCC 7937 (lanes 2, UniProt Q3M561), *Synechocystis* sp. strain PCC 6803 (lanes 3, UniProt P74490), *Thermosynechococcus elongatus* strain BP-1 (lanes 4, UniProt Q8DJQ3), *Gloeobacter violaceus* strain PCC 7421 (lanes 5, UniProt Q7NKE9), and higher plant *Arabidopsis thaliana* (lines 6, UniProt O24457), and mammal *Bos taurus* (lanes 7, UniProt A7MB35), *Sus scrofa* (lanes 8, UniProt P29804), *Homo sapiens* (lanes 9, UniProt P08559), and yeast *Saccharomyces cerevisiae* strain ATCC 204508 (lanes 10, UniProt P16387), *Kluyveromyces lactis strain* ATCC 8585 (lanes 11, UniProt O13366), *Schizosaccharomyces pombe* strain 972 (lanes 12, UniProt Q10489). A line above the alignment is used to mark strongly conserved positions with three characters ('*', ':' and '.'). Three serin residues of conserved phosphorylation site were highlighted by red box and red number respectively.

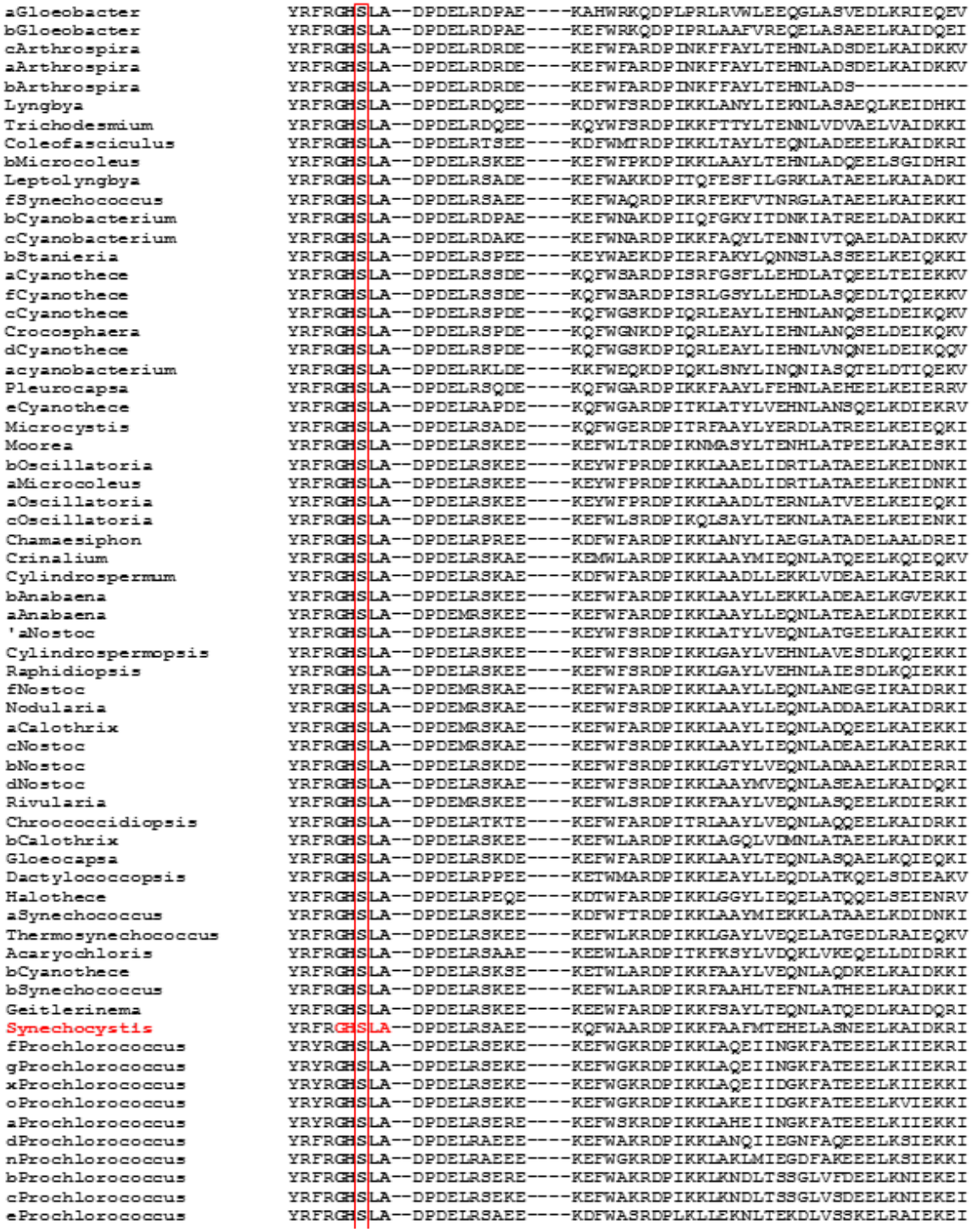
aGloeobacter YRFRGHSLA--DPDELRDPAE----KAHWRKQDPLPRLRVWLEEQGLASVEDLKRIEQEV
bGloeobacter YRFRGHSLA--DPDELRDPAE----KEFWRKQDPIPRLAAFVREQELASAEELKAIDQEI
cArthrospira YRFRGHSLA--DPDELRDRDE----KEFWFARDPINKFFAYLTEHNLADSDELKAIDKKV
aArthrospira YRFRGHSLA--DPDELRDRDE----KEFWFARDPINKFFAYLTEHNLADSDELKAIDKKV
bArthrospira YRFRGHSLA--DPDELRDRDE----KEFWFARDPINKFFAYLTEHNLADS----------
Lyngbya YRFRGHSLA--DPDELRDQEE----KDFWFSRDPIKKLANYLIEKNLASAEQLKEIDHKI
Trichodesmium YRFRGHSLA--DPDELRDQEE----KQYWFSRDPIKKFTTYLTENNLVDVAELVAIDKKI
Coleofasciculus YRFRGHSLA--DPDELRTSEE----KDFWMTRDPIKKLTAYLTEQNLADEEELKAIDKRI
bMicrocoleus YRFRGHSLA--DPDELRSKEE----KEFWFPKDPIKKLAAYLTEHNLADQEELSGIDHRI
Leptolyngbya YRFRGHSLA--DPDELRSADE----KEFWAKKDPITQFESFILGRKLATAEELKAIADKI
fSynechococcus YRFRGHSLA--DPDELRSAEE----KEFWAQRDPIKRFEKFVTNRGLATAEELKAIEKKI
bCyanobacterium YRFRGHSLA--DPDELRDPAE----KEFWNAKDPIIQFGKYITDNKIATREELDAIDKKI
cCyanobacterium YRFRGHSLA--DPDELRDAKE----KEFWNARDPIKKFAQYLTENNIVTQAELDAIDKKV
bStanieria YRFRGHSLA--DPDELRSPEE----KEYWAEKDPIERFAKYLQNNSLASSEELKEIQKKI
aCyanothece YRFRGHSLA--DPDELRSSDE----KQFWSARDPISRFGSFLLEHDLATQEELTEIEKKV
fCyanothece YRFRGHSLA--DPDELRSSDE----KQFWSARDPISRLGSYLLEHDLASQEDLTQIEKKV
cCyanothece YRFRGHSLA--DPDELRSPDE----KQFWGSKDPIQRLEAYLIEHNLANQSELDEIKQKV
Crocosphaera YRFRGHSLA--DPDELRSPDE----KQFWGNKDPIQRLEAYLIEHNLANQSELDEIKQKV
dCyanothece YRFRGHSLA--DPDELRSPDE----KQFWGSKDPIQRLEAYLIEHNLVNQNELDEIKQQV
acyanobacterium YRFRGHSLA--DPDELRKLDE----KKFWEQKDPIQKLSNYLINQNIASQTELDTIQEKV
Pleurocapsa YRFRGHSLA--DPDELRSQDE----KQFWGARDPIKKFAAYLFEHNLAEHEELKEIERRV
eCyanothece YRFRGHSLA--DPDELRAPDE----KQFWGARDPITKLATYLVEHNLANSQELKDIEKRV
Microcystis YRFRGHSLA--DPDELRSADE----KQFWGERDPITRFAAYLYERDLATREELKEIEQKI
Moorea YRFRGHSLA--DPDELRSKEE----KEFWLTRDPIKNMASYLTENHLATPEELKAIESKI
bOscillatoria YRFRGHSLA--DPDELRSKEE----KEYWFPRDPIKKLAAELIDRTLATAEELKEIDNKI
aMicrocoleus YRFRGHSLA--DPDELRSKEE----KEYWFPRDPIKKLAADLIDRTLATAEELKEIDNKI
aOscillatoria YRFRGHSLA--DPDELRSKEE----KEYWFPRDPIKKLAADLTERNLATVEELKEIEQKI
cOscillatoria YRFRGHSLA--DPDELRSKEE----KEFWLSRDPIKQLSAYLTEKNLATAEELKEIENKI
Chamaesiphon YRFRGHSLA--DPDELRPREE----KDFWFARDPIKKLANYLIAEGLATADELAALDREI
Crinalium YRFRGHSLA--DPDELRSKAE----KEMWLARDPIKKLAAYMIEQNLATQEELKQIEQKV
Cylindrospermum YRFRGHSLA--DPDELRSKAE----KDFWFARDPIKKLAADLLEKKLVDEAELKAIERKI
bAnabaena YRFRGHSLA--DPDELRSKEE----KEFWFARDPIKKLAAYLLEKKLADEAELKGVEKKI
aAnabaena YRFRGHSLA--DPDEMRSKEE----KEFWFARDPIKKLAAYLLEQNLATEAELKDIEKKI
'aNostoc YRFRGHSLA--DPDELRSKEE----KEYWFSRDPIKKLATYLVEQNLATGEELKAIEKKI
Cylindrospermopsis YRFRGHSLA--DPDELRSKEE----KEFWFSRDPIKKLGAYLVEHNLAVESDLKQIEKKI
Raphidiopsis YRFRGHSLA--DPDELRSKEE----KEFWFSRDPIKKLGAYLVEHNLAIESDLKQIEKKI
fNostoc YRFRGHSLA--DPDEMRSKAE----KEFWFARDPIKKLAAYLLEQNLANEGEIKAIDRKI
Nodularia YRFRGHSLA--DPDEMRSKAE----KEFWFSRDPIKKLAAYLLEQNLADDAELKAIDRKI
aCalothrix YRFRGHSLA--DPDEMRSKAE----KEFWFARDPIKKLAAYLIEQNLADQEELKAIEKKI
cNostoc YRFRGHSLA--DPDEMRSKAE----KEFWFSRDPIKKLAAYLIEQNLADEAELKAIERKI
bNostoc YRFRGHSLA--DPDELRSKDE----KEFWFSRDPIKKLGTYLVEQNLADAAELKDIERRI
dNostoc YRFRGHSLA--DPDELRSKAE----KEFWFSRDPIKKLAAYMVEQNLASEAELKAIDQKI
Rivularia YRFRGHSLA--DPDEMRSKEE----KEFWLSRDPIKKFAAYLVEQNLASQEELKDIERKI
Chroococcidiopsis YRFRGHSLA--DPDELRTKTE----KEFWFARDPITRLAAYLVEQNLAQQEELKAIDRKI
bCalothrix YRFRGHSLA--DPDELRSKEE----KEFWLARDPIKKLAGQLVDMNLATAEELKAIDKKI
Gloeocapsa YRFRGHSLA--DPDELRSKDE----KEFWFARDPIKKLAAYLTEQNLASQAELKQIEQKI
Dactylococcopsis YRFRGHSLA--DPDELRPPEE----KETWMARDPIKKLEAYLLEQDLATKQELSDIEAKV
Halothece YRFRGHSLA--DPDELRPEQE----KDTWFARDPIKKLGGYLIEQELATQQELSEIENRV
aSynechococcus YRFRGHSLA--DPDELRSKEE----KDFWFTRDPIKKLAAYMIEKKLATAAELKDIDNKI
Thermosynechococcus YRFRGHSLA--DPDELRSKEE----KEFWLKRDPIKKLGAYLVEQELATGEDLRAIEQKV
Acaryochloris YRFRGHSLA--DPDELRSAAE----KEEWLARDPITKFKSYLVDQKLVKEQELLDIDRKI
bCyanothece YRFRGHSLA--DPDELRSKSE----KETWLARDPIKKFAAYLVEQNLAQDKELKAIDKKI
bSynechococcus YRFRGHSLA--DPDELRSKEE----KEFWLARDPIKRFAAHLTEFNLATHEELKAIDKKI
Geitlerinema YRFRGHSLA--DPDELRSKEE----KEEWFARDPIKKFSAYLTEQNLATQEDLKAIDQRI
Synechocystis YRFRGHSLA--DPDELRSAEE----KQFWAARDPIKKFAAFMTEHELASNEELKAIDKRI
fProchlorococcus YRYRGHSLA--DPDELRSEKE----KEFWGKRDPIKKLAQEIINGKFATEEELKIIEKRI
gProchlorococcus YRYRGHSLA--DPDELRSEKE----KEFWGKRDPIKKLAQEIINGKFATEEELKIIEKRI
xProchlorococcus YRYRGHSLA--DPDELRSEKE----KEFWGKRDPIKKLAQEIIDGKFATEEELKIIEKKI
oProchlorococcus YRYRGHSLA--DPDELRSEKE----KEFWGKRDPIKKLAKEIIDGKFATEEELKVIEKKI
aProchlorococcus YRYRGHSLA--DPDELRSERE----KEFWSKRDPIKKLAHEIINGKFATEEELKIIEKKI
dProchlorococcus YRFRGHSLA--DPDELRAEEE----KEFWAKRDPIKKLANQIIEGNFAQEEELKSIEKKI
nProchlorococcus YRFRGHSLA--DPDELRAEEE----KEFWGKRDPIKKLAKLMIEGDFAKEEELKSIEKKI
bProchlorococcus YRFRGHSLA--DPDELRSERE----KEFWAKRDPIKKLKNDLTSSGLVFDEELKNIEKEI
cProchlorococcus YRFRGHSLA--DPDELRSEKE----KEFWAKRDPIKKLKNDLTSSGLVSDEELKNIEKEI
eProchlorococcus YRFRGHSLA--DPDELRSAEE----KDFWASRDPLKLLEKNLTEKDLVSSKELRAIEKEI

Fig. 4.3.4.2.2. Multiple sequence alignment of the complete amino acid sequence of pyruvate dehydrogenase E1 component subunit alpha from all sequenced cyanobacteria, *Homo sapiens* (human), *Bos taurus* (cattle) and *Mus musculus* (mouse). Protein sequences of all sequenced cyanobacteria are extracted from Cyanobase (http://genome.annotation.jp/cyanobase, till 2015). The first and second conserved phosphorylation sites were highlighted by red box respectively. The motif GHSLA with serine at the conserved position was highlighted in boldface. *Synechocystis* was marked in red. Strains carrying a deviating sequence with the serine at the conserved position were marked in green.

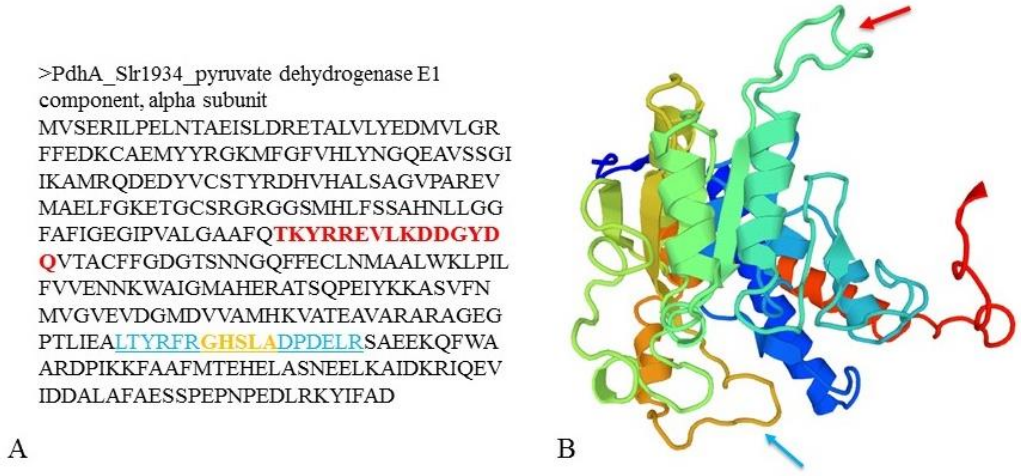

Fig. 4.3.4.2.3. The protein sequence and predicted 3D structure of PDHA from *Synechocystis*. A: The sequence of PDHA was obtained from Cyanobase (Slr1934 in http://genome.annotation.jp/cyanobase/). The specific peptide marked in dark red was used as antibody synthesis. The conserved region with serine was highlighted in blue and underline. B: 3D structure was predicated by SWISS-MODEL with L8AT42 from *Bacillus subtilis* BEST7613 as reference. Red arrow means the specific peptide for antibody synthesis and blue arrow means the conserved region with serine (site 1).

4.3.4.3 Detection of the phosphorylation of the PDH complex in *Synechocystis* by Western blot

In order to study if the PDH complex is phosphorylated under mixotrophic conditions, *Synechocystis* WT cells and Δ*pfor* were grown under photoautotrophic and mixotrophic conditions in order to identify the days on which PFOR is physiologically relevant for growth. Xi Chen determined the NADH/NAD$^+$ ratio in parallel as depicted in Fig. 4.3.4.3.1 (Chen 2014). WT cells were harvested from day 2 to day 7, as the NADH/NAD$^+$ ratio raised within these days and as the growth of *Δpfor* displayed its characteristic growth phenotype. Proteins were isolated from the samples subjected to SDS-PAGE followed by immunoblot analysis with a specific antibody against the E1 subunit of PdhA (α-PdhA-E1) and an antibody that binds specifically to phosphorylated serine residues (α –phosphoserine).

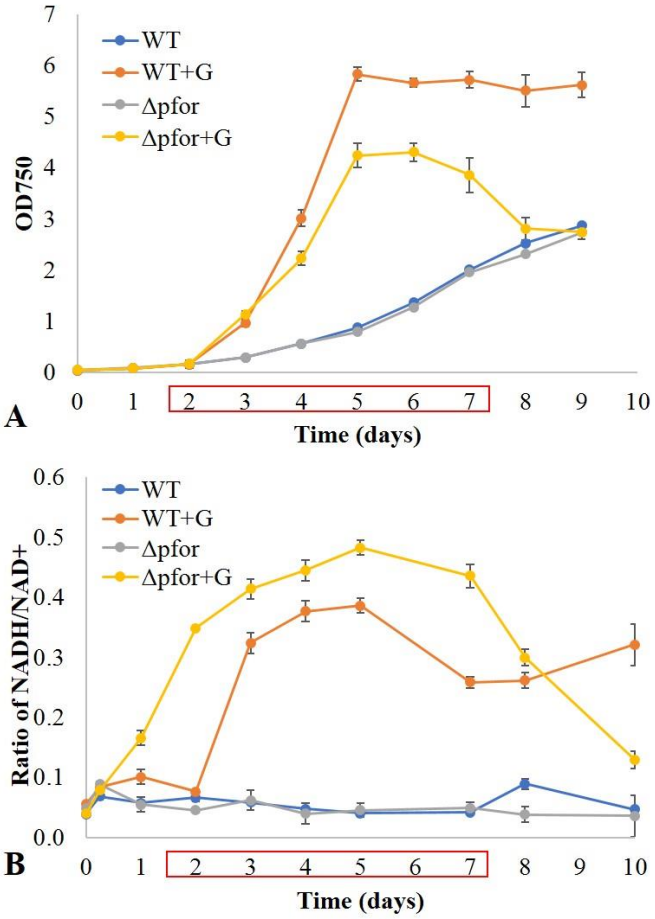

Fig. 4.3.4.3.1. Sampling days for the Western blot analysis. WT and *Δpfor* were grown under auto- and mixotrophic conditions in order to identify the days on which PFOR gets physiologically relevant. The NADH/NAD$^+$ ratio of the cultures was determined in parallel from Xi Chen (Chen 2014). Cells from the WT were harvested daily from day 2 to day 7 for Western blotting.

As we were not able to delete the PDH complex from the genome of *Synechocystis* (Chen 2014), we unfortunately could not use a negative control for our Western blotting analyses. However, the expected molecular weight of the E1 subunit of the PDH complex is 38 kDa, and a corresponding strong signal of this size was detected both under autotrophic and mixotrophic conditions in the WT with α-PdhA-E1 (band 1 in Fig. 4.3.4.3.2). In line with our hypothesis additional bands appeared on the blots from mixotrophically grown cells only within the course of the growth experiment, especially in the nonexponential late growth phase (bands 2-4 in Fig. 4.3.4.3.2). These bands appeared in the range between 26 to 36 kDa. The phosphorylation of a protein results in an additional negative charge which again can result in a faster running behavior in the SDS gel. All four bands were excised from the gel and analyzed via mass spectrometry at Turku University (Finnland) from Natalia Battchikova. The E1 subunit of the PDH-complex could be detected in all four bands. Phosphorylated forms could not be detected via mass spectrometry as they were below the detection limit. Phosphorylated proteins are commonly present in sub-stoichiometric concentrations in the samples due to the instability of the phosphorylation during sample preparation.

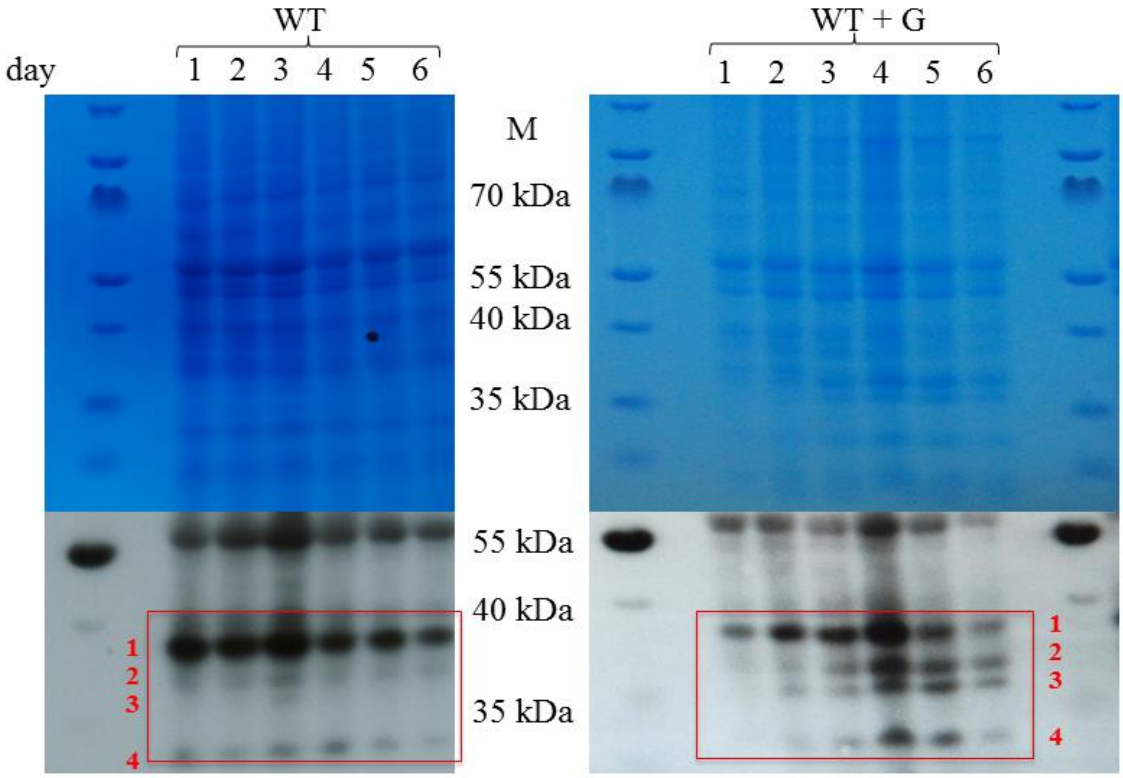

Fig. 4.3.4.3.2. Immunoblot of total protein extracts from *Syenechocytis* WT under autotrophic and mixotrophic conditions with a specific antibody against PdhA35 (α-PdhA-E1). The pdhA-E1 subunit has a molecular weight of 38 kDa. A respective band was detected both under autotrophic and mixotrophic conditions (band 1). Under mixotrophic conditions additional bands (2-4) appeared in the course of the growth experiment from day three on with increasing intensity that were suspected as potential phosphorylated E1 subunits from the PDH complex.

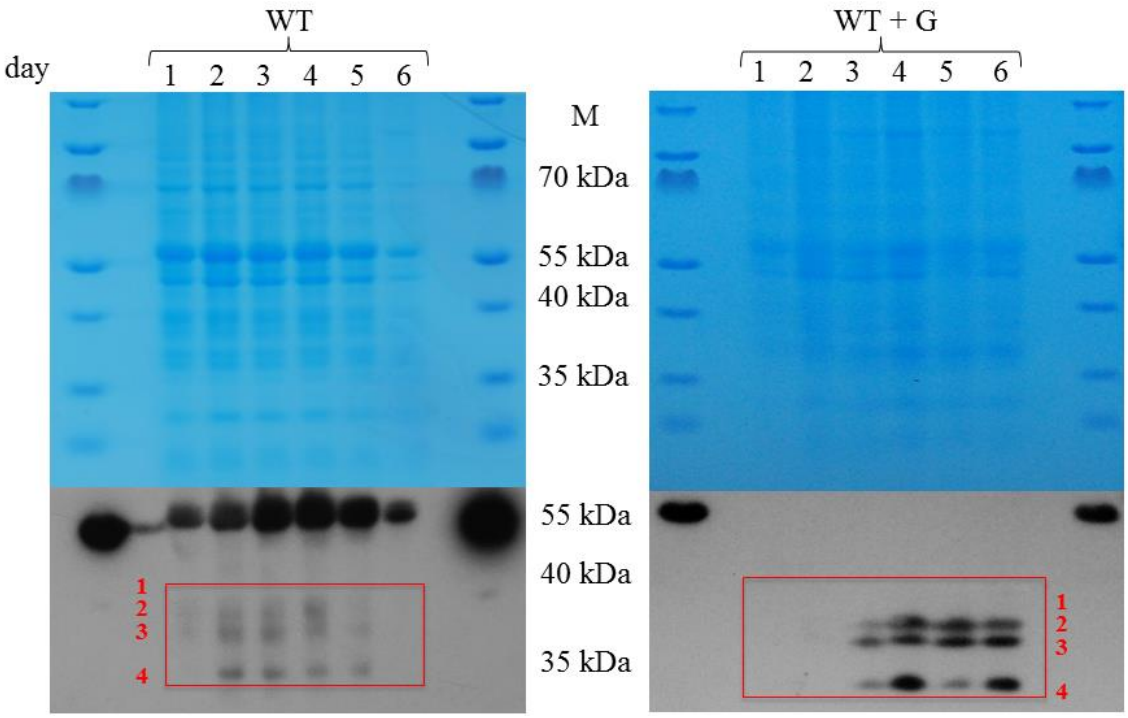

Fig. 4.3.4.3.3. Immunoblot of total protein extracts from *Syenechocytis* WT under autotrophic and mixotrophic conditions with anti-phosphoserine antibody. Phosphorylated proteins with similar size as PDHA protein were indicated in red box and numbered from large to small order.

Therefore, another approach was chosen to check if the additional bands that exclusively appeared on blots from mixotrophically grown cells originated from phosphorylated E1 subunits. The blots were thus subjected to a specific antibody against phosphoserins (α–phosphor-serine). As expected, the phosphoserin antibody did not give a signal for band 1, (which we had assumed as being the unphosphorylated form of E1 from the PDH complex) but precisely detected those bands 2-4 that appeared in addition on the blot from mixotrophically grown cells (which we had assumed as being the phosphorylated form of E1) (Fig. 4.3.4.3.3). These results confirm the hypothesis, that the PDH complex gets phosphorylated in the course of mixotrophic growth. As the PDH complex catalyzes exactly the same reaction as PFOR (the decarboxylation of pyruvate to acetyl-CoA) it is highly likely that PFOR compensates for the inactivated PDH complex in the WT. The impaired growth of Δ*pfor* is thus a result of the inability to decarboxylate pyruvate at high NADH/NAD^+ ratios. The cells thus seem to switch from the NADH/NAD^+ pool to the ferredoxin pool as an acceptor for electrons from carbohydrate oxidation. This scenario is also supported by the growth behavior of ferredoxin deletion mutants (such as *Δfx3*, *Δfx9*, *ΔisiB*), which show a similar growth phenotype as Δ*pfor* (Fig. 4.3.1.3 and 3.1.2). Ferredoxins that are thus involved in this process under mixotrophic conditions and serve as pool to accept electrons for carbohydrate oxidation in the late nonexponential growth phase are thus Fx3, Fx9 and IsiB (Fig. 4.3.1.3 and 3.1.2).

4.4 Characterization of the ferredoxin deletion mutants in *Synechocystis* under heterotrophic (LAHG) conditions

It has been previously shown that a *Chlamydomonas reinhardtii* ferredoxin-5 (FDX5)-deletion mutant is unable to grow in the dark, whereas its growth in the light is unaffected (Yang et al. 2015). The importance of ferredoxins for growth under heterotrophic conditions in darkness (LAHG: light-activated heterotrophic growth) in *Synechocystis* has not been studied so far.

4.4.1 Screening and characterization of *Synechocystis* ferredoxin deletion mutants under LAHG conditions

In order to investigate the function of *Synechocystis* ferredoxins under light-activated heterotrophic growth (LAHG) conditions, all available ferredoxin and flavodoxin deletion mutants (*fx2/Δfx2, Δfx3, Δfx4, fx5/Δfx5, Δfx6, Δfx7, Δfx9, Δfx7Δfx9, Δfx9ΔisiB, ΔisiB*) and *Δpfor* were analyzed under these conditions.

The absence of Fx9 either alone or in combination with other deletions (*Δfx9, Δfx7Δfx9, Δfx9ΔisiB*) had the strongest negative impact on growth under LAHG conditions in comparison to the WT (Fig.4.4.1.1).

Remarkably, *Δpfor* grew much better than the Fx9 deletion mutants under LAHG conditions (Fig. 4.4.1.1 and Fig. 4.4.1.2), which indicates that PFOR is not the only enzyme that reduces Fx9 under these conditions.

4.4.2 Characterization of the ferredoxin deletion mutant *Δfx9* grown on different nitrogen source under LAHG conditions

In order to check if *Δfx9* stays alive under LAHG conditions, the mutant was transferred back to the light on day 7. The mutant immediately regained its ability to grow, which indicates that *Δfx9* stayed alive but rather entered a dormant state under LAHG conditions (Fig. 4.4.2.1A).

As described in Section 4.3.2, *Δfx9* cannot grow on arginine and glucose in the light (Fig. 4.3.2.1). Cultivation of *Δfx9* on arginine and glucose under LAHG conditions resulted in the same phenotype, whereas the WT grew during the first 5 days (Fig. 4.4.2.1B). The transfer from these cultures from LAHG conditions to the light did not result in a regaining of growth as had been observed on nitrate (Fig. 4.4.2.1B).

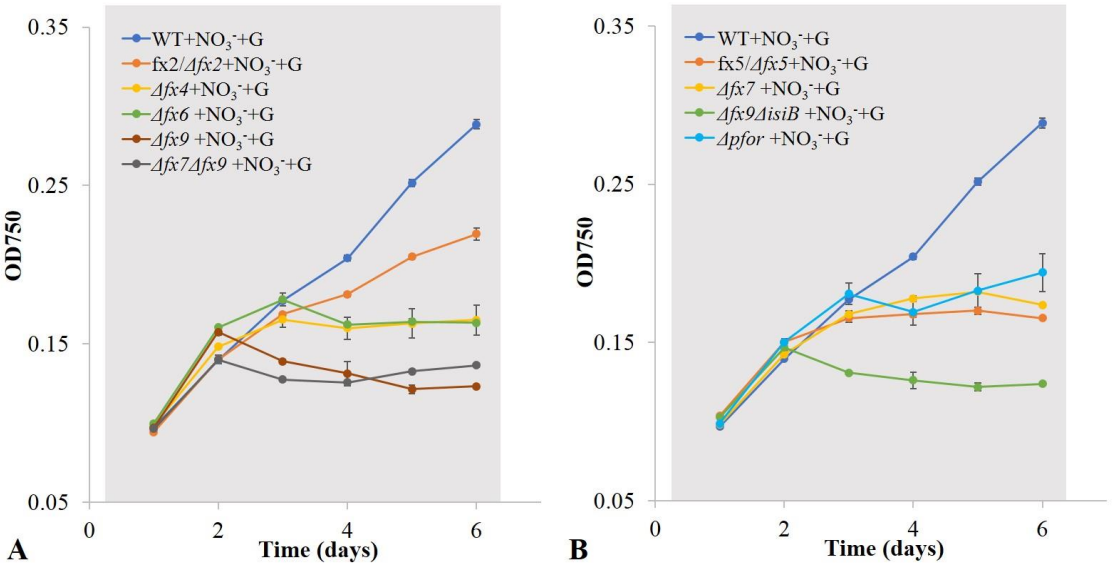

Fig. 4.4.1.1. Growth of all the ferredoxin and PFOR deletion mutants under LAHG conditions. When strains were grown under LAHG conditions, cells were kept in complete darkness except for one 10-min light period (white light at 20 µmol photons m^{-2} s^{-1}) every 24 h and supplemented with 10 mM glucose (+G). The error bars are standard deviations from two biological replicates and three technical replicates.

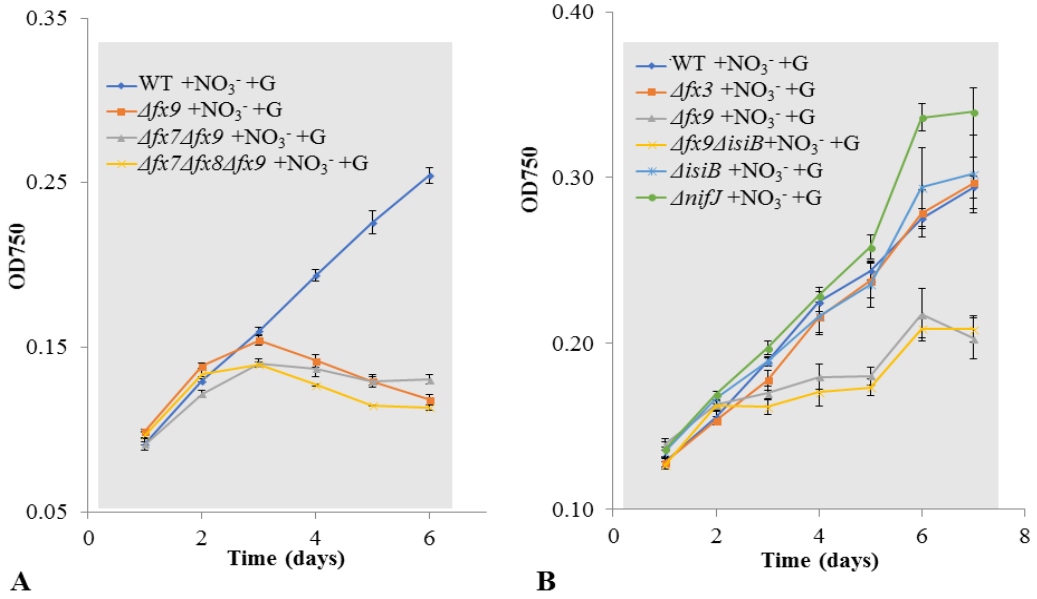

Fig. 4.4.1.2. Growth of *Δfx3, Δfx9, Δfx7Δfx9, Δfx7Δfx8Δfx9, Δfx9ΔisiB, ΔisiB* under LAHG conditions. The error bars are standard deviations from three biological replicates and three technical replicates.

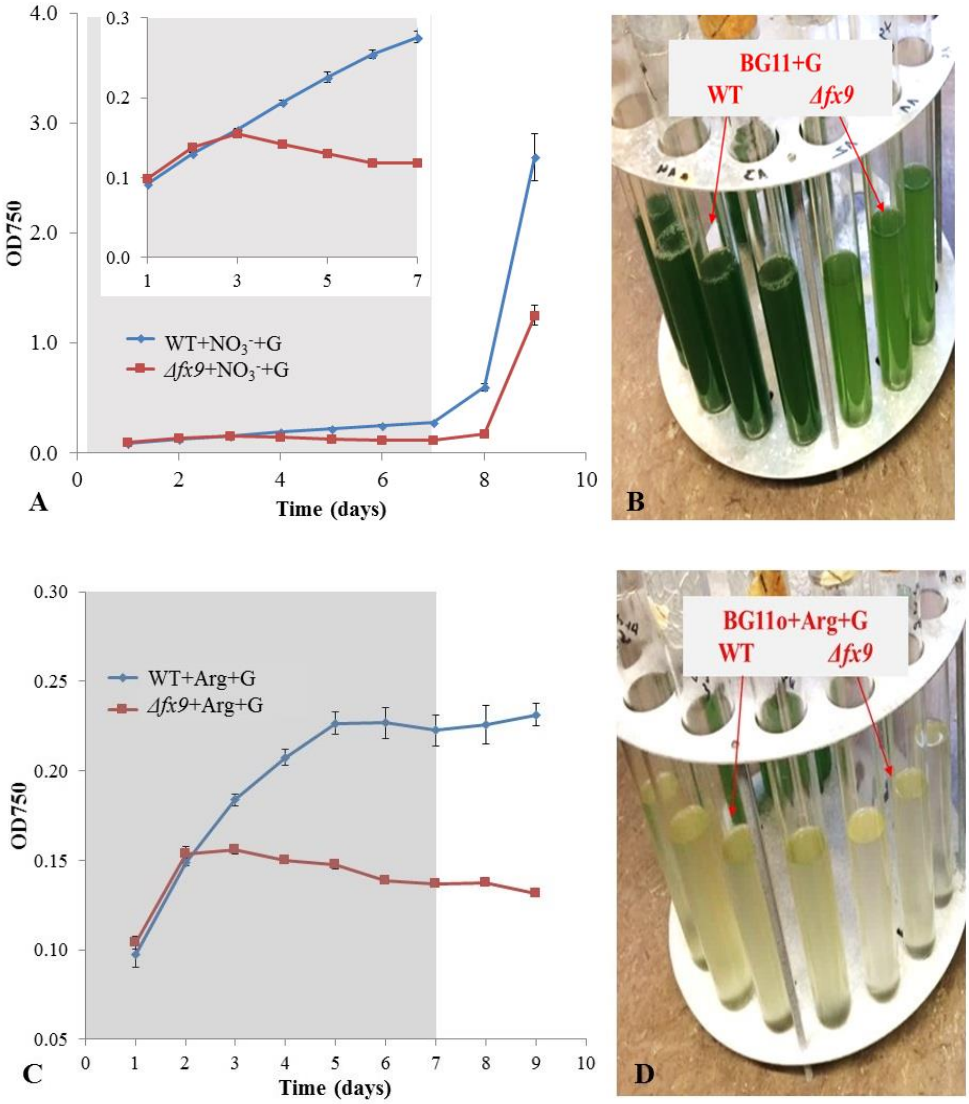

Fig. 4.4.2.1. Growth of *Δfx9* with 17.6 mM nitrate (+NO_3^- , A and B) or 5 mM arginine (+Arg, C and D) under LAHG conditions (gray background), followed by transfer to mixotrophic conditions (white background, continuously illuminated at 55 µmol photons m^{-2} s^{-1}) from 7th day. The error bars are standard deviations from three biological replicates and three technical replicates. The right photos of cultures (C and D) are taken on the 9th day.

Synechocystis possess both bacterial-type and plant-type ferredoxins. Fx9 belongs to the bacterial-type ferredoxins whereas Fx5 from *Chlamydomonas reinhardtii* belongs to the plant-type ferredoxins (Figure phylogenetic tree in the discussion part). Although both ferredoxins were shown to be essential for growth in darkness it can thus be assumed that they fulfill distinct functions. Fx5 in *Chlamydomonas reinhardtii* is involved in the desaturation of fatty acids which is required for maintaining the correct ratio of the dominant lipids in the thylakoid membranes (Yang et al. 2015).

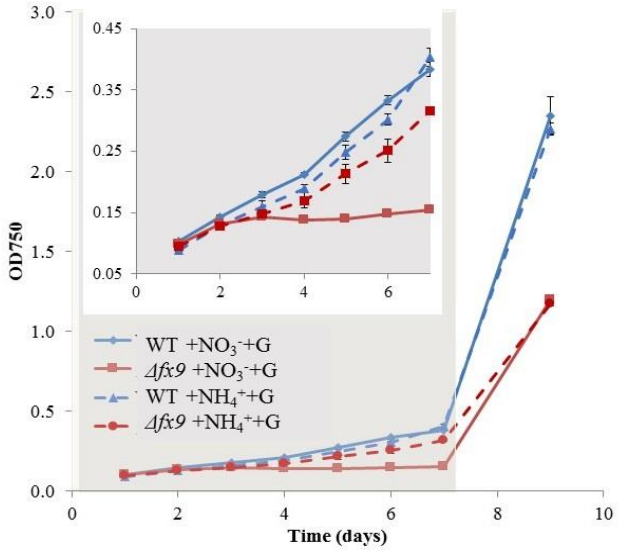

Fig. 4.4.2.2. Growth *Δfx9* with 17.6 mM nitrate ($+NO_3^-$, A and B) or 10 mM ammonium ($+NH_4^+$) under LAHG conditions (gray background), followed by transfer to mixotrophic conditions (white background, continuously illuminated at 55 μmol photons m^{-2} s^{-1}) on the 7th day. The error bars are standard deviations from three biological replicates and three technical replicates.

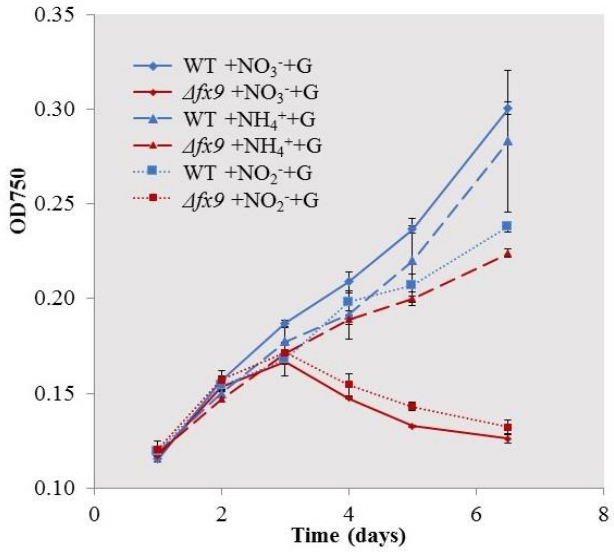

Fig. 4.4.2.3. Growth of *Δfx9* on 17.6 mM nitrate ($+NO_3^-$), 10 Mm nitrite ($+NO_2^-$) or 10 mM ammonium ($+NH_4^+$) under LAHG conditions. The error bars are standard deviations from three biological replicates and three technical replicates.

As the reduction of nitrate to ammonium requires reduced ferredoxin, we further checked if Fx9 might be involved either in the ferredoxin-dependent nitrate or nitrite reduction in *Synechocystis*. For this purpose, *Δfx9* was grown on 17.6 mM nitrate or 10 mM ammonium under LAHG conditions. Interestingly, addition of ammonium, the final product of nitrate reduction, could restore the inhibited growth of *Δfx9* which appears

on nitrate under LAGH conditions (Fig. 4.4.2.2). Transferring the cultures to light stimulated growth of *Δfx9* both on nitrate and on ammonium (Fig. 4.4.2.2).

Nitrate is first reduced via the nitrate reductase to nitrite and further via the nitrite reductase. Both enzymes are ferredoxin-dependent in cyanobacteria (Flores and Herrero 2005b). Therefore, *Δfx9* was grown under LAHG conditions on either 17.6 mM nitrate, 17.6 mM nitrite or 10 mM ammonium, in order to check if Fx9 might be the electron donor to one of these reactions. *Δfx9* could neither grow on nitrate or nitrite but exclusively on ammonium (Fig. 4.4.2.3).

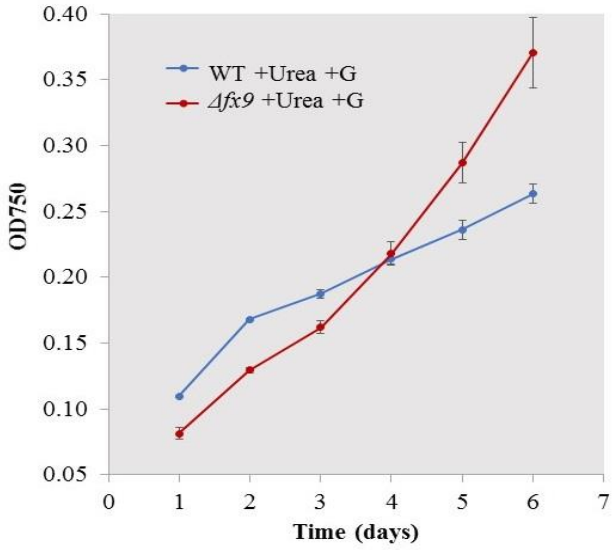

Fig. 4.4.2.4. Growth of *Δfx9* on 5 mM urea under LAHG conditions. The error bars are standard deviations from three biological replicates and three technical replicates.

However, ammonium is able to uncouple the proton gradient across membranes and might thus induce physiological artifacts (Dean and Miskiewicz 2003). Therefore, in order to further test the hypothesis that Fx9 is involved in nitrate and/or nitrite reduction, *Δfx9* was grown on urea which is broken down to ammonium without the need for an electron donor. As expected, when urea was added in the medium as sole nitrogen source, *Δfx9* could grow as well as WT (Fig. Fig. 4.4.2.4). These results indicate that Fx9 might be involved in the reduction of either nitrate or nitrite under LAHG conditions.

4.4.3 Metabolic characterization of *Δfx9* grown on nitrate or nitrite under LAHG conditions

As shown in Fig.4.3.1B, *Δfx9* contains more Chl a on nitrate but less Chl a on nitrite compared to the WT. The WT stopped its growth after 6 days under LAHG conditions as the glucose had been completely consumed at this point (Fig. 4.4.3.1A and 4.4.3.2A).

When grown on nitrate *Δfx9* stopped its growth on the second day even though glucose was still present in the medium (Fig. 4.4.3.1A and 4.4.3.2A). On nitrite *Δfx9* was impaired in its ability to consume nitrite from the medium in comparison to the WT, whereas the uptake of glucose was unaffected (Fig. 4.4.3.2A and 4.4.3.3A). Furthermore, WT excreted more nitrite into the medium than the *Δfx9* when grown on nitrate (Fig.4.3.3B). These results imply that the absence of Fx9 might not only inhibit the nitrite reduction but also affect the nitrate reduction under LAHG conditions.

In order to check the morphology of the cells under LAHG conditions, WT and *Δfx9* on nitrate were harvested on the 3rd and 5th day of cultivation and monitored via a transmission electron microscope (TEM). The pictures show that the WT accumulated more glycogen than *Δfx9* cells (Fig. 4.4.3.4)

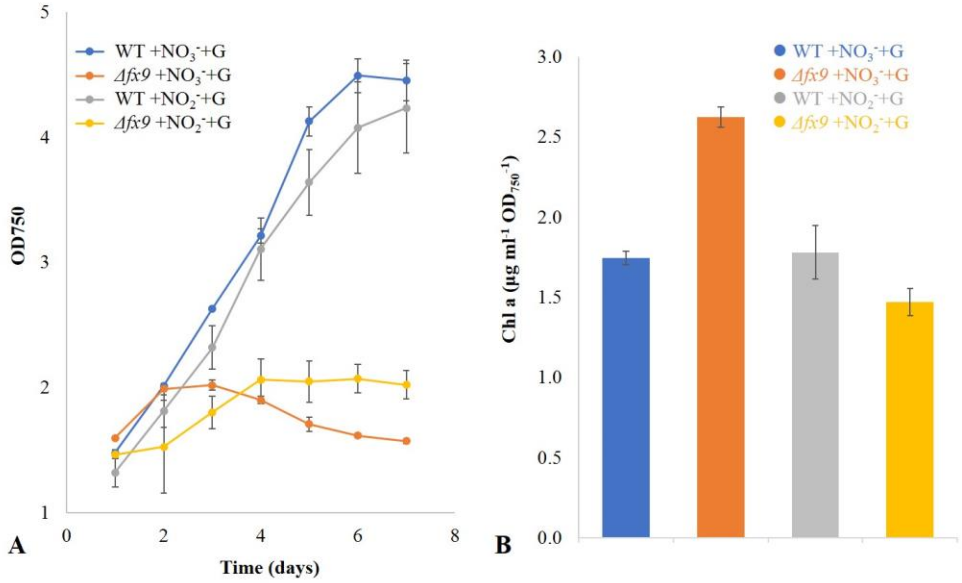

Fig. 4.4.3.1. Growth of *Δfx9* with either 17.6 mM nitrate (+NO_3^-) or 10 mM nitrite (+NO_2^-) under LAHG conditions. A: The growth curve of *Δfx9* under LAHG conditions with nitrate or nitrite. Cells were kept in complete darkness except for one 10-min light period (white light at 20 µmol photons m^{-2} s^{-1}) every 24 h and supplemented with10 mM glucose (+Glu). B: The chlrophyll a (Chl a) content of Wild-type and *Δfx9* cells on the 6th day. The error bars are standard deviations from three biological replicates and three technical replicates.

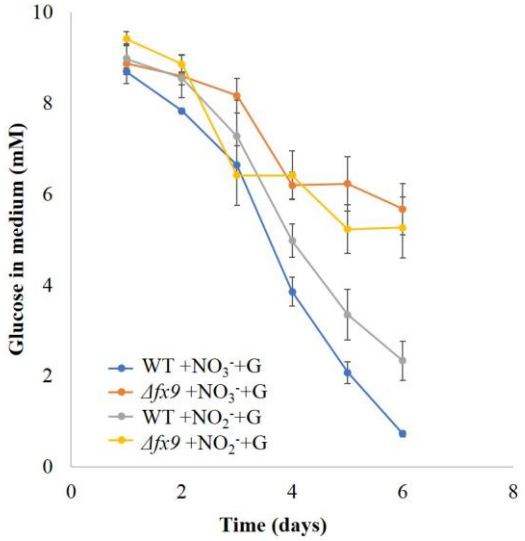

Fig. 4.4.3.2. The carbon metabolism changes in Wild-type and *Δfx9* cells from cultures in Fig.4.3.1A. Glucose concentration left in the supernatant of WT and *Δfx9* was determined every day. The error bars are standard deviations from three biological replicates and three technical replicates.

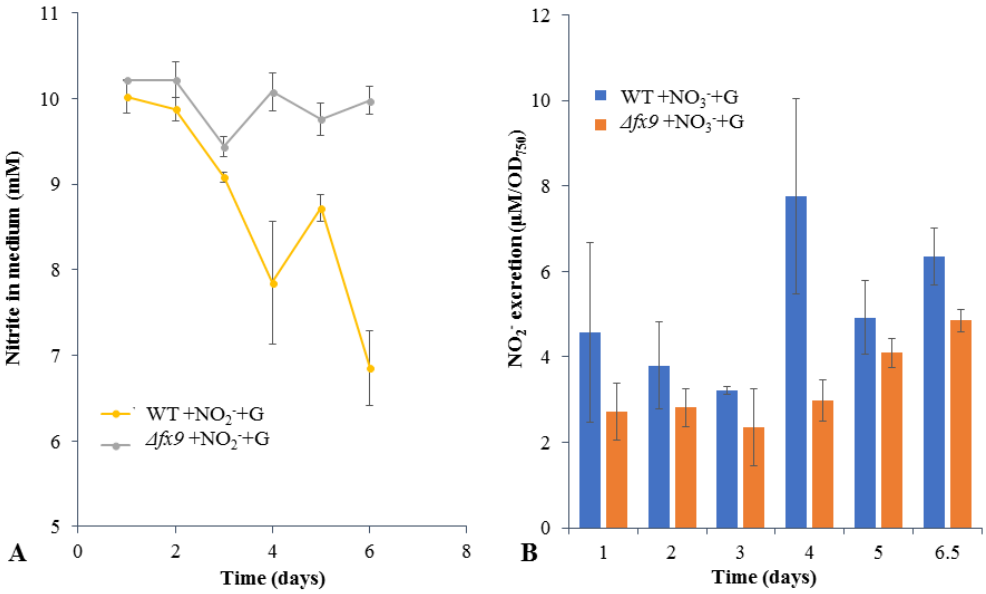

Fig. 4.4.3.3. Consumption (A) and excretion (B) of nitrite in WT and *Δfx9* under LAHG conditions. Samples from Fig.4.2.3 was used to determine nitrite excretion.

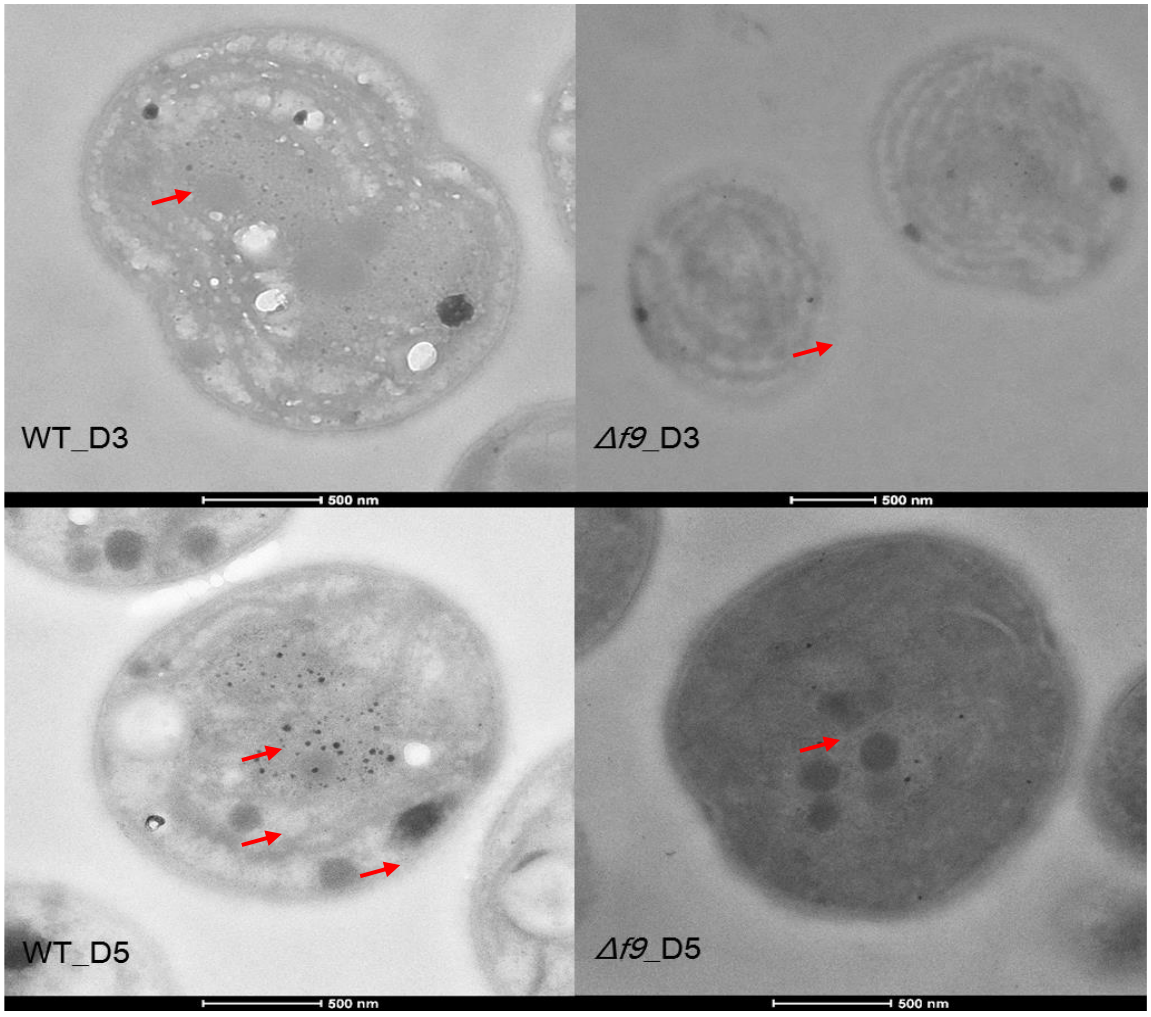

Fig. 4.4.3.4. Identification of glycogen (red arrows) and the phenotype of whole cells of WT and *Δfx9* under LAHG conditions via transmission electron microscopy (TEM). Cells grown on 3rd and 5th day in Fig. 4.4.3.1A were separately harvested for TEM imaging.

4.4.4 Characterization of ferredoxin deletion mutant *Δfx9* grown in the day/night cycle

When grown photo-autotrophically in continuous light *Δfx9* and *Δpfor* grew like the WT (Fig. 4.2.1.2). When grown mixotrophically in continuous light *Δfx9* and *Δpfor* displayed impaired growth at the nonexponential late growth phase (Fig. 4.3.1.2). However, when grown under photoautotrophic conditions in a circadian dark/light cycle (12h:12h), both *Δfx9* and *Δpfor* grew less than the WT (Fig. 4.4.4A). When grown under mixotrophic conditions in a circadian dark/light cycle (12h:12h), *Δpfor* performed like the WT while *Δfx9* had problems to grow (Fig. 4.4.4).

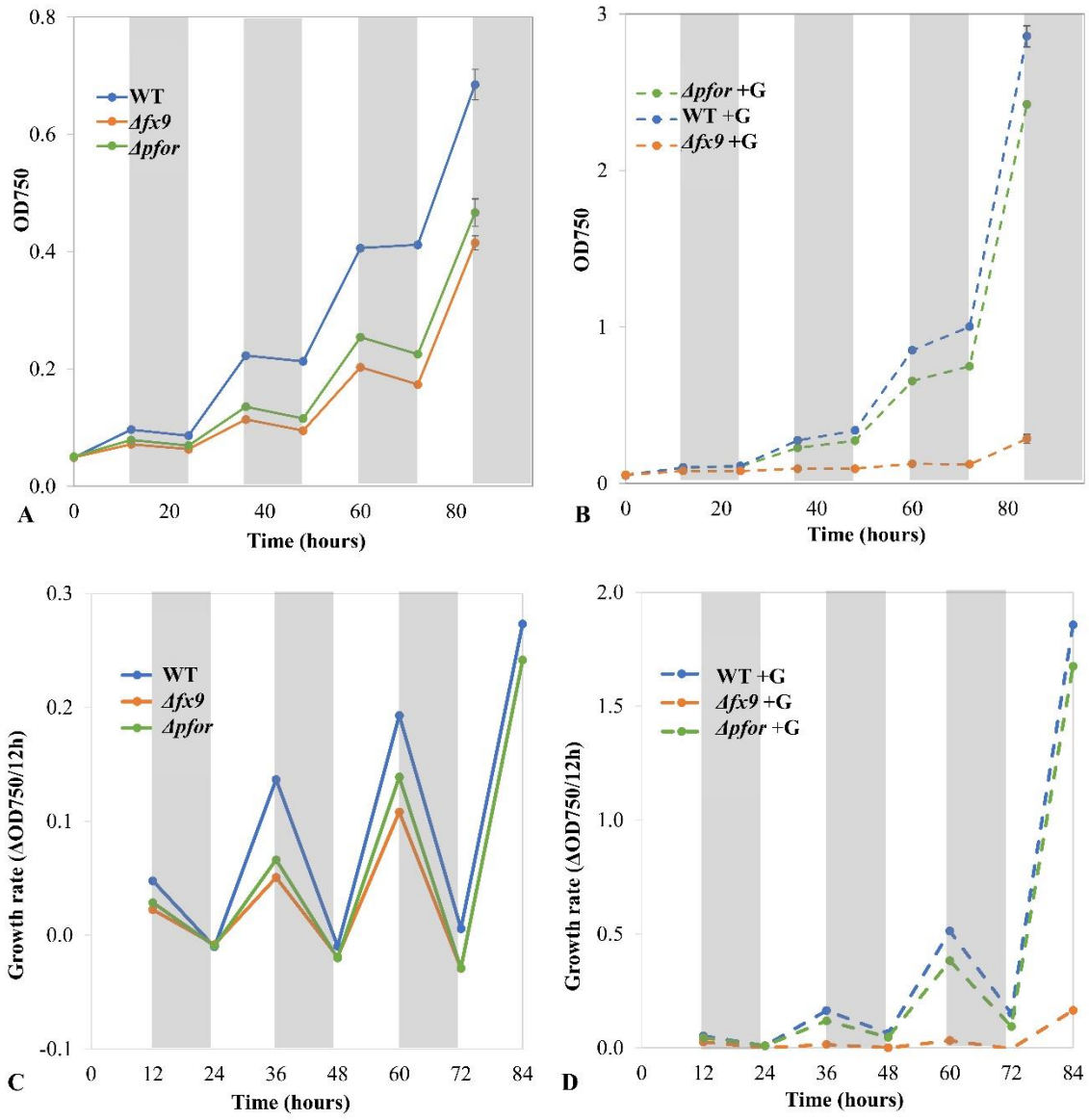

Fig. 4.4.4. A and B: Growth of *Δfx9*, *Δpfor* and WT under autotrophic and mixotrophic (+G) conditions in a 12h day/12h night cycle; C and D: Growth rate (ΔOD750/12h) of *Δfx9*, *Δpfor* and WT under autotrophic and mixotrophic (+G) conditions in a 12h day/12h night cycle. Darkness or light (55 µmol photons m^{-2} s^{-1}) is indicated as gray or white background, respectively.

4.5 Characterization of the ferredoxin deletion mutants under fermentative conditions

4.5.1 Determination of the NAD(P)H/NAD(P)+ ratio in parallel to production of high amounts of hydrogen

It has been assumed for several decades that NAD(P)H is the electron donor to the bidirectional NiFe-hydrogenase in *Synechocystis* (Appel et al. 2000a, Schmitz and Bothe 1996). However, more recent results point to ferredoxin as the direct electron donor to the enzyme (Gutekunst et al. 2014). As this issue has been the subject of some debate (Dutta and Vermaas 2016), additional experiments were done. Electrons can be transferred with ease from a partner with a highly negative redox potential to a partner with a more positive redox potential. If electrons need to be transferred the other way around an input of energy is required. The redox potential of NAD(P)H/NAD(P)$^+$ is about -320 mV (at pH 7.0), whereas Fdx_{red}/Fdx_{ox} has a redox potential around -440 mV (at pH 7.0) and H_2/H^+ of about -414 mV (at pH 7.0) (Gutekunst et al. 2014). It is therefore obviously energetically unfavorable to produce hydrogen (H_2) on the basis of NAD(P)H as an input of energy is required, whereas hydrogen production on the basis of reduced ferredoxin is energetically favorable. However, the redox potentials given above refer to standard conditions. The actual redox potential of any couple like NAD(P)H/NAD(P)$^+$ or Fdx_{red}/Fdx_{ox} in the cell does therefore not have a constant value but is influenced by the concentration and ratio of the partners to each other and the pH value in the cell. The pH value in cells is normally around pH 7. Fig. 4.5.1.1 shows the required ratios of NAD(P)H/NAD(P)$^+$ or Fdx_{red}/Fdx_{ox} for the production of distinct amounts of hydrogen at pH 5 to pH 8.

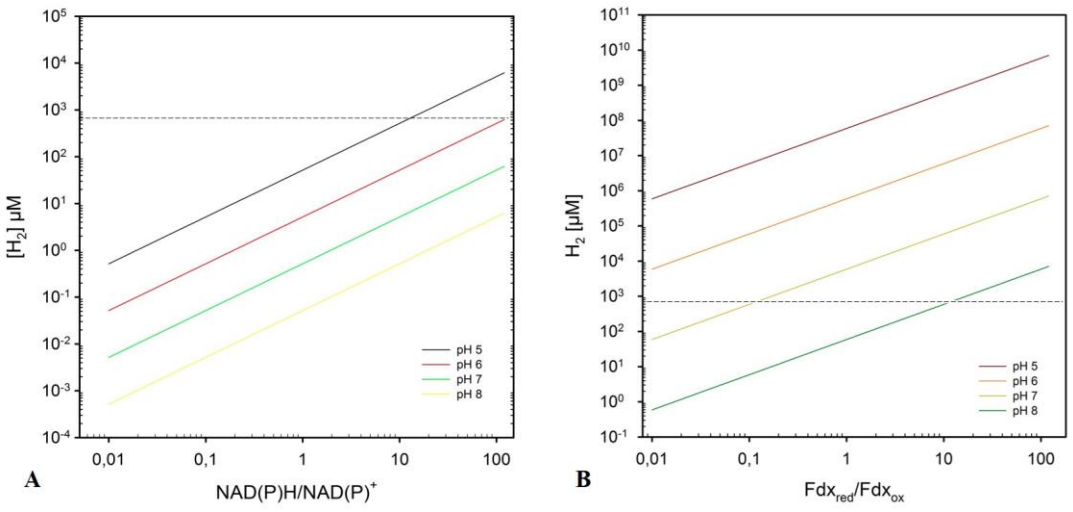

Fig. 4.5.1.1. H_2 concentration in µM that can be produced by a specific (A) NAD(P)H/NAD(P)$^+$ or (B) Fdx_{red}/Fdx_{ox} ratio at different pH values. The broken lines indicate the saturating H_2 concentration of about 758 µM. Note that all H_2 concentrations above 758 µM are beyond saturation and cannot be reached (Gutekunst and Schulz 2018)).

Table 4.5.1.1 The required ratio of NAD(P)H/NAD(P)$^+$ or Fdx_{red}/Fdx_{ox} for the production of certain amounts of hydrogen that have been reported in the literature at different pH values (Gutekunst and Schulz 2018).

H_2 concentrations	pH 5	pH 6	pH 7	pH 8
	required NAD(P)H/NAD(P)$^+$ ratios			
4 µM H_2	0.08	0.8	8	80
12 µM H_2	0.25	2.5	25	250
20 µM H_2	0.45	4.5	45	450
50 µM H_2	1	10	100	1000
160 µM H_2	3	30	300	3000
	required Fdx_{red}/Fdx_{ox} ratios			
4 µM H_2	0.00007	0.0007	0.007	0.07
12 µM H_2	0.0002	0.002	0.02	0.2
50 µM H_2	0.00085	0.0085	0.085	0.85
160 µM H_2	0.003	0.03	0.3	3

In order to test if NAD(P)H might be the electron donor for hydrogen production as stated by Dutta and Vermaas (2016) under fermentative conditions, the concentration of fermentative hydrogen and the ratio of NAD(P)H/NAD(P)$^+$ were determined in cultures in parallel. In order to trigger the production of high amounts of hydrogen, cells were measured in the presence of arginine and glucose. For this purpose, cells were pre-cultivated photoautotrophically in BG11medium until they reached an OD_{750} of about 3.0. They were then resuspended in fresh BG11 or $BG11_0$ with arginine. After an incubation time of approximately 12 hours, the fermentative H_2 production and in parallel the ratio of NADH/NAD$^+$ was measured and in a second experiment the NADPH/NADP$^+$ ratio determined. The hydrogen production was monitored with H_2 microsensors from Unisense, Denmark and the NAD(P)$^+$/NAD(P)H ratio quantification was performed by a Quantification Colorimetric Kit (BioVision, USA).

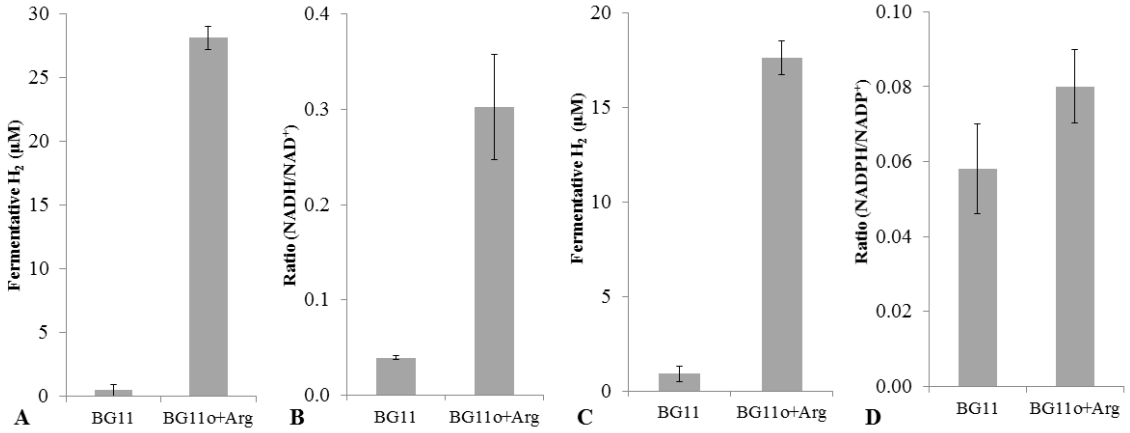

Fig. 4.5.1.2. Fermentative hydrogen production (A and D) and ratio of NADH/NAD$^+$ (B) NADPH/NADP$^+$ (D) either in the presence of nitrate (BG11) or in the presence of arginine ($BG11_0$+Arg). The error bars are standard deviations from three biological replicates and three technical replicates.

Table 4.5.1.2. The measured NADH/NAD$^+$ and NADPH/NADP$^+$ ratios are given together with H_2 in µM that could theoretically be attained based on these ratios and furthermore H_2 in µM that was actually measured in the respective cultures. The calculated attainable H_2 concentrations are based on the assumption of a pH of 7.

Medium	BG11	BG11o+Arg	Medium	BG11	BG11o+Arg
NADH/NAD$^+$	0.039	0.302	NADPH/NADP$^+$	0.058	0.080
attainable H_2 in µM	0.01	0.13	attainable H_2 in µM	0.025	0.030
measured H_2 in µM	0.5	28.1	measured H_2 in µM	0.9	17.6

Under fermentative conditions *Synechocystis* produced significantly more H_2 in the presence of arginine (28.1 µM and 17.6 µM) compared to nitrate (0.5 µM and 0.9 µM) (Fig. 4.5.1.2). In the presence of nitrate an NADH/NAD$^+$ ratio of 0.039 was determined that could support a hydrogen production of 0.01 µM H_2. However, a 50 times higher amount of hydrogen (0.5 µM) was measured. The NADH/NAD$^+$ ratio in the presence of arginine was 0.309 which could support a hydrogen production of 0.13 µM H_2. In this case a 216 times higher amount of hydrogen (28.1 µM H_2) was produced. The NADPH/NADP$^+$ ratio in the presence of nitrate was 0.058 which could support a hydrogen production of 0.025 µM, whereas 36 times more hydrogen was measured. In the case of arginine, the hydrogen that was produced reached an even 586 times higher H_2 concentration than the measured NADPH/NADP$^+$ could support. All the calculations assume that the pH in the cells is around pH7, which is a reasonable assumption. Lowering the pH to pH6 would result in a 10-times higher and lowering it further to a pH of pH5 (which is anyway not realistic) would result in a 100-times higher H_2 concentration. Even at a pH of 5, the hydrogen produced would be twice and five times higher than the NAD(P)H/NAD(P)$^+$ could support. In summary, these results thus convincingly demonstrate that the intracellular ratio of NAD(P)H/ NAD(P)$^+$ does not suffice to support the observed H_2 production in *Synechocystis*. Therefore, NAD(P)H is most likely not the sole electron donor to the NiFe-hydrogenase in *Synechocystis*. In contrast a Fdx_{red}/Fdx_{ox} ratio of approximately 0.005 would be required at pH7 to support a production of 28.1 µM H_2, as measured in the presence of arginine. We therefore conclude for a second time that rather reduced ferredoxin than NAD(P)H is the direct electron donor to the NiFe-hydrogenase in *Synechocystis*.

4.5.2 Determination of the fermentative hydrogen production of the ferredoxin deletion mutants

Under fermentative conditions PFOR was supposed to be responsible for the supply of reduced ferredoxin/flavodoxin for hydrogen production (Gutekunst et al. 2014). However, until now it is unknown if only one of the many ferredoxins or several of them are able to transfer electrons to the hydrogenase. In order to check if one of the ferredoxins might be especially important for fermentative hydrogen production, all ferredoxin deletion mutants we checked for their fermentative hydrogen

production. Please note that a mutant in which ferredoxin 1 was deleted is missing, as this ferredoxin is essential for survival. The mutants (*fx2/Δfx2, Δfx3, Δfx4, fx5/Δfx5, Δfx6, Δfx7, Δfx9, Δfx7Δfx9, Δfx9ΔisiB, ΔisiB*) were grown for 3 days under photoautotrophic conditions until they reached an OD_{750} of about 3.0. They were subsequently pelleted and resuspended in fresh $BG11_0$ medium containing 5 mM arginine, and finally kept under anaerobic conditions for fermentative hydrogen production. Hydrogen production was monitored with a H_2 microsensor from Unisense, Denmark. The relative fermentative hydrogen production (WT hydrogen production was set to 1) all mutants (*fx2/Δfx2, Δfx3, Δfx4, fx5/Δfx5, Δfx6, Δfx7, Δfx9, Δfx7Δfx9, Δfx9ΔisiB, ΔisiB*) is shown in Fig. 4.5.2.1. Compared to the WT, *Δfx4, fx5/Δfx5, Δfx9, ΔisiB* and especially the double mutant *Δfx9ΔisiB* produced more hydrogen (Fig. 4.5.2.1). Only, the putative *fx8/Δfx8* mutant produced significantly less fermentative hydrogen than the WT (Fig. 4.5.2.1 and 4.5.2.2). It might thus be that Fx8 is a direct electron donor to the hydrogenase under fermentative conditions. Those ferredoxins that were deleted and resulted in mutants with higher fermentative hydrogen production, might be involved in pathways that compete with the hydrogenase for electrons.

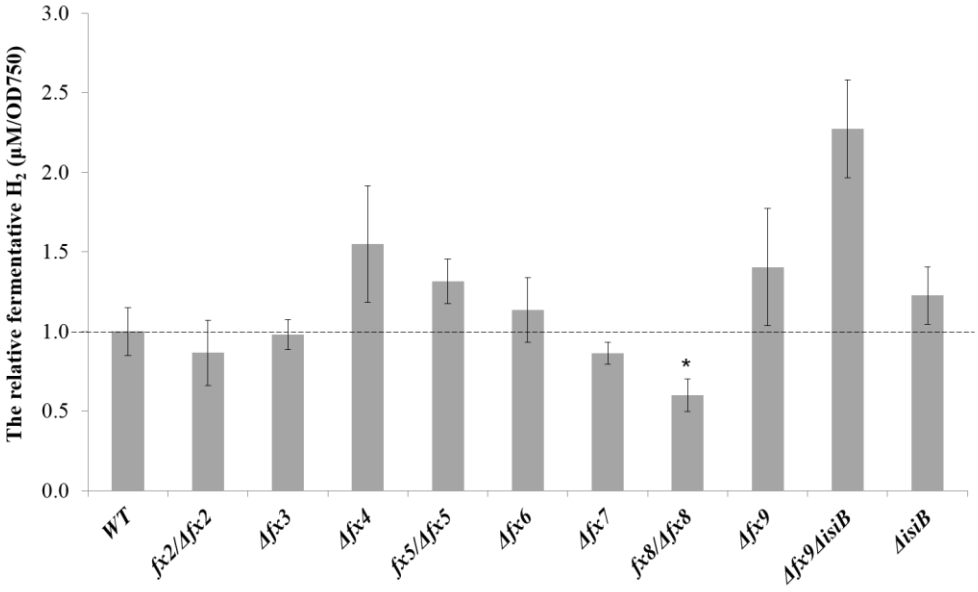

Fig. 4.5.2.1 Relative fermentative hydrogen production in 12 hours (WT set to 1.0). Wild-type and all ferredoxin deletion mutants are autotrophically pre-grown in standard BG11 medium, and subsequently transfer to $BG11_0$ medium containing 5 mM arginine before being incubated under fermentative conditions for hydrogen evolution measurement. Stars on the column diagram indicates differences between mutant and WT by Tukey's HSD test (*$P < 0.05$). The error bars are standard deviations from three biological replicates and three technical replicates.

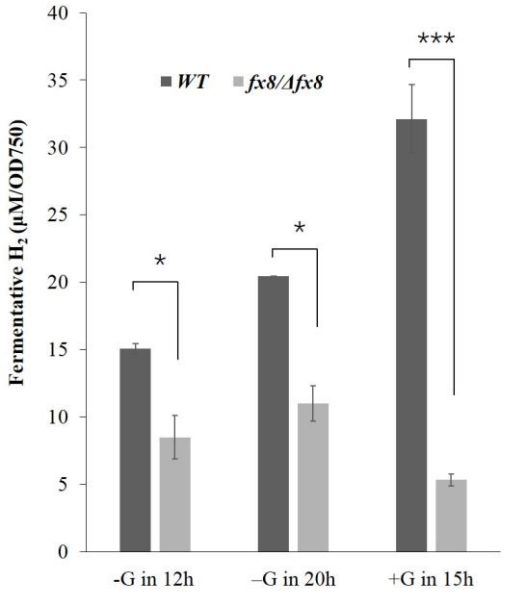

Fig. 4.5.2.2. Fermentative hydrogen production of Fx8 mutant pre-grown under standard autotrophic conditions (-G) or mixotrophic conditions (+G). Other details see Fig. 4.5.2.1. Stars on the column diagram indicates differences between mutant and WT by Tukey's HSD test (*P < 0.05 and ***P < 0.001). The error bars are standard deviations from three biological replicates and three technical replicates.

4.5.3 The growth and fermentative hydrogen production of *Δfx7Δfx8Δfx9*

In the triple mutant *Δfx7Δfx8Δfx9* all bacterial-type ferredoxins are deleted. Its growth under mixotrophic, heterotrophic and fermentative conditions resembles the growth of the single mutant *Δfx9* (Fig. 4.3.1.2, Fig. 4.3.2.1 and Fig. 4.4.1.2, Fig.4.5.3A

The deletion of either *Fx8* or *Fx9* has a converse influence on the fermentative hydrogen production. Therefore, the fermentative hydrogen production was measured in *Δfx7Δfx8Δfx9* in order to check which of the phenotypes prevailed in the triple mutant. As shown in Fig. 4.5.3B, *Δfx7Δfx8Δfx9* produced almost twice as much hydrogen as the WT under fermentative conditions.

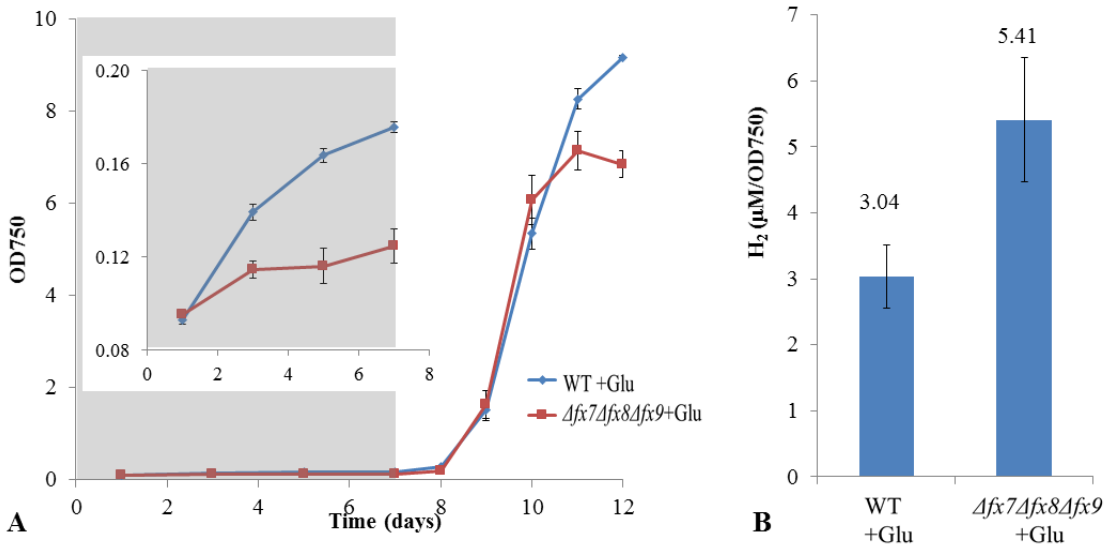

Fig. 4.5.3. Growth and hydrogen production in *Δfx7Δfx8fx9* under fermentative conditions. A: Growth under fermentative conditions followed by exposure to light from day 7 on. B: Fermentative hydrogen production.

5. Discussion

Ferredoxin, functioning as a mediator and messenger between the thylakoid and stroma, occupies a very unique position in photosynthesis and thereafter was even regarded as the center of the universe (Hanke 2017). Most studies on ferredoxin in cyanobacteria were performed in *Synechocystis* sp. PCC 6803 (Cassier-Chauvat and Chauvat 2014), a widely used photosynthetic model strain, which possesses multiple different kinds of ferredoxins (Hase et al. 1991). Recent work proposed that ferredoxin/flavodoxin instead of NAD(P)H serves as a direct electron donor to the bidirectional hydrogenase in *Synechocystis* and is thus of importance for applications such as biofuel production (Cassier-Chauvat and Chauvat 2014, Gutekunst et al. 2014). As a consequence of this finding, research on ferredoxins regained more attention recently (Cassier-Chauvat and Chauvat 2014, Dutta and Vermaas 2016, Hanke 2017). However, only the most abundant Ferredoxin 1 (Fx1or PetF or Fed1) was shown to play a main role in mediating electron transfer from donors to the majority of important metabolic reactions, such as NADPH reduction by ferredoxin: NADP reductase (FNR), CET (cyclic electron transfer) around PSI, nitrogen assimilation, hydrogen production, glutamate biosynthesis and the thioredoxin system, either in prokaryotic cyanobacteria or eukaryotic higher plants and green algae (Cassier-Chauvat and Chauvat 2014, Hanke and Mulo 2013, Peden et al. 2013). In contrast to Fx1, the remaining ferredoxins are weakly expressed under photoautotrophic conditions, and therefore, received much less attention with the exception of a few specific functional studies (Bottin and Lagoutte 1992, Cassier-Chauvat and Chauvat 2014, Houot et al. 2007, Mazouni et al. 2003, Poncelet et al. 1998). In this work, the functions of various *Synechocystis* ferredoxins and their functional counterpart flavodoxin were characterized and explored under different growth conditions, including photoautotrophic, mixotrophic, LAHG and fermentative conditions, with the supplement of different forms of nitrogen.

5.1. The evolution of *Synechocystis* ferredoxins

The green alga *Chlamydomonas reinhardtii*, a model organism to study eukaryotic photosynthesis and hydrogen production, was proposed to possess thirteen ferredoxins in total, of which six (PetF and FDX2-6) have been characterized so far (Sawyer and Winkler 2017). Indeed, each ferredoxin appears to be involved in a specific metabolic reaction under distinct conditions. For example, PetF (FDX1) as well as its highly structural homolog FDX2 were found to donate electrons to the FeFe-hydrogenase for photohydrogen production (Peden et al. 2013). FDX5 was described to function in fatty acid desaturation and in maintaining the composition and functionality of the thylakoid membrane in the dark (Yang et al. 2015).

Compared to green algae, which only possesses plant-type [2Fe-2S] ferredoxins (Sawyer and Winkler 2017), the cyanobacterium *Synechocystis* in addition also holds bacterial-type [3Fe-4S] or [4Fe-4S] ferredoxins, which are otherwise widespread in anaerobic fermenters (Bruschi and Guerlesquin 1988). Like PetF and FDX2-6 in *Chlamydomonas reinhardtii*, Fx1-4 in *Synechocystis* belong to the plant-type [2Fe-2S] ferredoxins. Furthermore, Fx5-6 and the candidate adrenodoxin-like homolog Ssl3044 are classified as

bacterial-type [2Fe-2S] ferredoxins according to protein sequence similarities (Fig. 5.2). Fx7-9 in *Synechocystis*, contain at least one bacterial-type [4Fe-4S] cluster and therefore clearly belong to the bacterial-type ferredoxins as well (Cassier-Chauvat and Chauvat 2014, Mustila et al. 2014).

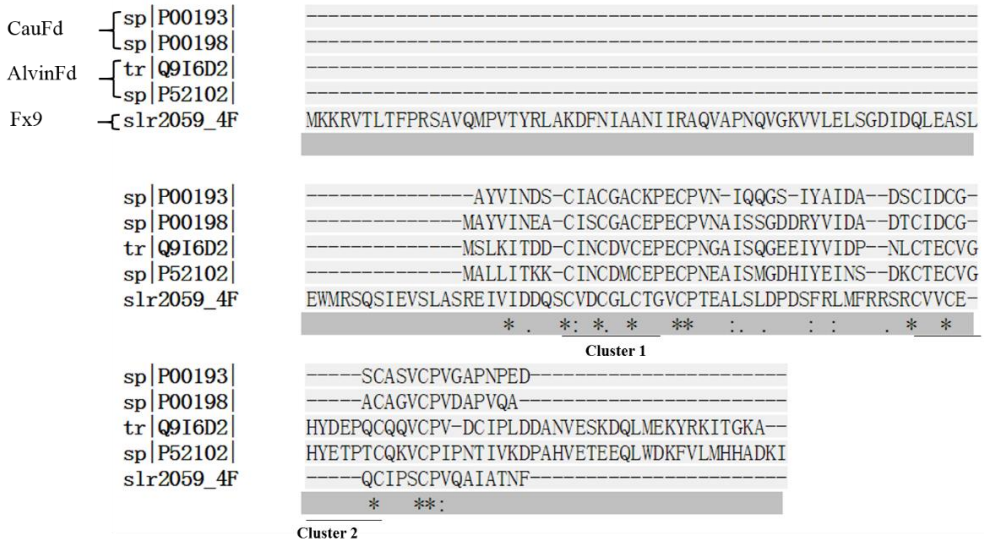

Fig. 5.1. Multiple sequence alignment of the complete amino acid sequence of *Synechocystis* Fx9 and other 2[4Fe-4S] ferredoxins (CauFd: P00193 from *Peptoniphilus asaccharolyticus* and P00198 from *Clostridium acidurici* ATCC 7906/DSM 604; AlvinFd: Q9I6D2 from *Pseudomonas aeruginosa* ATCC 15692 and P52102 from *Escherichia coli* K12). All the structures of these ferredoxins except for Fx9 have been characterized and were reviewed in Proteopedia (http://proteopedia.org/wiki/index.php/Ferredoxin).

Fx9 contains two bacterial-type [4Fe-4S] clusters. According to difference in the amino acid sequences, 2[4Fe–4S] ferredoxins could be assigned to two distinct subfamilies: Clostridial 2[4Fe–4S] ferredoxins (CauFd) and Alvin-like 2[4Fe–4S] ferredoxins (AlvinFd) (Giastas et al. 2006). In comparison to CauFd (C-X_2-C-X_2-C-X_n-C), AlvinFd contain a fragment of six amino acids, which is inserted between two cysteines (C-X_2-C-X_8-C-X_n-C) in the second iron-sulfur cluster and an extensive C-terminal α-helix (approximately 20 residues) (Elsen et al. 2010, Giastas et al. 2006, Fig. 5.1). *Synechocystis* Fx9 contains two domains, one iron-sulfur cluster binding domain and another NIL domain, which is normally found at the C-terminus of ABC transporter proteins as well as a number of ferredoxin-like proteins. Fx9 is a unique 2[4Fe–4S] ferredoxin because it contains the same iron-sulfur clusters as CauFd but with an extraordinarily long N-terminus (in the NIL domain) instead of a C-terminus (Fig. 5.1). By searching all ferredoxins marked in the NCBI by BlastP (till July 2018), a total of 249 homologs of Fx9 were found that are exclusively present in cyanobacteria with an only exception (BAM51618) in the bacterium *Bacillus subtilis* BEST7613. Therefore, the bacterial-type Fx9 in *Synechocystis* and its homologs, which are exclusively conserved in cyanobacteria, might constitute a new type of 2[4Fe–4S] ferredoxin.

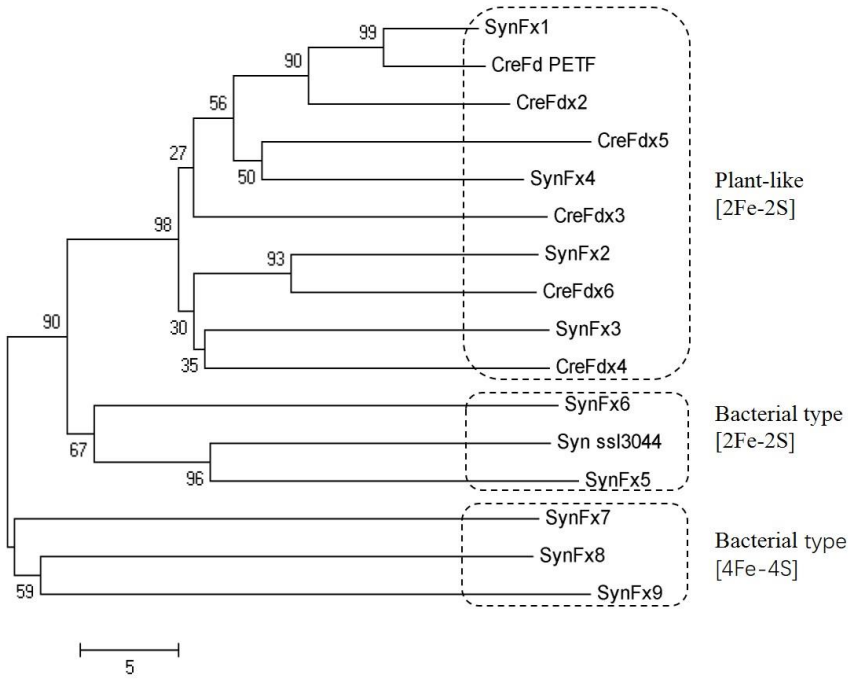

Fig. 5.2 Phylogenetic tree of ferredoxins (Fx=FDX) in the cyanobacterium *Synechocystis* (Syn) and the green alga *Chlamydomonas reinhardtii* (Cre). The protein sequences of 10 ferredoxins (Fx1-9 and the ferredoxin homolog Ssl3044) in *Synechocystis* and 6 ferredoxins (PETF and FDX2-6) in *Chlamydomonas reinhardtii* (Sawyer and Winkler 2017) were used for the multiple sequence alignment by ClustalW and the phylogenetic tree was constructed by MEGA.

As shown in the phylogenetic tree of ferredoxins from the cyanobacterium *Synechocystis* and the green alga *Chlamydomonas reinhardtii* (Fig. 5.2), plant-like ferredoxins and bacteria ferredoxins have a common ancestral form, which is well in line with past conclusion (Matsubar.H et al. 1969, Matsubara et al. 1979, Schwartz and Dayhoff 1978). Furthermore, this phylogenetic tree might be helpful to get a first idea for the prediction of functions of a distinct ferredoxin in *Synechocystis* when compared to the most structurally similar ferredoxin in *Chlamydomonas reinhardtii*.

5.2. Characterization of ferredoxin deletion mutants in *Synechocystis* under autotrophic conditions

5.2.1 Fx9 is of importance for the growth of *Synechocystis* on arginine instead of nitrate

The plant-type Fx1 (or PetF) is the most abundant protein in *Synechocystis* (Bottin and Lagoutte 1992a), which is in agreement with the highly expressed transcripts of *fx1* under photoautotrophic conditions (Poncelet et al. 1998). In contrast to Fx1, the other ferredoxin genes of *Synechocystis* are only weakly expressed under these conditions. These results, combined with the failures to completely delete Fx1 from

the genome of *Synechocystis*, shows that Fx1 is essential for photoautotrophic growth in *Synechocystis* (Cassier-Chauvat and Chauvat 2014a). This is well in line with our growth results, which showed that all the ferredoxin deletion mutants (*fx2/Δfx2, Δfx3, Δfx4, fx5/Δfx5, Δfx6, Δfx7, Δfx9, Δfx7Δfx9, Δfx7Δfx8Δfx9, Δfx9ΔisiB, ΔisiB*) had no significant growth difference compared to the Wild-type of *Synechocystis* under photoautotrophic conditions (Fig.4.2.1.1A-C).

However, ferredoxin Fx7 and Fx9 were found to play a prominent role in the tolerance to oxidative and metal stresses, whereas the expression of *fx1* was negatively regulated under these conditions (Cassier-Chauvat and Chauvat 2014). In order to test all the ferredoxin mutants under similar stress conditions, arginine instead of nitrate was used as a nitrogen source. When cells are grown on arginine, *Synechocystis* accumulates cyanophycin and shows a phenotype of nitrogen starvation and oxidative stress (Stephan et al. 2000). Interestingly, the absence of *fx9*, but not *fx7* caused impaired growth on arginine (Fig.4.2.1.1E-H), whereas the stressed phenotypes, including the accumulation of cyanophycin and the degraded thylakoid membranes, in *fx9*'s double mutant, *Δfx7Δfx9*, were less pronounced than in the WT (Fig. 4.2.1.7). Moreover, the higher ratio of carotenoid to chlorophyll in *Δfx9*, as shown in Fig. 4.2.2, indicates that this mutant suffers from surplus electrons under such conditions. Like *Δfx9* and *Δfx7Δfx9*, the deletion of PFOR and as well as flavodoxin IsiB also displayed similar phenotypes (Fig.4.2.1.1 and 4.2.2).

From the results above, it can be concluded that IsiB, PFOR and Fx9 might help the cells to dissipate surplus electrons when cells are grown on arginine and to switch their cell morphology and metabolism in a way that allows growth under these conditions. It is known that PFOR is able to reduce IsiB (Flavodoxin) as indicated by the name pyruvate: ferredoxin/flavodoxin oxidoreductase (Neuer and Bothe 1982). The results indicate that also Fx9 might be reduced by PFOR as the phenotypes of *Δfx9* and *Δpfor* are similar as well. However, this has to be proven in more detail.

5.2.2 Fx9 may not be an electron donor to flavodiiron protein Flv3 in *Synechocystis*

The bacterial-type Fx9 physically interacts *in vitro* with the flavodiiron protein Flv3, which functions in the NAD(P)H-driven photoreduction of O_2 to H_2O, known as Mehler-like reaction (Allahverdiyeva et al. 2011, Cassier-Chauvat and Chauvat 2014, Helman et al. 2003). It has been proposed that electrons from arginine oxidation are fed into the respiratory/photosynthetic electron transport chain (Schriek et al. 2009). Therefore, we hypothesized that Fx9 might be involved in a Mehler-like via Flv3 on arginine as an electron dissipating reaction for surplus electrons.

However, the growths of *Δflv3* (flv3: flavodiiron protein 3) and *Δfx9* were differently regulated in response to light intensities when grown autotrophically on arginine (Fig. 4.2.3.1). As expected, low light (15 µmol photons m^{-2} s^{-1}) could effectively rescue the completely absent growth of *Δflv3* on high light (300 µmol photons m^{-2} s^{-1}) and led to a O_2 evolution rate similar to the WT (Fig. 4.2.3.1A and D). This indicates that the protection of an overreduced photosynthetic electron chain via the photoreduction of O_2 catalyzed by

Flv3 is indispensable for *Synechocystis* under the described conditions. In contrast to *Δflv3*, *Δfx9* was not distinctly affected by light and displayed impaired growth under both low and high light (Fig. 4.2.3.1). Furthermore, *Δfx9* produced less oxygen than the WT and *Δflv3* at low light intensities (Fig. 4.2.3.1C and D). As shown in Fig. 4.2.3.2, the knockout of Flv3 caused a significantly slower oxidation of P700 in PSI because of the absence of the Flv3 mediated Mehler-like reaction in its function as an electron sink. However, *Δfx9* grown on either arginine or nitrate behaved like the WT and did not possess the P700 oxidation characteristics as *Δflv3* (Fig. 4.2.3.2).

In summary, these results show that Flv3, which is involved in the Mehler-like reaction, is indispensable under autotrophic conditions on arginine at high light. The function of Fx9 as an electron donor to Flv3 can either be replaced by e.g. Fx1 or alternatively, Fx9 does not interact with Flv3 *in vivo* at all. Fx9 is clearly not essential for the Mehler-like reaction in the presence of arginine or nitrate under photoautotrophic conditions.

5.2.3 Fx9 might be involved in a competitive pathway to the cyclic electron flow (CET) around PSI

Ferredoxins are proposed to be involved in at least four parallel operating routes of cyclic electron flow (CET) around PSI in *Synechocystis*, however, if any of the ferredoxins beside Ferredoxin-1 (Fx1) are involved is unknown (Yeremenko, et al. 2005). In this work, all available ferredoxin and flavodoxin mutant strains (*fx2/Δfx2, Δfx3, Δfx4, fx5/Δfx5, Δfx6, Δfx7, Δfx9, Δfx7Δfx9, Δfx7Δfx8Δfx9, Δfx9ΔisiB, ΔisiB*) grown under photoautotrophic conditions were characterized according to their $P700^+$ reduction kinetics by a pulse amplitude-modulated measurement (DUAL-PAM-100) in order to identify ferredoxins in *Synechocystis* which are involved in the CET pathway. However, we did not find a ferredoxin deletion mutant that showed a similar phenotype as the NDH-1 complex mutant M55, which has almost no CET around PSI (Fig. 4.2.2.3). This indicates that Fx1 is the principle electron carrier for the CET around PSI under standard photoautotrophic conditions or alternatively that different ferredoxins can replace each other in this function.

Interestingly, the Fx9-deletion mutant (*Δfx9*) and its double mutant *Δfx7Δfx9* displayed a faster CET around PS, which indicates that Fx9 might be involved in competitive pathways that dissipate electrons that are otherwise cycled around PSI. This is in agreement with our observations on NDH-CET activity around PSI using chlorophyll florescence analysis by Multi-Color PAM, in which the PQ pool of *Δfx9* is more reduced in the post-illumination phase compared to the WT on nitrate (Fig. 4.2.4.3). However, the reduction of the PQ pool on arginine during the post-illumination phase is lower both in WT and *Δfx9* when compared to conditions on nitrate (Fig. 4.2.4.3). Furthermore, the post-illumination rise in *Δfx9* is lower compared to the WT, while the rest of the chlorophyll fluorescence curves of WT and *Δfx9* on arginine are similar to each other (Fig. 4.2.4.3). These results suggest that contrary to the condition on nitrate, the absence of Fx9 slows

down NDH-CET around PSI when grown on arginine, which might contribute to the impaired phototrophic growth of *Δfx9* on arginine.

5.2.4 Fx9 might be involved in ferredoxin-dependent glutamate synthesis

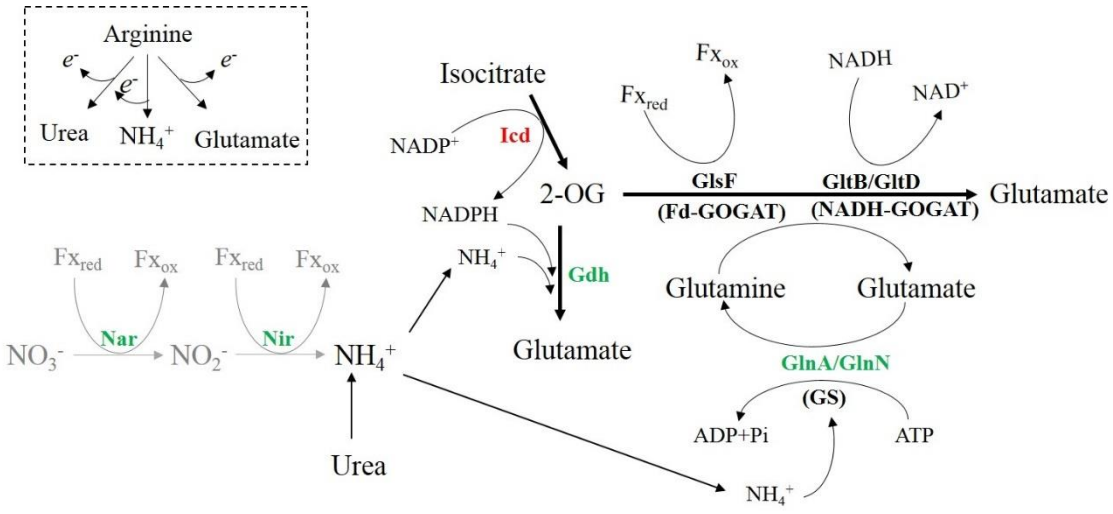

Fig. 5.2. Integration between carbon and nitrogen metabolisms in *Synechocystis*. Carbon source 2-oxoglutarate (2-OG) comes from open TCA cycle. Ammonium (NH_4^+) can be supplemented directly or it can originate from nitrate reduction or urea decomposition. The upregulated and downregulated enzymes in response to nitrogen starvation limitation (no nitrogen source (Krasikov et al. 2012) or the presence of arginine (Schriek et al. 2008)) are marked in red and green, respectively. Arginine oxidation could produce urea, ammonium or glutamate with the release of electrons (refer to the dotted rectangle). Fx_{red} or Fx_{ox}: reduced or oxidized ferredoxin. Icd: Isocitrate dehydrogenase; Gdh: Glutamate dehydrogenase; GlsF: ferredoxin-dependent glutamate synthase (Fd-GOGAT); GltB/GltD: NADH-dependent glutamate synthase (NADH-GOGAT); GlnA/GlnN: Glutamine synthase (GS); Nar: Nitrate reductase; Nir: Nitrite reductase.

When grown under photoautotrophic conditions with nitrate, the Fx9 deletion mutant grows similar as the WT (Fig. 4.2.1.1). It is assumed that under photoautotrophic conditions, Fx1, which is reduced at photosystem I (PSI), reduces nitrate to ammonium, which can be further incorporated into 2-oxoglutarate (2-OG) via glutamate dehydrogenase (GDH) or glutamine synthase (GS) and is furthermore assimilated via the GOGAT pathway (Fig. 5.2). Analogously, when urea or ammonium are supplemented under photoautotrophic conditions, *Δfx9* grows like the WT. This result is expected as urea provides ammonium (Fig. 5.2).

As shown in Fig. 4.2.1.2 and 4.2.4.1, the addition of arginine impairs the growth of *Δfx9* and the mutant develops a phenotype, which is typical for cells that suffer from nitrogen starvation. This indicates that ammonium might be lacking in the *Δfx9* cells. Nitrogen starvation is mainly sensed via the level of 2-OG, which increases at low levels of nitrogen (Muro-Pastor et al. 2001, Schriek et al. 2008). Arginine is converted via three alternative pathways to urea, ammonium and finally glutamate during its catabolic pathways (see

Fig. 1.7.4) (Quintero et al. 2000, Schriek et al. 2007). No reduction or oxidation occurs for the nitrogen that is part of the arginine. However, the carbon skeleton of arginine needs to be oxidized and it was shown that electrons are fed via the arginine dehydrogenase into the PQ-pool of the photosynthetic electron chain (Schriek et al. 2009, Schriek et al. 2007). The inability of *Δfx9* to grow on arginine might thus indicate that Fx9 plays a role to balance the redox state of the cells under these conditions. The enhanced CET around PSI in *Δfx9* (Fig.4.2.4.3) furthermore indicates that Fx9 might be involved in electron dissipation from the photosynthetic electron chain.

Another possibility is that Fx9 is involved in the ferredoxin-dependent glutamate synthesis (Fd-GOGAT) under photoautotrophic growth on arginine. In order to test this hypothesis, cells were grown on glutamate. However, both WT and *Δfx9* turned yellow and grew extremely slowly without any differences between each other (Fig. 4.2.5.1). In order to check if glutamate was consumed at all, the WT was grown in the absence of any nitrogen source. Growth of the WT on either glutamate or in the complete absence of any nitrogen source were similar, which reveals that glutamate is probably not metabolized from the cells at all (Fig. 4.2.5.2). Glutamate is obviously not a good nitrogen source for *Synechocystis*. This might be due to the fact that the activity of the glutamate dehydrogenase (GDH) which catalyzes the conversion from 2-oxoglutarate to glutamate in *Synechocystis* is low, as shown for both fungi and bacteria (Pateman 1969). This might explain why neither the addition of glutamate nor 2-oxoglutarate could rescue the growth of *Δfx9* on arginine (Fig. 4.2.5.1).

In order to further examine if Fx9 works as an electron donor for *Synechocystis* Fd-GOGAT, WT and *Δfx9* cells were grown with glutamine (Fig. 4.2.5.2). Glutamine can be taken up by cyanobacteria and can be used as a substrate for Fd-GOGAT or NADH-GOGAT (Fig. 5.2) (Flores and Herrero 2005b, Muro-Pastor et al. 2005). The growth phenotype in Fig. 4.2.5.2A shows that *Δfx9* displayed a sigmoidal growth curve when grown on glutamine, which is in line with the growth of the Fd-GOGAT deletion mutant, *ΔglsF*, in the cyanobacterium *Plectonema boryanum* (Okuhara et al. 1999). Growth of *Δfx9* was thus significantly impaired on glutamine compared to the WT which indicates its involvement in Fd-GOGAT. Furthermore, deletion of Fd-GOGAT in *Plectonema boryanum* resulted in impaired performance of the mutant under mixotrophic conditions similar as observed for *Δfx9* in *Synechocystis.* These results indicate that Fx9 could potentially be an electron donor to Fd-GOGAT (see Fig. 5.2). This hypothesis is difficult to test as there is no data available concerning the physiological role of Fd-GOGAT and NADH-GOGAT. It is not known under which conditions both enzymes can replace each other and under which conditions Fd-GOGAT is absolutely required.

Transcript profiling indicates that the glutamate synthase (GOGAT) plays a more important role in nitrogen assimilation in response to nitrogen starvation conditions, including the absence of any external nitrogen source (Krasikov et al. 2012) or the presence of arginine (Schriek et al. 2008) (Fig. 5.2). Both Fd-GOGAT and NADH-dependent were additionally found to be putative targets of glutathionylation, which is an important mechanism for signal transduction and regulation of protein function in response to oxidative stress

(Chardonnet et al. 2015, Sakr et al. 2013). Therefore, we hypothesized that the absence of Fx9 might affect the glutamate synthesis by interacting with the Fd-GOGAT (Fig. 5.2).

This new finding is of great significance for providing another possibility to work out the disagreement about whether the Ferredoxin:Fd-GOGAT complex stoichiometry is 1:1 or 1:2 (Garcia-Sanchez et al. 1997, Hirasawa et al. 2017, Schmitz et al. 1996, van den Heuvel et al. 2003). In contrast to the mostly studied plant-like Fx1 which contains one [2Fe-2S] cluster, the bacterial-type Fx9 contains two [4Fe-4S] clusters and can therefore transfer two electrons to Fd-GOGAT for the formation of two molecules of glutamate, therefore, the stoichiometry of the Ferredoxin:Fd-GOGAT complex could be 1:1 rather than 2:1. It was shown likewise, that in the hydrogen-oxidizing chemoautotrophic bacterium *Hydrogenobacter thermophilus* a ferredoxin with a [4Fe-4S] cluster, but not a ferredoxin with a [2Fe-2S] cluster, works as an electron donor for the Fd-GOGAT (Ikeda et al. 2005, Kameya et al. 2007).

In summary, *Synechocystis* Fx9 might play an important role in the glutamate synthesis by potentially interacting with the Fd-GOGAT (Fig. 5.2). However, this hypothesis needs further support. It would be especially helpful to construct Fd-GOGAT and NADH-GOGAT mutants and to characterize their growth in order to understand under which conditions the ferredoxin-dependent enzyme is of importance. These results should then be compared with the growth behavior of the Fx9 deletion mutant.

5.3. Characterization of ferredoxin deletion mutants in *Synechocystis* under mixotrophic conditions

5.3.1 Fx9 is of importance for the growth of *Synechocystis* under mixotrophic conditions

Previous work in our group showed that the absence of PFOR (Pyruvate: Ferredoxin/Flavodoxin Oxidoreductase) results in impaired growth under mixotrophic conditions as the optical density of the cultures drops at the end of the cultivation time (Chen 2014). This is astonishing as PFOR is known as an oxygen sensitive enzyme (Hughes et al. 1995, Meinecke et al. 1989, Williams et al. 1987), whose absence should thus not result in a growth phenotype under oxic conditions. All available ferredoxin deletion mutants (*fx2/Δfx2, Δfx3, Δfx4, fx5/Δfx5, Δfx6, Δfx7, Δfx9, Δfx7Δfx9, Δfx7Δfx8Δfx9, Δfx9ΔisiB, ΔisiB*) and the PFOR mutant (*Δpfor*) were cultivated under mixotrophic conditions and it was found that *Δfx3, Δfx9* and *ΔisiB* and their respective double- and triple- mutants exhibit impaired growths at the nonexponential phase, which are similar to the growth phenotype of *Δpfor* (Fig. 4.3.1.1 and Fig. 4.3.1.2A). *Δfx9* and the triple mutant *Δfx7Δfx8Δfx9* showed a lower content of Chl a and higher carotenoid-to-chlorophyll (Car/Chl) ratio (Fig. 4.3.1.2), which indicates that these mutants suffered from more oxidative stress than the WT under mixotrophic conditions. Previous work in our group proposed that those surplus electrons might be responsible for the impaired growth of *Δpfor* as PFOR might be an important electron sink for *Synechocystis* under mixotrophic conditions, especially at the nonexponential phase (Chen 2014). Therefore, the plant-like

Fx3, the bacterial-type ferredoxin Fx9 and the flavodoxin IsiB could be involved in accepting electrons from PFOR under mixotrophic conditions.

When grown on arginine and glucose, the deletion of either PFOR or the hydrogenase inhibited the growth of *Synechocystis* (Burgstaller 2017, Chen 2014, Chen et al. 2016). This indicates that the hydrogenase functions as an essential electron sink under these conditions, in which the two most important electron sinks, CO_2 fixation and nitrogen reduction, are downregulated (Burgstaller 2017). Furthermore, like *ΔhoxH* (Burgstaller 2017), *Δpfor* also suffered from surplus electrons under those conditions, as the addition of the photosynthetic inhibitor, DCMU, could rescue the repressed mixotrophic growth of *Δpfor* on arginine (Fig. 4.3.3.3A). This is astonishing as well as the hydrogenase, besides PFOR, is known as an oxygen sensitive enzyme (Tamagnini et al. 2002). The reduced ferredoxin/flavodoxin from PFOR or PSI is able to directly donate electrons to the bidirectional NiFe-hydrogenase in *Synechocystis* (Gutekunst et al. 2014). However, which ferredoxins besides Fx1 are reduced by PFOR or are involved in the hydrogen production is still unknown. In comparison to the standard mixotrophic growth conditions on nitrate, *Δfx3, Δfx9* and *ΔisiB* and their respective double- and triple- mutants grew even worse under mixotrophic conditions on arginine, which resembles the growth phenotype of *Δpfor* and *ΔhoxH* (Fig. 4.3.2.1). However, unlike *ΔhoxH* (Burgstaller 2017) and *Δpfor*, the repressed growth of *Δfx9* cannot be rescued by the supplement of DCMU (Fig. 4.3.3.3). This indicates that Fx9 might be involved in the nitrogen catabolism and/or carbon catabolism instead of functioning as an electron shuttle between PFOR and the hydrogenase. In order to check if the growth phenotype of *Δfx9* under mixotrophic conditions on arginine is rather due to the absence of nitrate as an electron sink or due to the presence of arginine itself, the mutant was mixotrophically grown on either urea or ammonium instead of arginine (Fig. 4.3.3.3 and 4.3.2.2). Urea can be taken up directly and is converted to ammonium by the urease in cyanobacteria (Erratt 2017). The deletion of Fx9 also affected the mixotrophic growth of *Synechocystis* on both urea and ammonium, even though to a much lesser extent (Fig. 4.3.2.2 and Fig. 4.3.3.3). These results indicate that the impaired growth of *Δfx9* under mixotrophic conditions might thus be partly due to a special effect of arginine and partly to the absence of nitrate as an electron sink.

Given that *Δfx9* displays a reduced growth in the presence of glucose (under mixotrophic conditions) on nitrate, ammonium, arginine and urea (Fig. 4.3.1.2, Fig. 4.3.2.1, Fig. 4.3.2.2, and Fig. 4.3.3.3), another possibility is that Fx9 is of importance as soon as carbohydrates are provided externally. Furthermore, growth on arginine alone in the absence of glucose also results in poorer growth of *Δfx9* (Fig. 4.2.1.2). The supplement of external glucose makes *Δfx9* cells suffer greatly from much more oxidative stress (Narainsamy et al. 2013), this might explain why its growth is worst on glucose and arginine and best on glucose and nitrate. In contrast to urea, ammonium, and nitrate, arginine is a carbon source due to its carbon content (C/N 2:1) and thus cultivation on arginine without glucose could be regarded as partly mixotrophic conditions as well (Schriek et al. 2008).

In summary, Fx9 in *Synechocystis* might be important for carbohydrates metabolism under mixotrophic conditions. However, the interacting target of Fx9, besides PFOR, during carbohydrates metabolism needs to be further investigated.

5.3.2 The NiFe-hydrogenase is of importance for the growth of *Synechocystis* under oxic conditions

Synechocystis possesses a bidirectional NiFe-hydrogenase that produces or takes up hydrogen (Appel et al. 2000b). This hydrogenase is sensitive to oxygen and thus can't produce hydrogen under oxic conditions (Appel et al. 2000b, Burgstaller 2017). The hydrogen evolution only occurs in anaerobic darkness or alternatively can proceed at the onset of illumination after the dark-adapted period (Appel et al. 2000a, Gutekunst et al. 2014). However, previous work from our group found that the deletion of the hydrogenase subunit HoxH inhibits mixotrophic growth on glucose and arginine ($BG11_0$+AG) in continuous light (Burgstaller 2017). Cells incubated under these condition should be subjected to a high concentration of reduced ferredoxin and a higher electron pressure because of the absence or down regulation of the two most important electron sinks, the CBB cycle and nitrate reduction (Burgstaller 2017). This hypothesis could be substantiated as the repressed growth phenotype of the hydrogenase deletion mutant could be rescued by reducing the photosynthetic electron pressure either via low light intensity or in the presence of the photosynthesis inhibitor DCMU (Burgstaller 2017). The highest carotenoid-to-chlorophyll (Car/Chl) ratio in $BG11_0$+AG compared to that in autotrophic mediums (BG11 and $BG11_0$+A) and mixotrophic medium (BG11+G) also indicates that *Synechocystis* WT cells suffer from the strongest oxidative stress (Burgstaller 2017). It was originally hypothesized that the severe impaired growth of *ΔhoxH* was caused by the inability to metabolize arginine because HoxH is missing as an electron sink.

Surprisingly, in contrast to the stressed WT cells carrying the severe stressed phenotype, *ΔhoxH* cells look as healthy and normal under mixotrophic conditions on arginine as under photoautotrophic conditions even though they are not able to grow (Fig. 4.3.3.1.1 and 4.3.3.1.2). Furthermore, *ΔhoxH* remarkably reduces its photosynthetic and respiratory activity (Fig. 4.3.3.1.2), even though the mutant cells look normal and healthy with complete thylakoid membranes and only small amounts of cyanophycin granules (Fig. 4.3.3.1.1). It might thus be that *ΔhoxH* enters a dormant state and does not switch its metabolism as does the WT under mixotrophic conditions on arginine. Carbon and nitrogen metabolism analysis showed that WT cells consumed glucose as carbon source and arginine as nitrogen source and grew continuously with the accumulation of large amounts of cyanophycin, whereas *ΔhoxH* as well as *Δfx9* cells that had a poor growth did only consume minor amounts of glucose and arginine and accumulated much smaller amounts of cyanophycin (Fig. 4.3.3.2.1). These results concerning the cyanophycin content in WT and *ΔhoxH* are well in line with the results from the TEM photographs (Fig. 4.3.3.2.1D).

For cyanobacteria, arginine has several roles. It can be used as a substrate to synthesize cyanophycin, which is a storage form of arginine, or it can alternatively be used as an amino acid directly or oxidized to ammonia for protein synthesis via glutamate and ornithine (Maheswaran et al. 2006). It has been proposed that electrons that are liberated during the oxidation of arginine are fed into the plastoquinone (PQ) pool of the thylakoid membrane utilizing O_2as an electron acceptor via the cytochrome oxidase (Schriek et al. 2009). The oxidation of arginine might thus result in a reduced PQ pool. *ΔhoxH* and *Δfx9*, in contrast to WT, barely consume glucose and arginine which thus leaves the PQ pool less reduced as indicated by higher values of q_p (Fig. 4.3.3.2.2). This further suggests that the deletion of HoxH makes cells suffer from surplus photosynthetic electrons.

Calculating the ratio of intracellular cyanophycin content to the total amount of arginine taken up by cells revealed that both WT and *Δfx9* display similar ratios. Almost 1/3 of the arginine was used for cyanophycin biosynthesis, the residual arginine was probably utilized for protein synthesis (Fig. 4.3.3.2.1B, C and E), whereas *ΔhoxH* has a much lower ratio (Fig. 4.3.3.2.1E). This suggests that the knockout of HoxH reduces the arginine uptake and assimilation and simultaneously switches the application of arginine from cyanophycin synthesis to other metabolic reactions such as protein synthesis. This result also further suggests that the reasons for the impaired growth of *Δfx9* and *ΔhoxH* are different.

In summary, the hydrogenase is needed as electron valve to allow the cells to metabolize arginine in the presence of glucose. The deletion of the hydrogenase results in cells that suffer from nitrogen-deficiency and a surplus of electrons. However, the hydrogenase does not produce hydrogen under such conditions so it probably uses an unknown electron acceptor instead.

5.3.3 The regulation of the PDH complex by phosphorylation under mixotrophic conditions in *Synechocystis*

Previous work in our group found that the deletion of PFOR causes impaired growth and higher NADH/NAD^+ ratios in *Synechocystis* under mixotrophic conditions, especially at the nonexponential phase (Fig. 4.3.1.2) (Chen 2014). Even though PFOR is known to be sensitive to O_2(McNeely et al. 2011, Plaga et al. 1992, Schmitz et al. 2001), it has been reported to be expressed under oxic conditions in the cyanobacteria *Synechococcus* PCC7002, *Synechococcus* PCC6301, and *Synechocystis* and an oxygen resistant enzyme is furthermore known in *Desulfovibrio africanus* (Chabriere et al. 1999, Chen 2014, Schmitz et al. 2001). This indicates that the oxygen-sensitive PFOR in *Synechocystis* has a function under aerobic conditions that cannot be compensated for by the PDH complex under mixotrophic conditions.

It is known from eukaryotes and gram-negative bacteria that the PDH complex gets phosphorylated and thereby inactivated at high NADH/NAD^+ ratios (de Kok et al. 1998, Korotchkina and Patel 2000, 2001, Patel and Korotchkina 2001). Therefore, the *Synechocystis* PDH complex is hypothesized to be inactive via phosphorylation in response to higher NADH/NAD^+ ratios at the nonexponential phase of mixotrophic

growth, and thus ferredoxin/flavodoxin-dependent PFOR becomes of crucial importance for the decarboxylation of pyruvate to acetyl-CoA during this growth period.

Firstly, the cyanobacterium *Synechocystis* was predicted to possess seven STKs (Sll0776, Sll1574-75, Slr0152, Slr0599, Slr1225, Slr1443, Slr1697) and seven STPs (Sll1365, Sll1387, Sll0114, Slr0328, Slr1860, Slr1983, Slr2031) (Table 1.6.1), which could overtake the phosphorylation and dephosphorylation of the PDH complex catalyzed by the PDH kinases and the PDH phosphatase in eukaryotes (Zhang et al. 1998, Zhang et al. 2005, Zhang et al. 2007).

Secondly, the multiple sequence alignment analysis showed, in contrast to the presence of three phosphorylation sites conserved in E1 of PDHc in mammals, only the first phosphorylation site of E1, site 1, is conserved in cyanobacteria, however, sites 2 and 3 are neither conserved in yeast, in higher plant nor in cyanobacteria (Fig. 4.3.4.2.1 and 4.3.4.2.2.). Furthermore, as phosphorylation of the first phosphorylation site suffices to inactivate the PDH complex also in mammals (Korotchkina and Patel 2001, Patel and Korotchkina 2001, 2003), it can be assumed that the conserved serine residue at site 1 that is found in cyanobacteria should be adequate to allow a regulation of the PDH complex via phosphorylation as well.

Thirdly, in order to further study if the PDH complex is phosphorylated at site 1 of E1 subunit of PdhA under mixotrophic conditions, α-PdhA-E1, a specific antibody against the E1 subunit of PdhA and in addition α–phosphoserine, an antibody that binds specifically to phosphorylated serine residues, were used in immunoblot analyses. The expected molecular weight of the E1 subunit of the PDH complex is 38 kDa, and a corresponding strong signal of this size was detected both under autotrophic and mixotrophic conditions in the WT with α-PdhA-E1 (band 1 in Fig. 4.3.4.3.2). In line with our hypothesis additional bands in the range between 26-36 kDa appeared on the blots from mixotrophically grown cells only within the course of the growth experiment, especially in the nonexponential late growth phase (bands 2-4 in Fig. 4.3.4.3.2). These bands could be the phosphorylated E1 subunit of the PDH complex as the phosphorylation of a protein results in an additional negative charge which again can result in a faster running behavior in the SDS gel. This hypothesis was further confirmed by the immunoblot analysis subjected to the phosphoserine- antibody, which did not give a signal for band 1, (which we had assumed as being the unphosphorylated form of E1 subunit from the PDH complex) but precisely detected those bands 2-4 that appeared in addition on the blot from mixotrophically grown cells (which we had assumed as being the phosphorylated form of E1) (Fig. 4.3.4.3.3).

In summary, as shown in Fig. 5.3, the PDH complex could be essential for the standard photoautotrophic growth of *Synechocystis* according to the impossibility to completely delete its encoding gene (Fig. 4.2.1.1A-C). When grown under mixotrophic conditions under low NADH/NAD^+ ratios, the PDH complex is still functioning with NAD^+ as electron acceptor in the exponential growth phase (Fig. 5.3). However, it becomes phosphorylated due to high NADH/NAD^+ ratios and thereafter inactive in the nonexponential growth phase. At the same time, PFOR compensates for the inactivated PDH complex in the WT (Fig. 5.3). The impaired mixotrophic growth of PFOR deletion mutant is thus a result of the inability to decarboxylate pyruvate by

the inactive PDH complex at high NADH/NAD$^+$ ratios. The cells thus seem to switch from the NADH/NAD$^+$ pool to the ferredoxin/flavodoxin pool (such as Fx3, Fx9 and IsiB) as an acceptor for electrons from carbohydrate oxidation (Fig. 5.3).

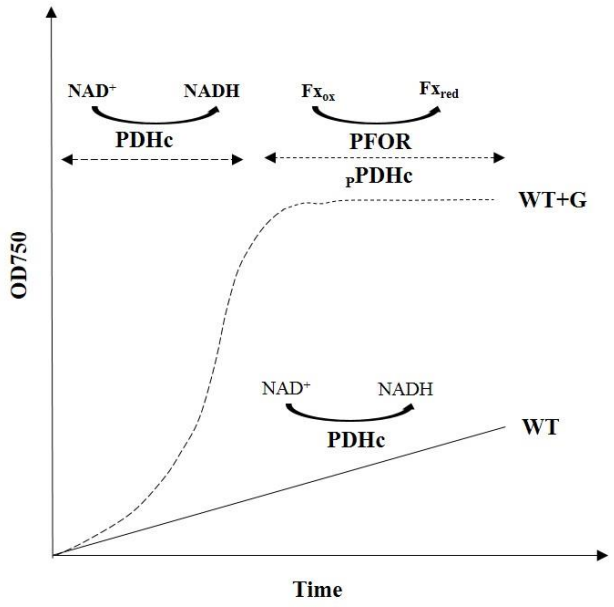

Fig. 5.3. Hypothetical scheme for the function of PFOR and PDHc during autotrophic and mixotrophic (+G) growth of *Synechocystis*. When grown with glucose, the PDH complex is initially functioning in the exponential growth phase and becomes phosphorylated due to high NADH/NAD$^+$ ratio and thereafter inactive in the nonexponential growth phase. NAD$^+$ and ferredoxin, both as electron acceptor, are reduced by PDHc and PFOR, respectively.

5.4. Characterization of ferredoxin deletion mutants in *Synechocystis* in the dark

5.4.1 Fx9 is essential for *Synechocystis* under LAHG conditions and might be involved in the nitrate/nitrite reduction as electron donors

In contrast to the highly abundant transcripts in the light, the *fx1* transcripts are downregulated in low light and become scarce after a 15-min shift to darkness (Mazouni et al. 2003, Poncelet et al. 1998). The low abundance of Fx1 in darkness could probably give other less-abundant ferredoxins the opportunity to play a role in electron transfer in *Synechocystis*. As expected, we found that the knockout of bacterial-type Fx9 causes an inhibited growth of *Synechocystis* under LAHG conditions with glucose as external carbon source (Fig. 4.4.1.1 and 4.4.1.2). This is the first ferredoxin/flavodoxin mutant to be found that cannot grow under LAGH conditions in cyanobacteria.

Yang and his cooperators found that a ferredoxin-5 (FDX5) deletion strain of *Chlamydomonas reinhardtii* was unable to grow in the dark with acetate as carbon source, but it's growth in the light was unaffected (Yang et al. 2015). According to the phylogenetic relationship of ferredoxins in the *Chlamydomonas reinhardtii* and *Synechocystis* (Fig. 5.2), the functions of bacterial-type Fx9 of *Synechocystis* might be totally different from the plant-type FDX5 of *Chlamydomonas reinhardtii* in the dark.

Further characterization of the LAGH growth of the Fx9 deletion mutant (*Δfx9*) in *Synechocystis* on various nitrogen sources, revealed that it cannot grow on nitrate, nitrite, or arginine but could grow on ammonium or urea (Fig. 4.4.2.3 and 4.4.2.4). The reduction of nitrate to nitrite and further to ammonium is catalyzed by two ferredoxin-dependent enzymes, namely nitrate reductase (Nar) and nitrite reductase (Nir) in *Synechocystis*, which require 2 and 6 electrons respectively (Flores et al. 2005). The conversion of urea to ammonium is catalyzed by the urease which does not require any electrons (Erratt 2017). It was therefore hypothesized that the knockout of Fx9 might affect the reduction of nitrate to nitrite or of nitrite to ammonium in the dark.

When grown on nitrite as sole nitrogen source under LAHG conditions, *Δfx9* is impaired in its ability to consume nitrite from the medium in comparison to the WT, whereas the uptake of glucose is unaffected (Fig. 4.4.3.2A and 4.4.3.3A). Furthermore, *Δfx9* also excretes less nitrite into the medium than the WT when grown on nitrate (Fig.4.3.3B). Thus, the absence of *Synechocystis* Fx9 not only inhibits the nitrite reduction but also affects the nitrate reduction under LAHG conditions. This could also explain why *Δfx9* holds an impaired growth in a circadian dark/light cycle (12h:12h) irrespective of the absence or the presence of glucose (Fig. 4.4.4).

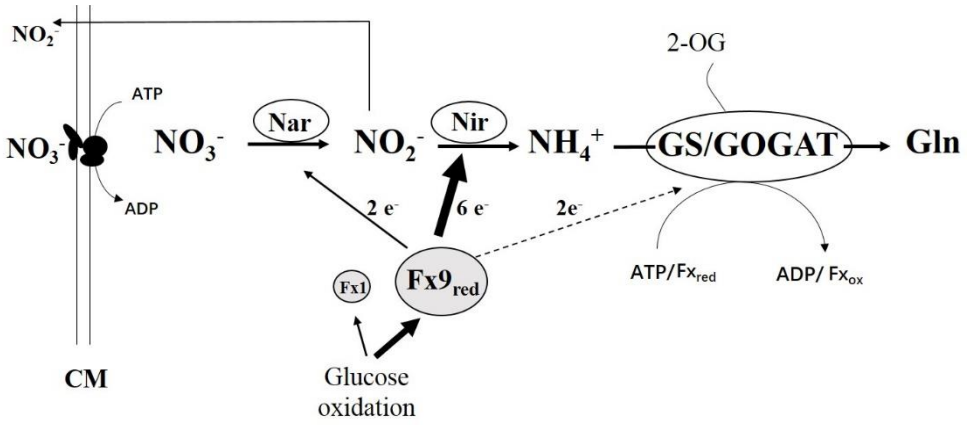

Fig. 5.4. Hypothetical scheme for the function of *Synechocystis* Fx9 in nitrogen assimilation under LAHG conditions. $Fx9_{red}$, the reduced form of Fx9, comes from glucose oxidation. CM: cytoplasmic membrane. More details could be found in Fig. 1.7.1.

In summary, as shown in the hypothetical scheme for the function of Fx9 (Fig. 5.4), when grown under LAHG conditions, Fx9, instead of Fx1, could be reduced during the oxidation of glucose. Reduced Fx9 would subsequently transfer its electrons to the ferredoxin-dependent enzyme Nar and Nir, which is reduced

by 2-electron and 6-electron reductions (equal to 1 and 3 molecules of $Fx9_{red}$), respectively. The absence of Fx9 inhibits the nitrite reduction and partly affects the nitrate reduction as the loss or limit of electron donor under LAHG conditions. Similar to the autotrophic growth on arginine, growth under LAHG conditions is characterized as nitrogen-starvation or oxidative stress conditions due to the imbalance in the C/N metabolism (Plohnke et al. 2015), the replacement of Fx1 by Fx9 functioning in the dark further indicates that Fx9 plays a crucial protective role in the tolerance to oxidative stress.

5.4.2 NAD(P)H is most likely not the sole direct electron donor to the NiFe-hydrogenase in *Synechocystis*

Previous work in our group revealed that ferredoxin/flavodoxin, but not NAD(P)H, functions as the direct electron donor to the bidirectional NiFe-hydrogenase in *Synechocystis* (Gutekunst et al. 2014). As this issue has been the subject of some debate (Dutta and Vermaas 2016), additional experiments were done in this work. In order to test if NAD(P)H might be the electron donor for hydrogen production as stated by Dutta and Vermaas (2016) under fermentative conditions, the concentration of fermentative hydrogen and the ratio of NAD(P)H/NAD(P)$^+$ were determined in cultures in parallel.

Table 5.4. The intracellular ratio of NADH/NAD$^+$ or NADPH/NADP$^+$ determined in cyanobacteria

Species	NADPH /NADP$^+$ ratio	NADH /NAD$^+$ ratio	Growth conditions	Methods	Reference
Synechococcus sp. PCC 7002	-	0.25	fermentative, nitrate-free, anoxic	LC-MS, MeOH-CAN-H_2O	McNeely et al. 2010
	0.16-0.18	0.05		LC-QQQ MS, MeOH	Kumaraswamy et al. 2013
Synechocystis sp. PCC 6803	0.007	0.0021	autotrophic, nitrogen-depleted (+N)	LC/MS/MS, MeOH/solvent mixture	Osanai et al. 2014
	0.0042	0.0021	autotrophic, nitrogen-depleted(-N)	LC/MS/MS, MeOH/solvent mixture	
Synechocystis sp. PCC 6803	0.058	0.039	fermentative, anoxic	enzymatic cycling kit	This work
	0.08	0.302	fermentative, nitrate-free, anoxic	enzymatic cycling kit	

Due to the absence of nitrate reduction as a competitive electron sink to hydrogen production, after an incubation for 12 hours under fermentative conditions, *Synechocystis* produced significantly more H_2 in the presence of arginine (28.1 μM and 17.6 μM) compared to nitrate (0.5 μM and 0.9 μM) (Fig. 4.5.1.2 and Table 4.5.1.2). However, the intracellular ratio of NADH/NAD$^+$ or NADPH/NADP$^+$ determined in parallel is not sufficient to support the observed H_2 production in *Synechocystis* (Fig. 4.5.1.2 and Table 4.5.1.2). Similar ranges of the ratios of NADH/NAD$^+$ or NADPH/NADP$^+$ were also found in *Synechococcus* sp. PCC7002 and *Synechocystis* before (Table 5.4). Furthermore, the metabolome analysis showed that the NADH and

NADPH levels did not increase in the merodiploid *hoxH* mutant of *Synechocystis* under fermentative conditions (Iijima et al. 2016).

In summary, NAD(P)H is most likely not the sole electron donor to the NiFe-hydrogenase in *Synechocystis*. In contrast a Fx_{red}/Fx_{ox} ratio of approximately 0.005 would be required at pH 7.0 to support a production of 28.1 μM H_2, as measured in the presence of arginine (Fig. 4.5.1.1 and Table 4.5.1.1). We therefore conclude for a second time that rather reduced ferredoxin than NAD(P)H is the direct electron donor to the NiFe-hydrogenase in *Synechocystis*.

5.4.3 Fx1 is most likely the primary electron donor to the NiFe-hydrogenase in *Synechocystis*

In order to screen which ferredoxins might be involved in the fermentative hydrogen production, all the available ferredoxin deletion mutants were incubated in nitrate-free medium for 12 hours under fermentative condition. The concentration of hydrogen produced in theses cultures was determined. None of the ferredoxin mutants except the putative merodiploid *fx8/Δfx8* mutant produced significantly less fermentative hydrogen than the WT (Fig. 4.5.2.1 and 4.5.2.2). As Fx1 in *Synechocystis* cannot be deleted, it might compensate for the loss of other low abundant ferredoxin for hydrogen production. Additionally, several ferredoxins might replace each other in donating electrons to the hydrogenase. Those ferredoxins that were deleted and resulted in mutants with higher fermentative hydrogen production, might be involved in pathways that compete with the hydrogenase for electrons (Fig. 4.5.2.1). For example, the absence of Fx9, which might function as electron donor for the reduction of nitrate to ammonium in darkness (Fig. 5.4), causes a shift of surplus electrons from the nitrate reduction to other ferredoxin-dependent pathways, such as hydrogen production. This is in well line with the results from nitrate reductase and nitrite reductase deletion mutants in *Synechocystis* (Baebprasert et al. 2011).

As shown in Fig. 5.1.2, the *Synechocystis* Fx1 has the closest phylogenetic relationship with the PETF and FDX2, which are reported to be involved in the hydrogen production in the green alga *Chlamydomonas reinhardtii*. It can thus be hypothesized that Fx1 may function as the primary electron donor to NiFe-hydrogenase in *Synechocystis* as well.

In summary, from our analyses it is not possible to identify distinct ferredoxins that might be involved in fermentative hydrogen production due to the fact that Fx1 cannot be deleted from the genome and might be the principal electron donor to the reaction. In addition, several ferredoxins might replace each other in donating electrons to the hydrogenase.

6. Summary

The cyanobacterium *Synechocystis* possesses nine ferredoxins (Fx) and one flavodoxin (IsiB), which function as electron carriers with low reduction potentials. They participate in a variety of metabolic reactions. In contrast to the highly abundant protein Fx1, which is well studied, the functions of the low-abundant ferredoxins (Fx2-Fx9), are only poorly understood. In this thesis, various ferredoxin/flavodoxin mutants were constructed and studied under different growth conditions. To assign distinct functions to single ferredoxins in deletion mutants is a challenge as most of them can probably replace each other physiologically. A special emphasis was put on the characterization of *Δfx9*.

In this thesis it was found that the bacterial-type Fx9 is probably involved in the nitrogen metabolism in *Synechocystis*. Three reactions that are involved in nitrogen assimilation require ferredoxin as an electron donor in cyanobacteria: nitrate (Nar) and nitrite (Nir) reductase and the ferredoxin-dependent glutamate synthase (Fd-GOGAT) reaction, which is present in addition to an NADH dependent NADH-GOGAT reaction. In this thesis it was found that Fx9 is of importance on organic nitrogen sources (arginine or glutamine) under photoautotrophic conditions. Fx9 is as well important for the growth of *Synechocystis* under mixotrophic conditions on several nitrogen sources (nitrate, arginine, urea). Under LAHG conditions in the dark *Δfx9* cannot grow on nitrate, nitrite or arginine, but it can grow on ammonium or urea. These results indicate that Fx9 might be involved in the ferredoxin-dependent nitrate and nitrite reduction under LAHG conditions. Its impaired growth under mixotrophic conditions and its inability to grow on glutamine indicates that Fx9 might be the electron donor to Fd-GOGAT in the presence of organic nitrogen sources as well as in the presence of additional carbohydrates. This hypothesis needs to be further substantiated.

A central reaction in the carbon and energy metabolism of all living cells is the decarboxylation of pyruvate to acetyl-CoA. It connects lower glycolysis to the TCA cycle. The TCA cycle provides among other intermediates 2-oxoglutarate, which serves as the carbon skeleton in nitrogen assimilation via GS/GOGAT. The decarboxylation of pyruvate is catalyzed by two enzymes in *Synechocystis*: pyruvate:ferredoxin oxidoreductase (PFOR) and the pyruvate dehydrogenase complex (PDHc). Whereas PFOR transfers electrons to ferredoxins, the PDHc reduces NAD^+. It is generally assumed that PFOR is involved in fermentation, as the enzyme is known to be oxygen sensitive, whereas PDHc is involved in respiration in the presence of oxygen. However, a mutant in which PFOR was deleted displayed impaired growth under mixotrophic conditions in the presence of oxygen. In this thesis it was found that PDHc is phosphorylated and therefore inactivated (or degraded) at high NADH/NAD^+ ratios during the nonexponential phase of mixotrophic growth and functionally replaced by PFOR. This observation is well in line with the fact that cells lacking Fx9 or IsiB, display a similar growth as the PFOR deletion mutant under mixotrophic conditions. It was thus hypothesized that PFOR reduces Fx9 under mixotrophic conditions which is probably involved in nitrogen assimilation as already stated above. This finding is quite remarkable as PFOR is known as an oxygen-sensitive enzyme.

Furthermore, the bidirectional NiFe-hydrogenase, which functions as an electron valve, is essential for growth under highly reducing conditions on arginine and glucose in the presence of oxygen. This is likewise remarkable as the hydrogenase is known as an oxygen-sensitive enzyme in cyanobacteria. In this thesis it was found that the absence of the hydrogenase provokes the cells to enter a dormant state. The respective mutant consumes neither glucose nor arginine at comparable amounts as Wild-type cells. Obviously, the hydrogenase is essential for growth on arginine and glucose in the presence of oxygen. It was further confirmed that rather ferredoxin/flavodoxin than NAD(P)H is the direct electron donor to the NiFe-hydrogenase in *Synechocystis*.

In summary, the transition of PDHc to PFOR, maybe also of NADH-GOGAT to Fd-GOGAT, suggests that the NADH pool is reduced first under highly reducing conditions and that thereafter electrons are transferred to the ferredoxin pool with a more negative redox potential. *Synechocystis* cells seem to switch from the utilization of NADH- to ferredoxin-dependent enzymes under highly reducing conditions. Low abundant ferredoxins and especially Fx9 are of physiological importance under these conditions.

7. Zusammenfassung

Das Cyanobakterium *Synechocystis* besitzt neun Ferredoxine (Fx) und ein Flavodoxin (IsiB), die als Elektronenüberträger mit niedrigem Redoxpotential fungieren. Sie sind an einer Vielzahl von metabolischen Reaktionen beteiligt. Im Gegensatz zu dem stark exprimierten Ferredoxin 1 (Fx1), welches gut untersucht ist, sind die physiologischen Bedeutungen der schwach exprimierten Ferredoxine (Fx2-Fx9) nur lückenhaft bekannt. In dieser Arbeit wurden verschiedene Ferredoxin/Flavodoxin Mutanten konstruiert und unter verschiedenen Wachstumsbedingungen untersucht. Die Funktionen verschiedener Ferredoxine über Deletionsmutanten zu identifizieren ist herausfordernd, da die meisten Ferredoxine sich in den Mutanten vermutlich gegenseitig ersetzen können. Besonderes Gewicht wurde auf die Charakterisierung von *Δfx9* gelegt.

In dieser Arbeit konnte gezeigt werden, dass das bakterientypische Fx9 vermutlich in den Stickstoffmetabolismus in *Synechocystis* involviert ist. Drei Reaktionen der Stickstoffassimilation sind in Cyanobakterien auf Ferredoxin als Elektronendonor angewiesen: Nitrat- (Nir) und Nitrit- (Nir) Reduktase und die Ferredoxin-abhängige Glutamatsynthase (Fd-GOGAT), die zusätzlich zur NADH-abhängigen NADH-GOGAT vorhanden ist. In dieser Arbeit konnte gezeigt werden, dass Fx9 unter photoautotrophen Bedingungen auf organischen Stickstoffquellen (Arginin und Glutamin) von Bedeutung ist. Fx9 ist außerdem wichtig für mixotrophes Wachstum in *Synechocystis* auf verschiedenen Stickstoffquellen (Nitrat, Nitrit, Harnstoff). *Δfx9* kann unter LAHG Bedingungen im Dunkeln weder auf Nitrat, Nitrit oder Arginin, aber auf Ammonium und Harnstoff wachsen. Diese Ergebnisse weisen darauf hin, dass Fx9 in die Ferredoxin-abhängige Nitrat- und Nitritreduktion unter LAHG Bedingungen involviert sein könnte. Das verminderte Wachstum unter mixotrophen Bedingungen und die Unfähigkeit auf Glutamin zu wachsen, weisen darauf hin, dass Fx9 zusätzlich der Elektronendonor für Fd-GOGAT in Gegenwart von organischen Stickstoffquellen sowie von Kohlenhydraten sein könnte. Diese Vermutung muss weiter untermauert werden.

Eine zentrale Reaktion im Kohlenhydrat- und Energiestoffwechsel aller lebender Zellen ist die Decarboxylierung von Pyruvat zu Acetyl-CoA. Sie verbindet die untere Glykolyse mit dem Citratzyklus. Der Citratzyklus liefert neben anderen Intermediaten 2-Oxoglutarat, welches als Kohlenstoffgerüst für die Stickstoffassimilation über GS/GOGAT dient. Die Decarboxylierung von Pyruvat wir in *Synechocystis* von zwei Enzymen katalysiert: der Pyruvat:Ferredoxin Oxidoreduktase (PFOR) und dem Pyruvat-Dehydrogenase-Komplex (PDHc). Während PFOR Elektronen auf Ferredoxin überträgt, reduziert PDHc NAD^+. Es wird allgemein angenommen, dass PFOR in die Fermentation involviert ist, da das Enzym sauerstoffsensitiv ist, wohingegen PDHc eine Rolle in der Atmung in Gegenwart von Sauerstoff spielt. Eine Mutante, in der PFOR deletiert wurde, zeigte jedoch unter mixotrophen Bedingungen in Gegenwart von Sauerstoff vermindertes Wachstum. In dieser Arbeit konnte gezeigt werden, dass PDHc unter hohen $NADH/NAD^+$ Verhältnissen in der nichtexponetiellen Phase mixotrophen Wachstums phosphoryliert und inaktiviert (oder degradiert) und funktionell von PFOR ersetzt wird. Diese Beobachtungen stimmen gut mit

der Tatsache überein, dass Zellen, denen Fx9 oder IsiB fehlen unter mixotrophen Bedingungen ein ähnliches Wachstum zeigen wie die PFOR Deletionsmutante. Auf Grundlage dieser Daten wurde die Hypothese formuliert, dass PFOR unter mixotrophen Bedingungen Fx9 reduziert, welches vermutlich in die Stickstoffassimilation involviert ist, wie bereits oben beschrieben. Diese Beobachtung ist bemerkenswert, weil PFOR als ein sauerstoffsensitives Enzym bekannt ist.

Desweiteres ist die bidirektionale NiFe-Hydrogenase, welche als Elektronenventil fungiert, essentiell für das Wachstum unter stark reduzierenden Bedingungen auf Arginin und Glukose in Gegenwart von Sauerstoff. Dies ist wiederum bemerkenswert, da auch die Hydrogenase als Sauerstoff-sensitives Enzym in Cyanobakterien bekannt ist. In dieser Arbeit konnte gezeigt werden, dass die Abwesenheit der Hydrogenase dazu führt, dass die Zellen in ein dormantes Stadium verfallen. Die entsprechenden Mutanten nehmen weder Arginin noch Glukose in zum Wildtyp vergleichbaren Mengen auf. Die Hydrogenase ist offensichtlich für das Wachstum auf Argin und Glukose essentiell. Darüber hinaus wurde bestätigt, dass Ferredoxin/Flavodoxin und nicht NAD(P)H die direkten Elektronendonoren der NiFe-Hydrogenase in *Synechocystis* sind.

Zusammenfassend legt die Ablösung von PDHc durch die PFOR, eventuell auch der Übergang von NADH-GOGAT zu Fd-GOGAT, nahe, dass unter stark reduzierenden Bedingungen zunächst der NADH Pool reduziert wird und Elektronen anschließend in den Ferredoxinpool, mit seinem negativeren Redoxpotential, fließen. *Synechocystis* scheint unter stark reduzierenden Bedingungen vom Gebrauch NADH-abhängiger Enzyme zum Einsatz Ferredoxin-abhängiger Enzyme zu wechseln. Schwach exprimierte Ferredoxine und insbesondere Fx9 sind unter diesen Bedingungen von physiologischer Bedeutung.

8. Future perspectives

Some more experiments are supposed to be carried out in order to understand the physiological functions of various ferredoxins/flavodoxin, especially Fx9, more deeply. They are marked as follows:

1. It has been shown that Fx9 might be involved in the ferredoxin-dependent glutamate synthesis under autotrophic conditions on arginine as well as glutamine. This reaction is catalyzed by GlsF. In order to further verify this assumption, the expression of GlsF in WT and *Δfx9* under these conditions could be analyzed by Western blots. In addition, growth of WT and *Δfx9* could be checked on glutamine under mixotrophic and heterotrophic conditions as well. Furthermore, NADH-GOGAT and Fd-GOGAT could be deleted from the genome in *Synechocystis* and the growth of the respective mutants could be compared with the growth of WT, PFOR and *Δfx9.* Additionally, characterization of both NADH-GOGAT and Fd-GOGAT deletion mutants would help to understand under which conditions either of these reactions are of physiological importance.
2. When grown under mixotrophic conditions, the knockout of Fx9 might affect the carbohydrates metabolism instead of nitrogen assimilation. However, PFOR is the only known enzyme that reduces ferredoxin in glycolytic pathways. Additional enzymes that might interact with Fx9 need to be searched for and identified according to Hanke's work (Hanke et al. 2011).
3. Fx9 is assumed to be involved in the nitrate/nitrite reductase under LAHG conditions. In order to further verify this assumption, cellular nitrite reductase and nitrate reductase activity in WT and *Δfx9* grown in the dark should be determined *in situ* (Herrero and Guerrero 1986).
4. A Southern blot which was done at the very end of this work revealed that the mutant, in which Fx8 should have been deleted, is either merodiploid (putative *fx8/Δfx8)* and thus contains a reduced amount of Fx8, or alternatively the resistance cassette was integrated into another place in the genome, which would result in a mutant that might possess as much Fx8 as the WT. The mutant should thus be characterized further and possibly constructed again. Results that are shown in this thesis regarding putative *fx8/Δfx8* therefore need to be interpreted cautiously and respective experiments should possibly be repeated in a new mutant.

Acknowledgement

This PhD study was performed in the Plant Cell Physiology and Biotechnology Group at the University of Kiel under the supervision of Prof. Dr. Rüdiger Schulz and Dr. Kirstin Gutekunst. The whole project continued for four years from September 2014 to September 2018.

Firstly, I am deeply grateful to Prof. Dr. Rüdiger Schulz for giving me the opportunity to purse my PhD degree in the laboratory and for the encouragement and guidance both in work and in the life, especially at the beginning when I came to Germany. I also appreciate for his review and comments on my thesis.

So many thanks go to my co-supervisor Dr. Kirstin Gutekunst. I cannot necessarily finish my PhD work without her help and support. She offered me the precious opportunity to start a PhD study in Germany and really helped me a lot from the beginning to the end. She really changed me a lot on the attitude to science and life. For the research, think more before taking acting. She encouraged me to think about the question independently and patiently and put forward the innovative idea, which is the most important in science. She was very kind and patient to talk with me about my results and answer my question every time when I was confused. For the life, I am also impressed that her endeavor, optimism and independence, which are three of the most valuable personalities for one person. She was so nice to encourage me whenever I was at sea or in trouble. In addition, I would also express my particular gratitude for her comments and helps on language editing and summary translation of my thesis.

I am grateful to Dr. Jens Appel and Dr. Marko Böhm. I am impressed by their knowledgeability, intelligence and professional experimental skills. Discussion with Jens was a great experience, which brought me much valuable information on my projects. Working with Marko was also an enjoyable experience because he can carry out every experiment more efficient and professional, which really make me learn a lot.

I am grateful to Prof. Dr. Bilger for being my second referee and his consent to use the Hitachi 850 fluorescence spectrophotometer for the 77 K Fluorescence Measurements.

Many thanks to Alexander Makowka. It was surprisingly enjoyable to have the trips with you, especially the road trip in the American West, which I would remember through my life. He also gave me a lot of help on the projects, such as the glucose/glycogen determination.

I am grateful to Berit Faehnrich. She is so nice and kind to help and encourage me constantly. Her little daughter was so cute and made me a lot of happiness.

Special thanks to Claudia Marquardt, Vannessa Hueren, Jannik Faustmann, Johanna Callebe, Sinje Leitzke for their technical assistances, such as mutant construction, hydrogenase activity measurement, nitrate/nitrite determination and arginine determination, in my project. I am also grateful to Katharina Spengler, Dr. Lars Nichelmann, Sarah Hildebrandt, Rafael Meichßner, Dr. Karoline Schreiber, Dr. Heiner Burgstaller, Dr. Xi Chen, Dr. Opayi Mudium, Inga Koopmann, Marie Schröder and the others in our group. Their presences

make a lot of fun in the lab and my daily life in Germany. I am so glad to be their friends and colleagues in the past four years.

I am grateful to Mr. Jan Bensien from International Center in Kiel University. Four years ago, he helped me apply for a dormitory belonging to the Studentenwerk Schleswig-Holstein, where is very convenient and I still live till now. It's really great help for me because everyone knows that finding a good place to live in Kiel, even the whole country, is very difficult.

Financial support from the China Scholarship Council (CSC) for my living costs in Germany is gratefully acknowledged. University of Kiel is appreciated for supporting me the travel scholarships to attend the international conferences in Sweden and the United States.

Last but not least, I would like to express my deepest gratitude to my parents, my old brother (and his family) and my old sister (and her family) for their support and loves, which are the most important source of strength for me to keep moving forward through my whole life. During the past four years, meeting with my fiancee, Chunyan Shen, is the most important, valuable and memorable thing for me. Honey, thanks a lot for your loves, supports, efforts and adamancy in the past four years. This thesis is not only for me but also for you.

Affidavit

Herewith, I declare that the work is my genuine work apart from the supervisors' guidance and nothing but the references and tools mentioned in my thesis have been used to conduct this work.

The thesis has not been submitted either partially or wholly as part of a doctoral degree to another examining body.

Besides this, I declare that the thesis has been prepared subject to the Rules of Good Scientific Practice of the German Research Foundation.

The oral examination is carried out in the form of a disputation and is held in English.

Yingying Wang

Curriculum Vitae

Name	Yingying Wang
Date of birth	09.12.1988
Place of birth	Shandong, China
Nationality	P.R. China

Education:

2014.10 – now	PhD student, Department of Biology, Christian-Albrechts-Universität zu Kiel, Germany
	Thesis: The physiological functions of different ferredoxins in *Synechocystis* sp. PCC 6803
	Supervisors: Prof. Dr. Rüdiger Schulz and Dr. Kirstin Gutekunst
2011.09 – 2014.03	Master of Science, Institute of Crop Science, Zhejiang University, Hangzhou, China
	Thesis: Studies on biological and agronomic traits of Gu (*Zizania latifolia*)
	Supervisor: Prof. Dr. Longjiang Fan
2007.09 – 2011.06	Bachelor of Science, College of Bioengineering, Weifang University, Weifang, China
	Thesis: Research progress on biomass energy
	Supervisor: Guanzhao Cheng
2004.09 – 2007.06	High School, Zoucheng Experimental Middle School, Jining, Shandong, China
2001.09 – 2004.06	Middle School, Jining, Shandong, China
1996.09 -2001.06	Elementary School, Jining, Shandong, China

Reference

Adams, D.G. (2000) The ecology of cyanobacteria, pp. 523-561, Springer.

Aichi, M., Takatani, N. and Omata, T. (2001) Role of NtcB in activation of nitrate assimilation genes in the cyanobacterium Synechocystis sp strain PCC 6803. Journal of Bacteriology 183(20), 5840-5847.

Allahverdiyeva, Y., Ermakova, M., Eisenhut, M., Zhang, P., Richaud, P., Hagemann, M., Cournac, L. and Aro, E.M. (2011) Interplay between flavodiiron proteins and photorespiration in Synechocystis sp. PCC 6803. Journal of Biological Chemistry 286(27), 24007-24014.

Allahverdiyeva, Y., Isojarvi, J., Zhang, P. and Aro, E.M. (2015) Cyanobacterial Oxygenic Photosynthesis is Protected by Flavodiiron Proteins. Life (Basel) 5(1), 716-743.

Allahverdiyeva, Y., Mustila, H., Ermakova, M., Bersanini, L., Richaud, P., Ajlani, G., Battchikova, N., Cournac, L. and Aro, E.M. (2013) Flavodiiron proteins Flv1 and Flv3 enable cyanobacterial growth and photosynthesis under fluctuating light. Proceedings of the National Academy of Sciences of the United States of America 110(10), 4111-4116.

Allen, J.F. and Martin, W. (2007) Evolutionary biology - Out of thin air. nature 445(7128), 610-612.

Alvarez, F.J., Ermer, J., Hubner, G., Schellenberger, A. and Schowen, R.L. (1991) Catalytic Power of Pyruvate Decarboxylase - Rate-Limiting Events and Microscopic Rate Constants from Primary Carbon and Secondary Hydrogen Isotope Effects. Journal of the American Chemical Society 113(22), 8402-8409.

Anderson, S.L. and Mcintosh, L. (1991) Light-Activated Heterotrophic Growth of the Cyanobacterium Synechocystis Sp Strain Pcc-6803 - a Blue-Light-Requiring Process. Journal of Bacteriology 173(9), 2761-2767.

Angeleri, M., Zorina, A., Aro, E.M. and Battchikova, N. (2018) Interplay of SpkG kinase and the Slr0151 protein in the phosphorylation of ferredoxin 5 in Synechocystis sp strain PCC 6803. Febs Letters 592(3), 411-421.

Appel, J., Phunpruch, S., Steinmuller, K. and Schulz, R. (2000a) The bidirectional hydrogenase of Synechocystis sp PCC 6803 works as an electron valve during photosynthesis. Archives of Microbiology 173(5-6), 333-338.

Appel, J., Phunpruch, S., Steinmüller, K. and Schulz, R. (2000b) The bidirectional hydrogenase of Synechocystis sp. PCC 6803 works as an electron valve during photosynthesis. Archives of Microbiology 173(5-6), 333-338.

Arnon, D.I. and Chain, R.K. (1979) Regulatory Electron-Transport Pathways in Cyclic Photophosphorylation - Reduction of C-550 and Cytochrome-B6 by Ferredoxin in the Dark. Febs Letters 102(1), 133-138.

Asada, K., Kiso, K. and Yoshikaw.K (1974) Univalent Reduction of Molecular-Oxygen by Spinach-Chloroplasts on Illumination. Journal of Biological Chemistry 249(7), 2175-2181.

Baebprasert, W., Jantaro, S., Khetkorn, W., Lindblad, P. and Incharoensakdi, A. (2011) Increased H2 production in the cyanobacterium Synechocystis sp. strain PCC 6803 by redirecting the electron supply via genetic engineering of the nitrate assimilation pathway. Metabolic Engineering 13(5), 610-616.

Balakrishnan, A., Nemeria, N.S., Chakraborty, S., Kakalis, L. and Jordan, F. (2012) Determination of Pre-Steady-State Rate Constants on the Escherichia coli Pyruvate Dehydrogenase Complex Reveals That Loop Movement Controls the Rate-Limiting Step. Journal of the American Chemical Society 134(45), 18644-18655.

Ball, S.G. and Morell, M.K. (2003) From bacterial glycogen to starch: understanding the biogenesis of the plant starch granule. Annual Review of Plant Biology 54, 207-233.

Batie, C.J. and Kamin, H. (1986) Association of ferredoxin-NADP+ reductase with NADP(H) specificity and oxidation-reduction properties. Journal of Biological Chemistry 261(24), 11214-11223.

Battchikova, N. and Aro, E.M. (2007) Cyanobacterial NDH-1 complexes: multiplicity in function and subunit composition. Physiologia Plantarum 131(1), 22-32.

Battchikova, N., Eisenhut, M. and Aro, E.M. (2011) Cyanobacterial NDH-1 complexes: Novel insights and remaining puzzles. Biochimica Et Biophysica Acta-Bioenergetics 1807(8), 935-944.

Bekker, A., Holland, H.D., Wang, P.L., Rumble, D., Stein, H.J., Hannah, J.L., Coetzee, L.L. and Beukes, N.J. (2004) Dating the rise of atmospheric oxygen. nature 427(6970), 117-120.

Berla, B.M., Saha, R., Immethun, C.M., Maranas, C.D., Moon, T.S. and Pakrasi, H.B. (2013) Synthetic biology of cyanobacteria: unique challenges and opportunities. Frontiers in Microbiology 4.

Bernat, G., Waschewski, N. and Rogner, M. (2009) Towards efficient hydrogen production: the impact of antenna size and external factors on electron transport dynamics in Synechocystis PCC 6803. Photosynthesis Research 99(3), 205-216.

Berry, S., Schneider, D., Vermaas, W.F.J. and Rogner, M. (2002) Electron transport routes in whole cells of Synechocystis sp strain PCC 6803: The role of the cytochrome bd-type oxidase. Biochemistry 41(10), 3422-3429.

Bersanini, L., Battchikova, N., Jokel, M., Rehman, A., Vass, I., Allahverdiyeva, Y. and Aro, E.M. (2014) Flavodiiron Protein Flv2/Flv4-Related Photoprotective Mechanism Dissipates Excitation Pressure of PSII in Cooperation with Phycobilisomes in Cyanobacteria. Plant Physiology 164(2), 805-818.

Bertini, I., Luchinat, C., Provenzani, A., Rosato, A. and Vasos, P.R. (2002) Browsing gene banks for Fe2S2 ferredoxins and structural modeling of 88 plant-type sequences: An analysis of fold and function. Proteins-Structure Function and Genetics 46(1), 110-127.

Bhattacharya, J., GhoshDastidar, K., Chatterjee, A., Majee, M. and Majumder, A.L. (2004) Synechocystis Fe superoxide dismutase gene confers oxidative stress tolerance to Escherichia coli. Biochem Biophys Res Commun 316(2), 540-544.

Bottin, H. and Lagoutte, B. (1992a) Ferredoxin and Flavodoxin from the Cyanobacterium Synechocystis Sp Pcc-6803. Biochim Biophys Acta 1101(1), 48-56.

Bottin, H. and Lagoutte, B. (1992b) Ferrodoxin and flavodoxin from the cyanobacterium Synechocystis sp PCC 6803. Biochimica et Biophysica Acta (BBA)-Bioenergetics 1101(1), 48-56.

Bradford, M.M. (1976) A rapid and sensitive method for the quantitation of microgram quantities of protein utilizing the principle of protein-dye binding. Anal Biochem 72, 248-254.

Bricker, T.M. and Frankel, L.K. (2011) Auxiliary functions of the PsbO, PsbP and PsbQ proteins of higher plant Photosystem II: A critical analysis. Journal of Photochemistry and Photobiology B-Biology 104(1-2), 165-178.

Bricker, T.M., Roose, J.L., Fagerlund, R.D., Frankel, L.K. and Eaton-Rye, J.J. (2012) The extrinsic proteins of Photosystem II. Biochimica Et Biophysica Acta-Bioenergetics 1817(1), 121-142.

Briggs, L.M., Pecoraro, V.L. and Mcintosh, L. (1990) Copper-Induced Expression, Cloning, and Regulatory Studies of the Plastocyanin Gene from the Cyanobacterium Synechocystis Sp Pcc-6803. Plant Molecular Biology 15(4), 633-642.

Bruland, K.W., Coale, K.H. and Mart, L. (1985) Analysis of Seawater for Dissolved Cadmium, Copper and Lead - an Intercomparison of Voltammetric and Atomic-Absorption Methods. Marine Chemistry 17(4), 285-300.

Bruschi, M. and Guerlesquin, F. (1988) Structure, function and evolution of bacterial ferredoxins. FEMS Microbiol Rev 4(2), 155-175.

Buchanan, B.B. (1991) Regulation of Co2 Assimilation in Oxygenic Photosynthesis - the Ferredoxin Thioredoxin System - Perspective on Its Discovery, Present Status, and Future-Development. Archives of Biochemistry and Biophysics 288(1), 1-9.

Buchanan, B.B., Schurmann, P., Wolosiuk, R.A. and Jacquot, J.P. (2002) The ferredoxin/thioredoxin system: from discovery to molecular structures and beyond. Photosynthesis Research 73(1-3), 215-222.

Burgstaller, H.M. (2017) Physiologie der bidirektionalen [NiFe]-Hydrogenase im Cyanobakterium Synechocystis sp. PCC6803 unter oxischen Bedingungen, Christian-Albrechts Universität Kiel.

Caldovic, L. and Tuchman, M. (2003) N-acetylglutamate and its changing role through evolution. Biochemical Journal 372, 279-290.

Campbell, D., Hurry, V., Clarke, A.K., Gustafsson, P. and Oquist, G. (1998) Chlorophyll fluorescence analysis of cyanobacterial photosynthesis and acclimation. Microbiology and Molecular Biology Reviews 62(3), 667-+.

Cannon, G.C., Bradburne, C.E., Aldrich, H.C., Baker, S.H., Heinhorst, S. and Shively, J.M. (2001) Microcompartments in prokaryotes: Carboxysomes and related polyhedra. Applied and Environmental Microbiology 67(12), 5351-5361.

Carrieri, D., Lombardi, T., Paddock, T., Cano, M., Goodney, G.A., Nag, A., Old, W., Maness, P.C., Seibert, M., Ghirardi, M. and Yu, J.P. (2017) Transcriptome and proteome analysis of nitrogen starvation responses in Synechocystis 6803 Delta glgC, a mutant incapable of glycogen storage. Algal Research-Biomass Biofuels and Bioproducts 21, 64-75.

Carrieri, D., McNeely, K., De Roo, A.C., Bennette, N., Pelczer, I. and Dismukes, G.C. (2009) Identification and quantification of water-soluble metabolites by cryoprobe-assisted nuclear magnetic resonance spectroscopy applied to microbial fermentation. Magnetic Resonance in Chemistry 47, S138-S146.

Carrieri, D., Momot, D., Brasg, I.A., Ananyev, G., Lenz, O., Bryant, D.A. and Dismukes, G.C. (2010) Boosting Autofermentation Rates and Product Yields with Sodium Stress Cycling: Application to Production of Renewable Fuels by Cyanobacteria. Applied and Environmental Microbiology 76(19), 6455-6462.

Cassier-Chauvat, C. and Chauvat, F. (2014a) Function and Regulation of Ferredoxins in the Cyanobacterium, Synechocystis PCC6803: Recent Advances. Life (Basel) 4(4), 666-680.

Cassier-Chauvat, C. and Chauvat, F. (2014b) Responses to oxidative and heavy metal stresses in cyanobacteria: recent advances. International Journal of Molecular Sciences 16(1), 871-886.

Chabriere, E., Charon, M.H., Volbeda, A., Pieulle, L., Hatchikian, E.C. and Fontecilla-Camps, J.C. (1999) Crystal structures of the key anaerobic enzyme pyruvate : ferredoxin oxidoreductase, free and in complex with pyruvate. Nature Structural Biology 6(2), 182-190.

Chardonnet, S., Sakr, S., Cassier-Chauvat, C., Le Marechal, P., Chauvat, F., Lemaire, S.D. and Decottignies, P. (2015) First proteomic study of S-glutathionylation in cyanobacteria. J Proteome Res 14(1), 59-71.

Chen, X. (2014) Characterization of Synechocystis sp. PCC 6803 under mixotrophic conditions, Kiel University.

Chen, X., Schreiber, K., Appel, J., Makowka, A., Fahnrich, B., Roettger, M., Hajirezaei, M.R., Sonnichsen, F.D., Schonheit, P., Martin, W.F. and Gutekunst, K. (2016) The Entner-Doudoroff pathway is an overlooked glycolytic route in cyanobacteria and plants. Proceedings of the National Academy of Sciences of the United States of America 113(19), 5441-5446.

Cooley, J.W., Howitt, C.A. and Vermaas, W.F.J. (2000) Succinate : quinol oxidoreductases in the cyanobacterium Synechocystis sp strain PCC 6803: Presence and function in metabolism and electron transport. Journal of Bacteriology 182(3), 714-722.

de Kok, A., Hengeveld, A.F., Martin, A. and Westphal, A.H. (1998) The pyruvate dehydrogenase multi-enzyme complex from Gram-negative bacteria. Biochimica Et Biophysica Acta-Protein Structure and Molecular Enzymology 1385(2), 353-366.

Dean, R.L. and Miskiewicz, E. (2003) Rates of electron transport in the thylakoid membranes of isolated, illuminated chloroplasts are enhanced in the presence of ammonium chloride. Biochemistry and Molecular Biology Education 31(6), 410-417.

Deibel, R.H. and Niven, C.F. (1964) Pyruvate Fermentation by Streptococcus Faecalis. Journal of Bacteriology 88(1), 4-&.

Deng, M.D. and Coleman, J.R. (1999) Ethanol synthesis by genetic engineering in cyanobacteria. Applied and Environmental Microbiology 65(2), 523-528.

Dereeper, A., Guignon, V., Blanc, G., Audic, S., Buffet, S., Chevenet, F., Dufayard, J.F., Guindon, S., Lefort, V., Lescot, M., Claverie, J.M. and Gascuel, O. (2008) Phylogeny.fr: robust phylogenetic analysis for the non-specialist. Nucleic Acids Research 36, W465-W469.

DeRuyter, Y.S. and Fromme, P. (2008) Molecular structure of the photosynthetic apparatus. The cyanobacteria: molecular biology, genomics and evolution, 217-269.

Dupont, C.L., Butcher, A., Valas, R.E., Bourne, P.E. and Caetano-Anolles, G. (2010) History of biological metal utilization inferred through phylogenomic analysis of protein structures. Proceedings of the National Academy of Sciences of the United States of America 107(23), 10567-10572.

Dur n, R.V., Herv s, M., De la Rosa, M.A. and Navarro, J.A. (2004) The efficient functioning of photosynthesis and respiration in Synechocystis sp PCC 6803 strictly requires the presence of either cytochrome c(6) or plastocyanin. Journal of Biological Chemistry 279(8), 7229-7233.

Dutta, I. and Vermaas, W.F.J. (2016) The electron transfer pathway upon H2 oxidation by the NiFe bidirectional hydrogenase of Synechocystis sp. PCC 6803 in the light shares components with the photosynthetic electron transfer chain in thylakoid membranes. International Journal of Hydrogen Energy 41(28), 11949-11959.

Eisenhut, M., Aguirre von Wobeser, E., Jonas, L., Schubert, H., Ibelings, B.W., Bauwe, H., Matthijs, H.C.P. and Hagemann, M. (2007) Long-term response toward inorganic carbon limitation in wild type and glycolate turnover mutants of the cyanobacterium Synechocystis sp strain PCC 6803(1[W]). Plant Physiology 144(4), 1946-1959.

Ellersiek, U., Berger, S. and Steinmuller, K. (1991) Cyanobacteria Contain a Mitochondrial Complex I-Homologous Nadh-Dehydrogenase. Biological Chemistry Hoppe-Seyler 372(8), 549-549.

Elsen, S., Efthymiou, G., Peteinatos, P., Diallinas, G., Kyritsis, P. and Moulis, J.M. (2010) A bacteria-specific 2[4Fe-4S] ferredoxin is essential in Pseudomonas aeruginosa. Bmc Microbiology 10.

Ermakova, M., Huokko, T., Richaud, P., Bersanini, L., Howe, C.J., Lea-Smith, D.J., Peltier, G. and Allahverdiyeva, Y. (2016) Distinguishing the Roles of Thylakoid Respiratory Terminal Oxidases in the Cyanobacterium Synechocystis sp PCC 6803. Plant Physiology 171(2), 1307-1319.

Erratt, K.J. (2017) Urea as an Effective Nitrogen Source for Cyanobacteria.

Falkowski, P.G. and Raven, J.A. (1997) Aquatic Photosynthesis, Blackwell Science.

Fang, L.F., Ge, H.T., Huang, X.H., Liu, Y., Lu, M., Wang, J.L., Chen, W.Y., Xu, W. and Wang, Y.C. (2017) Trophic Mode-Dependent Proteomic Analysis Reveals Functional Significance of Light-Independent Chlorophyll Synthesis in Synechocystis sp PCC 6803. Molecular Plant 10(1), 73-85.

Finnegan, M.G., Knaff, D.B., Qin, H., Gray, K.A., Daldal, F., Yu, L.D., Yu, C.A., Francisco, S.K.S. and Johnson, M.K. (1996) Axial heme ligation in the cytochrome bc(1) complexes of mitochondrial and photosynthetic membranes. A near-infrared magnetic circular dichroism and electron paramagnetic resonance study. Biochimica Et Biophysica Acta-Bioenergetics 1274(1-2), 9-20.

Flores, E., Frías, J.E., Rubio, L.M. and Herrero, A. (2005) Photosynthetic nitrate assimilation in cyanobacteria. Photosynthesis Research 83(2), 117-133.

Flores, E. and Herrero, A. (2005a) Nitrogen assimilation and nitrogen control in cyanobacteria. Biochemical Society Transactions 33, 164-167.

Flores, E. and Herrero, A. (2005b) Nitrogen assimilation and nitrogen control in cyanobacteria, Portland Press Limited, Biochemical Society Transactions.

Flores, E. and Muropastor, A.M. (1990) Mutational and Kinetic-Analysis of Basic-Amino-Acid Transport in the Cyanobacterium Synechocystis Sp Pcc-6803. Archives of Microbiology 154(6), 521-527.

Forchhammer, K. (2004) Global carbon/nitrogen control by PII signal transduction in cyanobacteria: from signals to targets. FEMS Microbiol Rev 28(3), 319-333.

Foyer, C.H. and Noctor, G. (2000) Oxygen processing in photosynthesis: regulation and signalling. New Phytologist 146(3), 359-388.

Fromme, P. and Grotjohann, I. (2008) Overview of photosynthesis. Wiley-VCH Verlag, Weinheim, Germany.

Fujita, Y., Murakami, A. and Ohki, K. (1987) Regulation of Photosystem Composition in the Cyanobacterial Photosynthetic System - the Regulation Occurs in Response to the Redox State of the Electron Pool Located between the 2 Photosystems. Plant and Cell Physiology 28(2), 283-292.

Garcia-Sanchez, M.I., Gotor, C., Jacquot, J.P., Stein, M., Suzuki, A. and Vega, J.M. (1997) Critical residues of Chlamydomonas reinhardtii ferredoxin for interaction with nitrite reductase and glutamate synthase revealed by site-directed mutagenesis. Eur J Biochem 250(2), 364-368.

Gardner, A.M., Helmick, R.A. and Gardner, P.R. (2002) Flavorubredoxin, an inducible catalyst for nitric oxide reduction and detoxification in Escherichia coli. Journal of Biological Chemistry 277(10), 8172-8177.

Gasteiger, E., Gattiker, A., Hoogland, C., Ivanyi, I., Appel, R.D. and Bairoch, A. (2003) ExPASy: the proteomics server for in-depth protein knowledge and analysis. Nucleic Acids Research 31(13), 3784-3788.

Giastas, P., Pinotsis, N., Efthymiou, G., Wilmanns, M., Kyritsis, P., Moulis, J.M. and Mavridis, I.M. (2006) The structure of the 2[4Fe-4S] ferredoxin from Pseudomonas aeruginosa at 1.32-A resolution: comparison with other high-resolution structures of ferredoxins and contributing structural features to reduction potential values. Journal of Biological Inorganic Chemistry 11(4), 445-458.

Goss, T. and Hanke, G. (2014) The End of the Line: Can Ferredoxin and Ferredoxin NADP(H) Oxidoreductase Determine the Fate of Photosynthetic Electrons? Current Protein & Peptide Science 15(4), 385-393.

Grasshoff, K., Kremling, K. and Ehrhardt, M. (2009) Methods of seawater analysis, John Wiley & Sons.

Gutekunst, K. (2018) Hypothesis on the Synchronistic Evolution of Autotrophy and Heterotrophy. Trends in Biochemical Sciences 43(6), 402-411.

Gutekunst, K., Chen, X., Schreiber, K., Kaspar, U., Makam, S. and Appel, J. (2014) The Bidirectional NiFe-hydrogenase in Synechocystis sp PCC 6803 Is Reduced by Flavodoxin and Ferredoxin and Is Essential under Mixotrophic, Nitrate-limiting Conditions. Journal of Biological Chemistry 289(4), 1930-1937.

Gutekunst, K. and Schulz, R. (2018) Microalgal Hydrogen Production, pp. 107-138.

Gutthann, F., Egert, M., Marques, A. and Appel, J. (2007) Inhibition of respiration and nitrate assimilation enhances photohydrogen evolution under low oxygen concentrations in Syneehocystis sp PCC 6803. Biochimica Et Biophysica Acta-Bioenergetics 1767(2), 161-169.

Hall, T., Biosciences, I. and Carlsbad, C. (2011) BioEdit: an important software for molecular biology. GERF Bull Biosci 2(1), 60-61.

Hanada, S. (2016) Anoxygenic Photosynthesis -A Photochemical Reaction That Does Not Contribute to Oxygen Reproduction. Microbes Environ 31(1), 1-3.

Hanke, G. (2017) Preface: ferredoxin. Photosynthesis Research 134(3), 233-234.

Hanke, G. and Mulo, P. (2013) Plant type ferredoxins and ferredoxin-dependent metabolism. Plant Cell Environ 36(6), 1071-1084.

Hanke, G.T., Satomi, Y., Shinmura, K., Takao, T. and Hase, T. (2011) A screen for potential ferredoxin electron transfer partners uncovers new, redox dependent interactions. Biochim Biophys Acta 1814(2), 366-374.

Harel, A., Bromberg, Y., Falkowski, P.G. and Bhattacharya, D. (2014) Evolutionary history of redox metal-binding domains across the tree of life. Proceedings of the National Academy of Sciences of the United States of America 111(19), 7042-7047.

Hase, T., Kimata, Y., Yonekura, K., Matsumura, T. and Sakakibara, H. (1991) Molecular-Cloning and Differential Expression of the Maize Ferredoxin Gene Family. Plant Physiology 96(1), 77-83.

Hasunuma, T., Matsuda, M. and Kondo, A. (2016) Improved sugar-free succinate production by Synechocystis sp. PCC 6803 following identification of the limiting steps in glycogen catabolism. Metab Eng Commun 3, 130-141.

He, Z.H., Zheng, F.F., Wu, Y.Z., Li, Q.H., Lv, J., Fu, P.C. and Mi, H.L. (2015) NDH-1L interacts with ferredoxin via the subunit NdhS in Thermosynechococcus elongatus. Photosynthesis Research 126(2-3), 341-349.

Heinrich, A., Maheswaran, M., Ruppert, U. and Forchhammer, K. (2004) The Synechococcus elongatus P-II signal transduction protein controls arginine synthesis by complex formation with N-acetyl-L-glutamate kinase. Molecular Microbiology 52(5), 1303-1314.

Helman, Y., Tchernov, D., Reinhold, L., Shibata, M., Ogawa, T., Schwarz, R., Ohad, I. and Kaplan, A. (2003) Genes encoding a-type flavoproteins are essential for photoreduction of O-2 in cyanobacteria. Current Biology 13(3), 230-235.

Herrero, A., Flores, E. and Guerrero, M.G. (1981) Regulation of Nitrate Reductase Levels in the Cyanobacteria Anacystis-Nidulans, Anabaena Sp Strain 7119, and Nostoc Sp Strain 6719. Journal of Bacteriology 145(1), 175-180.

Herrero, A. and Guerrero, M.G. (1986) Regulation of Nitrite Reductase in the Cyanobacterium Anacystis-Nidulans. Journal of General Microbiology 132, 2463-2468.

Herrero, A., Muro-Pastor, A.M. and Flores, E. (2001) Nitrogen control in cyanobacteria. Journal of Bacteriology 183(2), 411-425.

Hervas, M., Navarro, J.A. and De La Rosa, M.A. (2003) Electron transfer between membrane complexes and soluble proteins in photosynthesis. Accounts of Chemical Research 36(10), 798-805.

Heyer, H. and Krumbein, W.E. (1991) Excretion of Fermentation Products in Dark and Anaerobically Incubated Cyanobacteria. Archives of Microbiology 155(3), 284-287.

Hihara, Y., Kamei, A., Kanehisa, M., Kaplan, A. and Ikeuchi, M. (2001) DNA microarray analysis of cyanobacterial gene expression during acclimation to high light. Plant Cell 13(4), 793-806.

Hirasawa, M., Hurley, J.K., Salamon, Z., Tollin, G. and Knaff, D.B. (1996) Oxidation-reduction and transient kinetic studies of spinach ferredoxin-dependent glutamate synthase. Archives of Biochemistry and Biophysics 330(1), 209-215.

Hirasawa, M., Solis, J., Vaidyanathan, N., Srivastava, A.P., Wynn, R.M., Sutton, R.B. and Knaff, D.B. (2017) Identification of the ferredoxin interaction sites on ferredoxin-dependent glutamate synthase from Synechocystis sp PCC 6803. Photosynthesis Research 134(3), 317-328.

Hisbergues, M., Jeanjean, R., Joset, F., de Marsac, N.T. and Bedu, S. (1999) Protein PII regulates both inorganic carbon and nitrate uptake and is modified by a redox signal in Synechocystis PCC 6803. Febs Letters 463(3), 216-220.

Hoare, D.S. and Hoare, S.L. (1966) Feedback regulation of arginine biosynthesis in blue-green algae and photosynthetic bacteria. Journal of Bacteriology 92(2), 375-379.

Hosoya-Matsuda, N., Motohashi, K., Yoshimura, H., Nozaki, A., Inoue, K., Ohmori, M. and Hisabori, T. (2005) Anti-oxidative stress system in cyanobacteria. Significance of type II peroxiredoxin and the role of 1-Cys peroxiredoxin in Synechocystis sp. strain PCC 6803. Journal of Biological Chemistry 280(1), 840-846.

Houot, L., Floutier, M., Marteyn, B., Michaut, M., Picciocchi, A., Legrain, P., Aude, J.C., Cassier-Chauvat, C. and Chauvat, F. (2007) Cadmium triggers an integrated reprogramming of the metabolism of Synechocystis PCC6803, under the control of the Slr1738 regulator. Bmc Genomics 8, 350.

Howitt, C.A., Udall, P.K. and Vermaas, W.F.J. (1999) Type 2 NADH dehydrogenases in the cyanobacterium Synechocystis sp strain PCC 6803 are involved in regulation rather than respiration. Journal of Bacteriology 181(13), 3994-4003.

Howitt, C.A. and Vermaas, W.F.J. (1998) Quinol and cytochrome oxidases in the cyanobacterium Synechocystis sp. PCC 6803. Biochemistry 37(51), 17944-17951.

Hughes, N.J., Chalk, P.A., Clayton, C.L. and Kelly, D.J. (1995) Identification of carboxylation enzymes and characterization of a novel four-subunit pyruvate:flavodoxin oxidoreductase from Helicobacter pylori. Journal of Bacteriology 177(14), 3953-3959.

Hugler, M. and Sievert, S.M. (2011) Beyond the Calvin Cycle: Autotrophic Carbon Fixation in the Ocean. Annual Review of Marine Science, Vol 3 3, 261-289.

Ihlenfeldt, M. and Gibson, J. (1977) Acetate uptake by the unicellular cyanobacteria Synechococcus and Aphanocapsa. Archives of Microbiology 113(3), 231-241.

Iijima, H., Shirai, T., Okamoto, M., Pinto, F., Tamagnini, P., Hasunuma, T., Kondo, A., Hirai, M.Y. and Osanai, T. (2016) Metabolomics-based analysis revealing the alteration of primary carbon metabolism by the genetic manipulation of a hydrogenase HoxH in Synechocystis sp. PCC 6803. Algal Research 18, 305-313.

Ikeda, T., Yamamoto, M., Arai, H., Ohmori, D., Ishii, M. and Igarashi, Y. (2005) Two tandemly arranged ferredoxin genes in the Hydrogenobacter thermophilus genome: Comparative characterization of the recombinant [4Fe-4S] ferredoxins. Bioscience Biotechnology and Biochemistry 69(6), 1172-1177.

Johnson, M., Zaretskaya, I., Raytselis, Y., Merezhuk, Y., McGinnis, S. and Madden, T.L. (2008) NCBI BLAST: a better web interface. Nucleic Acids Research 36(Web Server issue), W5-9.

Jordan, P., Fromme, P., Witt, H.T., Klukas, O., Saenger, W. and Krauss, N. (2001) Three-dimensional structure of cyanobacterial photosystem I at 2.5 A resolution. nature 411(6840), 909-917.

Kameda, H., Hirabayashi, K., Wada, K. and Fukuyama, K. (2011) Mapping of Protein-Protein Interaction Sites in the Plant-Type [2Fe-2S] Ferredoxin. Plos One 6(7).

Kameya, M., Ikeda, T., Nakamura, M., Arai, H., Ishii, M. and Igarashi, Y. (2007) A novel ferredoxin-dependent glutamate synthase from the hydrogen-oxidizing chemoautotrophic bacterium Hydrogenobacter thermophilus TK-6. Journal of Bacteriology 189(7), 2805-2812.

Kaneko, T., Nakamura, Y., Sasamoto, S., Watanabe, A., Kohara, M., Matsumoto, M., Shimpo, S., Yamada, M. and Tabata, S. (2003) Structural analysis of four large Plasmids harboring in a unicellular cyanobacterium, Synechocystis sp PCC 6803. DNA Research 10(5), 221-228.

Kaneko, T., Sato, S., Kotani, H., Tanaka, A., Asamizu, E., Nakamura, Y., Miyajima, N., Hirosawa, M., Sugiura, M., Sasamoto, S., Kimura, T., Hosouchi, T., Matsuno, A., Muraki, A., Nakazaki, N., Naruo, K., Okumura, S., Shimpo, S., Takeuchi, C., Wada, T., Watanabe, A., Yamada, M., Yasuda, M. and Tabata, S. (1996a) Sequence analysis of the genome of the unicellular cyanobacterium Synechocystis sp. strain PCC6803. II. Sequence determination of the entire genome and assignment of potential protein-coding regions. DNA Res 3(3), 109-136.

Kaneko, T., Sato, S., Kotani, H., Tanaka, A., Asamizu, E., Nakamura, Y., Miyajima, N., Hirosawa, M., Sugiura, M., Sasamoto, S., Kimura, T., Hosouchi, T., Matsuno, A., Muraki, A., Nakazaki, N., Naruo, K., Okumura, S., Shimpo, S., Takeuchi, C., Wada, T., Watanabe, A., Yamada, M., Yasuda, M. and Tabata, S. (1996b) Sequence analysis of the genome of the unicellular cyanobacterium Synechocystis sp. strain PCC6803. II. Sequence determination of the entire genome and assignment of potential protein-coding regions (supplement). DNA Res 3(3), 185-209.

Karlusich, J.J.P. and Carrillo, N. (2017) Evolution of the acceptor side of photosystem I: ferredoxin, flavodoxin, and ferredoxin-NADP(+) oxidoreductase. Photosynthesis Research 134(3), 235-250.

Kendall, A.C., Wallsgrove, R.M., Hall, N.P., Turner, J.C. and Lea, P.J. (1986) Carbon and Nitrogen-Metabolism in Barley (Hordeum-Vulgare-L) Mutants Lacking Ferredoxin-Dependent Glutamate Synthase. Planta 168(3), 316-323.

Kloft, N. and Forchhammer, K. (2005) Signal transduction protein PII phosphatase PphA is required for light-dependent control of nitrate utilization in Synechocystis sp. strain PCC 6803. Journal of Bacteriology 187(19), 6683-6690.

Knaff, D.B. (1996) Oxygenic photosynthesis: the light reactions, pp. 333-361, Springer.

Knight, R., Jansson, J., Field, D., Fierer, N., Desai, N., Fuhrman, J.A., Hugenholtz, P., van der Lelie, D., Meyer, F., Stevens, R., Bailey, M.J., Gordon, J.I., Kowalchuk, G.A. and Gilbert, J.A. (2012) Unlocking the potential of metagenomics through replicated experimental design. Nature Biotechnology 30(6), 513-520.

Knoop, H., Grundel, M., Zilliges, Y., Lehmann, R., Hoffmann, S., Lockau, W. and Steuer, R. (2013) Flux Balance Analysis of Cyanobacterial Metabolism: The Metabolic Network of Synechocystis sp PCC 6803. Plos Computational Biology 9(6).

Knoop, H., Zilliges, Y., Lockau, W. and Steuer, R. (2010) The metabolic network of Synechocystis sp. PCC 6803: systemic properties of autotrophic growth. Plant Physiol 154(1), 410-422.

Knowles, V.L. and Plaxton, W.C. (2003) From genome to enzyme: Analysis of key glycolytic and oxidative pentose-phosphate pathway enzymes in the cyanobacterium Synechocystis sp PCC 6803. Plant and Cell Physiology 44(7), 758-763.

Kobayashi, M., Ishizuka, T., Katayama, M., Kanehisa, M., Bhattacharyya-Pakrasi, M., Pakrasi, H.B. and Ikeuchi, M. (2004) Response to oxidative stress involves a novel peroxiredoxin gene in the unicellular cyanobacterium Synechocystis sp PCC 6803. Plant and Cell Physiology 45(3), 290-299.

Kopp, R.E., Kirschvink, J.L., Hilburn, I.A. and Nash, C.Z. (2005) The paleoproterozoic snowball Earth: A climate disaster triggered by the evolution of oxygenic photosynthesis. Proceedings of the National Academy of Sciences of the United States of America 102(32), 11131-11136.

Korotchkina, L.G. and Patel, M.S. (2000) Site-specificity of four pyruvate dehydrogenase kinase (PDK) isoenzymes. Faseb Journal 14(8), A1527-A1527.

Korotchkina, L.G. and Patel, M.S. (2001) Site specificity of four pyruvate dehydrogenase kinase isoenzymes toward the three phosphorylation sites of human pyruvate dehydrogenase. Journal of Biological Chemistry 276(40), 37223-37229.

Kramer, D.M. and Evans, J.R. (2011) The Importance of Energy Balance in Improving Photosynthetic Productivity. Plant Physiology 155(1), 70-78.

Krasikov, V., Aguirre von Wobeser, E., Dekker, H.L., Huisman, J. and Matthijs, H.C. (2012) Time-series resolution of gradual nitrogen starvation and its impact on photosynthesis in the cyanobacterium Synechocystis PCC 6803. Physiol Plant 145(3), 426-439.

Krebs, H.A. (1970) The history of the tricarboxylic acid cycle. Perspect Biol Med 14(1), 154-170.

Kujat, S.L. and Owttrim, G.W. (2000) Redox-regulated RNA helicase expression. Plant Physiology 124(2), 703-713.

Kurian, D., Jansen, T. and Maenpaa, P. (2006) Proteomic analysis of heterotrophy in Synechocystis sp. PCC 6803. Proteomics 6(5), 1483-1494.

Kurisu, G., Kusunoki, M., Katoh, E., Yamazaki, T., Teshima, K., Onda, Y., Kimata-Ariga, Y. and Hase, T. (2001) Structure of the electron transfer complex between ferredoxin and ferredoxin-NADP(+) reductase. Nature Structural Biology 8(2), 117-121.

Kyle, D.J., Ohad, I. and Arntzen, C.J. (1984) Membrane-Protein Damage and Repair - Selective Loss of a Quinone-Protein Function in Chloroplast Membranes. Proceedings of the National Academy of Sciences of the United States of America-Biological Sciences 81(13), 4070-4074.

Laemmli, U.K. (1970) Cleavage of structural proteins during the assembly of the head of bacteriophage T4. nature 227(5259), 680.

Lang, N.J. (1968) The fine structure of blue-green algae. Annu Rev Microbiol 22, 15-46.

Larkin, M.A., Blackshields, G., Brown, N.P., Chenna, R., McGettigan, P.A., McWilliam, H., Valentin, F., Wallace, I.M., Wilm, A., Lopez, R., Thompson, J.D., Gibson, T.J. and Higgins, D.G. (2007) Clustal W and clustal X version 2.0. Bioinformatics 23(21), 2947-2948.

Latifi, A., Ruiz, M. and Zhang, C.C. (2009) Oxidative stress in cyanobacteria. Fems Microbiology Reviews 33(2), 258-278.

Lau, N.S., Matsui, M. and Abdullah, A.A.A. (2015) Cyanobacteria: Photoautotrophic Microbial Factories for the Sustainable Synthesis of Industrial Products. Biomed Research International.

Lawrence, C.L., Botting, C.H., Antrobus, R. and Coote, P.J. (2004) Evidence of a new role for the high-osmolarity glycerol mitogen-activated protein kinase pathway in yeast: Regulating adaptation to citric acid stress. Molecular and Cellular Biology 24(8), 3307-3323.

Lea-Smith, D.J., Bombelli, P., Vasudevan, R. and Howe, C.J. (2016) Photosynthetic, respiratory and extracellular electron transport pathways in cyanobacteria. Biochim Biophys Acta 1857(3), 247-255.

Lea-Smith, D.J., Ross, N., Zori, M., Bendall, D.S., Dennis, J.S., Scott, S.A., Smith, A.G. and Howe, C.J. (2013) Thylakoid Terminal Oxidases Are Essential for the Cyanobacterium Synechocystis sp PCC 6803 to Survive Rapidly Changing Light Intensities(1[C][W][OA]). Plant Physiology 162(1), 484-495.

Lee, J.Z., Burow, L.C., Woebken, D., Everroad, R.C., Kubo, M.D., Spormann, A.M., Weber, P.K., Pett-Ridge, J., Bebout, B.M. and Hoehler, T.M. (2014) Fermentation couples Chloroflexi and sulfate-reducing bacteria to cyanobacteria in hypersaline microbial mats. Frontiers in Microbiology 5.

Lee, R.B., Purves, J.V., Ratcliffe, R.G. and Saker, L.R. (1992) Nitrogen Assimilation and the Control of Ammonium and Nitrate Absorption by Maize Roots. Journal of Experimental Botany 43(256), 1385-1396.

Lelong, C., Setif, P., Bottin, H., Andre, F. and Neumann, J.M. (1995) 1H and 15N NMR sequential assignment, secondary structure, and tertiary fold of [2Fe-2S] ferredoxin from Synechocystis sp. PCC 6803. Biochemistry 34(44), 14462-14473.

Lex, M. and Carr, N.G. (1974) The metabolism of glucose by heterocysts and vegetative cells of Anabaena cylindrica. Archives of Microbiology 101(2), 161-167.

Lichtenthaler, H.K. (1987) Chlorophylls and Carotenoids - Pigments of Photosynthetic Biomembranes. Methods in Enzymology 148, 350-382.

Lillo, C. (2004) Nitrogen acquisition and assimilation in higher plants, pp. 149-184, Springer.

Liu, J., Chakraborty, S., Hosseinzadeh, P., Yu, Y., Tian, S.L., Petrik, I., Bhagi, A. and Lu, Y. (2014) Metalloproteins Containing Cytochrome, Iron-Sulfur, or Copper Redox Centers. Chemical Reviews 114(8), 4366-4469.

Lubner, C.E., Applegate, A.M., Knorzer, P., Ganago, A., Bryant, D.A., Happe, T. and Golbeck, J.H. (2011) Solar hydrogen-producing bionanodevice outperforms natural photosynthesis. Proceedings of the National Academy of Sciences of the United States of America 108(52), 20988-20991.

Lubner, C.E., Applegate, A.M., Knorzer, P., Ganago, A., Bryant, D.A., Happe, T. and Golbeck, J.H. (2013) Solar hydrogen-producing bionanodevice that outperforms natural photosynthesis. Abstracts of Papers of the American Chemical Society 246.

Ludwig, M. and Bryant, D.A. (2011) Transcription profiling of the model cyanobacterium Synechococcus sp strain PCC 7002 by Next-Gen (SOLiD (TM)) sequencing of cDNA. Frontiers in Microbiology 2.

Luque, I., Flores, E. and Herrero, A. (1994a) Molecular Mechanism for the Operation of Nitrogen Control in Cyanobacteria. Embo Journal 13(12), 2862-2869.

Luque, I., Flores, E. and Herrero, A. (1994b) Molecular Mechanism for the Operation of Nitrogen Control in Cyanobacteria (Vol 13, Pg 2862, 1994). Embo Journal 13(23), 5794-5794.

Ma, W. and Ogawa, T. (2015) Oxygenic photosynthesis-specific subunits of cyanobacterial NADPH dehydrogenases. Iubmb Life 67(1), 3-8.

Maheswaran, M., Urbanke, C. and Forchhammer, K. (2004) Complex formation and catalytic activation by the PII signaling protein of N-acetyl-L-glutamate kinase from Synechococcus elongatus strain PCC 7942. Journal of Biological Chemistry 279(53), 55202-55210.

Maheswaran, M., Ziegler, K., Lockau, W., Hagemann, M. and Forchhammer, K. (2006) P-II-regulated arginine synthesis controls accumulation of cyanophycin in Synechocystis sp strain PCC 6803. Journal of Bacteriology 188(7), 2730-2734.

Marteyn, B., Domain, F., Legrain, P., Chauvat, F. and Cassier-Chauvat, C. (2009) The thioredoxin reductase-glutaredoxins-ferredoxin crossroad pathway for selenate tolerance in Synechocystis PCC6803. Molecular Microbiology 71(2), 520-532.

Matsubar.H, Jukes, T.H. and Cantor, C.R. (1969) Structural and Evolutionary Relationships of Ferredoxins. Brookhaven Symposia in Biology 1(21), 201-&.

Matsubara, H., Hase, T., Wakabayashi, S. and Wada, K. (1979) Structural and evolution of chloroplast-and bacterial-type ferredoxins, pp. 245-266.

Matthijs, H.C.P., Jeanjean, R., Yeremenko, N., Huisman, J., Joset, F. and Hellingwerf, K.J. (2002) Hypothesis: versatile function of ferredoxin-NADP(+) reductase in cyanobacteria provides regulation for transient photosystem I-driven cyclic electron flow. Functional Plant Biology 29(2-3), 201-210.

Mazouni, K., Domain, F., Chauvat, F. and Cassier-Chauvat, C. (2003) Expression and regulation of the crucial plant-like ferredoxin of cyanobacteria. Molecular Microbiology 49(4), 1019-1029.

McDonald, A.E., Ivanov, A.G., Bode, R., Maxwell, D.P., Rodermel, S.R. and Hüner, N.P.A. (2011) Flexibility in photosynthetic electron transport: The physiological role of plastoquinol terminal oxidase (PTOX). Biochimica Et Biophysica Acta-Bioenergetics 1807(8), 954-967.

McNeely, K., Xu, Y., Ananyev, G., Bennette, N., Bryant, D.A. and Dismukes, G.C. (2011) Synechococcus sp. strain PCC 7002 nifJ mutant lacking pyruvate: ferredoxin oxidoreductase. Applied and Environmental Microbiology 77(7), 2435-2444.

McNeely, K., Xu, Y., Bennette, N., Bryant, D.A. and Dismukes, G.C. (2010) Redirecting Reductant Flux into Hydrogen Production via Metabolic Engineering of Fermentative Carbon Metabolism in a Cyanobacterium. Applied and Environmental Microbiology 76(15), 5032-5038.

Mehler, A.H. (1951a) Studies on Reactions of Illuminated Chloroplasts .1. Mechanism of the Reduction of Oxygen and Other Hill Reagents. Archives of Biochemistry and Biophysics 33(1), 65-77.

Mehler, A.H. (1951b) Studies on Reactions of Illuminated Chloroplasts .2. Stimulation and Inhibition of the Reaction with Molecular Oxygen. Archives of Biochemistry and Biophysics 34(2), 339-351.

Mehler, A.H. and Brown, A.H. (1952) Studies on Reactions of Illuminated Chloroplasts .3. Simultaneous Photoproduction and Consumption of Oxygen Studied with Oxygen Isotopes. Archives of Biochemistry and Biophysics 38(Jul), 365-370.

Meinecke, B., Bertram, J. and Gottschalk, G. (1989) Purification and characterization of the pyruvate-ferredoxin oxidoreductase from Clostridium acetobutylicum. Archives of Microbiology 152(3), 244-250.

Mendel, R.R., Marton, L. and Muller, A.J. (1986) Comparative Biochemical-Characterization of Mutants at the Nitrate Reductase Molybdenum Cofactor Loci Cnxa, Cnxb, and Cnxc of Nicotiana-Plumbaginifolia. Plant Science 43(2), 125-129.

Mi, H.L., Endo, T., Schreiber, U., Ogawa, T. and Asada, K. (1992) Electron Donation from Cyclic and Respiratory Flows to the Photosynthetic Intersystem Chain Is Mediated by Pyridine-Nucleotide Dehydrogenase in the Cyanobacterium Synechocystis Pcc-6803. Plant and Cell Physiology 33(8), 1233-1237.

Mondal, J. and Bruce, B.D. (2018) Ferredoxin: the central hub connecting photosystem I to cellular metabolism. Photosynthetica 56(1), 279-293.

Montesinos, M.L., Herrero, A. and Flores, E. (1997) Amino acid transport in taxonomically diverse cyanobacteria and identification of two genes encoding elements of a neutral amino acid permease putatively involved in recapture of leaked hydrophobic amino acids. Journal of Bacteriology 179(3), 853-862.

Montesinos, M.L., Muro-Pastor, A.M., Herrero, A. and Flores, E. (1998) Ammonium/Methylammonium permeases of a cyanobacterium - Identification and analysis of three nitrogen-regulated amt genes in Synechocystis sp. PCC 6803. Journal of Biological Chemistry 273(47), 31463-31470.

Mortenson, L.E., Carnahan, J.E. and Valentine, R.C. (1962) An Electron Transport Factor from Clostridium Pasteurianum. Biochemical and Biophysical Research Communications 7(6), 448-&.

Muro-Pastor, M.I. and Florencio, F.J. (2003) Regulation of ammonium assimilation in cyanobacteria. Plant Physiology and Biochemistry 41(6-7), 595-603.

Muro-Pastor, M.I., Reyes, J.C. and Florencio, F.J. (2001) Cyanobacteria perceive nitrogen status by sensing intracellular 2-oxoglutarate levels. Journal of Biological Chemistry 276(41), 38320-38328.

Muro-Pastor, M.I., Reyes, J.C. and Florencio, F.J. (2005) Ammonium assimilation in cyanobacteria. Photosynthesis Research 83(2), 135-150.

Mus, F., Dubini, A., Seibert, M., Posewitz, M.C. and Grossman, A.R. (2007) Anaerobic acclimation in Chlamydomonas reinhardtii - Anoxic gene expression, hydrogenase induction, and metabolic pathways. Journal of Biological Chemistry 282(35), 25475-25486.

Mustila, H. (2017) Photoprotective auxiliary electron transport pathways in cyanobacteria, fi= Turun yliopisto| en= University of Turku.

Mustila, H., Allahverdiyeva, Y., Isojarvi, J., Aro, E.M. and Eisenhut, M. (2014) The bacterial-type [4Fe-4S] ferredoxin 7 has a regulatory function under photooxidative stress conditions in the cyanobacterium Synechocystis sp. PCC 6803. Biochim Biophys Acta 1837(8), 1293-1304.

Mustila, H., Paananen, P., Battchikova, N., Santana-Sanchez, A., Muth-Pawlak, D., Hagemann, M., Aro, E.M. and Allahverdiyeva, Y. (2016) The Flavodiiron Protein Flv3 Functions as a Homo-Oligomer During Stress Acclimation and is Distinct from the Flv1/Flv3 Hetero-Oligomer Specific to the O-2 Photoreduction Pathway. Plant and Cell Physiology 57(7), 1468-1483.

Nakajima, T., Kajihata, S., Yoshikawa, K., Matsuda, F., Furusawa, C., Hirasawa, T. and Shimizu, H. (2014) Integrated Metabolic Flux and Omics Analysis of Synechocystis sp PCC 6803 under Mixotrophic and Photoheterotrophic Conditions. Plant and Cell Physiology 55(9), 1605-1612.

Nakao, M., Okamoto, S., Kohara, M., Fujishiro, T., Fujisawa, T., Sato, S., Tabata, S., Kaneko, T. and Nakamura, Y. (2010) CyanoBase: the cyanobacteria genome database update 2010. Nucleic Acids Research 38, D379-D381.

Narainsamy, K., Cassier-Chauvat, C., Junot, C. and Chauvat, F. (2013) High performance analysis of the cyanobacterial metabolism via liquid chromatography coupled to a LTQ-Orbitrap mass spectrometer: evidence that glucose reprograms the whole carbon metabolism and triggers oxidative stress. Metabolomics 9(1), 21-32.

Narayana, B. and Sunil, K. (2009) A spectrophotometric method for the determination of nitrite and nitrate. Eurasian Journal of Analytical Chemistry 4(2), 204-214.

Navarro, F., Martin-Figueroa, E., Candau, P. and Florencio, F.J. (2000) Ferredoxin-dependent iron-sulfur flavoprotein glutamate synthase (GlsF) from the cyanobacterium Synechocystis sp PCC 6803: Expression and assembly in Escherichia coli. Archives of Biochemistry and Biophysics 379(2), 267-276.

Nemeria, N., Baykal, A., Joseph, E., Zhang, S., Yan, Y., Furey, W. and Jordan, F. (2004) Tetrahedral intermediates in thiamin diphosphate-dependent decarboxylations exist as a 1 ',4 '-imino tautomeric form of the coenzyme, unlike the Michaelis complex or the free coenzyme. Biochemistry 43(21), 6565-6575.

Neuer, G. and Bothe, H. (1982) The pyruvate: ferredoxin oxidoreductase in heterocysts of the cyanobacterium Anabaena cylindrica. Biochim Biophys Acta 716(3), 358-365.

Ninfa, A.J., Ninfa, E.G., Lupas, A.N., Stock, A., Magasanik, B. and Stock, J. (1988) Crosstalk between Bacterial Chemotaxis Signal Transduction Proteins and Regulators of Transcription of the Ntr Regulon - Evidence That Nitrogen Assimilation and Chemotaxis Are Controlled by a Common Phosphotransfer Mechanism. Proceedings of the National Academy of Sciences of the United States of America 85(15), 5492-5496.

Nomura, C.T., Persson, S., Shen, G.Z., Inoue-Sakamoto, K. and Bryant, D.A. (2006) Characterization of two cytochrome oxidase operons in the marine cyanobacterium Synechococcus sp PCC 7002: Inactivation of ctaDI affects the PSI : PS II ratio. Photosynthesis Research 87(2), 215-228.

Noth, J., Krawietz, D., Hemschemeier, A. and Happe, T. (2013) Pyruvate:ferredoxin oxidoreductase is coupled to light-independent hydrogen production in Chlamydomonas reinhardtii. Journal of Biological Chemistry 288(6), 4368-4377.

Ogawa, T. (1991) A gene homologous to the subunit-2 gene of NADH dehydrogenase is essential to inorganic carbon transport of Synechocystis PCC6803. Proceedings of the National Academy of Sciences 88(10), 4275-4279.

Okuhara, H., Matsumura, T., Fujita, Y. and Hase, T. (1999) Cloning and inactivation of genes encoding ferredoxin- and NADH-dependent glutamate synthases in the cyanobacterium Plectonema boryanum. Imbalances in nitrogen and carbon assimilations caused by deficiency of the ferredoxin-dependent enzyme. Plant Physiology 120(1), 33-41.

Omata, T., Andriesse, X. and Hirano, A. (1993) Identification and Characterization of a Gene-Cluster Involved in Nitrate Transport in the Cyanobacterium Synechococcus Sp-Pcc7942. Molecular & General Genetics 236(2-3), 193-202.

Orme-Johnson, W. (1973) Tryptic Cleavage of Clostridium acidi-urici Apoferredoxin, and Reconstitution of the Separated Fragments, Portland Press Limited.

Ort, D.R. and Yocum, C.F. (1996) Oxygenic photosynthesis: the light reactions, Springer Science & Business Media.

Osanai, T. and Tanaka, K. (2007) Keeping in touch with PII: PII-interacting proteins in unicellular cyanobacteria. Plant and Cell Physiology 48(7), 908-914.

Paneque, A., Ramirez, J.M., Delcampo, F.F. and Losada, M. (1964) Light and Dark Reduction of Nitrite in a Reconstituted Enzymic System. Journal of Biological Chemistry 239, 1737-1741.

Patel, M.S. and Korotchkina, L.G. (2001) Regulation of mammalian pyruvate dehydrogenase complex by phosphorylation: complexity of multiple phosphorylation sites and kinases. Exp Mol Med 33(4), 191-197.

Patel, M.S. and Korotchkina, L.G. (2003) The biochemistry of the pyruvate dehydrogenase complex. Biochemistry and Molecular Biology Education 31(1), 5-15.

Patel, M.S., Nemeria, N.S., Furey, W. and Jordan, F. (2014) The pyruvate dehydrogenase complexes: structure-based function and regulation. Journal of Biological Chemistry 289(24), 16615-16623.

Patel, M.S. and Roche, T.E. (1990) Molecular biology and biochemistry of pyruvate dehydrogenase complexes. Faseb Journal 4(14), 3224-3233.

Patel, M.S., Roche, T.E. and Harris, R.A. (2012) Alpha-keto acid dehydrogenase complexes, Birkhäuser.

Pateman, J.A. (1969) Regulation of Synthesis of Glutamate Dehydrogenase and Glutamine Synthetase in Micro-Organisms. Biochemical Journal 115(4), 769-&.

Pearce, J. and Carr, N.G. (1967) The metabolism of acetate by the blue-green algae, Anabaena variabilis and Anacystis nidulans. Journal of General Microbiology 49(2), 301-313.

Peden, E.A., Boehm, M., Mulder, D.W., Davis, R., Old, W.M., King, P.W., Ghirardi, M.L. and Dubini, A. (2013) Identification of Global Ferredoxin Interaction Networks in Chlamydomonas reinhardtii. Journal of Biological Chemistry 288(49), 35192-35209.

Pelroy, R.A., Rippka, R. and Stanier, R.Y. (1972) Metabolism of glucose by unicellular blue-green algae. Archiv Fur Mikrobiologie 87(4), 303-322.

Pietrocola, F., Galluzzi, L., Bravo-San Pedro, J.M., Madeo, F. and Kroemer, G. (2015) Acetyl coenzyme A: a central metabolite and second messenger. Cell Metabolism 21(6), 805-821.

Pieulle, L., Guigliarelli, B., Asso, M., Dole, F., Bernadac, A. and Hatchikian, E.C. (1995) Isolation and Characterization of the Pyruvate-Ferredoxin Oxidoreductase from the Sulfate-Reducing Bacterium Desulfovibrio-Africanus. Biochimica Et Biophysica Acta-Protein Structure and Molecular Enzymology 1250(1), 49-59.

Pieulle, L., Magro, V. and Hatchikian, E.C. (1997) Isolation and analysis of the gene encoding the pyruvate-ferredoxin oxidoreductase of Desulfovibrio africanus, production of the recombinant enzyme in Escherichia coli, and effect of carboxy-terminal deletions on its stability. Journal of Bacteriology 179(18), 5684-5692.

Pils, D., Gregor, W. and Schmetterer, G. (1997) Evidence for in vivo activity of three distinct respiratory terminal oxidases in the cyanobacterium Synechocystis sp strain PCC6803. FEMS microbiology letters 152(1), 83-88.

Plaga, W., Lottspeich, F. and Oesterhelt, D. (1992) Improved Purification, Crystallization and Primary Structure of Pyruvate-Ferredoxin Oxidoreductase from Halobacterium-Halobium. European Journal of Biochemistry 205(1), 391-397.

Plohnke, N., Seidel, T., Kahmann, U., Rogner, M., Schneider, D. and Rexroth, S. (2015) The proteome and lipidome of Synechocystis sp. PCC 6803 cells grown under light-activated heterotrophic conditions. Molecular & Cellular Proteomics 14(3), 572-584.

Pogoryelov, D., Reichen, C., Klyszejko, A.L., BrunisholZ, R., Muller, D.J., Dimroth, P. and Meier, T. (2007) The oligomeric state of c rings from cyanobacterial F-ATP synthases varies from 13 to 15. Journal of Bacteriology 189(16), 5895-5902.

Poncelet, M., Cassier-Chauvat, C., Leschelle, X., Bottin, H. and Chauvat, F. (1998) Targeted deletion and mutational analysis of the essential (2Fe-2S) plant-like ferredoxin in Synechocystis PCC6803 by plasmid shuffling. Molecular Microbiology 28(4), 813-821.

Prabha, R., Singh, D.P., Somvanshi, P. and Rai, A. (2016) Functional profiling of cyanobacterial genomes and its role in ecological adaptations. Genomics Data 9, 89-94.

Purich, D.L. (1998) Advances in the enzymology of glutamine synthesis. Advances in Enzymology, Vol 72 72, 9-+.

Quintana, N., Van der Kooy, F., Van de Rhee, M.D., Voshol, G.P. and Verpoorte, R. (2011) Renewable energy from Cyanobacteria: energy production optimization by metabolic pathway engineering. Applied Microbiology and Biotechnology 91(3), 471-490.

Quintero, M.a.J., Montesinos, M.a.L., Herrero, A. and Flores, E. (2001) Identification of genes encoding amino acid permeases by inactivation of selected ORFs from the Synechocystis genomic sequence. Genome Research 11(12), 2034-2040.

Quintero, M.J., Muro-Pastor, A.M., Herrero, A. and Flores, E. (2000) Arginine catabolism in the cyanobacterium Synechocystis sp strain PCC 6803 involves the urea cycle and arginase pathway. Journal of Bacteriology 182(4), 1008-1015.

Rasmussen, B., Fletcher, I.R., Brocks, J.J. and Kilburn, M.R. (2008) Reassessing the first appearance of eukaryotes and cyanobacteria. nature 455(7216), 1101-U1109.

Reed, L.J. (1981) Regulation of mammalian pyruvate dehydrogenase complex by a phosphorylation-dephosphorylation cycle. Curr Top Cell Regul 18, 95-106.

Rexroth, S., Mullineaux, C.W., Ellinger, D., Sendtko, E., Rogner, M. and Koenig, F. (2011) The Plasma Membrane of the Cyanobacterium Gloeobacter violaceus Contains Segregated Bioenergetic Domains. Plant Cell 23(6), 2379-2390.

Rippka, R. (1972) Photoheterotrophy and Chemoheterotrophy among Unicellular Blue-Green-Algae. Archiv Fur Mikrobiologie 87(1), 93-&.

Rippka, R., Deruelles, J., Waterbury, J.B., Herdman, M. and Stanier, R.Y. (1979) Generic Assignments, Strain Histories and Properties of Pure Cultures of Cyanobacteria. Journal of General Microbiology 111(Mar), 1-61.

Robinson, B.H., MacKay, N., Chun, K. and Ling, M. (1996) Disorders of pyruvate carboxylase and the pyruvate dehydrogenase complex. Journal of Inherited Metabolic Disease 19(4), 452-462.

Rose, A.S. and Hildebrand, P.W. (2015) NGL Viewer: a web application for molecular visualization. Nucleic Acids Research 43(W1), W576-579.

Roughan, P.G. and Ohlrogge, J.B. (1994) On the Assay of Acetyl-Coa Synthetase-Activity in Chloroplasts and Leaf Extracts. Analytical Biochemistry 216(1), 77-82.

Rowland, J.G., Pang, X., Suzuki, I., Murata, N., Simon, W.J. and Slabas, A.R. (2010) Identification of Components Associated with Thermal Acclimation of Photosystem II in Synechocystis sp PCC6803. Plos One 5(5).

Saha, R., Liu, D., Hoynes-O'Connor, A., Liberton, M., Yu, J.J., Bhattacharyya-Pakrasi, M., Balassy, A., Zhang, F.Z., Moon, T.S., Maranas, C.D. and Pakrasi, H.B. (2016) Diurnal Regulation of Cellular Processes in the

Cyanobacterium Synechocystis sp Strain PCC 6803: Insights from Transcriptomic, Fluxomic, and Physiological Analyses. Mbio 7(3).

Sakamoto, T., Inoue-Sakamoto, K. and Bryant, D.A. (1999) A novel nitrate/nitrite permease in the marine cyanobacterium Synechococcus sp strain PCC 7002. Journal of Bacteriology 181(23), 7363-7372.

Sakr, S., Dutheil, J., Saenkham, P., Bottin, H., Leplat, C., Ortega-Ramos, M., Aude, J.C., Chapuis, V., Guedeney, G., Decottignies, P., Lemaire, S., Cassier-Chauvat, C. and Chauvat, F. (2013) The activity of the Synechocystis PCC6803 AbrB2 regulator of hydrogen production can be post-translationally controlled through glutathionylation. International Journal of Hydrogen Energy 38(31), 13547-13555.

Sanger, F., Nicklen, S. and Coulson, A.R. (1977) DNA Sequencing with Chain-Terminating Inhibitors. Proceedings of the National Academy of Sciences of the United States of America 74(12), 5463-5467.

Saux, C., Gabard, J. and Morotgaudry, J.F. (1986) Metabolic Deviations Linked to the Loss of Nitrate Reductase-Activity in Nicotiana-Plumbaginifolia. Comptes Rendus De L Academie Des Sciences Serie Iii-Sciences De La Vie-Life Sciences 302(10), 391-394.

Savary, B.J. and Flores, H.E. (1994) Biosynthesis of defense-related proteins in transformed root cultures of Trichosanthes kirilowii Maxim. var japonicum (Kitam.). Plant Physiol 106(3), 1195-1204.

Sawyer, A. and Winkler, M. (2017) Evolution of Chlamydomonas reinhardtii ferredoxins and their interactions with [FeFe]-hydrogenases. Photosynthesis Research 134(3), 307-316.

Schmetterer, G. (1994) The molecular biology of cyanobacteria, pp. 409-435, Springer.

Schmetterer, G., Alge, D. and Gregor, W. (1994) Deletion of cytochrome c oxidase genes from the cyanobacterium Synechocystis sp. PCC6803: Evidence for alternative respiratory pathways. Photosynthesis Research 42(1), 43-50.

Schmitz, O. and Bothe, H. (1996) The diaphorase subunit HoxU of the bidirectional hydrogenase as electron transferring protein in cyanobacterial respiration? Naturwissenschaften 83(11), 525-527.

Schmitz, O., Gurke, J. and Bothe, H. (2001) Molecular evidence for the aerobic expression of nifJ, encoding pyruvate: ferredoxin oxidoreductase, in cyanobacteria. FEMS microbiology letters 195(1), 97-102.

Schmitz, S., Navarro, F., Kutzki, C.K., Florencio, F.J. and Bohme, H. (1996) Glutamate 94 of [2Fe-2S]-ferredoxins is important for efficient electron transfer in the 1:1 complex formed with ferredoxin-glutamate synthase (GltS) from Synechocystis sp PCC 6803. Biochimica Et Biophysica Acta-Bioenergetics 1277(1-2), 135-140.

Schopf, J.W. and Packer, B.M. (1987) Early Archean (3.3-Billion to 3.5-Billion-Year-Old) Microfossils from Warrawoona Group, Australia. Science 237(4810), 70-73.

Schreiber, K. (2016) Aufklärung verschiedener Glukoseabbauwege und deren Einfluss auf den Wasserstoffmetabolismus im Cyanobakterium Synechocystis spec. PCC 6803, Christian-Albrechts Universität Kiel.

Schreiber, U., Klughammer, C. and Kolbowski, J. (2012) Assessment of wavelength-dependent parameters of photosynthetic electron transport with a new type of multi-color PAM chlorophyll fluorometer. Photosynthesis Research 113(1-3), 127-144.

Schriek, S., Aguirre-Von-Wobeser, E., Nodop, A., Becker, A., Ibelings, B.W., Bok, J., Staiger, D., Matthijs, H.C.P., Pistorius, E.K. and Michel, K.P. (2008) Transcript profiling indicates that the absence of PsbO affects the coordination of C and N metabolism in Synechocystis sp PCC 6803. Physiologia Plantarum 133(3), 525-543.

Schriek, S., Kahmann, U., Staiger, D., Pistorius, E.K. and Michel, K.P. (2009) Detection of an L-amino acid dehydrogenase activity in Synechocystis sp PCC 6803. Journal of Experimental Botany 60(3), 1035-1046.

Schriek, S., Ruckert, C., Staiger, D., Pistorius, E.K. and Michel, K.P. (2007) Bioinformatic evaluation of L-arginine catabolic pathways in 24 cyanobacteria and transcriptional analysis of genes encoding enzymes of L-arginine catabolism in the cyanobacterium Synechocystis sp. PCC 6803. Bmc Genomics 8, 437.

Schuurmans, R.M., Schuurmans, J.M., Bekker, M., Kromkamp, J.C., Matthijs, H.C.P. and Hellingwerf, K.J. (2014) The Redox Potential of the Plastoquinone Pool of the Cyanobacterium Synechocystis Species Strain PCC 6803 Is under Strict Homeostatic Control. Plant Physiology 165(1), 463-475.

Schwartz, R. and Dayhoff, M. (1978) Other electron transport proteins. Atlas of Protein Sequence and Structure.(Dayhoff, MO, Ed.) 5, 45-48.

Schwarz, D., Nodop, A., Huge, J., Purfurst, S., Forchhammer, K., Michel, K.P., Bauwe, H., Kopka, J. and Hagemann, M. (2011) Metabolic and transcriptomic phenotyping of inorganic carbon acclimation in the Cyanobacterium Synechococcus elongatus PCC 7942. Plant Physiol 155(4), 1640-1655.

Selim, K.A., Haase, F., Hartmann, M.D., Hagemann, M. and Forchhammer, K. (2018) PII-like signaling protein SbtB links cAMP sensing with cyanobacterial inorganic carbon response. Proc Natl Acad Sci U S A 115(21), E4861-E4869.

Shastri, A.A. and Morgan, J.A. (2005) Flux balance analysis of photoautotrophic metabolism. Biotechnol Prog 21(6), 1617-1626.

Shikanai, T. (2007) Cyclic electron transport around photosystem I: genetic approaches. Annual Review of Plant Biology 58, 199-217.

Shikanai, T. (2014) Central role of cyclic electron transport around photosystem I in the regulation of photosynthesis. Curr Opin Biotechnol 26, 25-30.

Shikanai, T. (2016) Chloroplast NDH: A different enzyme with a structure similar to that of respiratory NADH dehydrogenase. Biochim Biophys Acta 1857(7), 1015-1022.

Shimakawa, G., Shaku, K., Nishi, A., Hayashi, R., Yamamoto, H., Sakamoto, K., Makino, A. and Miyake, C. (2015) FLAVODIIRON2 and FLAVODIIRON4 Proteins Mediate an Oxygen-Dependent Alternative Electron Flow in Synechocystis sp PCC 6803 under CO2-Limited Conditions. Plant Physiology 167(2), 472-U732.

Silaghi-Dumitrescu, R., Ng, K.Y., Viswanathan, R. and Kurtz, D.M., Jr. (2005) A flavo-diiron protein from Desulfovibrio vulgaris with oxidase and nitric oxide reductase activities. Evidence for an in vivo nitric oxide scavenging function. Biochemistry 44(9), 3572-3579.

Singh, A.K., Bhattacharyya-Pakrasi, M., Elvitigala, T., Ghosh, B., Aurora, R. and Pakrasi, H.B. (2009) A Systems-Level Analysis of the Effects of Light Quality on the Metabolism of a Cyanobacterium. Plant Physiology 151(3), 1596-1608.

Singh, A.K., Elvitigala, T., Bhattacharyya-Pakrasi, M., Aurora, R., Ghosh, B. and Pakrasi, H.B. (2008) Integration of carbon and nitrogen metabolism with energy production is crucial to light acclimation in the cyanobacterium Synechocystis. Plant Physiology 148(1), 467-478.

Singh, A.K., Elvitigala, T., Cameron, J.C., Ghosh, B.K., Bhattacharyya-Pakrasi, M. and Pakrasi, H.B. (2010) Integrative analysis of large scale expression profiles reveals core transcriptional response and coordination between multiple cellular processes in a cyanobacterium. BMC systems biology 4(1), 105.

Smith, A.J. (1983) Modes of Cyanobacterial Carbon Metabolism. Annales De Microbiologie B134(1), 93-113.

Solovchenko, A.E., Khozin-Goldberg, I., Cohen, Z. and Merzlyak, M.N. (2008) Carotenoid-to-chlorophyll ratio as a proxy for assay of total fatty acids and arachidonic acid content in the green microalga Parietochloris incisa. Journal of Applied Phycology 21(3), 361-366.

Somerville, C.R. and Ogren, W.L. (1980) Inhibition of Photosynthesis in Arabidopsis Mutants Lacking Leaf Glutamate Synthase Activity. nature 286(5770), 257-259.

Song, Z., Chen, L., Wang, J., Lu, Y., Jiang, W. and Zhang, W. (2014) A transcriptional regulator Sll0794 regulates tolerance to biofuel ethanol in photosynthetic Synechocystis sp. PCC 6803. Molecular & Cellular Proteomics 13(12), 3519-3532.

Stal, L.J. (1995) Physiological Ecology of Cyanobacteria in Microbial Mats and Other Communities. New Phytologist 131(1), 1-32.

Stal, L.J. (2009) Is the distribution of nitrogen-fixing cyanobacteria in the oceans related to temperature? Environmental Microbiology 11(7), 1632-1645.

Stal, L.J. and Moezelaar, R. (1997) Fermentation in cyanobacteria. Fems Microbiology Reviews 21(2), 179-211.

Stanier, R. and Bazine, G. (1977) Phototrophic prokaryotes: the cyanobacteria. Annual Reviews in Microbiology 31(1), 225-274.

Staples, C.R., Ameyibor, E., Fu, W.G., GardetSalvi, L., StrittEtter, A.L., Schurmann, P., Knaff, D.B. and Johnson, M.K. (1996) The function and properties of the iron-sulfur center in spinach ferredoxin:thioredoxin reductase: A new biological role for iron-sulfur clusters. Biochemistry 35(35), 11425-11434.

Steinhauser, D., Fernie, A.R. and Araujo, W.L. (2012) Unusual cyanobacterial TCA cycles: not broken just different. Trends in Plant Science 17(9), 503-509.

Stephan, D.P., Ruppel, H.G. and Pistorius, E.K. (2000) Interrelation between cyanophycin synthesis, L-arginine catabolism and photosynthesis in the cyanobacterium Synechocystis sp. strain PCC 6803. Zeitschrift für Naturforschung C 55(11-12), 927-942.

Stephens, P.E., Darlison, M.G., Lewis, H.M. and Guest, J.R. (1983) The pyruvate dehydrogenase complex of Escherichia coli K12. Nucleotide sequence encoding the dihydrolipoamide acetyltransferase component. Eur J Biochem 133(3), 481-489.

Stephens, P.J., Jollie, D.R. and Warshel, A. (1996) Protein control of redox potentials of iron-sulfur proteins. Chemical Reviews 96(7), 2491-2513.

Stock, D., Leslie, A.G.W. and Walker, J.E. (1999) Molecular architecture of the rotary motor in ATP synthase. Science 286(5445), 1700-1705.

Suzuki, A. and Knaff, D.B. (2005) Glutamate synthase: structural, mechanistic and regulatory properties, and role in the amino acid metabolism. Photosynthesis Research 83(2), 191-217.

Suzuki, I., Horie, N., Sugiyama, T. and Omata, T. (1995) Identification and characterization of two nitrogen-regulated genes of the cyanobacterium Synechococcus sp. strain PCC7942 required for maximum efficiency of nitrogen assimilation. Journal of Bacteriology 177(2), 290-296.

Suzuki, I., Sugiyama, T. and Omata, T. (1993) Primary Structure and Transcriptional Regulation of the Gene for Nitrite Reductase from the Cyanobacterium Synechococcus Pcc-7942. Plant and Cell Physiology 34(8), 1311-1320.

Sweetlove, L.J., Beard, K.F., Nunes-Nesi, A., Fernie, A.R. and Ratcliffe, R.G. (2010) Not just a circle: flux modes in the plant TCA cycle. Trends Plant Sci 15(8), 462-470.

Tabei, Y., Okada, K., Makita, N. and Tsuzuki, M. (2009) Light-induced gene expression of fructose 1,6-bisphosphate aldolase during heterotrophic growth in a cyanobacterium, Synechocystis sp PCC 6803. Febs Journal 276(1), 187-198.

Tagawa, K., Tsujimoto, H.Y. and Arnon, D.I. (1963) Role of chloroplast ferredoxin in the energy conversion process of photosynthesis. Proc Natl Acad Sci U S A 49, 567-572.

Takahashi, H., Uchimiya, H. and Hihara, Y. (2008) Difference in metabolite levels between photoautotrophic and photomixotrophic cultures of Synechocystis sp PCC 6803 examined by capillary electrophoresis electrospray ionization mass spectrometry. Journal of Experimental Botany 59(11), 3009-3018.

Tamagnini, P., Axelsson, R., Lindberg, P., Oxelfelt, F., Wunschiers, R. and Lindblad, P. (2002) Hydrogenases and hydrogen metabolism of cyanobacteria. Microbiol Mol Biol Rev 66(1), 1-20, table of contents.

Tamoi, M., Miyazaki, T., Fukamizo, T. and Shigeoka, S. (2005) The Calvin cycle in cyanobacteria is regulated by CP12 via the NAD(H)/NADP(H) ratio under light/dark conditions. Plant Journal 42(4), 504-513.

Tanaka, M., Nakashima, T., Benson, A., Mower, H. and Tasunobu, K.T. (1966) The amino acid sequence of Clostridium pasteurianum ferredoxin. Biochemistry 5(5), 1666-1681.

Tanigawa, R., Shirokane, M., Maeda, S., Omata, T., Tanaka, K., Takahashi, H. and Takahashi, H. (2002) Transcriptional activation of NtcA-dependent promoters of Synechococcus sp PCC 7942 by 2-oxoglutarate in vitro. Proceedings of the National Academy of Sciences of the United States of America 99(7), 4251-4255.

Taroncher-Oldenberg, G., Nishina, K. and Stephanopoulos, G. (2000) Identification and analysis of the polyhydroxyalkanoate-specific beta-ketothiolase and acetoacetyl coenzyme A reductase genes in the cyanobacterium Synechocystis sp strain PCC6803. Applied and Environmental Microbiology 66(10), 4440-4448.

Temple, S.J., Vance, C.P. and Gantt, J.S. (1998) Glutamate synthase and nitrogen assimilation. Trends in Plant Science 3(2), 51-56.

Thomas, P., Starlinger, J., Vowinkel, A., Arzt, S. and Leser, U. (2012) GeneView: a comprehensive semantic search engine for PubMed. Nucleic Acids Research 40(W1), W585-W591.

Tittmann, K. (2009) Reaction mechanisms of thiamin diphosphate enzymes: redox reactions. Febs Journal 276(9), 2454-2468.

Tovar-Mendez, A., Miernyk, J.A. and Randall, D.D. (2003) Regulation of pyruvate dehydrogenase complex activity in plant cells. European Journal of Biochemistry 270(6), 1043-1049.

Tripathy, J.N., Hirasawa, M., Sutton, R.B., Dasgupta, A., Vaidyanathan, N., Zabet-Moghaddam, M., Florencio, F.J., Srivastava, A.P. and Knaff, D.B. (2015) A loop unique to ferredoxin-dependent glutamate synthases is not absolutely essential for ferredoxin-dependent catalytic activity. Photosynthesis Research 123(2), 129-139.

Valladares, A., Montesinos, M.L., Herrero, A. and Flores, E. (2002) An ABC-type, high-affinity urea permease identified in cyanobacteria. Molecular Microbiology 43(3), 703-715.

van de Meene, A.M.L., Hohmann-Marriott, M.F., Vermaas, W.F.J. and Roberson, R.W. (2006) The three-dimensional structure of the cyanobacterium Synechocystis sp PCC 6803. Archives of Microbiology 184(5), 259-270.

van den Heuvel, R.H.H., Curti, B., Vanoni, M.A. and Mattevi, A. (2004) Glutamate synthase: a fascinating pathway from L-glutamine to L-glutamate. Cellular and Molecular Life Sciences 61(6), 669-681.

van den Heuvel, R.H.H., Svergun, D.I., Petoukhov, M.V., Coda, A., Curti, B., Ravasio, S., Vanoni, M.A. and Mattevi, A. (2003) The active conformation of glutamate synthase and its binding to ferredoxin. Journal of Molecular Biology 330(1), 113-128.

van Lis, R., Baffert, C., Coute, Y., Nitschke, W. and Atteia, A. (2013) Chlamydomonas reinhardtii Chloroplasts Contain a Homodimeric Pyruvate: Ferredoxin Oxidoreductase That Functions with FDX1. Plant Physiology 161(1), 57-71.

van Thor, J.J., Jeanjean, R., Havaux, M., Sjollema, K.A., Joset, F., Hellingwerf, K.J. and Matthijs, H.C.P. (2000) Salt shock-inducible Photosystem I cyclic electron transfer in Synechocystis PCC6803 relies on binding of ferredoxin : NADP(+) reductase to the thylakoid membranes via its CpcD phycobilisome-linker homologous N-terminal domain. Biochimica Et Biophysica Acta-Bioenergetics 1457(3), 129-144.

Vanoni, M.A. and Curti, B. (2008) Structure-function studies of glutamate synthases: A class of self-regulated iron-sulfur flavoenzymes essential for nitrogen assimilation. Iubmb Life 60(5), 287-300.

VanWalraven, H.S., Strotmann, H., Schwarz, O. and Rumberg, B. (1996) The H+/ATP coupling ratio of the ATP synthase from thiol-modulated chloroplasts and two cyanobacterial strains is four. Febs Letters 379(3), 309-313.

Varman, A.M., Xiao, Y., Pakrasi, H.B. and Tang, Y.J.J. (2013a) Metabolic Engineering of Synechocystis sp Strain PCC 6803 for Isobutanol Production. Applied and Environmental Microbiology 79(3), 908-914.

Varman, A.M., Yu, Y., You, L. and Tang, Y.J.J. (2013b) Photoautotrophic production of D-lactic acid in an engineered cyanobacterium. Microbial Cell Factories 12.

Vermaas, W. (1996) Molecular genetics of the cyanobacterium Synechocystis sp. PCC 6803: Principles and possible biotechnology applications. Journal of Applied Phycology 8(4-5), 263-273.

Vermaas, W.F. (2001) Photosynthesis and respiration in cyanobacteria. Encyclopedia of Life Sciences 1, 1-7.

Vermaas, W.F.J., Shen, G.Z. and Styring, S. (1994) Electrons Generated by Photosystem-Ii Are Utilized by an Oxidase in the Absence of Photosystem-I in the Cyanobacterium Synechocystis Sp Pcc-6803. Febs Letters 337(1), 103-108.

Vicente, J.B., Carrondo, M.A., Teixeira, M. and Frazao, C. (2008) Structural studies on flavodiiron proteins. Globins and Other Nitric Oxide-Reactive Proteins, Part B 437, 3-19.

Vicente, J.B., Gomes, C.M., Wasserfallen, A. and Teixeira, M. (2002) Module fusion in an A-type flavoprotein from the cyanobacterium Synechocystis condenses a multiple-component pathway in a single polypeptide chain. Biochem Biophys Res Commun 294(1), 82-87.

Vinyard, D.J., Ananyev, G.M. and Dismukes, G.C. (2013) Photosystem II: The Reaction Center of Oxygenic Photosynthesis. Annual Review of Biochemistry, Vol 82 82, 577-606.

Wachtershauser, G. (2007) On the chemistry and evolution of the pioneer organism. Chemistry & Biodiversity 4(4), 584-602.

Wan, N., Abernathy, M., Tang, J.K.-H., Tang, Y.J. and You, L. (2015) Cyanobacterial photo-driven mixotrophic metabolism and its advantages for biosynthesis. Frontiers of Chemical Science and Engineering 9(3), 308-316.

Wegener, K.M., Welsh, E.A., Thornton, L.E., Keren, N., Jacobs, J.M., Hixson, K.K., Monroe, M.E., Camp, D.G., Smith, R.D. and Pakrasi, H.B. (2008) High sensitivity proteomics assisted discovery of a novel operon involved in the assembly of photosystem II, a membrane protein complex. Journal of Biological Chemistry 283(41), 27829-27837.

Whitton, B.A. and Potts, M. (2007) The ecology of cyanobacteria: their diversity in time and space, Springer Science & Business Media.

Wildman, R.B. and Bowen, C.C. (1974) Phycobilisomes in Blue-Green-Algae. Journal of Bacteriology 117(2), 866-881.

Williams, J.G.K. (1988) Construction of Specific Mutations in Photosystem-Ii Photosynthetic Reaction Center by Genetic-Engineering Methods in Synechocystis-6803. Methods in Enzymology 167, 766-778.

Williams, K., Lowe, P.N. and Leadlay, P.F. (1987) Purification and characterization of pyruvate: ferredoxin oxidoreductase from the anaerobic protozoon Trichomonas vaginalis. Biochemical Journal 246(2), 529-536.

Wright, R.T. and Hobbie, J.E. (1966) Use of Glucose and Acetate by Bacteria and Algae in Aquatic Ecosystems. Ecology 47(3), 447-&.

Xiong, W., Brune, D. and Vermaas, W.F.J. (2014) The gamma-aminobutyric acid shunt contributes to closing the tricarboxylic acid cycle in Synechocystis sp PCC 6803. Molecular Microbiology 93(4), 786-796.

Xu, Y. (2010) Synechococcus sp. PCC 7002: A robust and versatile cyanobacterial platform for biofuels development.

Yamamoto, H. and Shikanai, T. (2013) In Planta Mutagenesis of Src Homology 3 Domain-like Fold of NdhS, a Ferredoxin-binding Subunit of the Chloroplast NADH Dehydrogenase-like Complex in Arabidopsis A CONSERVED ARG-193 PLAYS A CRITICAL ROLE IN FERREDOXIN BINDING. Journal of Biological Chemistry 288(51), 36328-36337.

Yang, C., Hua, Q. and Shimizu, K. (2002a) Integration of the information from gene expression and metabolic fluxes for the analysis of the regulatory mechanisms in Synechocystis. Appl Microbiol Biotechnol 58(6), 813-822.

Yang, C., Hua, Q. and Shimizu, K. (2002b) Metabolic flux analysis in Synechocystis using isotope distribution from C-13-labeled glucose. Metabolic Engineering 4(3), 202-216.

Yang, W.Q., Wittkopp, T.M., Li, X.B., Warakanont, J., Dubini, A., Catalanotti, C., Kim, R.G., Nowack, E.C.M., Mackinder, L.C.M., Aksoy, M., Page, M.D., D'Adamo, S., Saroussi, S., Heinnickel, M., Johnson, X., Richaud, P., Alric, J., Boehm, M., Jonikas, M.C., Benning, C., Merchant, S.S., Posewitz, M.C. and Grossman, A.R. (2015) Critical role of Chlamydomonas reinhardtii ferredoxin-5 in maintaining membrane structure and dark metabolism. Proceedings of the National Academy of Sciences of the United States of America 112(48), 14978-14983.

Ye, J., Coulouris, G., Zaretskaya, I., Cutcutache, I., Rozen, S. and Madden, T.L. (2012) Primer-BLAST: A tool to design target-specific primers for polymerase chain reaction. Bmc Bioinformatics 13.

Yeremenko, N., Jeanjean, R., Prommeenate, P., Krasikov, V., Nixon, P.J., Vermaas, W.F.J., Havaux, M. and Matthijs, H.C.P. (2005) Open reading frame ssr2016 is required for antimycin A-sensitive photosystem I-driven cyclic electron flow in the cyanobacterium Synechocystis sp PCC 6803. Plant and Cell Physiology 46(8), 1433-1436.

Yoon, K.S., Ishii, M., Kodama, T. and Igarashi, Y. (1997) Carboxylation reactions of pyruvate:ferredoxin oxidoreductase and 2-oxoglutarate: Ferredoxin oxidoreductase from Hydrogenobacter thermophilus TK-6. Bioscience Biotechnology and Biochemistry 61(3), 510-513.

Yoshikawa, K., Hirasawa, T., Ogawa, K., Hidaka, Y., Nakajima, T., Furusawa, C. and Shimizu, H. (2013) Integrated transcriptomic and metabolomic analysis of the central metabolism of Synechocystis sp. PCC 6803 under different trophic conditions. Biotechnol J 8(5), 571-580.

You, L., Berla, B., He, L., Pakrasi, H.B. and Tang, Y.J. (2014) 13C-MFA delineates the photomixotrophic metabolism of Synechocystis sp. PCC 6803 under light- and carbon-sufficient conditions. Biotechnol J 9(5), 684-692.

You, L., He, L. and Tang, Y.J. (2015) Photoheterotrophic Fluxome in Synechocystis sp Strain PCC 6803 and Its Implications for Cyanobacterial Bioenergetics. Journal of Bacteriology 197(5), 943-950.

Yu, Y., You, L., Liu, D.Y., Hollinshead, W., Tang, Y.J.J. and Zhang, F.Z. (2013) Development of Synechocystis sp PCC 6803 as a Phototrophic Cell Factory. Marine Drugs 11(8), 2894-2916.

Zavřel, T., Sinetova, M.A. and Červený, J. (2015) Measurement of chlorophyll a and carotenoids concentration in cyanobacteria. Bio-protocol 5, e1467.

Zehr, J.P., Bench, S.R., Carter, B.J., Hewson, I., Niazi, F., Shi, T., Tripp, H.J. and Affourtit, J.P. (2008) Globally Distributed Uncultivated Oceanic N(2)-Fixing Cyanobacteria Lack Oxygenic Photosystem II. Science 322(5904), 1110-1112.

Zhang, C.C., Gonzalez, L. and Phalip, V. (1998) Survey, analysis and genetic organization of genes encoding eukaryotic-like signaling proteins on a cyanobacterial genome. Nucleic Acids Research 26(16), 3619-3625.

Zhang, C.C., Jang, J.C., Sakr, S. and Wang, L. (2005) Protein phosphorylation on Ser, Thr and Tyr residues in cyanobacteria. Journal of Molecular Microbiology and Biotechnology 9(3-4), 154-166.

Zhang, P., Allahverdiyeva, Y., Eisenhut, M. and Aro, E.M. (2009) Flavodiiron proteins in oxygenic photosynthetic organisms: photoprotection of photosystem II by Flv2 and Flv4 in Synechocystis sp. PCC 6803. Plos One 4(4), e5331.

Zhang, P., Eisenhut, M., Brandt, A.M., Carmel, D., Silen, H.M., Vass, I., Allahverdiyeva, Y., Salminen, T.A. and Aro, E.M. (2012) Operon flv4-flv2 provides cyanobacterial photosystem II with flexibility of electron transfer. Plant Cell 24(5), 1952-1971.

Zhang, S.Y. and Bryant, D.A. (2011) The Tricarboxylic Acid Cycle in Cyanobacteria. Science 334(6062), 1551-1553.

Zhang, S.Y. and Bryant, D.A. (2015) Biochemical Validation of the Glyoxylate Cycle in the Cyanobacterium Chlorogloeopsis fritschii Strain PCC 9212. Journal of Biological Chemistry 290(22), 14019-14030.

Zhang, X.W., Zhao, F.Q., Guan, X.G., Yang, Y., Liang, C.W. and Qin, S. (2007) Genome-wide survey of putative serine/threonine protein kinases in cyanobacteria. Bmc Genomics 8.

Zhou, Y., Feng, J.T., He, H.W., Hou, L.F., Jiang, W., Xie, D., Feng, L.L., Cai, M. and Peng, H. (2017) Design, Synthesis, and Potency of Pyruvate Dehydrogenase Complex E1 Inhibitors against Cyanobacteria. Biochemistry 56(49), 6491-6502.

Zorina, A., Stepanchenko, N., Novikova, G.V., Sinetova, M., Panichkin, V.B., Moshkov, I.E., Zinchenko, V.V., Shestakov, S.V., Suzuki, I., Murata, N. and Los, D.A. (2011) Eukaryotic-like Ser/Thr protein kinases SpkC/F/K are involved in phosphorylation of GroES in the Cyanobacterium synechocystis. DNA Res 18(3), 137-151.

Appendix

I. **Schematic representations of the ferredoxin (Fx2, Fx3, Fx4, Fx7, Fx9) or flavodoxin (IsiB) deletion construct and the positions of the primers used.** The ORF of the gene targeted for mutagenesis (a) was replaced by various antibiotic resistance gene (b). The restriction sites of *Hind III* and *EcoR I* were marked on the fragment containing the region upstream and downstream of target gene. Km: Kanamycin, Cm: Chloramphenicol, Spec: Spectinomycin, Em: Erythromycin, Gm: Gentamycin.

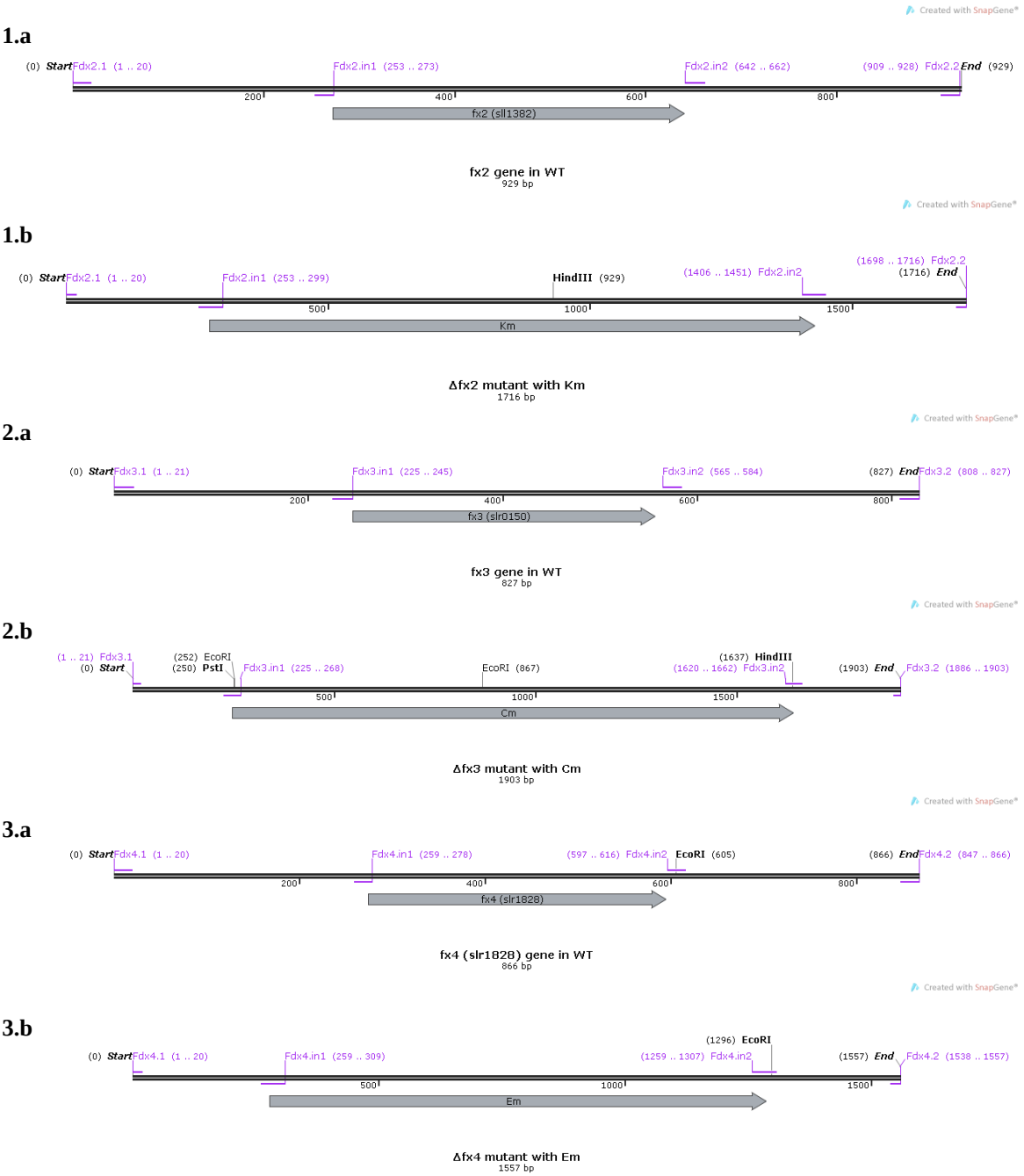

4.a

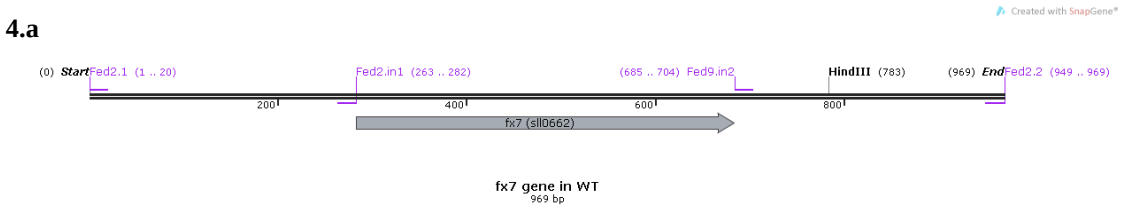

fx7 gene in WT
969 bp

4.b

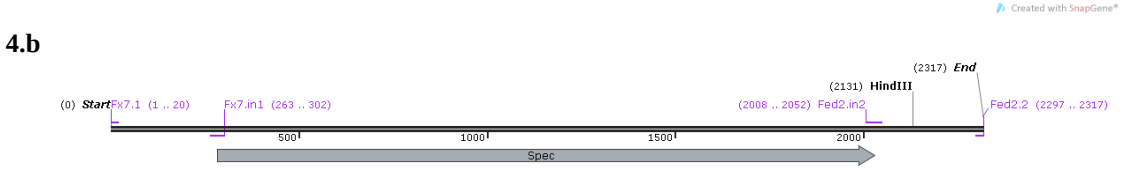

Δfx7 mutant with Spec
2317 bp

5.a

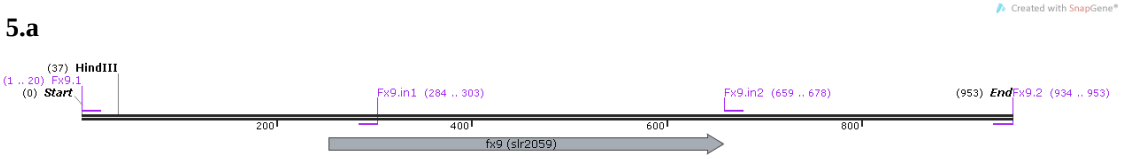

fx9 gene in WT
953 bp

5.b

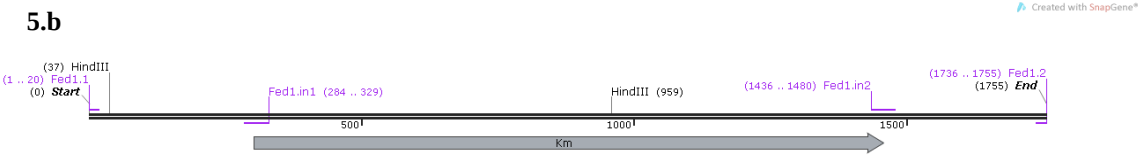

Δfx9 mutant with Km
1755 bp

6.a

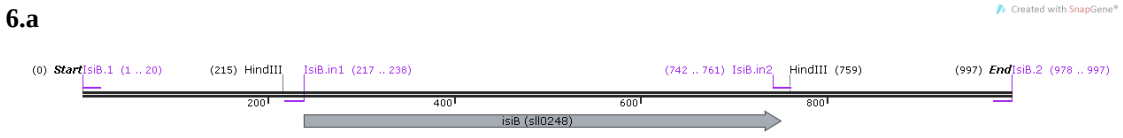

isiB gene in WT
997 bp

6.b

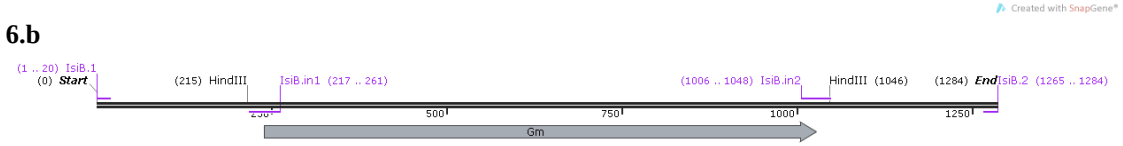

ΔisiB mutant with Gm
1284 bp

II. **Schematic representations of the recombinant ferredoxins (Fx1 and Fx9) that carry Strep II-tag or 6xHistidine-tag (6xHis-tag) at the C-terminus and the positions of the primers used.** Erythromycin (Em) and Kanamycin (Km) resistance cassette were inserted following the ORFs of ferredoxin-encoding genes in *Synechocystis*. More details about primers used could be found in Table 3.3.3.

A. F1s (*fx1* with Strep-tag)

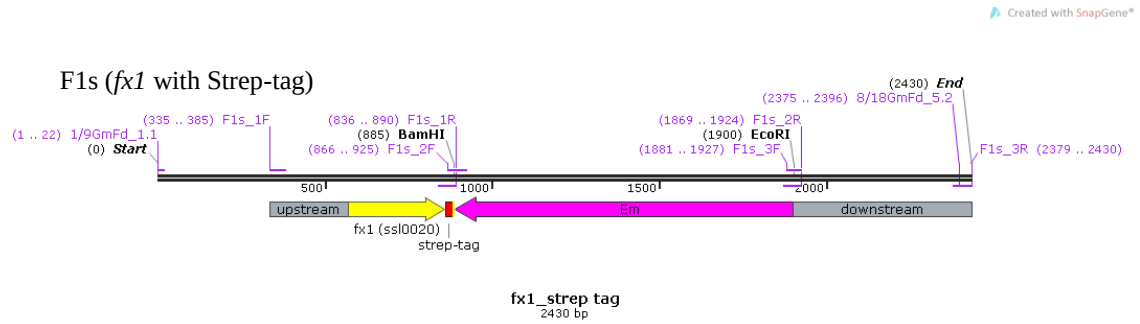

B. F9s (*fx9* with Strep-tag)

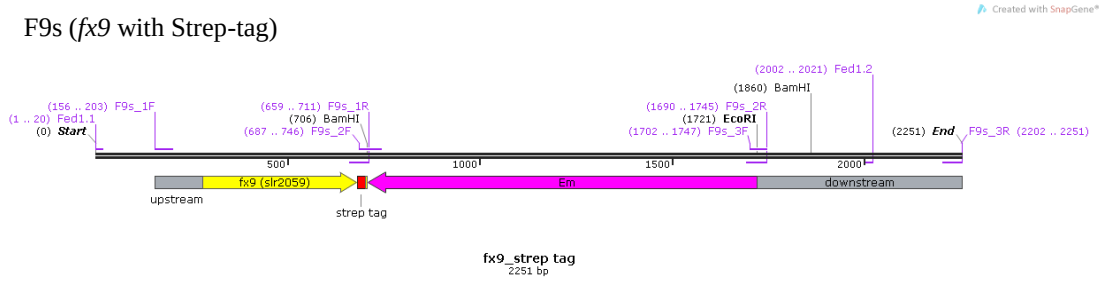

C. F1h (*fx1* with 6xHis-tag)

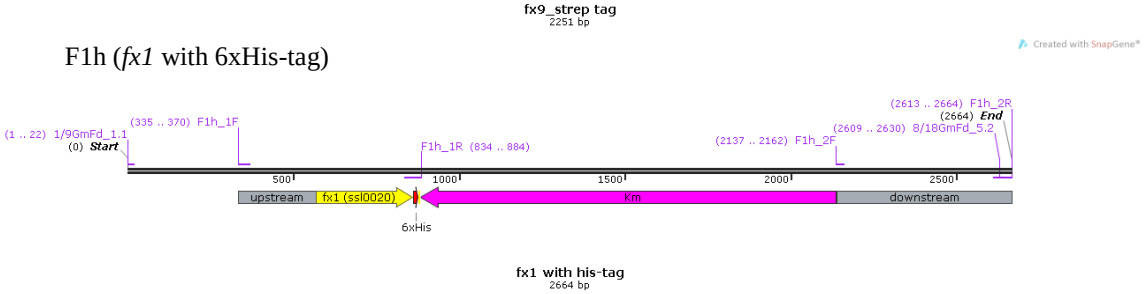

D. F9h (*fx9* with 6xHis-tag)

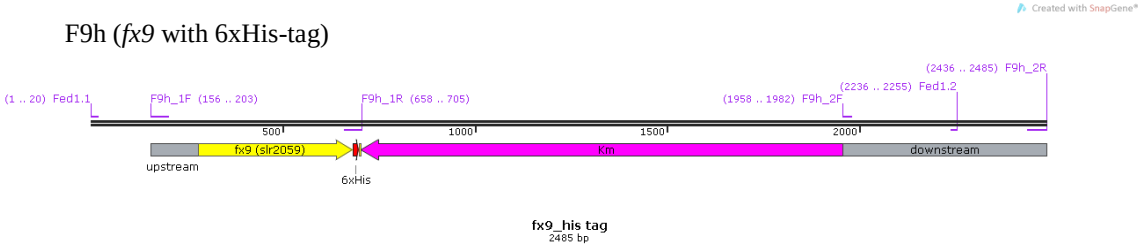

III. TEM images of *Synechocystis* WT and *Δfx7Δfx9* cells under autotrophic conditions with ammonium ($+NH_4^+$) or arginine (+Arg) as sole nitrogen source. Cells were harvested on the 6th day for TEM images. Carboxysome granules were marked as red stars in the images.

a) WT $+NH_4^+$

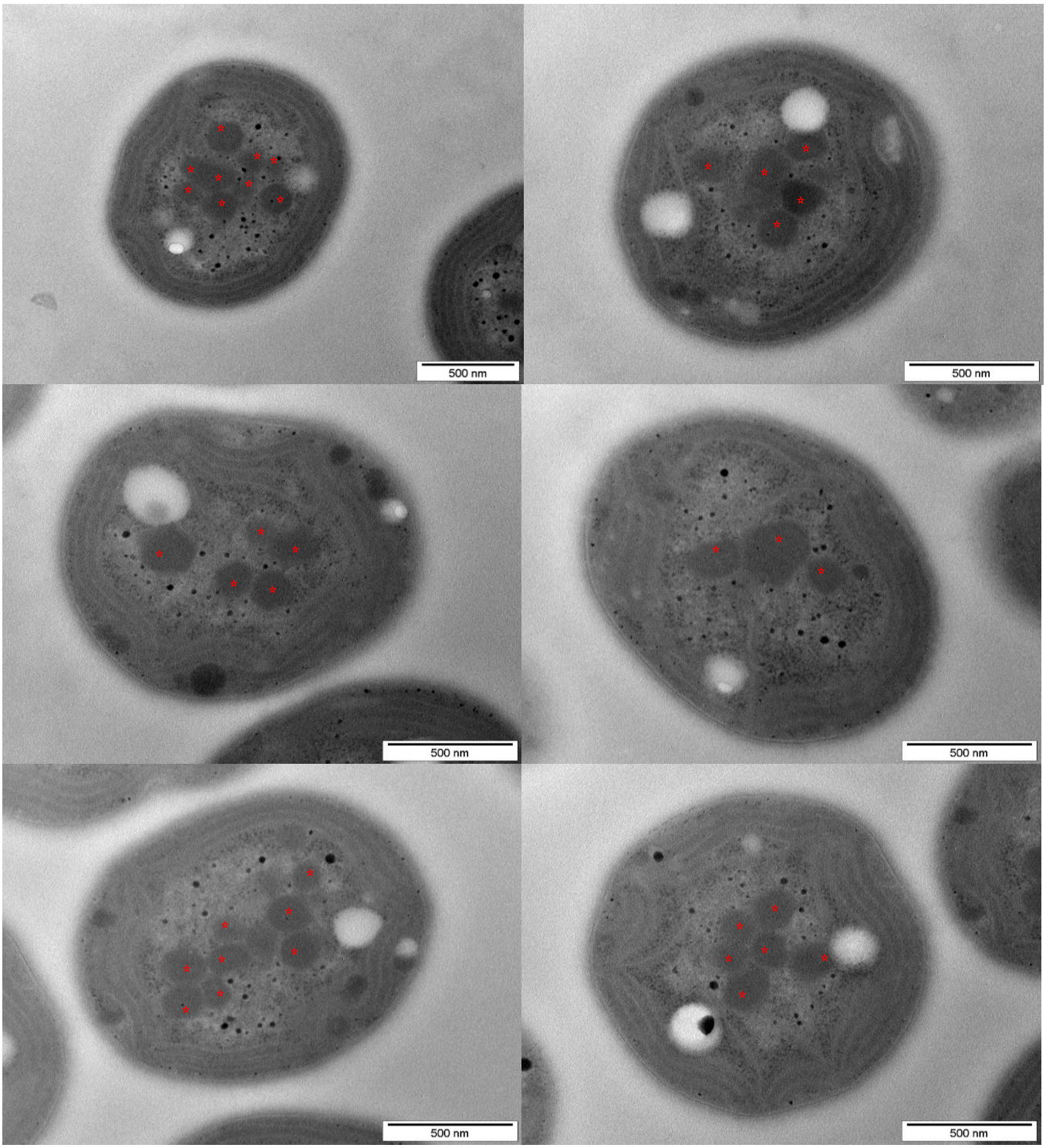

b) WT +Arg

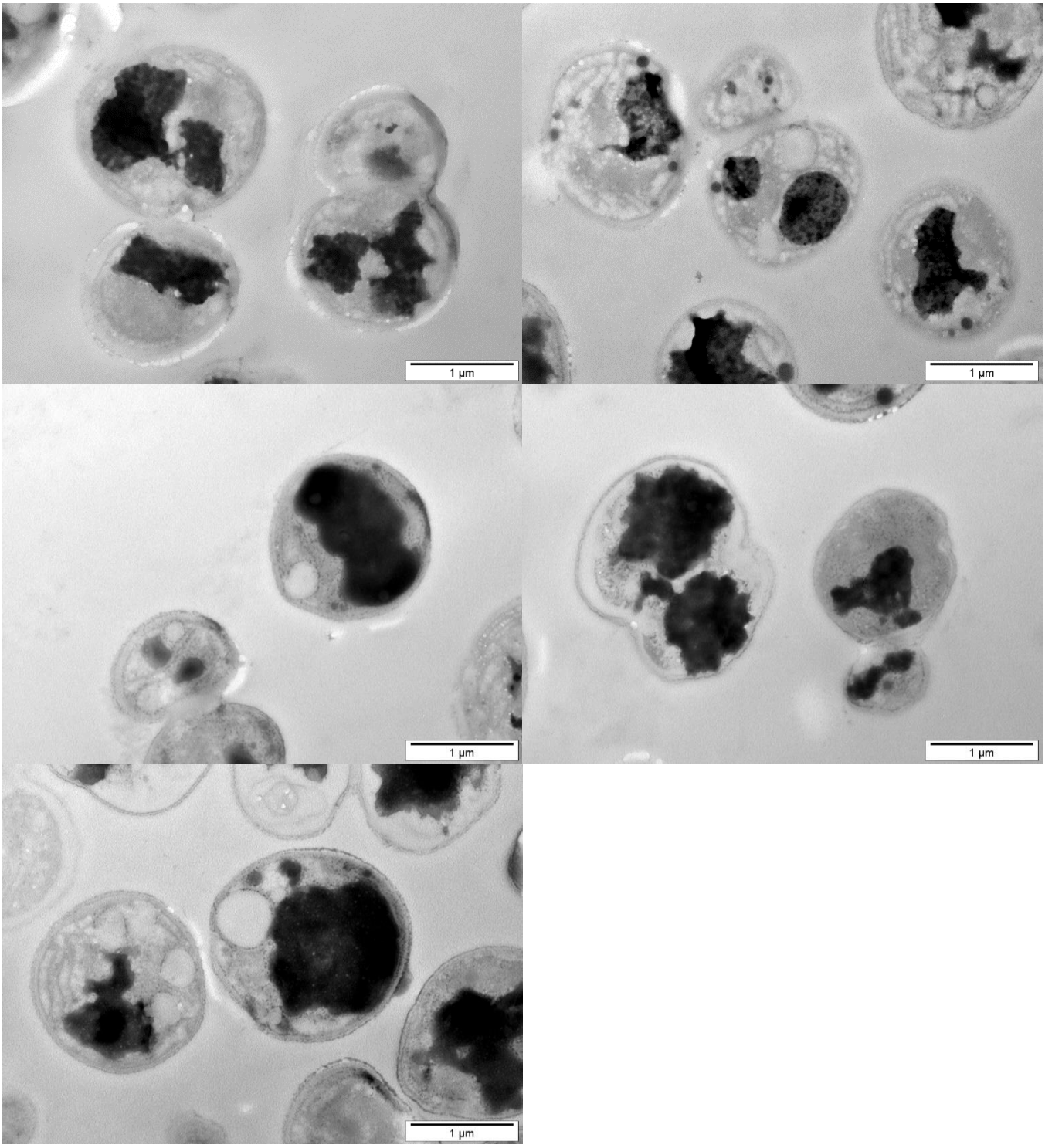

c) *Δfx7Δfx9* +NH_4^+

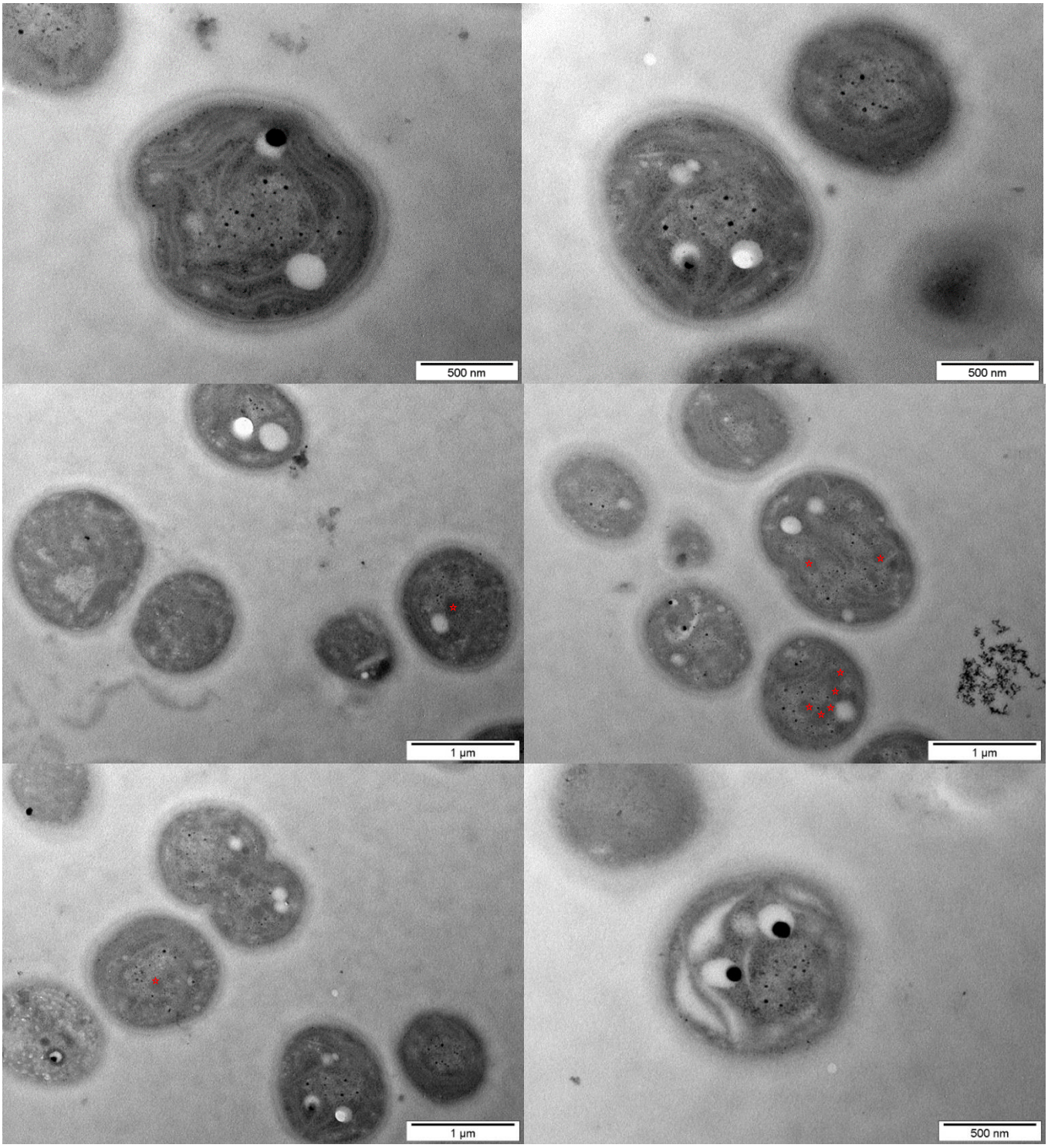

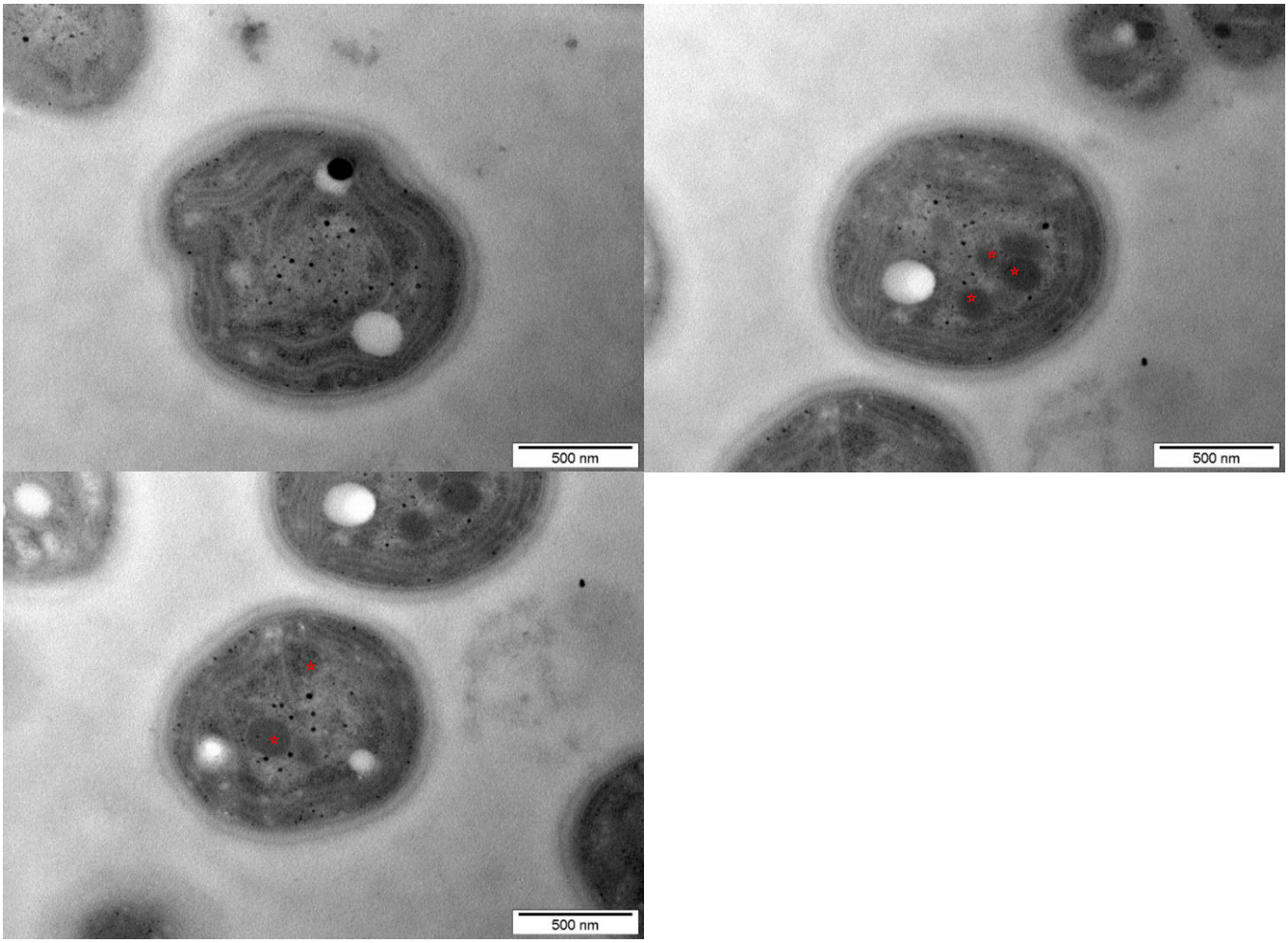

d) *Δfx7Δfx9* +Arg

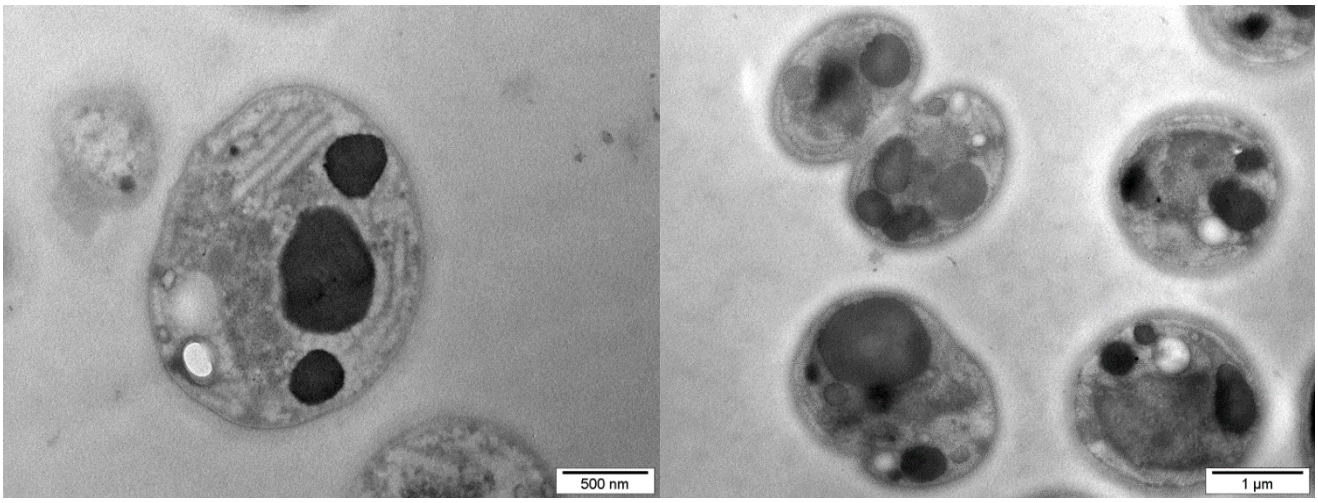

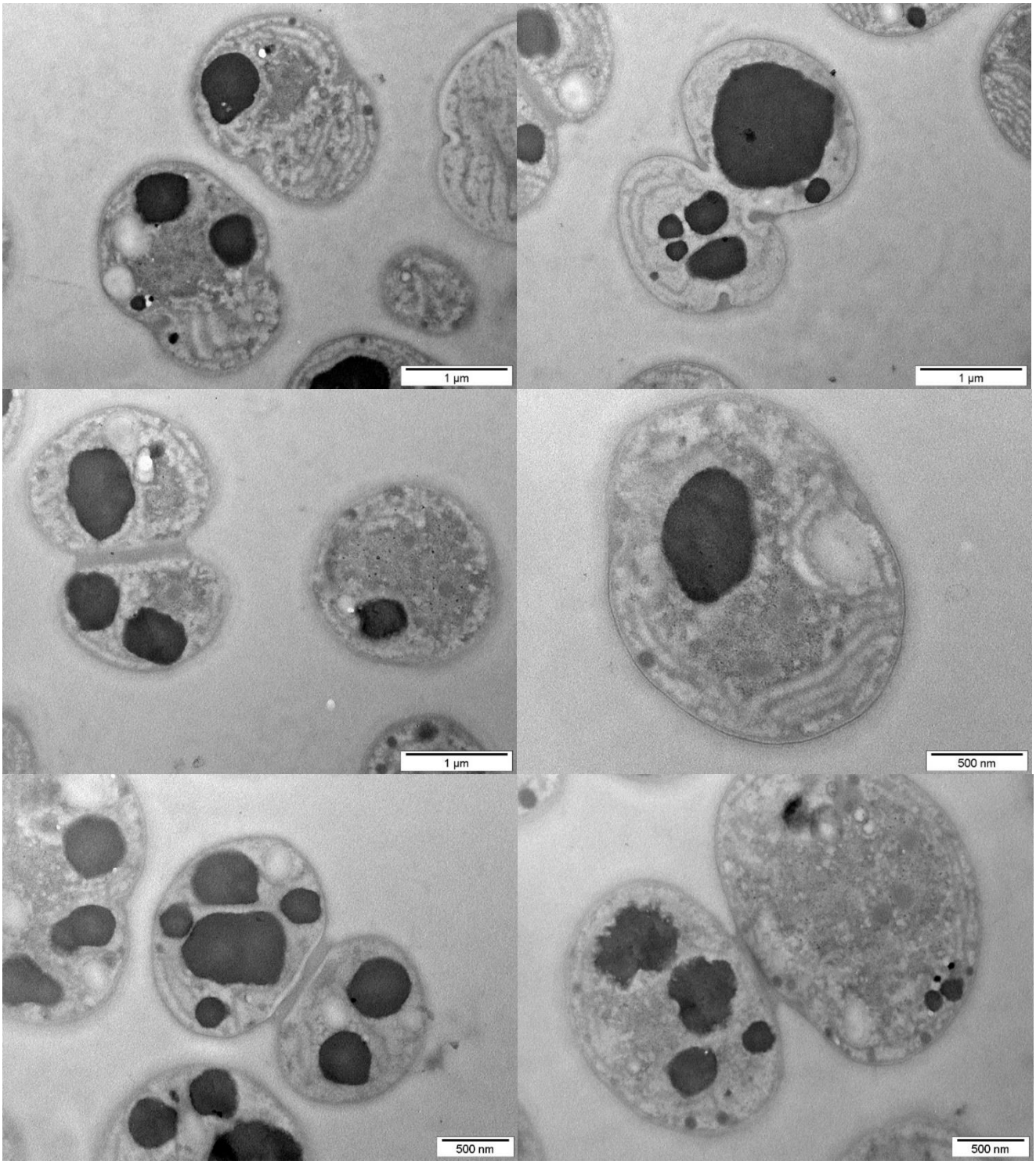
1 µm
1 µm
1 µm
500 nm
500 nm
500 nm

IV. Equilibrium concentrations of oxygen (µmol O_2/litre) at ambient partial pressure of 0.21 atm. in water as a function of temperature and salinity. At 20 ˚C and 1 atm.: 1 µmol O_2/l = 0.032 mg O_2/l = 0.024 ml O_2. Detailed tables are available at our web page: http://www.unisense.com/technical_information/

‰ /˚C	0.0	5.0	10.0	15.0	20.0	25.0	30.0	35.0	40.0
0.0	456.6	398.9	352.6	314.9	283.9	257.9	235.9	217.0	200.4
2.0	450.4	393.6	348.1	311.1	280.6	255.0	233.3	214.7	198.3
4.0	444.2	388.5	343.7	307.3	277.3	252.1	230.8	212.4	196.3
6.0	438.1	383.3	339.4	303.6	274.0	249.3	228.3	210.2	194.3
8.0	432.1	378.3	335.1	299.9	270.8	246.5	225.8	207.9	192.3
10.0	426.1	373.3	330.8	296.2	267.6	243.7	223.3	205.7	190.3
12.0	420.3	368.4	326.7	292.6	264.5	240.9	220.9	203.6	188.4
14.0	414.5	363.5	322.5	289.1	261.4	238.2	218.5	201.4	186.5
16.0	408.8	358.7	318.4	285.5	258.3	235.5	216.1	199.3	184.6
18.0	403.2	354.0	314.4	282.1	255.3	232.8	213.7	197.2	182.7
20.0	397.7	349.3	310.4	278.6	252.3	230.2	211.4	195.1	180.8
22.0	392.2	344.7	306.5	275.2	249.3	227.6	209.1	193.0	179.0
24.0	386.8	340.2	302.6	271.9	246.4	225.0	206.8	191.0	177.1
26.0	381.5	335.7	298.7	268.5	243.5	222.5	204.5	189.0	175.3
28.0	376.2	331.2	294.9	265.3	240.6	219.9	202.3	187.0	173.5

V. Equilibrium hydrogen concentrations (µmol/litre) at ambient hydrogen partial pressure of 1 atm. in water as a function of temperature. Ref. Wiesenburg and Guinasso 1979. J.Chem Eng. Data 24(4):356-360.

	Salinity (parts per thousand)								
Temp. °C	**0**	**10**	**20**	**30**	**32**	**34**	**36**	**38**	**40**
-2	901.34	851.79	841.96	832.59	823.21	813.84	804.46	813.84	804.46
-1	890.18	841.52	832.14	822.77	813.84	804.46	795.54	804.46	795.54
0	982.59	929.46	879.46	832.14	822.77	813.84	804.46	795.98	787.05
1	969.64	917.86	869.20	822.77	813.84	804.91	795.98	787.50	778.57
2	957.59	907.14	858.93	813.84	804.91	796.43	787.50	779.02	770.98
3	945.54	896.43	849.55	805.36	796.43	787.95	779.91	771.43	763.39
4	934.38	886.16	840.18	796.88	788.39	780.36	771.88	763.84	755.80
5	923.66	876.34	831.70	789.29	780.80	772.77	764.73	756.70	748.66
6	912.95	866.96	823.21	781.70	773.66	765.63	757.59	749.55	741.96
8	893.30	849.11	807.14	767.41	759.38	751.79	744.20	736.61	729.46
10	875.45	833.04	792.41	754.02	746.43	739.29	731.70	724.55	717.41
12	858.93	817.86	779.02	741.96	734.82	727.68	720.54	713.39	706.70
14	843.75	804.02	766.52	730.80	723.66	716.96	710.27	703.13	696.43
16	829.46	791.52	755.36	720.54	713.84	707.14	700.45	693.75	687.50
18	816.96	779.91	744.64	711.16	704.46	698.21	691.52	685.27	679.02
20	805.36	769.64	735.27	702.68	695.98	689.73	683.48	677.23	671.43
22	794.64	759.82	726.34	694.64	688.39	682.14	676.34	670.09	664.29
24	785.27	751.34	718.75	687.50	681.70	675.45	669.64	663.84	657.59
26	776.79	743.30	711.61	681.25	675.00	669.20	663.39	657.59	651.79
28	768.75	736.16	704.91	675.45	669.64	663.84	658.04	652.23	646.88
30	762.05	729.91	699.55	670.09	664.29	658.48	653.13	647.32	641.96